CORA Cork Open Research Archive
Cartlann Taighde Oscailte Chorcaí

Title	Simulation chamber studies of the atmospheric degradation of naphthalene, 1-nitronaphthalene and phthaldialdehyde
Authors	Chen, Yang
Publication date	2012-04
Original Citation	Chen, Y, 2012. Simulation chamber studies of the atmospheric degradation of naphthalene, 1-nitronaphthalene and phthaldialdehyde. PhD Thesis, University College Cork.
Type of publication	Doctoral thesis
Rights	© 2012, Yang Chen - http://creativecommons.org/licenses/by-nc-nd/3.0/
Download date	2026-11-12 10:46:03
Item downloaded from	https://hdl.handle.net/10468/622

UCC
University College Cork, Ireland
Coláiste na hOllscoile Corcaigh

Simulation Chamber Studies of the Atmospheric Degradation of Naphthalene, 1-Nitronaphthalene and Phthaldialdehyde

A thesis submitted to

THE NATIONAL UNIVERSITY OF IRELAND



For the degree of

DOCTOR OF PHILOSOPHY

By

Yang Chen, **M.Sc.**

Based on Research Performed in the

Department of Chemistry

and at

Environmental Research Institute,

University College Cork

and at

European PhotoReactor,

Spain

Under the Supervision of

Dr. John C. Wenger

Head of Department

Prof. Mick Morris

April 2012

Table of Contents

Chapter 1 Introduction

1.1 Chemical Transformation in the Troposphere……... 2

1.1.1 Reaction with the Hydroxyl Radical (OH)…….4

1.1.2 Reaction with the Nitrate Radical (NO_3)……...9

1.1.3 Reaction with Ozone (O_3)…….....……... 11

1.1.4 Photolysis by Sunlight…… 11

1.2. Secondary Organic Aerosol (SOA) Formation…….……12

1.2.1 Gas/Particle Phase Partitioning Theory……13

1.2.2 Measurements of SOA…….14

1.2.3 Simulation Chamber Studies……16

1.3 Polycyclic Aromatic Hydrocarbons (PAHs) in the Atmosphere…… 17

1.4 Atmospheric Degradation of Naphthalene……19

1.5 References…… 22

Chapter 2 Secondary Organic Aerosol Formation from Photooxidation of Naphthalene

2.1 Introduction……...…...……31

2.1.1 Influence of Hydrocarbon/NO_x Ratio on SOA Formation…….…… 31

2.1.2 Influence of Relative Humidity on SOA Formation……..... 32

2.1.3 Previous Studies of SOA Formation from Photooxidation of Naphthalene… 32

2.1.4 Aim of this Work…….....…… 34

2.2 Experimental…… 35

2.2.1 Materials……....…..…… 35

2.2.2 Atmospheric Simulation Chamber……..…...….…… 36

2.2.3 Procedure…… 37

2.3 Results and Discussion…… 38

2.3.1 Effects of Hydrocarbon to NO_x Ratio on SOA yield …… 41

2.3.2. Comparison with Previous Studies……..... 45

2.3.3 Effect of Relative Humidity on SOA Yields……...…… 46

2.4 Conclusions…….. 52

2.5 References…… 53

Chapter 3 On-line and Off-line Analysis of Products from the Photooxidation of Naphthalene

3.1 Introduction……..…… 60

3.1.1 Previous Product Studies on the Photooxidation of Naphthalene……...…… 60

3.1.2 Photooxidation Mechanism for Naphthalene……...61

3.1.3 Denuder-Filter Sampling System……....…….64

3.1.4 Aerosol Time-of-Flight Mass Spectrometer (ATOFMS)…….……65

3.1.5 Aim of this Study……..67

3.2 Experimental…….68

3.2.1 Materials……...……68

3.2.2 Off-line Analysis using GC-MS with Derivatization…….....68

3.2.2.1 Denuder-Filter Sampling System…….....69

3.2.2.2 Derivatization with PFBHA……..……70

3.2.2.3 Derivatization of Quinones…….……71

3.2.2.4 Derivatization with BSTFA……... 72

3.2.2.5 Derivatization with PFBBr…… 74

3.2.3 On-line Analysis of SOA using ATOFMS……...75

3.2.3.1 Atmospheric Simulation Chamber…… 75

3.2.3.2 The Aerosol Time-of-Flight Mass Spectrometer (ATOFMS)……...… 77

3.2.3.3 Procedure……... 78

3.3 Results and Discussion…… 80

3.3.1 PFBHA Derivatization…… 80

3.3.2 Quinone Derivatization……... 86

3.3.3 PFBBr Derivatization…….. 86

3.3.4 BSTFA Derivatization……. 90

3.3.5 On-line Analysis of SOA using ATOFMS……..…… 98

3.3.5.1 Effect of OH Precursor…….. 98

3.3.5.2 Effect of Relative Humidity…… 103

3.3.5.3 Chemical Evolution of SOA ……106

3.4 Conclusions…… 109

3.5 References……..…… 110

Chapter 4 Photolysis of Phthaldialdehyde

4.1 Introduction……....……..... 117

4.1.1 Photolysis in the Troposphere……..... 118

4.1.2 Previous studies of the photolysis of aromatic aldehydes……. 119

4.1.3 Aim of this work…… 123

4.2 Experimental……...……124

4.2.1 Experiments in EUPHORE Chamber…….……124

4.2.1.1 Apparatus…… 124

4.2.1.2 Procedure and Analysis……126

4.2.2 Experiments in the Indoor Chamber……...……127

4.2.2.1 Apparatus……..……127

4.2.2.2 Procedure and Analysis……....…….....……128

4.3 Results and Discussion…….…… 130

4.3.1 Photolysis Rate Coefficient…….…….. 130

4.3.1.1 EUPHORE Chamber……...…… 130

4.3.1.2 Indoor Chamber……...…… 138

4.3.1.3 Comparison with Previous Studies…….…… 142

4.3.2 Photolysis Products……143

4.3.2.1 EUPHORE Chamber……144

4.3.2.2 Indoor Chamber……149

4.3.2.3 Comparison with previous studies……...…… 151

4.3.2.4 Photolysis Mechanism.....152

4.3.3 Secondary Organic Aerosol (SOA) Formation……..……154

4.3.3.1 EUPHORE Chamber……155

4.3.3.2 Indoor Chamber……... 164

4.3.4 On-line Analysis of SOA using ATOFMS…… 168

4.4 Conclusions……175

4.5 References…….. 176

Chapter 5 Photolysis of 1-Nitronaphthalene

5.1 Introduction……180

5.1.1 Previous studies of Atmospheric Chemistry of 1-Nitronaphthalene……..180

5.1.2 Aim of this Work……182

5.2 Experimental……...183

5.2.1 Materials…….....…….183

5.2.2 Experiments in EUPHORE Chamber…….....…….183

5.2.3 Experiments in the Indoor Chamber……...184

5.3 Results and Discussion……...186

5.3.1 Photolysis Rate Coefficient……186

5.3.1.1 EUPHORE Chamber……186

5.3.1.2 Indoor Chamber……194

5.3.1.3 Comparison with Previous Studies……...196

5.3.2 Photolysis Products and Mechanism……..198

5.3.3 Secondary organic aerosol (SOA) Formation……199

5.3.3.1 EUPHORE Chamber……200

5.3.3.2 Indoor Chamber……207

5.3.4 On-line Analysis of SOA using ATOFMS……207

5.3.4.1 Effect of Laser Power Density……..209

5.3.4.2 Effect of Nitrobenzene and NO on Naphthoxy Dimerization……...…..216

5.4 Conclusions……...…….220

5.5 References……...221

Chapter 6 Conclusions and Future Work

6.1 Conclusions…….226

6.2 Suggestions for Future Work……228

6.3 References……...230

Declaration

The work presented in this thesis was performed in the Department of Chemistry and the Environmental Research Institute, University College Cork during the academic years 2008-2012. This thesis is the independent work of the author and has not been submitted to any institution for the purpose of obtaining any other qualification.

Yang Chen

Abstract

A detailed series of simulation chamber experiments has been performed on the atmospheric degradation pathways of the primary air pollutant naphthalene and two of its photooxidation products, phthaldialdehyde and 1-nitronaphthalene.

The measured yields of secondary organic aerosol (SOA) arising from the photooxidation of naphthalene varied from 6-20%, depending on the concentrations of naphthalene and nitrogen oxides as well as relative humidity. A range of carbonyls, nitro-compounds, phenols and carboxylic acids were identified among the gas- and particle-phase products. On-line analysis of the chemical composition of naphthalene SOA was performed using aerosol time-of-flight mass spectrometry (ATOFMS) for the first time. The results indicate that enhanced formation of carboxylic acids may contribute to the observed increase in SOA yields at higher relative humidity.

The photolysis of phthaldialdehyde and 1-nitronaphthalene was investigated using natural light at the European Photoreactor (EUPHORE) in Valencia, Spain. The photolysis rate coefficients were measured directly and used to confirm that photolysis is the major atmospheric loss process for these compounds. For phthaldialdehyde, the main gas-phase products were phthalide and phthalic anhydride. SOA yields in the range 2-11% were observed, with phthalic acid and dihydroxyphthalic acid identified among the particle phase products.

The photolysis of 1-nitronaphthalene yielded nitric oxide and a naphthoxy radical which reacted to form several products. SOA yields in the range 57-71% were observed, with 1,4-naphthoquinone, 1-naphthol and 1,4-naphthalenediol identified in the particle phase. On-line analysis of the SOA generated in an indoor chamber using ATOFMS provided evidence for the formation of high-molecular-weight products. Further investigations revealed that these products are oxygenated polycyclic compounds most likely produced from the dimerization of naphthoxy radicals.

These results of this work indicate that naphthalene is a potentially large source of SOA in urban areas and should be included in atmospheric models. The kinetic and mechanistic information could be combined with existing literature data to produce an overall degradation mechanism for naphthalene suitable for inclusion in photochemical models that are used to predict the effect of emissions on air quality.

Acknowledgement

I would like to thank Dr. John Wenger firstly for giving me the chance to pursue my PhD degree under his supervision. John is the best supervisor ever for scientific thinking, valuable and essential suggestion on my research, also his happy attitude, and good sense of humour. His guidance is the key reason for me to present this thesis, and make through my PhD study. John also taught me the spirit of dictation and critical thinking in scientific research. He also provided amazing chances for me to go to the United Kingdom, Spain and America, which were all unforgettable experiences. Financial support for this work was provided by the Irish Environmental Protection Agency STRIVE Doctoral Scholarships Programme (2008-PhD-AQ1).

I would like to thank two postdocs, Shouming and Rob. Shouming helped me to get into the field of atmospheric chemistry as soon as possible, and help me to learn the principle of simulation chamber study. He trained me for operation of the instruments in the lab, and the related data collecting and processing. Shouming influenced me very much on the serious and cautious attitude and critical thinking on scientific research. His experience on scientific research helped me to save a lot of time. I would thank Rob for his help, especially on the ATOFMS study of SOA, operation and data processing, for his valuable experience on simulation chamber study, for his patience on the trouble we confronted with.

I would like to thank the colleagues in both CRAC lab and ERI. I would thank Ivan, Kristina and Jennie on their help on the GC-MS analysis. I would thank Jun for his help in my life in Cork, and the interdisciplinary view on my study. I would thank Ian and Trevor who helped me settle in the CRAC lab and got registered my attendance to the University. I would also thank Arnaud, Danny, Daves, Ruairi, Eoins, Tina, Stephen and Jovanna, for their kindly help in the lab.

I would thank Shumin, my wife, on the contribution on my PhD study. Thank her for being my lover and my soulmate, for her decision to spend the rest of her life with me, for her understanding on my choice of career, for her patience and tolerance when away from me during these tough three years, for her support on my research. Marrying her is the best thing that happened in my life, and travelling in Europe after our wedding was the best time I had in these three years!

采薇采薇，薇亦作止。

日归日归，岁亦莫止。

——诗经《采薇》

To my parents and my wife

Chapter

1

Introduction

1.1 Chemical Transformation in the Troposphere

The troposphere is the lowest layer of Earth's atmosphere which extends upwards from the surface to an altitude of 10-15 km (Finlayson-Pitts et al. 2000). It is characterized by a decrease in temperature of approximately 7 K km^{-1} with altitude until the tropopause, where the temperature starts to rise with altitude due to the formation and destruction of ozone in the stratosphere. The presence of ozone is vital as it, along with molecular oxygen, absorbs the most energetic part of the ultraviolet radiation emitted by the Sun, ensuring that only radiation with $\lambda \geq 290$ nm reaches the troposphere, **Figure 1.1.** The lower region of the troposphere, from the surface up to an altitude of 0.5 to 2 km, is called the boundary layer. In this layer, turbulent weather systems, combined with both natural and anthropogenic emissions, lead to a highly complex and chemically active air mass.

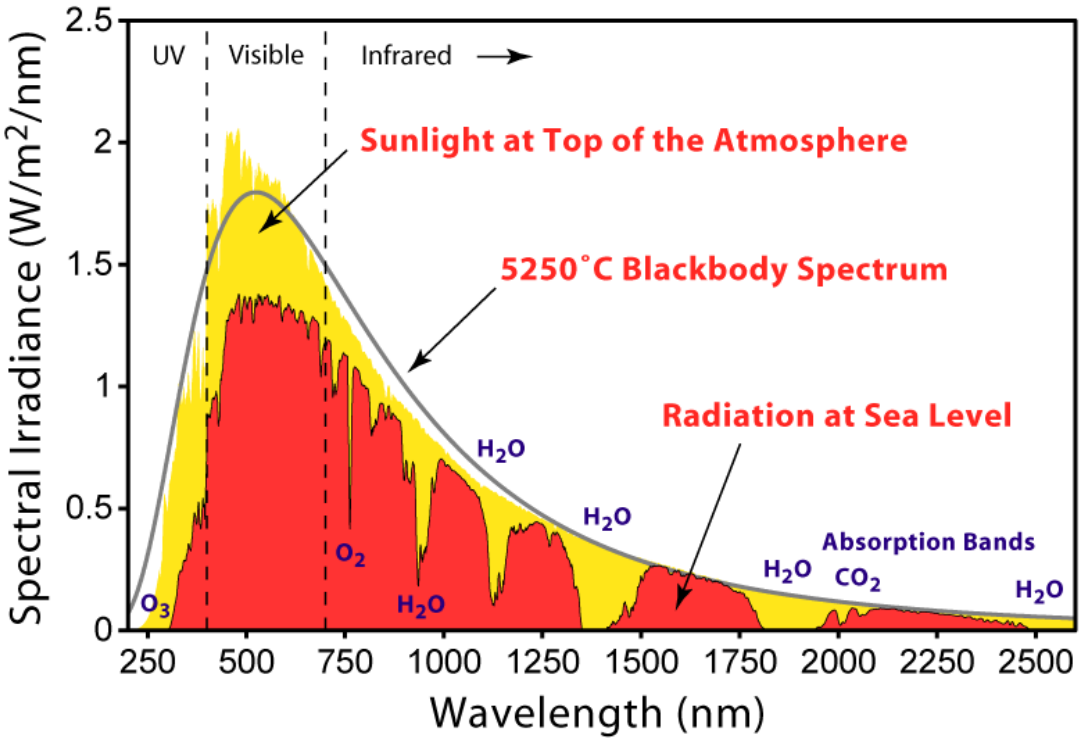


Figure 1.1 Solar spectrum from the top of atmosphere to sea level (ISO 1992).

A wide variety of gases and particles are emitted into the atmosphere from the biosphere, lithosphere and the oceans. Natural sources include volcanic eruptions, emissions from vegetation, microorganisms, peat bogs, swamps and forest fires. Anthropogenic sources include industrial activities, fossil fuel, biomass burning and

agricultural practices. These combined emissions result in a wide range of organic and inorganic gases and particles being present in the atmosphere. Although the abundance of these trace species is limited to part per billion (ppb) or part per trillion (ppt) levels, there are a range of physical and chemical processes that can lead to transportation, transformation and removal from the atmosphere. The simplest removal process is dry deposition, whereby particles and gases, such as ozone and SO_2, can be absorbed by soil, plants, water surfaces or man-made materials (Wesely et al. 2000). Wet deposition, or removal by precipitation, is also important for gases and particles that are soluble in water (Jacob 2000), Some species can undergo direct photolysis by sunlight in the troposphere, however, the most important removal process is chemical conversion via gas-phase reactions initiated by oxidising species such as the hydroxyl radical (OH), nitrate radical (NO_3) and ozone.

One of the most important categories of atmospheric trace gases is volatile organic compounds (VOCs). These organic chemicals have sufficient vapour pressure to be present in the gas phase at ambient temperature and pressure. VOCs comprise many classes of compounds including pure hydrocarbons (e.g. alkanes, alkenes and aromatic hydrocarbons) and organic compounds containing oxygen, nitrogen, sulfur and halogens. Other terms used to describe VOCs in the atmosphere include hydrocarbons (HCs), reactive organic gases (ROGs) and non-methane volatile organic compounds (NMVOCs) (Finlayson-Pitts et al. 2000). VOCs are emitted into the troposphere from biogenic (Atkinson et al. 2003) and anthropogenic sources (Sawyer et al. 2000), but can also be formed *in situ* via the atmospheric degradation of other organic compounds (Atkinson et al. 2003). The principal biogenic sources are terrestrial plants, forests, animal and microbial organisms, while oil-refining, motor vehicle exhaust, solvent use, food manufacture and agriculture (Kirchstetter et al. 1998; Lu et al. 2005) are the main anthropogenic sources. On a global basis, the biogenic emissions of VOCs are significantly higher, however, anthropogenic emissions are dominant in urban environments and can have a large impact on local and regional air quality. Indeed, VOCs are one of the key chemical species responsible for the formation of photochemical smog (Finlayson-Pitts et al. 2000).

Photochemical smog, first observed in Los Angeles in the mid-1940s (Finlayson-Pitts et al. 2000), is now a major world-wide environment issue. It is a form of air pollution that can cause plant damage, visibility degradation, eye irritation and is also

harmful to the human respiratory system, causing asthma and in severe cases, even death. Photochemical smog results from emissions of VOCs and NO from motor vehicles, which react in the atmosphere to form secondary pollutants such as ozone, NO_2, nitric acid, aldehydes, formic acid, peroxyacyl nitrates (PAN) and organic aerosol (Finlayson-Pitts et al. 2000). The general reaction mechanism for photochemical smog formation was discovered by Haagen-Smit and further details have been added over the last few decades. The key species that initiates the process is the hydroxyl radical.

1.1.1 Reaction with the Hydroxyl Radical (OH)

During the day time, the major removal process for many species, including volatile organic compounds (VOCs), is gas-phase reaction with hydroxyl (OH) radicals. The hydroxyl radical is generated in a number of different reactions. On a global level, the principal process for production of OH in the troposphere is the photolysis of ozone. Electronically excited $O(^1D)$ atoms are produced, which can be deactivated by collisions with nitrogen and oxygen molecules to ground-state oxygen $O(^3P)$, or react with water vapour to produce hydroxyl radicals (Atkinson 2000):

$$O_3 + h\nu\ (\lambda \leq 335\ \text{nm}) \rightarrow O_2 + O(^1D) \quad (1)$$

$$O(^1D) + M \rightarrow O(^3P) + M\ (N_2, O_2) \quad (2)$$

$$O(^3P) + O_2 + M \rightarrow O_3 + M \quad (3)$$

$$O(^1D) + H_2O \rightarrow 2OH \quad (4)$$

The reaction of $O(^3P)$ with H_2O to generate the OH radical is thermodynamically unfavourable under atmospheric conditions and reaction with O_2 to regenerate ozone is preferred.

At 298 K and atmospheric pressure, with a relative humidity of 50%, approximately 0.2 OH radicals are produced per $O(^1D)$ atom formed (Atkinson et al. 2003). Hydroxyl radicals then react mainly with CO and CH_4 (Atkinson 2000).

$$OH + CO \rightarrow H + CO_2 \quad (5)$$

$$OH + CH_4 \rightarrow CH_3 + H_2O \quad (6)$$

In the clean atmosphere, approximately 70% of hydroxyl radicals react with CO, and 30% with methane. The H and CH_3 radicals produced in reactions (5) and (6) can react with molecular oxygen to form hydroperoxy and methylperoxy radicals, respectively:

$$H + O_2 + M \rightarrow HO_2 + M \quad (7)$$

$$CH_3 + O_2 + M \rightarrow CH_3O_2 + M \quad (8)$$

In regions with a low concentration of NO, the peroxy radicals are generally consumed by reaction with itself and the hydroperoxy and methylperoxy radical (Atkinson 2000):

$$HO_2 + HO_2 \rightarrow H_2O_2 + O_2 \quad (9)$$

$$CH_3O_2 + HO_2 \rightarrow ROOH + O_2 \quad (10)$$

Under low NO conditions, the hydroperoxy radical can also react with ozone to regenerate the hydroxyl radical.

$$HO_2 + O_3 \rightarrow OH + 2O_2 \quad (11)$$

However, in the presence of NO, hydroperoxy radicals form NO_2 and a hydroxyl radical. In a similar way methylperoxy radicals can react with NO to form NO_2 and a methoxy radical, which subsequently reacts with O_2 to produce formaldehyde:

$$HO_2 + NO \rightarrow OH + NO_2 \quad (12)$$

$$CH_3O_2 + NO \rightarrow CH_3O + NO_2 \quad (13)$$

$$CH_3O + O_2 \rightarrow CH_2O + HO_2 \quad (14)$$

Thus, in the case of reaction (12), the hydroxyl radical is regenerated. For both reactions, the formation of NO_2 is important, as it can photolyse to form ozone.

$$NO_2 + h\nu\ (\lambda<420\ \text{nm}) \rightarrow O(^3P) + NO \quad (15)$$

$$O(^3P) + O_2 + M \rightarrow O_3 + M \quad (3)$$

Ozone can also react with NO as follows:

$$NO + O_3 \rightarrow NO_2 + O_2 \quad (16)$$

From this series of reactions it appears that there is no net formation of ozone in the clean troposphere. However, in other environments, e.g., polluted urban areas, the reaction of peroxy radicals with NO will cause an increase in NO_2 and in turn net

ozone production. An important sink for both hydroxyl radicals and nitrogen oxides (NO_x) is the gas-phase reaction of OH and NO_2 to form nitric acid, which can dissolve in water droplets and be removed by wet deposition:

$$OH + NO_2 \rightarrow HNO_3 \quad (17)$$

In polluted urban areas, the photolysis of nitrous acid, HONO, is also a major source of OH radicals. HONO is believed to be generated in the atmosphere via heterogeneous reactions of NO_2 including that with water absorbed on various surfaces and particles in the atmosphere (Kleffmann 2007). During the daytime, it can also be formed by the reaction of OH with NO:

$$OH + NO + M \rightarrow HONO \quad (18)$$

HONO is photolysed very quickly during the day time, generating OH:

$$HONO + h\nu\,(\lambda < 400\ \text{nm}) \rightarrow OH + NO \quad (19)$$

HONO can also react with OH

$$OH + HONO \rightarrow H_2O + NO_2 \quad (20)$$

The major sources of OH radicals in the troposphere are photolytic and hence the OH radical concentration depends on a number of factors including time of day, season, latitude, and cloud cover (Atkinson 1986; Atkinson 2000).

In urban environments, the OH radical can react with a large number of VOCs including, alkanes, alkenes and aromatic hydrocarbons. The hydroxyl radical initiated oxidation of an alkane proceeds via H atom abstraction:

$$OH + RCH_3 \rightarrow H_2O + RCH_2 \quad (21)$$

$$RCH_2 + O_2 + M \rightarrow RCH_2O_2 + M \quad (22)$$

The alkyl peroxy radical reacts with NO to form an alkoxy radical and NO_2. Alkyl nitrates can also be formed through the reaction of organic peroxy radicals with NO (Atkinson et al. 1992). Furthermore, organic nitrate formation is a sink for both radicals and NO_x.

$$RCH_2O_2 + NO \rightarrow RCH_2O + NO_2 \quad (23)$$

$$\rightarrow RCH_2ONO_2 \quad (24)$$

$$RCH_2O + O_2 \rightarrow RCHO + HO_2 \quad (25)$$

$$HO_2 + NO \rightarrow OH + NO_2 \quad (12)$$

The alkoxy radical (RCH_2O) reacts with oxygen by H atom abstraction to form an aldehyde and HO_2 radical, which can oxidise NO to NO_2 and thus form ozone, and the OH radical, which can start up a new reaction cycle.

More complicated, longer chain alkanes can form several alkoxy (RO) radicals, which can undergo a number of different reaction pathways, including bond dissociation and isomerization (Atkinson 2007). These reaction pathways give rise to a range of carbonyl and hydroxycarbonyl products.

The reaction of OH radicals with alkenes mainly occurs by addition of OH across the double bond. In unsymmetrical alkenes, two alkyl radicals can be produced, reaction (26), which react with O_2 to produce the corresponding peroxy radicals and in turn the respective oxy radicals. The oxy radicals can undergo reaction with oxygen, decomposition or isomerization as described earlier. Thus, a wide range of reaction products may be expected.

$$R_1R_2C{=}CR_3R_4 + OH \rightarrow R_1R_2C(OH){-}CR_3R_4 \quad (26a)$$

$$\rightarrow R_1R_2C{-}C(OH)R_3R_4 \quad (26b)$$

Reaction of OH with aromatic hydrocarbons is more complex and generally involves two competing mechanistic pathways (Atkinson 1989), as shown for toluene in **Figure 1.2**. H-atom abstraction from the alkyl-substituted groups results in the formation of aromatic aldehydes, while OH radical addition to the carbon atoms of the aromatic ring produces an alkyl-substituted hydroxyl-cyclohexadienyl radical (OH-adduct) which can react further to yield a range of ring-retaining and ring-opening products.

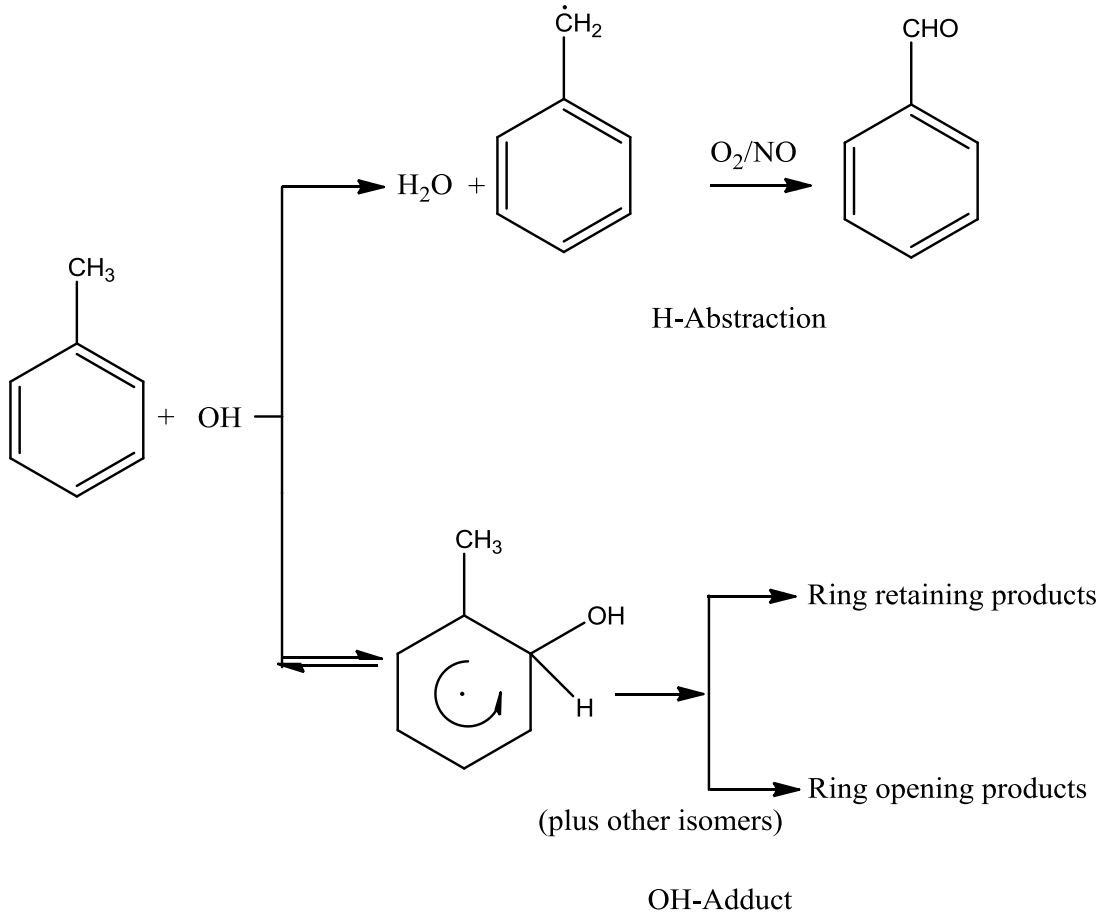


Figure 1.2 Initial steps in the OH initiated atmospheric degradation of toluene.

A general mechanism outlining the key reactions in the OH-initiated atmospheric oxidation of VOCs is shown **Figure 1.3**. In high-NO_x environments, carbonyls, hydroxycarbonyls, and organic nitrates are the major products, while hydroperoxides, carbonyls, hydroxycarbonyls and alcohols are dominant products in low-NO_x conditions.

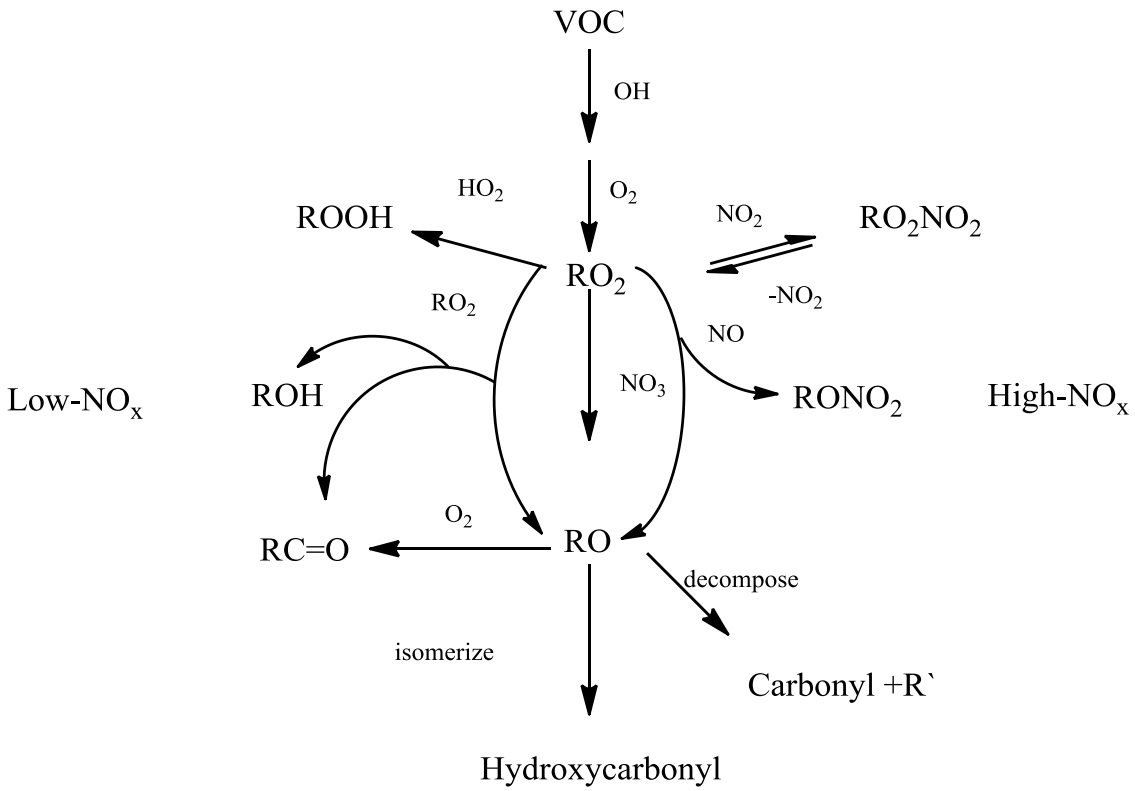


Figure 1.3 Simplified general reaction mechanism for the OH-initiated degradation of VOCs (Hallquist et al. 2009).

1.1.2 Reaction with the Nitrate Radical (NO_3)

OH plays a decisive role in the chemistry of the atmosphere during daytime. However, during night its concentration is negligible, and the NO_3 radical and O_3 are the main oxidants (Platt et al. 1984; Wayne et al. 1991). NO_3 reacts with a number of VOCs initiating their night time degradation (Atkinson 2000). NO_3 also contributes to the removal of NO_x mainly via HNO_3 and particulate nitrate formation.

The major source of NO_3 is the oxidation of nitrogen dioxide by ozone (Wayne et al. 1991).

$$NO_2 + O_3 \rightarrow NO_3 + O_2 \qquad (27)$$

During daytime, NO_3 has a very short lifetime (about 5 s) due to its strong absorption (Wayne et al. 1991) in the visible region of the solar spectrum (maximum absorption

662 nm) and rapid photodissociation, mainly to NO_2 and to a lesser extent to NO (Brauers et al. 1995):

$$NO_3 + h\nu\ (\lambda<700\ nm) \rightarrow NO_2 + O(^3P) \quad (28)$$

$$NO_3 + h\nu\ (\lambda<580\ nm) \rightarrow NO + O_2 \quad (29)$$

NO_3 reacts with NO_2 to produce N_2O_5 via the temperature-dependent equilibrium (Wangberg et al. 1996):

$$NO_3 + NO_2 + M \leftrightarrows N_2O_5 + M \quad (30)$$

Subsequent removal of nitrogen pentoxide (N_2O_5) leads to a net loss of NO_3 from the atmosphere. In the gas phase N_2O_5 can contribute to nitric acid formation following: first and second order reactions with water vapour (Wahner et al. 1998):

$$N_2O_5 + H_2O \rightarrow 2HNO_3 \quad (31)$$

$$N_2O_5 + 2H_2O \rightarrow 2HNO_3 + H_2O \quad (32)$$

NO_3 reacts with alkanes by H-abstraction from a C-H bond to form nitric acid and the resulting organic alkyl radical (R), which can convert to RO_2:

$$NO_3 + RH \rightarrow HNO_3 + R \quad (33)$$

$$R + O_2 + M \rightarrow RO_2 + M \quad (34)$$

The organic peroxy radicals can undergo the same series of reactions as outlined above. In addition, RO_2 can react with NO_3 as follows:

$$RO_2 + NO_3 \rightarrow RO + NO_2 + O_2 \quad (35)$$

$$RO + O_2 \rightarrow R_1R_2CO + HO_2 \quad (36)$$

NO_3 thus plays an important role as a night-time source of both RO_2 and HO_2 radicals.

The reaction of NO_3 with alkenes occurs via an addition mechanism to form peroxy nitrates:

$$NO_3 + >C=C< \rightarrow >C(ONO_2)\dot{C}<$$ (37)

The NO_3 adduct can eliminate NO_2 to yield an epoxide or react with O_2 leading to the formation of a peroxy radical, which can undergo similar reactions as described earlier.

1.1.3 Reaction with Ozone (O_3)

Reaction with ozone is an important removal process for unsaturated VOCs during the day and night time (Finlayson-Pitts et al. 2000). The ozonolysis of VOCs has been well studied (Johnson et al. 2008). A general mechanism for the alkene-ozone reaction is shown in **Figure 1.4**.The initial step is electrophilic addition of ozone to the C═C bond to form a 1,2,3-trioxolane adduct, or primary ozonide. The ozonide is unstable and quickly decomposes to produce a carbonyl and biradical species called a Criegee intermediate (Atkinson et al. 1993). The chemistry of Criegee intermediates is complex and involves the formation of a range of species, including the OH radical (Donahue et al. 1998).

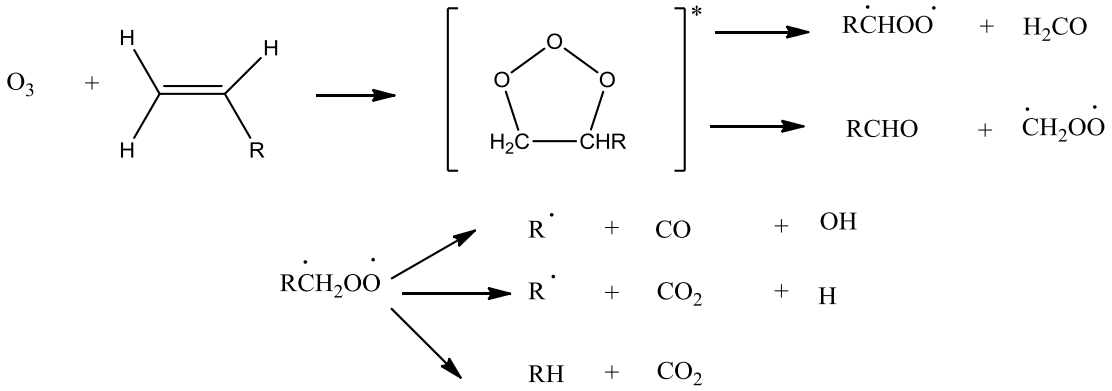


Figure 1.4 General mechanism for ozonolysis of an alkene.

1.1.4 Photolysis by Sunlight

It is possible for a compound to be photolysed in the troposphere if it has absorption at wavelengths > 290 nm. The photolysis rate coefficient, *j*, is described by the following equation:

$$j = \int \sigma_T(\lambda)\Phi(\lambda)F(\lambda)d\lambda$$ (I)

where j is the rate coefficient of photolysis, σ is the absorption cross-section (cm^2 $molecule^{-1}$) and dependent on temperature, F is the solar actinic flux (photons cm^{-2} s^{-1}), and Φ is the quantum yield of photolysis (molecule $photon^{-1}$). Each parameter could be different under various conditions. For example, the phase of compound can change the absorption cross-section, the solar actinic flux is influenced by the solar zenith angle and Φ often depends strongly on the wavelength of radiation absorbed by the compounds (Finlayson-Pitts et al. 2000; Wayne 2000). Photolysis is an important loss process for VOCs with strong absorption features at $\lambda > 290$ nm, such as aldehydes, nitrates, nitro aromatics and hydroperoxides (Atkinson 2007).

1.2. Secondary Organic Aerosol (SOA) Formation

The atmospheric oxidation of VOCs leads to polar and less volatile products containing oxygenated functional groups such as aldehyde, ketone, alcohol and nitrate. Oxidation products with sufficiently low volatility may undergo gas to particle transfer to produce secondary organic aerosol (SOA). The formation of SOA can occur via the condensation of oxidation products onto pre-existing particles or nucleation to form new particles. However, the detection of higher molecular weight species, such as oligomers and organosulfates, in organic aerosol, indicates that gas/particle transfer is not only a simple physical process, but may also involve reactive uptake of certain species. For example, the relatively volatile glyoxal (CHOCHO) can associate with other aldehydes and organic acids in particles (Kroll et al. 2005; Volkamer et al. 2007) or can be sulfated after gem-diol formation (Gómez-González et al. 2008). Glyoxal molecules can also undergo hemiacetal (Loeffler et al. 2006), and Aldol condensation reactions in the particle phase (Jang et al. 2002; Sareen et al. 2010). These chemical processes can dramatically increase the mass of SOA and represent mechanisms by which relatively volatile (and reactive) species can be involved in SOA formation.

The major precursors of SOA are biogenic compounds such as terpenes (Bahreini et al. 2005; Ng et al. 2007b), isoprene (Kroll et al. 2006; Surratt et al. 2006) and anthropogenic hydrocarbons like benzene, toluene (Ng et al. 2007a) and other substituted aromatics. Although some information is available on the yields of SOA formed from various precursors, there is uncertainty over the chemical composition of

the SOA produced and the nature of the oxidation products responsible for its formation (Hallquist et al. 2009). In addition, recent field measurements indicate that monocyclic aromatic hydrocarbons can only partially account for the amount of SOA present in urban areas and that significant additional anthropogenic sources exist (Volkamer et al. 2007). A range of organic compounds with intermediate volatility (IVOCs), e.g. higher alkanes, alkenes and polycyclic aromatic hydrocarbons have been identified as possible "missing" sources of SOA (Robinson et al. 2007). Since up to 70% of the organic material in ambient aerosols is secondary in nature, further information on the sources and composition of SOA is clearly required to understand its potential impact on air quality and climate. Moreover, recently research clearly showed that the Intermediate Volatile Organic Compound (IVOCs) play an important role on SOA formation (de Gouw et al. 2011).

1.2.1 Gas/Particle Phase Partitioning Theory

Fundamentally, SOA is a mixture of numerous semi-volatile compounds which can transfer from the gas phase to the particle phase (Hallquist et al. 2009). The partitioning behaviour of atmospheric oxidation products is characterised by a partitioning coefficient, which was first used by Pankow (Pankow 1994a; Pankow 1994b) to describe the gas/particle partitioning:

$$K_p = \frac{F_{i,om}/TSP}{A_i} = \frac{760RTf_{om}}{(MW_{om}10^{6}\xi_i p_{L.i}^{\circ})} \qquad \text{(II)}$$

where K_p is the partition coefficient, $F_{i,om}$ (ngm^{-3}) is the concentration of organic matter, *i*, in the particulate phase, TSP (μgm^{-3}) is the total suspended particles concentration, and A_i (ngm^{-3}) is the concentration in the gaseous phase. *R* is the gas constant (8.206×10^{-5} m^3 atm mol^{-1} K^{-1}), *T* is the temperature (K), f_{om} is the mass fraction of the total suspended particles (TSP) that is the a organic matter (om) phase, MW_{om} is the average molecular weight of the absorbed om (g/mol), ζ_i is the activity coefficient of compound *i* in the om phase and $p_{L,i}^{o}$ is the vapour pressure (Torr) of the absorbing compound as liquid.

Later on, this model was extended by Odum (Odum et al. 1996), who proposed that the yield of SOA, *Y*, can be described as:

$$Y = \frac{\Delta M_0}{\Delta HC} \quad \text{(III)}$$

where ΔM_0 is the organic aerosol mass concentration (μg m^{-3}) produced for a given amount of HC (hydrocarbon) reacted, ΔHC (μg m^{-3}). Odum developed a model to relate the overall aerosol yield to the amount of pre-existing aerosol (Odum et al. 1996):

$$Y = M_0 \sum_i \left(\frac{\alpha_i K_{om,i}}{1 + K_{om,i} M_0} \right) \quad \text{(IV)}$$

where M_0 is the aerosol mass concentration (μg m^{-3}), α_i is the mass-based stoichiometric coefficient for the reaction product *i* and $K_{om,i}$ is the partitioning coefficient of product *i* normalized by the mass concentration of the absorbing aerosol. Thus the aerosol yield is expressed as the sum of the contributions of each reaction product and is dependent on their partitioning coefficients and the aerosol mass concentration. However, due to the complexity of the oxidation pathways for SOA precursors, values for α_i and $K_{om,i}$ are not known for all products.

1.2.2 Measurements of SOA

A range of analytical methods have been employed to measure the chemical species present in ambient and laboratory-generated organic aerosols to obtain information on the sources, composition and formation mechanisms of SOA. These include traditional off-line methods such as FTIR spectroscopy and gas chromatography-mass spectrometry (GC-MS) and recently developed on-line techniques utilizing aerosol mass spectrometry.

Off-line methods require sample collection before analysis. Filters are the most common substrate used for the collection of suspended particles. Various materials have been employed including glass fibre (Turpin et al. 2000), polycarbonate, PTFE (Iinuma et al. 2004), and quartz (Forstner et al. 1997). Unfortunately, filter sampling is prone to artefacts arising from the volatilization of particle-phase species and adsorption of gas-phase species, which can cause errors in quantitative analysis.

However, the use of a denuder-filter can help to minimize these artefacts and also collect both gas-phase and particle-phase species simultaneously (Possanzini et al. 1983; Ye et al. 1991; Gundel et al. 1995; Temime et al. 2007; Healy et al. 2009).

FTIR spectroscopy was one of the first techniques used for analysis of the chemical content of SOA. It can be used to identify functional groups such as carbonyl, carboxylic acid and nitrate and provides qualitative information on the overall functionality of species present in particles (Odum et al. 1996; Blando et al. 1998; Sax et al. 2005). Advantages include low detection limits and no prior extraction or preparation steps. However this method does not provide any information on individual compounds.

In most cases, the composition of the particle phase is very complex and samples may contain hundreds or even thousands of different organic compounds (Hamilton et al. 2004). As a result, analytical techniques such as GC-MS and liquid chromatography – mass spectrometry (LC-MS), which involve the separation and identification of individual components, prove to be the most effective. However, the high polarity and often small amounts of oxygenated compounds present in SOA can cause difficulties for GC-MS analysis and derivatization methods are often employed to improve chromatographic efficiency and enhance detectability. For example, the derivatization agents *O*-(2,3,4,5,6-pentafluorobenzyl)- hydroxylamine (PFBHA) and bis(trimethylsilyl)-trifluoroacetamide (BSTFA), which convert carbonyls and hydroxyl-containing compounds into their more easily analysed oximes and trimethylsilyl derivatives respectively, have been widely used to prepare SOA extracts for GC-MS analysis (Pratt et al. 2012a). Despite this, the use of GC-MS for the detection of very highly functionalized oxygenated compounds and oligomers remains problematic, and LC-MS, which does not require prior derivatization of the products, is more suited for analysis of these types of species (Hallquist et al. 2009).

The principal advantage of the off-line analytical methods is that they provide detailed information on SOA composition at the molecular level. However, in order to achieve sufficient sensitivity, sampling times can be long (often hours) and it is usually not possible to monitor the chemical evolution of aerosol with high time resolution. Real-time measurements of the chemical composition of aerosols can only be afforded by on-line aerosol mass spectrometers (Pratt et al. 2012b). Two instruments are

commercially available - the Aerodyne aerosol mass spectrometer (AMS) and the TSI aerosol time-of-flight mass spectrometer (ATOFMS). The AMS provides bulk mass concentrations of non-refractory species, including organics, within submicron particles as a function of particle diameter. The ATOFMS can provide information on the mixing state of organic species in single particles containing both refractory and non-refractory components (Pratt et al. 2012b). These instruments work on different principles and can often provide complementary information on particle composition. The recent use of positive matrix factorization (PMF) and high-resolution time-of-flight mass analyzers has also allowed a more in-depth investigation into the sources and composition of organic aerosol. However, molecular information is often not provided by these on-line techniques and they are probably best used in combination with traditional off-line analytical methods (Pratt et al. 2012a).

1.2.3 Simulation Chamber Studies

Atmospheric simulation chambers are widely used to study the formation of SOA (Hallquist et al. 2009). Simulation chambers vary in size, shape and volume, but are typically made of transparent Fluorinated Ethylene Propylene (FEP) Teflon foil. They are generally equipped with a clean air supply, instruments to monitor the concentration of trace species, temperature, pressure, humidity in the chamber and associated devices such as mixing fans. Outdoor chambers have the advantage of using natural sunlight conditions whereas indoor chambers are equipped with ultraviolet and visible lamps to mimic sunlight.

Experiments carried out in simulation chambers usually involve the atmospheric oxidation of SOA precursors initiated by OH, NO_3, O_3 or light. A range of physical and chemical properties of SOA can be measured, including the aerodynamic diameter distribution, volatility, chemical composition and temporal trends of particular marker species during SOA aging processes. The yield of aerosol may also be determined under different reaction conditions. However, simulation chamber experiments are typically performed using much higher concentrations of the precursor and oxidant than those found in ambient air. This, combined with the fact that pre-existing particles can also affect SOA formation, means that extrapolation of the SOA yields determined from chamber experiments to real atmospheric conditions,

is problematic. Nevertheless, simulation chamber studies currently provide the best means of investigating SOA yields, composition and formation mechanisms.

1.3 Polycyclic Aromatic Hydrocarbons (PAHs) in the Atmosphere

Polycyclic aromatic hydrocarbons (PAHs), also known as poly aromatic hydrocarbons or poly-nuclear aromatic hydrocarbons are chemical compounds that consist of fused aromatic rings and do not contain heteroatoms or substituents. PAHs exist in oil, coal, and tar deposits, and are produced as by-products of fuel burning. PAHs are lipophilic, and as a result are also found in foods such as cereals, oils and fats (Larsson et al. 1983). PAHs are mainly emitted to the environment as emissions from combustion sources such as automobiles, forest fires, and solid fuel burning.

In the atmosphere, PAHs containing two and three rings are found predominantly in the gas-phase, whilst those containing six or more rings principally adsorb to particles (Finlayson-Pitts et al. 2000). PAHs with four or five rings are found in both phases (Calvert et al. 2002). The chemical structures of some of the most important PAHs detected in the gas-phase at urban locations around the world are shown in **Figure 1.5** .

As pollutants, PAHs are of concern because many of them have been identified as carcinogenic, mutagenic, and teratogenic (Albinet et al. 2007). Epidemiological studies have established that exposure to air pollution containing PAHs is associated with damaging effects on the respiratory and cardiovascular systems, and can lead to asthma, oxidative stress, health deterioration and even death (Dockery et al. 1993). The toxicity of PAHs is very structurally dependent, with isomers (PAHs with the same formula and number of rings) varying from being nontoxic to extremely toxic. One PAH compound, benzo[a]pyrene, is notable for being the first chemical carcinogen to be discovered, and is also one of many carcinogens found in cigarette smoke (Hecht 1999).

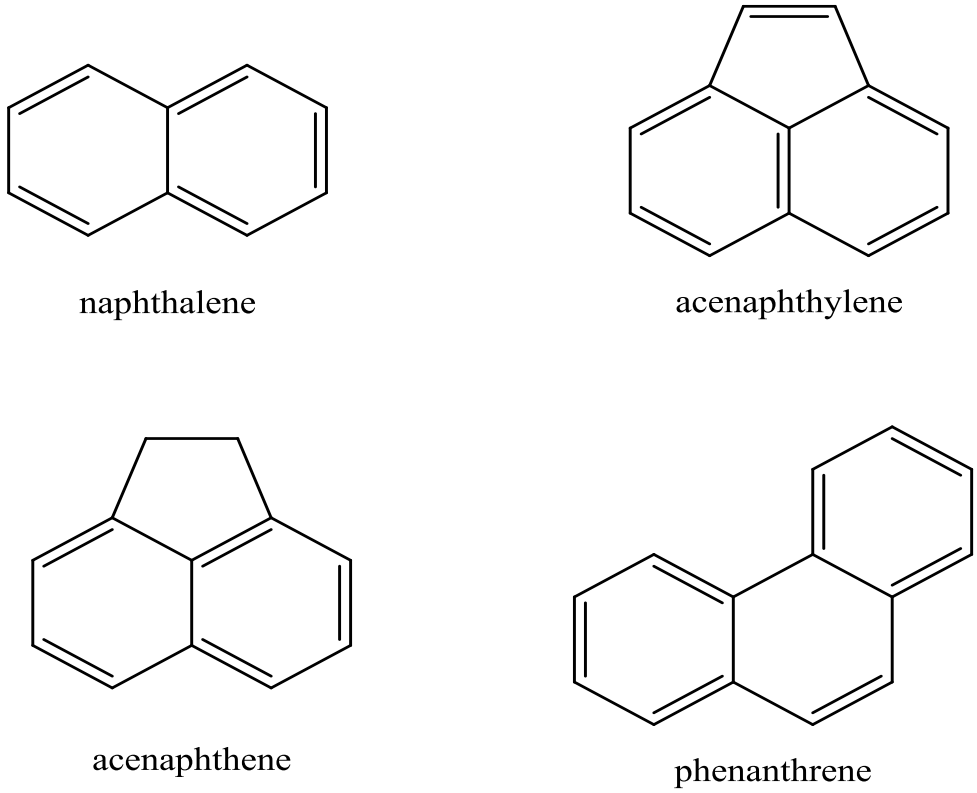


Figure 1.5 Chemical structures of some of the most abundant PAHs detected in ambient urban air (Finlayson-Pitts et al. 2000).

The environmental fate and impact of PAHs and their oxidation products has been the subject of several reviews (Bolton et al. 2000; Calvert et al. 2002; Srogi 2007).

The degradation of gaseous PAHs in the atmosphere is mainly initiated via reaction with the hydroxyl radical (OH), although, reaction with ozone and nitrate radicals may also be possible for certain species (Calvert et al. 2002). Research published in the peer-reviewed literature has largely focused on the kinetics of the atmospheric oxidation of naphthalene, acenaphthalene, acenaphthylene and phenanthrene. Product studies indicate that a range of ring retaining compounds, such as hydroxylated and nitrated PAHs, are formed as oxidation products (Calvert et al. 2002; Atkinson et al. 2007). The formation of SOA from the photooxidation of naphthalene, alkylnaphthalenes, acenaphthylene and acenaphthene has also recently been investigated (Chan et al. 2009; Shakya et al. 2010) and the results indicate that these light PAHs are potentially important precursors of SOA in urban atmospheres.

1.4 Atmospheric Degradation of Naphthalene

Naphthalene is the simplest PAH consisting of two fused benzene rings and has been detected in ambient air at urban locations around the world. Naphthalene is classified by the International Agency for Research on Cancer as a possible human carcinogen (Jia et al. 2010) and by the Californian EPA as a human carcinogen. Incomplete combustion processes are the main anthropogenic source of naphthalene, with over 40% of the naphthalene emissions into the atmosphere in Southern California being attributed to gasoline engine exhaust and evaporation (Lu et al. 2005). In the gas-phase, naphthalene can be chemically transformed in the lower troposphere via reaction with hydroxyl (OH) and nitrate (NO_3) radicals (Calvert et al. 2002). These reactions lead to the formation of a range of oxidation products including naphthols, nitronaphthalenes and ring-opening carbonyls (Atkinson et al. 1987; Lane et al. 1996; Bunce et al. 1997; Atkinson et al. 2007), in addition to other pollutants such as ozone and secondary organic aerosol (SOA) (Chan et al. 2009; Shakya et al. 2010).

Kinetic studies of the reaction of naphthalene with OH and NO_3 have been studied by Atkinson and others (Atkinson et al. 1984; Biermann et al. 1985; Atkinson et al. 1994; Kwok et al. 1994; Lane et al. 1994; Phousongphouang et al. 2002). The reported rate coefficients indicate that reaction with NO_3 and O_3 are of negligible importance under typical atmospheric conditions and that the major fate of naphthalene is reaction with OH during daylight hours. The recommended value of k(OH + naphthalene) at 298 K is 2.30×10^{-11} cm^3 $molecule^{-1}$ s^{-1} (Calvert et al. 2002), which yields a lifetime of around 12 hours for an average OH concentration of 1×10^6 molecule cm^{-3} (Seinfeld et al. 2006).

The gas-phase products arising from the photooxidation of naphthalene have been reported in the literature (Atkinson et al. 1994; Lane et al. 1996; Bunce et al. 1997; Sasaki et al. 1997; Mihele et al. 2002; Lee et al. 2009). The products include 2-formylcinnamaldehyde, phthaldialdehyde, glyoxal, naphthols, and nitronaphthalenes, **Figure 1.6**. These products indicate that the photooxidation mechanism is similar to that observed for monoaromatics (Calvert et al. 2002) and proceeds via OH addition to the aromatic ring followed by addition of oxygen and further reaction.

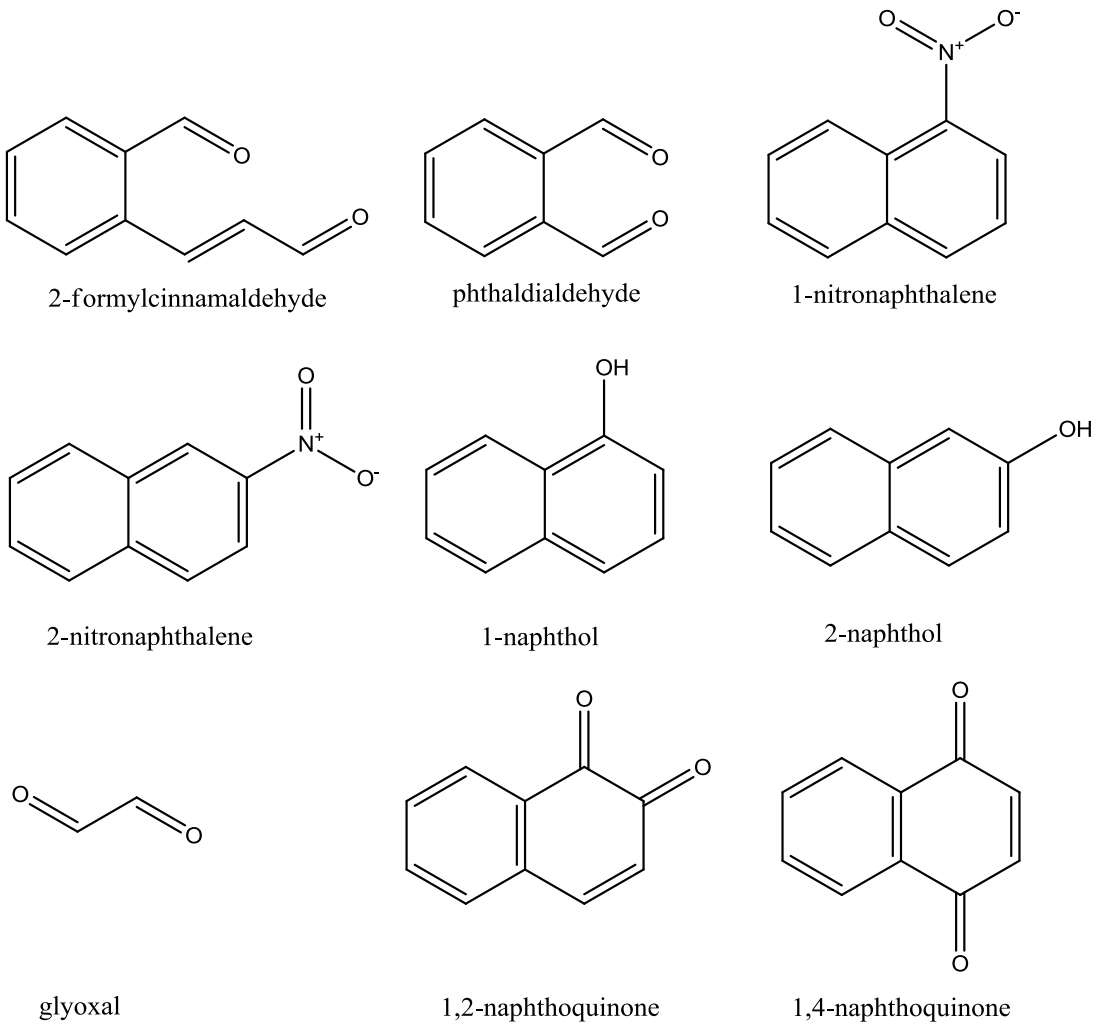


Figure 1.6 Major products of the atmospheric photooxidation of naphthalene.

1.5 Aim and Outline of this Study

The photooxidation of naphthalene produces a range of oxidation products, some of which are toxic, and can form secondary organic aerosol. The overall aim of this work was to perform a series of simulation chamber experiments on the photooxidation of naphthalene and selected oxidation products in order to improve the current understanding of the environmental impact of this important PAH.

In chapter 2, the SOA formation yield from photooxidation of naphthalene has been measured under a range of different reaction conditions. The results are compared to other recent studies on naphthalene and monoaromatic hydrocarbons. The chemical composition of the gas and particle phase photooxidation products has been investigated using on-line and off-line technology in Chapter 3. A denuder-filter system coupled with GC-MS was used to measure the gas/particle phase partitioning during the photooxidation, while ATOFMS was used to provide information of the composition and evolution of SOA in the simulation chamber.

The photolysis of two naphthalene photooxidation products, phthaldialdehyde and 1-nitronaphthalene, has been investigated in Chapters 4 and 5. Experiments were performed in both outdoor and indoor simulation chambers to determine the photolysis rate, gas-phase products, aerosol formation yields and the composition of SOA using on-line and off-line analytical techniques.

Chapter 6 includes a summary of the results, conclusions and suggestions for future studies in the area.

1.5 References

Albinet, A., E. Leoz-Garziandia, H. Budzinski and E. ViIlenave (2007). "Polycyclic aromatic hydrocarbons (PAHs), nitrated PAHs and oxygenated PAHs in ambient air of the Marseilles area (South of France): Concentrations and sources." Science of the Total Environment **384**(1-3): 280-292.

Atkinson, R. (1986). "Kinetics and mechanisms of the gas-phase reactions of the hydroxyl radical with organic compounds under atmospheric conditions." Chemical Reviews **86**(1): 69-201.

Atkinson, R. (1989). "Kinetics and Mechanisms of the Gas-Phase Reactions of the Hydroxyl Radical with Organic Compounds." Journal of Physical and Chemical Reference Data **Monograph 1**: 1-246.

Atkinson, R. (2000). "Atmospheric chemistry of VOCs and NO_x." Atmospheric Environment **34**(12-14): 2063-2101.

Atkinson, R. (2007). "Gas-phase tropospheric chemistry of organic compounds: a review." Atmospheric Environment **41, Supplement**(0): 200-240.

Atkinson, R. and J. Arey (2003). "Atmospheric Degradation of Volatile Organic Compounds." Chemical Reviews **103**(12): 4605-4638.

Atkinson, R. and J. Arey (2003). "Gas-phase tropospheric chemistry of biogenic volatile organic compounds: a review." Atmospheric Environment **37, Supplement 2**(0): 197-219.

Atkinson, R. and J. Arey (2007). "Mechanisms of the gas-phase reactions of aromatic hydrocarbons and PAHs with OH and NO_3 radicals." Polycyclic Aromatic Compounds **27**(1): 15-40.

Atkinson, R., J. Arey, B. Zielinska and S. M. Aschmann (1987). "Kinetics and Products of the Gas-Phase Reactions of OH Radicals and N_2O_5 with Naphthalene and Biphenyl." Environmental Science & Technology **21**(10): 1014-1022.

Atkinson, R. and S. M. Aschmann (1993). "Hydroxyl radical production from the gas-phase reactions of ozone with a series of alkenes under atmospheric conditions." Environmental Science & Technology **27**(7): 1357-1363.

Atkinson, R., S. M. Aschmann and J. N. Pitts (1984). "Kinetics of the Reactions of Naphthalene and Biphenyl with OH Radicals and with O_3 at 294±1 K." Environmental Science & Technology **18**(2): 110-113.

Atkinson, R., D. Baulch, R. Cox, R. Hampson Jr, J. Kerr and J. Troe (1992). "Evaluated kinetic and photochemical data for atmospheric chemistry: Supplement IV. IUPAC subcommittee on gas kinetic data evaluation for atmospheric chemistry." Journal of Physical and Chemical Reference Data **21**: 1125.

Atkinson, R., E. C. Tuazon, I. Bridier and J. Arey (1994). "Reactions of NO_3-Naphthalene Adducts with O_2 and NO_2." International Journal of Chemical Kinetics **26**(6): 605-614.

Bahreini, R., M. D. Keywood, N. L. Ng, V. Varutbangkul, S. Gao, R. C. Flagan, J. H. Seinfeld, D. R. Worsnop and J. L. Jimenez (2005). "Measurements of Secondary Organic Aerosol from Oxidation of Cycloalkenes, Terpenes, and m-Xylene Using an Aerodyne Aerosol Mass Spectrometer." Environmental Science & Technology **39**(15): 5674-5688.

Biermann, H. W., H. Mac Leod, R. Atkinson, A. M. Winer and J. N. Pitts (1985). "Kinetics of the gas-phase reactions of the hydroxyl radical with naphthalene, phenanthrene, and anthracene." Environmental Science & Technology **19**(3): 244-248.

Blando, J. D., R. J. Porcja, T.-H. Li, D. Bowman, P. J. Lioy and B. J. Turpin (1998). "Secondary Formation and the Smoky Mountain Organic Aerosol: An Examination of Aerosol Polarity and Functional Group Composition During SEAVS." Environmental Science & Technology **32**(5): 604-613.

Bolton, J. L. T., Michael A., T. M. Penning, G. Dryhurst and T. J. Monks (2000). "Role of Quinones in Toxicology." Chemical Research in Toxicology **13**(3): 135-160.

Brauers, T., M. Hausmann, U. Brandenburger and H.-P. Dorn (1995). "Improvement of differential optical absorption spectroscopy with a multichannel scanning technique." Applied Optics **34**(21): 4472-4479.

Bunce, N. J., L. Liu, J. Zhu and D. A. Lane (1997). "Reaction of Naphthalene and Its Derivatives with Hydroxyl Radicals in the Gas Phase." Environmental Science & Technology **31**(8): 2252-2259.

Calvert, J. G., R. Atkinson, K. H. Becker, R. M. Kamens, J. H. Seinfeld, T. J. Wallington and G. Yarwood (2002). The Mechanisms of Atmospheric Oxidation of Aromatic Hydrocarbons. Oxford, Oxford University Press.

Chan, A. W. H., K. E. Kautzman, P. S. Chhabra, J. D. Surratt, M. N. Chan, J. D. Crounse, A. Karten, P. O. Wennberg, R. C. Flagan and J. H. Seinfeld (2009). "Secondary Organic Aerosol Formation from Photooxidation of Naphthalene and Alkylnaphthalenes: Implications for Oxidation of Intermediate Volatility Organic Compounds (IVOCs)." Atmospheric Chemistry and Physics **9**(9): 3049-3060.

de Gouw, J. A., A. M. Middlebrook, C. Warneke, R. Ahmadov, E. L. Atlas, R. Bahreini, D. R. Blake, C. A. Brock, J. Brioude, D. W. Fahey, F. C. Fehsenfeld, J. S. Holloway, M. Le Henaff, R. A. Lueb, S. A. McKeen, J. F. Meagher, D. M. Murphy, C. Paris, D. D. Parrish, A. E. Perring, I. B. Pollack, A. R. Ravishankara, A. L. Robinson, T. B. Ryerson, J. P. Schwarz, J. R. Spackman, A. Srinivasan and L. A. Watts (2011). "Organic Aerosol Formation Downwind from the Deepwater Horizon Oil Spill." Science **331**(6022): 1295-1299.

Dockery, D. W., C. A. Pope, X. Xu, J. D. Spengler, J. H. Ware, M. E. Fay, B. G. Ferris and F. E. Speizer (1993). "An Association between Air Pollution and Mortality in Six U.S. Cities." New England Journal of Medicine **329**(24): 1753-1759.

Donahue, N. M., J. H. Kroll, J. G. Anderson and K. L. Demerjian (1998). "Direct observation of OH production from the ozonolysis of olefins." Geophysics Research Letters **25**(1): 59-62.

Finlayson-Pitts, B. J. and J. N. Pitts (2000). Chemistry of the upper and lower atmosphere: Theory, experiments, and applications, Academic Press.

Forstner, H. J. L., R. C. Flagan and J. H. Seinfeld (1997). "Secondary Organic Aerosol from the Photooxidation of Aromatic Hydrocarbons: Molecular Composition." Environmental Science & Technology **31**(5): 1345-1358.

Gómez-González, Y., J. D. Surratt, F. Cuyckens, R. Szmigielski, R. Vermeylen, M. Jaoui, M. Lewandowski, J. H. Offenberg, T. E. Kleindienst, E. O. Edney, F. Blockhuys, C. Van Alsenoy, W. Maenhaut and M. Claeys (2008). "Characterization of Organosulfates from the Photooxidation of Isoprene and Unsaturated Fatty Acids in Ambient Aerosol Using Liquid Chromatography/electrospray Ionization Mass Spectrometry." Journal of Mass Spectrometry **43**(3): 371-382.

Gundel, L. A., V. C. Lee, K. R. R. Mahanama, R. K. Stevens and J. M. Daisey (1995). "Direct determination of the phase distributions of semi-volatile polycyclic

aromatic hydrocarbons using annular denuders." Atmospheric Environment **29**(14): 1719-1733.

Hallquist, M., J. C. Wenger, U. Baltensperger, Y. Rudich, D. Simpson, M. Claeys, J. Dommen, N. M. Donahue, C. George, A. H. Goldstein, J. F. Hamilton, H. Herrmann, T. Hoffmann, Y. Iinuma, M. Jang, M. E. Jenkin, J. L. Jimenez, A. Kiendler-Scharr, W. Maenhaut, G. McFiggans, T. F. Mentel, A. Monod, A. S. H. Pravit, J. H. Seinfeld, J. D. Surratt, R. Szmigielski and J. Wildt (2009). "The formation, properties and impact of secondary organic aerosol: current and emerging issues." Atmospheric Chemistry and Physics **9**(14): 5155-5236.

Hamilton, J. F., P. J. Webb, A. C. Lewis, J. R. Hopkins, S. Smith and P. Davy (2004). "Partially oxidised organic components in urban aerosol using GCxGC-TOF/MS." Atmospheric Chemistry and Physics **4**(5): 1279-1290.

Healy, R. M., B. Temime, K. Kuprovskyte and J. C. Wenger (2009). "Effect of Relative Humidity on Gas/Particle Partitioning and Aerosol Mass Yield in the Photooxidation of *p*-Xylene." Environmental Science & Technology **43**(6): 1884-1889.

Hecht, S. S. (1999). "Tobacco Smoke Carcinogens and Lung Cancer." Journal of the National Cancer Institute **91**(14): 1194-1210.

Iinuma, Y., O. Böge, T. Gnauk and H. Herrmann (2004). "Aerosol-chamber study of the α-pinene/O_3 reaction: influence of particle acidity on aerosol yields and products." Atmospheric Environment **38**(5): 761-773.

ISO (1992). Solar energy -- Reference solar spectral irradiance at the ground at different receiving conditions. 9845-1.

Jacob, D. (2000). "Heterogeneous chemistry and tropospheric ozone." Atmospheric Environment **34**(12-14): 2131-2159.

Jang, M., N. M. Czoschke, S. Lee and R. M. Kamens (2002). "Heterogeneous Atmospheric Aerosol Production by Acid-Catalyzed Particle-Phase Reactions." Science **298**(5594): 814-817.

Jia, C. and S. Batterman (2010). "A critical review of naphthalene sources and exposures relevant to indoor and outdoor air." International journal of environmental research and public health **7**(7): 2903-2939.

Johnson, D. and G. Marston (2008). "The gas-phase ozonolysis of unsaturated volatile organic compounds in the troposphere." Chemical Society Reviews **37**(4): 699-716.

Kirchstetter, T. W., B. C. Singer, R. A. Harley, G. R. Kendall and M. Traverse (1998). "Impact of California Reformulated Gasoline on Motor Vehicle Emissions. 1. Mass Emission Rates." Environmental Science & Technology **33**(2): 318-328.

Kleffmann, J. (2007). "Daytime sources of nitrous acid (HONO) in the atmospheric boundary layer." Chemphyschem **8**(8): 1137-1144.

Kroll, J. H., N. L. Ng, S. M. Murphy, R. C. Flagan and J. H. Seinfeld (2006). "Secondary Organic Aerosol Formation from Isoprene Photooxidation." Environmental Science & Technology **40**(6): 1869-1877.

Kroll, J. H. and J. H. Seinfeld (2005). "Representation of Secondary Organic Aerosol Laboratory Chamber Data for the Interpretation of Mechanisms of Particle Growth." Environmental Science & Technology **39**(11): 4159-4165.

Kwok, E. S. C., R. Atkinson and J. Arey (1994). "Kinetics and Mechanisms of the Gas-Phase Reactions of the NO_3 Radical with Aromatic-Compounds." International Journal of Chemical Kinetics **26**(5): 511-525.

Lane, D. A., S. S. Fielder, S. J. Townsend, N. J. Bunce, J. Zhu, L. Liu, B. Wiens and P. Pond (1996). "Atmospheric Photochemistry of Naphthalene: a Practical and Theoretical Approach." Polycyclic Aromatic Compounds **9**(1): 53 - 59.

Lane, D. A. and H. Tang (1994). "Photochemical Degradation of Polycyclic Aromatic Compounds. I. Naphthalene." Polycyclic Aromatic Compounds **5**(1): 131 - 138.

Larsson, B. K., G. P. Sahlberg, A. T. Eriksson and L. A. Busk (1983). "Polycyclic aromatic hydrocarbons in grilled food." Journal of Agricultural and Food Chemistry **31**(4): 867-873.

Lee, J. Y. and D. A. Lane (2009). "Unique products from the reaction of naphthalene with the hydroxyl radical." Atmospheric Environment **43**(32): 4886-4893.

Loeffler, K. W., C. A. Koehler, N. M. Paul and D. O. De Haan (2006). "Oligomer Formation in Evaporating Aqueous Glyoxal and Methyl Glyoxal Solutions." Environmental Science & Technology **40**(20): 6318-6323.

Lu, R., J. Wu, R. P. Turco, A. M. Winer, R. Atkinson, J. Arey, S. E. Paulson, F. W. Lurmann, A. H. Miguel and A. Eiguren-Fernandez (2005). "Naphthalene distributions and human exposure in a Southern California." Atmospheric Environment **39**(3): 489-507.

Mihele, C. M., H. A. Wiebe and D. A. Lane (2002). "Particle Formation and Gas/Particle Partition Measurements of the Products of the Naphthalene-OH

Radical Reaction in a Smog Chamber." Polycyclic Aromatic Compounds **22**(3-4): 729-736.

Ng, N. L., P. S. Chhabra, A. W. H. Chan, J. D. Surratt, J. H. Kroll, A. J. Kwan, D. C. McCabe, P. O. Wennberg, A. Sorooshian, S. M. Murphy, N. F. Dalleska, R. C. Flagan and J. H. Seinfeld (2007b). "Effect of NO_x level on secondary organic aerosol (SOA) formation from the photooxidation of terpenes." Atmospheric Chemistry and Physics **7**(19): 5159-5174.

Ng, N. L., J. H. Kroll, A. W. H. Chan, P. S. Chhabra, R. C. Flagan and J. H. Seinfeld (2007a). "Secondary organic aerosol formation from m-xylene, toluene, and benzene." Atmospheric Chemistry and Physics **7**(14): 3909-3922.

Odum, J. R., T. Hoffmann, F. Bowman, D. Collins, R. C. Flagan and J. H. Seinfeld (1996). "Gas/particle partitioning and secondary organic aerosol yields." Environmental Science & Technology **30**(8): 2580-2585.

Pankow, J. F. (1994a). "An absorption model of gas/particle partitioning of organic compounds in the atmosphere." Atmospheric Environment **28**(2): 185-188.

Pankow, J. F. (1994b). "An absorption model of the gas/aerosol partitioning involved in the formation of secondary organic aerosol." Atmospheric Environment **28**(2): 189-193.

Phousongphouang, P. T. and J. Arey (2002). "Rate Constants for the Gas-Phase Reactions of a Series of Alkylnaphthalenes with the Nitrate Radical." Environmental Science & Technology **37**(2): 308-313.

Platt, U. F., A. M. Winer, H. W. Biermann, R. Atkinson and J. N. Pitts (1984). "Measurement of nitrate radical concentrations in continental air." Environmental Science & Technology **18**(5): 365-369.

Possanzini, M., A. Febo and A. Liberti (1983). "New design of a high-performance denuder for the sampling of atmospheric pollutants." Atmospheric Environment (1967) **17**(12): 2605-2610.

Pratt, K. A. and K. A. Prather (2012a). "Mass spectrometry of atmospheric aerosols—Recent developments and applications. Part I: Off-line mass spectrometry techniques." Mass Spectrometry Reviews **31**(1): 1-16.

Pratt, K. A. and K. A. Prather (2012b). "Mass spectrometry of atmospheric aerosols—Recent developments and applications. Part II: On-line mass spectrometry techniques." Mass Spectrometry Reviews **31**(1): 17-48.

Robinson, A. L., N. M. Donahue, M. K. Shrivastava, E. A. Weitkamp, A. M. Sage, A. P. Grieshop, T. E. Lane, J. R. Pierce and S. N. Pandis (2007). "Rethinking Organic Aerosols: Semivolatile Emissions and Photochemical Aging." Science **315**(5816): 1259-1262.

Sareen, N., A. N. Schwier, E. L. Shapiro, D. Mitroo and V. F. McNeill (2010). "Secondary organic material formed by methylglyoxal in aqueous aerosol mimics." Atmospheric Chemistry and Physics **10**(3): 997-1016.

Sasaki, J. C., J. Arey, D. A. Eastmond, K. K. Parks and A. J. Grosovsky (1997). "Genotoxicity induced in human lymphoblasts by atmospheric reaction products of naphthalene and phenanthrene." Mutation Research/Genetic Toxicology and Environmental Mutagenesis **393**: 23-35.

Sawyer, R. F., R. A. Harley, S. H. Cadle, J. M. Norbeck, R. Slott and H. A. Bravo (2000). "Mobile sources critical review: 1998 NARSTO assessment." Atmospheric Environment **34**(12-14): 2161-2181.

Sax, M., R. Zenobi, U. Baltensperger and M. Kalberer (2005). "Time Resolved Infrared Spectroscopic Analysis of Aerosol Formed by Photo-Oxidation of 1,3,5-Trimethylbenzene and α-Pinene." Aerosol Science and Technology **39**(9): 822-830.

Seinfeld, J. H. and S. N. Pandis (2006). Atmospheric chemistry and physics: from air pollution to climate change, Wiley.

Shakya, K. M. and R. J. Griffin (2010). "Secondary Organic Aerosol from Photooxidation of Polycyclic Aromatic Hydrocarbons." Environmental Science & Technology **44**(21): 8134-8139.

Srogi, K. (2007). "Monitoring of environmental exposure to polycyclic aromatic hydrocarbons: a review." Environmental Chemistry Letters **5**(4): 169-195.

Surratt, J. D., S. M. Murphy, J. H. Kroll, N. L. Ng, L. Hildebrandt, A. Sorooshian, R. Szmigielski, R. Vermeylen, W. Maenhaut, M. Claeys, R. C. Flagan and J. H. Seinfeld (2006). "Chemical Composition of Secondary Organic Aerosol Formed from the Photooxidation of Isoprene." The Journal of Physical Chemistry A **110**(31): 9665-9690.

Temime, B., R. M. Healy and J. C. Wenger (2007). "A Denuder-Filter Sampling Technique for the Detection of Gas and Particle Phase Carbonyl Compounds." Environmental Science & Technology **41**(18): 6514-6520.

Turpin, B. J., P. Saxena and E. Andrews (2000). "Measuring and simulating particulate organics in the atmosphere: problems and prospects." Atmospheric Environment **34**(18): 2983-3013.

Volkamer, R., F. San Martini, L. T. Molina, D. Salcedo, J. L. Jimenez and M. J. Molina (2007). "A missing sink for gas-phase glyoxal in Mexico City: Formation of secondary organic aerosol." Geophysical Research Letters **34**(19): L19807.

Wahner, A., T. F. Mentel and M. Sohn (1998). "Gas phase reaction of N_2O_5 with water vapor: Importance of heterogeneous hydrolysis of N_2O_5 and surface desorption of HNO_3 in a large Teflon chamber." Geophysical Research Letters **25**(12): 2169-2172.

Wangberg, I., I. Barnes and K. H. Becker (1996). "Atmospheric chemistry of bifunctional cycloalkyl nitrates." Chemical Physics Letters **261**(1-2): 138-144.

Wayne, R. P. (2000). Chemistry of Atmospheres. Oxford, Oxford Science Publications.

Wayne, R. P., I. Barnes, P. Biggs, J. P. Burrows, C. E. Canosa-Mas, J. Hjorth, G. Le Bras, G. K. Moortgat, D. Perner, G. Poulet, G. Restelli and H. Sidebottom (1991). "The nitrate radical: Physics, chemistry, and the atmosphere." Atmospheric Environment. Part A. General Topics **25**(1): 1-203.

Wesely, M. L. and B. B. Hicks (2000). "A review of the current status of knowledge on dry deposition." Atmospheric Environment **34**(12): 2261-2282.

Ye, Y., C. Tsai, D. Y. H. Pui and C. W. Lewis (1991). "Particle Transmission Characteristics of an Annular Denuder Ambient Sampling System." Aerosol Science and Technology **14**(1): 102 - 111.

Chapter

2

Secondary Organic Aerosol Formation from Photooxidation of Naphthalene

2.1 Introduction

Laboratory studies of SOA formation from the photooxidation of VOCs have mainly focused on determination of the aerosol yield under a variety of reaction conditions (Kroll et al. 2008). The aerosol yields show a strong dependence on temperature, hydrocarbon to NO_x ratios (Hurley et al. 2001; Johnson et al. 2004; Song et al. 2005; Kroll et al. 2006; Ng et al. 2007a; Ng et al. 2007b) and the OH concentration (Song et al. 2007a; Ng et al. 2007b; Song et al. 2007b; Warren et al. 2008) during the photooxidation process.

2.1.1 Influence of Hydrocarbon/NO_x Ratio on SOA Formation

In typical simulation chamber studies, the NO and NO_2 concentrations keep changing during the experiment and it is difficult to predict their single influence on SOA formation (Ng et al. 2007b). As a result, these species are normally coupled together as NO_x (nitrogen oxides) and even in the early studies of SOA formation, it was shown that the hydrocarbon to NO_x ratio strongly influenced the SOA formation (Odum et al. 1996; Odum et al. 1997a; Odum et al. 1997b). This effect was further confirmed in other chamber studies of SOA formation from photooxidation of aromatic hydrocarbons (Hurley et al. 2001; Johnson et al. 2004; Johnson et al. 2005; Song et al. 2007a; Ng et al. 2007b).

The concentration of NO_x in the photooxidation system can impact on SOA formation in a number of ways. In classical photooxidation experiments, where NO_x is used as the OH radical precursor, SOA formation is generally observed only when the NO concentration is near zero. It was initially suggested that the primary products of the RO_2 + NO reactions are too volatile to undergo condensation and that SOA formation is only possible when RO_2 + HO_2 reactions begin to dominate and generate a range of lower volatility products (Johnson et al. 2004; Johnson et al. 2005) . This, of course, implies that species such as aromatic hydrocarbons would not form SOA in urban areas and an alternative explanation was sought. Ng et al. subsequently showed that SOA formation can be observed in the presence of NO when the oxidation reactions are sufficiently fast, e.g., when HONO is used as the OH radical source (Ng et al. 2007b). The NO_x level may also affect the distribution of products, particularly in the case of aromatic hydrocarbons where the aromatic-OH adduct can react with NO_2

leading to the formation of nitro-aromatic products such as nitrobenzene, nitrotoluenes, and nitronaphthalene (Atkinson et al. 1989; Lane et al. 1996; Bunce et al. 1997; Koch et al. 2007). These species have lower volatility than many other oxidation products and are thus likely to contribute to SOA formation and growth. As a result of these effects, it is quite common to investigate the effect of NO_x concentration when determining SOA yields.

2.1.2 Influence of Relative Humidity on SOA Formation

Many atmospheric oxidation products are water-soluble and relative humidity is therefore a possible factor in influencing SOA formation and growth (Pöschl 2005). Water can participate in both gas phase and particle phase reactions, and model studies indicate that water vapour may impact on the equilibrium concentration of SOA mass (Seinfeld et al. 2001). The effect of relative humidity on SOA formation has been investigated in a number of simulation chamber studies (Edney et al. 2000; Tobias et al. 2000; Cocker III et al. 2001; Gao et al. 2004; Yu et al. 2008; Healy et al. 2009).

Water is known to react with NO_2 on the chamber walls to produce HONO and higher OH radical concentrations can thus be produced at higher relative humidity in the chamber (Finlayson-Pitts et al. 2003; Healy et al. 2009). The increase in OH radical concentration may, in turn, increase the oxidation rate to form higher amounts of less-volatile compounds that can transfer to the particle phase, thereby contributing to SOA formation (Ng et al. 2007b). In the particle phase, H_2O could also be part of condensed phase chemical processes, such as oligomerization, hydrolysis (Finlayson-Pitts et al. 2003) and organosulfate formation (Surratt et al. 2006; Gómez-González et al. 2008; Kautzman et al. 2010). Clearly, it is also important to investigate the effect of relative humidity on SOA formation.

2.1.3 Previous Studies of SOA Formation from Photooxidation of Naphthalene

Mihele et al. (Mihele et al. 2002) first reported the formation of SOA during the photooxidation of naphthalene a number of years ago, however, no attempt was made to determine the yield. More recently, Chan et al. investigated SOA formation from the gas-phase photooxidation of naphthalene, 1-methylnaphthalene, 2-methylnaphthalene and 1,2-dimethylnaphthalene to evaluate the importance of PAHs

as effective SOA precursors (Chan et al. 2009), with $Al_2(SO_4)_3$ as seed aerosol in high and low-NO_x conditions. Under high-NO_x conditions and aerosol mass loadings between 10 and 40 μg m^{-3}, the SOA yields (mass of SOA per mass of hydrocarbon reacted) ranged from 19-30% for naphthalene, while under low-NO_x conditions, the SOA yields were measured to be 73% for naphthalene. Shakya and Griffin (Shakya et al. 2010) also reported the SOA formation from photooxidation of naphthalene and other light PAHs using H_2O_2 and HONO as OH precursors, in the absence of seed aerosol. The SOA yield from naphthalene was 8-16%, depending on the type of precursor and starting amount of naphthalene (Shakya et al. 2010). Neither of these previous studies involved a systematic investigation of the effects of hydrocarbon to NO_x ratio or relative humidity on SOA yield.

2.1.4 Aim of this Work

The aim of this work was to determine the yield of SOA arising from naphthalene photooxidation under different reaction conditions. A series of simulation chamber experiments has been performed using NO_x and HONO as the OH precursor in the absence of seed aerosol. The effect of relative humidity on SOA yields has been investigated in a systematic manner. The results are compared to previous studies and used to improve our understanding of the potential contribution of naphthalene to SOA formation in urban environments.

2.2 Experimental

2.2.1 Materials

Materials used in this work are listed in the **Table 2.1**. All chemicals were used without further purification.

Table 2.1 Chemicals used in the experiments.

Material	Purity (%)	Manufacturer
Naphthalene	99	Aldrich
Nitric oxide	99	Aldrich
Hydrogen (GC)	99.9999	Air Products
Air (GC)	99.9999	Air Products
Sodium nitrite	>98	Aldrich
Sulfuric acid	30% in water solution	Aldrich

2.2.2 Atmospheric Simulation Chamber

Experiments were performed in a 6.5 m^3 simulation chamber (Temime et al. 2007) (**Figure 2.1**) at atmospheric pressure (1 atm) in the absence of seed aerosol. The chamber is a cuboid made of FEP Teflon foil and is surrounded by 12 Philips TL05 (40 W) lamps (λ_{max}=360 nm) and 12 Philips TL12 (40 W) lamps (λ_{max}=310 nm). The chamber and lamps are supported by a frame constructed of aluminium panels (60 mm thickness, Bosch) and covered with aluminium sheets. There are several ports for the introduction and sampling of gases and particles.



Figure 2.1 6.5 m^3 atmospheric simulation chamber in the Environmental Research Institute (ERI), University College Cork.

The chamber is operated at atmospheric pressure using purified air for the zero air

generator (Zander KMA 75). The temperature and relative humidity (RH) in the chamber are measured using a dewpoint meter (Vaisala DM70). Experiments are typically performed at 295 ± 2 K and at a relative humidity of 0.1-0.4% (dewpoint temperature of 223 ± 5 K), however, RH can be varied by adding water to the chamber. Between experiments the chamber is cleaned by flushing with purified air at a flow rate of 0.15 m^3 min^{-1} for at least 6 hours and preferably overnight.

A gas chromatograph (Varian CP3800) equipped with a flame ionization detector (GC-FID) is used to measure the concentration of organic compounds in the chamber. The GC-FID system is connected to the chamber through a 6 port gas sampling valve (Valco). The valve is fitted with a 1 cm^3 sampling loop and is equipped with a pneumatically controlled actuator to enable automated injection of reaction mixtures onto the column. NO and NO_x concentrations are measured with a chemiluminescence NO_x analyser (Thermo model 42*i*). Ozone concentration is measured with a UV photometric O_3 analyser (Thermo model 49*i*). The formation and evolution of particles in the range 10-470 nm is monitored using a scanning mobility particle sizer (SMPS, TSI Model 3034).

2.2.3 Procedure

Naphthalene was introduced to the clean chamber by passing dry purified air over a heated impinger containing a known amount of the compound. In most of the experiments, NO_x was used as the OH radical precursor. A known volume of NO was added to a small glass bulb and flushed directly into the chamber with dry purified air. Three experiments were performed using nitrous acid (HONO) as OH radical precursor. HONO was generated by adding a 1% $NaNO_2$ aqueous solution dropwise into a flask containing 30% sulfuric acid. In order to investigate the effect of water vapour on the SOA formation, the chamber was humidified by flowing purified air through the headspace of an impinger containing heated deionized (Milli-Q, HPLC) water.

After being introduced into the chamber, the reactants were kept in the dark for at least 30 minutes for mixing. The photooxidation of naphthalene was initiated by switching on the TL05 lamps around the chamber. The lamps were turned off when SOA volume concentrations had reached a maximum value, typically after 3-5 hours. The concentration of naphthalene was measured throughout the experiments by GC-

FID. Samples (1 cm^3 each) were injected automatically using the gas sampling valve and then separated using a Chrompack GC Capillary Column CP-Sil-8CB (5% phenyl, 95% dimethylpolysiloxane) column, 30 m in length, with an internal diameter of 0.25 mm and with hydrogen as the carrier gas (5 cm^3 min^{-1}). The column flow was 5.0 cm^3 min^{-1} with a pulse pressure of 10.0 psi. The oven temperature was programmed as follows: 50 ℃ held for 0.5 min, ramped to 110 at a rate of 80 ℃ min^{-1}, ramped to 160 ℃ at 40 ℃ min^{-1} and to 250 ℃ at70 ℃ min^{-1}, held for 0.62 min. The temperature of the injector was held at 250 ℃ for the duration of the 4.21 min run. The concentrations of NO_x and O_3 also were continuously monitored (1 minute time resolution) during the experiments, while the formation and evolution of particles was monitored every 3 minutes using the SMPS. The volume concentration of the particles was converted to mass concentration using a particle density of 1.48 g cm^{-1} (Chan et al. 2009). The wall loss rates of naphthalene and the SOA were determined after the lamps had been switched off. The derived first order rate coefficients were used to correct for the concentration of OH radical.

2.3 Results and Discussion

A series of experiments was performed on the photooxidation of naphthalene in the presence of NO_x. Details of the experimental conditions and associated parameters are summarized in **Table 2.2**. The concentration-time profiles were qualitatively similar in all experiments, with the decay of hydrocarbon accompanied by conversion of NO to NO_2 and the subsequent formation of ozone, as shown in **Figure 2.2**. The formation and evolution of SOA during the reaction is shown in **Figure 2.3**. SOA formation was observed after 24-83 min, depending on experimental conditions. Following nucleation, the particles continued to increase in both size and mass due to condensation and coagulation before reaching a maximum concentration after 180-300 min.

The typical wall loss rate of naphthalene was (1-2) $\times 10^{-6}$ s^{-1}, indicating that wall loss accounted for 4-5% of the overall naphthalene decay. The reproducibility of the experiments was tested by introducing similar initial concentrations of naphthalene and NO_x. The similar SOA yields from RH0_2 and RH0_3 in **Table 2.2** demonstrated that the experiments were reproducible.

Table 2.2 Experimental conditions and results for naphthalene/NO_x reactions.

Expt.	RH(%)	HC_0 [a] (ppbV)	NO_x [b] (ppbV)	HC_0/NO_x	ΔHC [c] ($\mu g/m^3$)	M_0 [d] ($\mu g/m^3$)	Y [e] (%)
RH0_1	0.2	1070	520	1.95	2198	285.5	13.0
RH0_2	0.6	1040	240	4.35	1807	330.1	18.3
RH0_3	0.8	1084	250	4.34	2118	379.6	17.9
RH0_4	0.7	1081	510	2.13	2135	237.3	11.1
RH0_5	0.8	830	690	1.20	1310	136	10.3
RH0_6	0.8	602	145	4.15	1470	248.5	16.9
RH0_7	1.9	508	500	1.02	954	63.4	6.64
RH0_8	1.3	611	202	3.02	1444	230.8	16.0
RH25_1	25.1	585	470	1.24	1022	118.6	11.6
RH25_2	25.3	593	540	1.01	926	103.8	11.2
RH25_3	25.1	532	520	1.02	1055	97.2	9.23
RH25_4	25.5	611	344	1.78	1408	229.4	15.5
RH25_5	25.6	626	517	1.21	1168	155	13.3
RH25_6	25.3	699	556	1.26	1745	271.3	15.5
RH50_1	50.3	629	590	1.07	1276	218.5	17.1
RH50_2	49.2	514	496	1.04	1061	159.4	15.0
RH50_3	50.6	602	370	1.63	1287	206.9	16.1
RH50_4	51.0	705	410	1.72	1651	309.7	18.8

[a] Initial mixing ratio of hydrocarbon (naphthalene). [b] Initial mixing ratio of NO_x. [c] Amount of parent hydrocarbon reacted, corrected for dilution and dark wall loss. [d] SOA mass concentration, determined at the time of measured maximum particle volume concentration, corrected for wall loss, assuming a density of 1.48 g cm^{-3}. [e] SOA yield calculated from $M_0/\Delta HC$.

One particularly interesting feature of the concentration-time profiles is that SOA nucleation started even while the NO concentration was as high as 150-200 ppbV. This is in sharp contrast to the classical photooxidation experiments performed on monocyclic aromatics, where SOA formation and growth is observed only when the NO concentration approaches zero (Cocker III et al. 2001; Song et al. 2007a; Ng et al. 2007b). It was initially proposed that the primary oxidation products of the RO_2 + NO reactions are too volatile to undergo condensation and that SOA formation is only observed at low NO concentrations when RO_2 + HO_2 reactions begin to dominate and

generate a range of lower volatility products such as peroxyhemiacetals and organic hydroperoxides (Johnson et al. 2004; Johnson et al. 2005). However, Ng et al. (Ng et al. 2007b) subsequently showed that products of the RO_2 + NO reactions are in fact condensable, but contribute to aerosol mass only when the oxidation reactions are fast, e.g., when direct injection of HONO is used as the OH radical source. Under classical photooxidation conditions, such as those performed in this work, it was proposed that the primary oxidation products of RO_2 + NO reactions are formed too slowly and competing processes such as further gas-phase reaction or wall deposition are favoured over nucleation and condensation. Although this explanation holds for the monocyclic aromatic hydrocarbons, e.g. toluene, xylene and 1,3,5-trimethylbenzene (Cocker III et al. 2001; Song et al. 2007a; Ng et al. 2007b), the observed formation of SOA at high NO_x levels in this work clearly indicates that the primary products of RO_2 + NO reactions during the photooxidation of naphthalene are able to undergo nucleation and condensation even when the reaction is relatively slow.

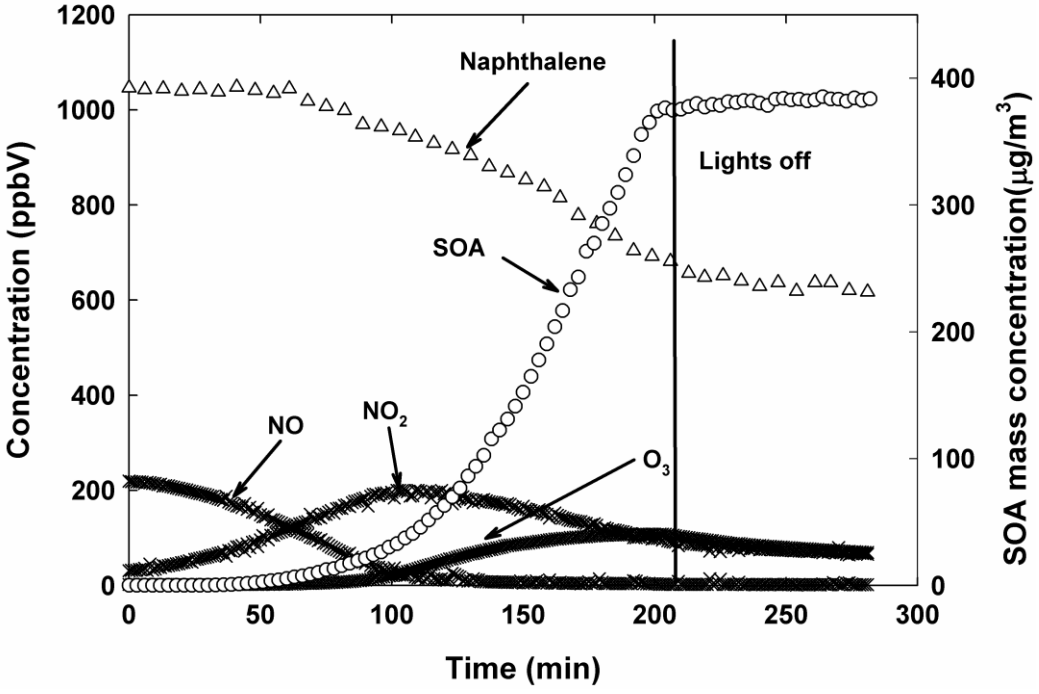


Figure 2.2 Typical concentration-time profiles for the photooxidation of naphthalene (Expt. RH0_3).

Naphthalene oxidation products such as 1- and 2-naphthol, 1- and 2-nitronaphthalene, 2-formyl-cinnamaldehyde, phthaldialdehyde (Bunce et al. 1997; Sasaki et al. 1997; Calvert et al. 2002; Mihele et al. 2002; Kautzman et al. 2010), have higher molecular

weight and higher polarity and thus lower volatility than their monocyclic counterparts and are thus more likely to undergo condensation. As the reaction progresses, these products may also contribute to SOA via further reaction with OH radicals, ozone and NO_3 radicals or photolysis.

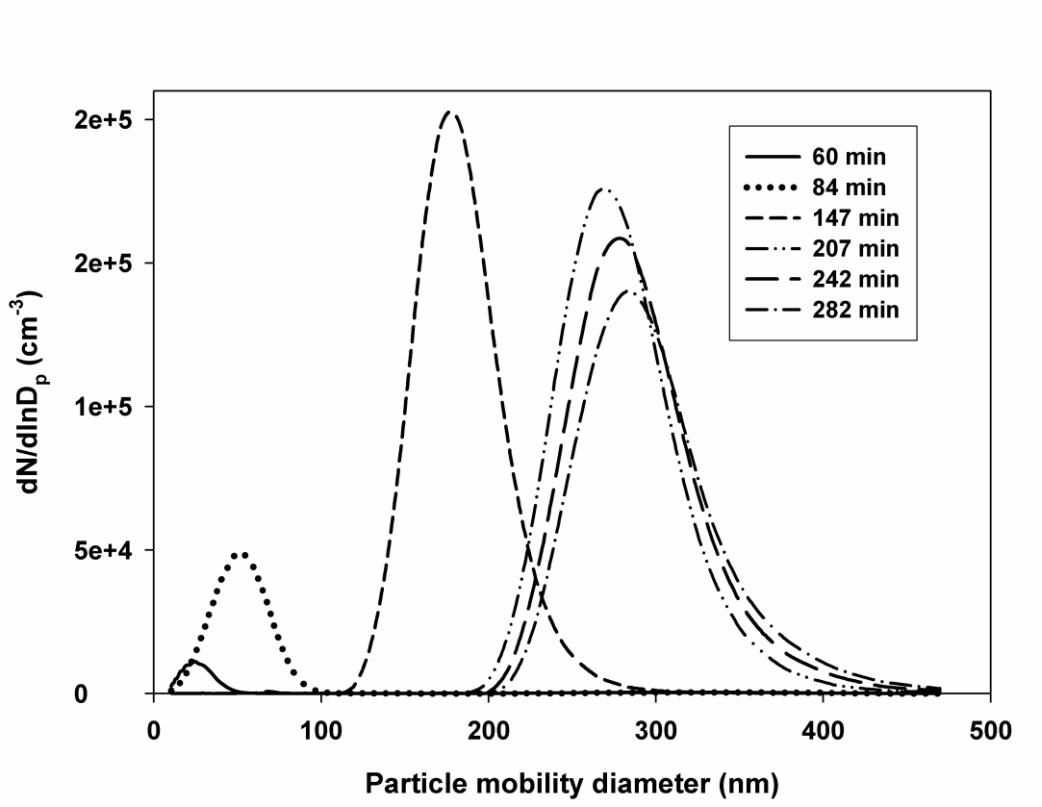


Figure 2.3 Evolution of the SOA distribution with reaction time (min) during the photooxidation of naphthalene (Expt. RH0_3).

2.3.1 Effects of Hydrocarbon to NO_x Ratio on SOA yield

The SOA formation yield, *Y*, is defined as the fraction of the hydrocarbon (ΔHC) which is converted into organic aerosol:

$$Y = \frac{M_0}{\Delta HC} \quad \text{(I)}$$

where M_0 is the total organic aerosol mass concentration. The yield of SOA produced in each experiment was determined from the values of reacted naphthalene (ΔHC) and M_0 at the point where the maximum particle concentration was observed. Both ΔHC and M_0 were corrected for wall losses and dilution by applying first order loss rates obtained from measuring the dark decay of naphthalene and particles at the end of each experiment. M_0 was calculated from the volume concentration of SOA by

assuming a density of 1.48 g cm^{-3} (Chan et al. 2009). The calculated yields are listed in **Table 2.2** and show a range of values which depend on the initial concentrations of naphthalene and NO_x, as well as RH.

The effect of the hydrocarbon to NO_x ratio (HC_0/NO_x) can be seen by comparing the results from the experiments performed under dry (RH<2%) conditions, RH0_1 to RH0_8. As indicated in **Table 2.2 and Figure 2.4**, higher SOA mass yields were obtained when HC_0/NO_x was higher. This effect has also been observed for monocyclic aromatic hydrocarbons (Cocker III et al. 2001; Song et al. 2007a; Ng et al. 2007b) and has generally been attributed to differences in peroxy radical chemistry under high and low NO_x conditions, as outlined above. The same explanation can be applied here because although SOA formation always occurred in the presence of NO_x, most of it is formed after NO is depleted (**Figure 2.2**), when $RO_2 + RO_2$ and $RO_2 + HO_2$ reactions dominate.

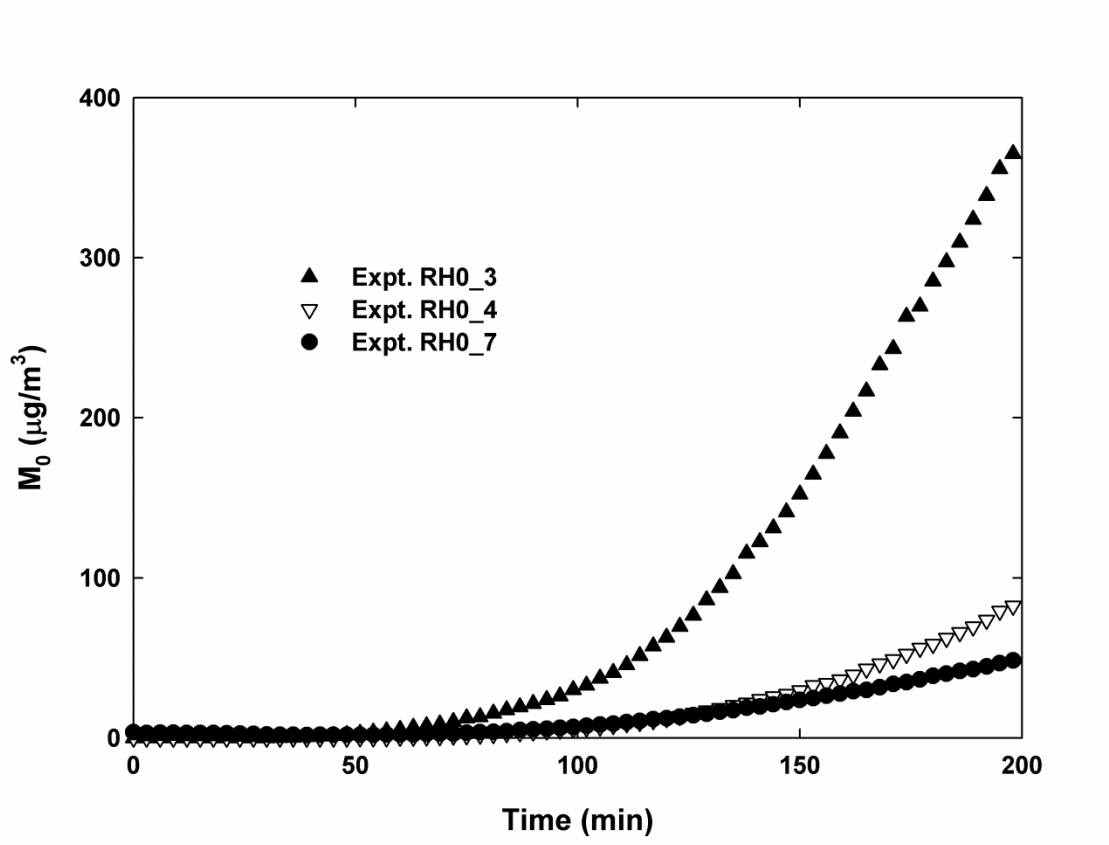


Figure 2.4 SOA mass concentration-time profiles to illustrate the effect of hydrocarbon to NO_x ratio on SOA yield.

Expt.RH0_3 means the 3rd of experiment in dry conditions.

The SOA yield (Y) obtained for each experiment is plotted against M_0 in **Figure 2.5**. The data points fall into four categories according to the different initial reaction conditions. For each category a yield curve was produced by fitting the data points to the gas-particle partitioning model proposed by Odum (Odum et al. 1997a; Odum et al. 1997b):

$$Y = M_0 \sum_{i=1}^{n} \left(\frac{\alpha_i K_i}{1 + M_0 K_i} \right) \qquad \text{(II)}$$

where α_i is the mass-based stoichiometric yield of the oxidation product *i*, K_i (in m^3 μg^{-1}) is the partitioning coefficient and n is the number of product species. Best-fit yield curves were generated using one-product models. Previous studies performed on aromatic compounds under similar conditions have generally found that a two-product model provides the best fit to the experimental data (Odum et al. 1997b; Song et al. 2007a) , indicating that two types of products with different volatility are responsible for SOA formation. However, Henry et al. (Henry et al. 2008) recently showed that SOA yields from the photooxidation of cresols are best described by a one-product model. The cresols, like naphthalene, mainly generate ring-retaining oxidation products with lower volatility than those produced by the alkylbenzenes (Calvert et al. 2002) and it is thus not surprising to find that products with higher volatility do not appear to be involved in SOA formation in both systems. The values of α and K determined using the one-product model are shown in **Table 2.3**. Under dry conditions, a larger value of α is obtained when HC_0/NO_x is higher, while the K values are similar, suggesting that the same types of products partition into the particle phase. The results also show that an increase in RH leads to a larger value for α, indicating a higher yield of aerosol-forming products.

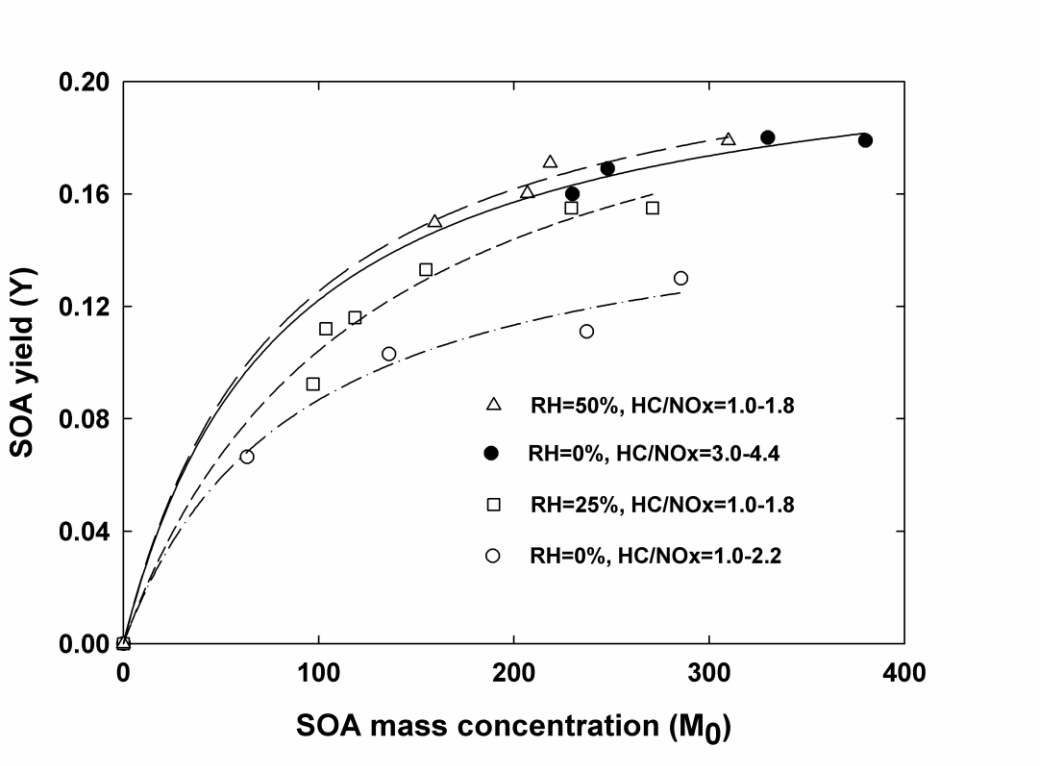


Figure 2.5 SOA yield curves for the photooxidation of naphthalene as a function of hydrocarbon to NOx ratio (HC_0/NO_x) and relative humidity (RH).

Table 2.3 Aerosol yield parameters obtained from the best-fit of the experimental data to the gas/particle partitioning model by assuming one product partitioning.

Expt.	α_1	K_1 (m^3 ug^{-1})	Average OH (10^6 molecule cm^{-3})
RH<2%, HC_0/NO_x=1.0-2.2	0.1645	0.0111	2.1-2.4
RH<2%, HC_0/NO_x=3.0-4.4	0.2246	0.0116	2.2-2.8
RH=25%, HC_0/NO_x=1.0-1.8	0.2324	0.0081	2.2-2.7
RH=50%, HC_0/NO_x=1.0-1.8	0.2595	0.0084	3.0-3.2

2.3.2. Comparison with Previous Studies

Two previous studies of SOA formation from the photooxidation of naphthalene appear in the literature. Chan et al (Chan et al. 2009) reported yields in the range 19-30% under high NO_x conditions at a RH of 5-8% and used a two-product model to generate yield curves for naphthalene, but found that a one-product model provided the best fit for SOA production from methylnaphthalenes. Although SOA yields from photooxidation of naphthalene obtained by Chan et al. (Chan et al. 2009) are somewhat higher than those obtained in the present work, there are a number of significant differences in the experimental conditions employed in the two studies. Chan et al. employed the direct injection of HONO as the OH radical source, which is known to produce higher concentrations of OH than in classical photooxidation experiments (Ng et al. 2007b). The experiments of Chan et al. were also performed in the presence of seed aerosol, which is expected to increase the yield of SOA via enhanced partitioning of the oxidation products (Kroll et al. 2007). Other factors that can influence SOA yield, such as temperature and light intensity are also different in the two studies.

In the only other study of SOA formation yields from photooxidation of naphthalene, Shakya and Griffin (Shakya et al. 2010) reported yields of 8-16%, using both H_2O_2/NO_x and HONO as the OH precursor. The results are in good agreement with those obtained in this work and although the hydrocarbon/NO_x ratio was varied from 4-11, no obvious pattern in the SOA yields was observed.

In order to gauge the relative importance of naphthalene as a potential SOA precursor, it is useful to compare these chamber-derived SOA yields with those obtained for other VOCs under similar experimental conditions. The SOA yields for naphthalene reported by Chan et al. were about three times those for monocyclic aromatics performed using HONO as the precursor in the same chamber (Ng et al., 2007). Similarly, the SOA yields for naphthalene obtained in this work are also much higher than those obtained for toluene, *p*-xylene and 1,3,5-trimethylbenzene (Temime et al. 2007; Healy et al. 2008; Healy et al. 2009) obtained during classical photooxidation experiments in the same chamber. This confirms the potential of naphthalene as an important source of SOA in urban areas. However, care should be taken when extrapolating laboratory-determined SOA yields to atmospheric conditions. The

majority of SOA formed in classical photooxidation experiments occurs after NO is depleted, a situation unlikely to be encountered in urban atmospheres where anthropogenic precursors are mainly emitted. The use of HONO as the OH source overcomes this limitation, but the levels of OH typically produced in these experiments are up to an order of magnitude higher than the global daytime average in the troposphere (Ng et al. 2007a).

2.3.3 Effect of Relative Humidity on SOA Yields

The effect of RH on SOA yields was investigated by performing a series of experiments in which initial water concentration was varied while the HC_0/NO_x ratios were maintained in a similar range, i.e., HC_0/NO_x=1-2. Comparison of the results shown in Table 2.2 from experiments RH0_7, RH25_3 and RH50_2, where the initial reactant concentrations were similar but the RH was varied, shows that there is an increase in the SOA yields at higher RH .This is also apparent in the yield curves (**Figure 2.5**) where the value of α increases by a factor of 1.5 over the RH range 0-50%. However, the value of K does not change significantly, indicating that products with similar volatility (probably the same products) are formed in all cases (**Table 2.2**).

Several studies on the effect of water vapour on SOA formation during the photooxidation of monocyclic aromatic hydrocarbons have been performed (Kleindienst et al. 1999; Edney et al. 2000; Cocker III et al. 2001) studied the hygroscopicity of SOA formed from the photooxidation of toluene, *p*-xylene, and 1,3,5-trimethylbenzene in the presence of dry ammonium sulfate seed aerosol and determined that water uptake by the organic fraction was negligible. Edney et al. (Edney et al. 2001) reported similar findings for SOA produced from toluene photooxidation and two other independent studies have shown that SOA yields from m-xylene and 1,3,5-trimethylbenzene are largely unaffected by the presence of gas-phase water up to a RH of 50% (Baltensperger et al. 2005) .

The effect of RH on SOA yields from the classical photooxidation of p-xylene was reported by Healy et al. (Healy et al. 2009). The SOA yields increased by a factor of approximately two over the RH range 5-75% and were found to correlate with OH concentration. In classical photooxidation experiments, OH is initially produced from

the photolysis of HONO. It is known that HONO is generated from the heterogeneous reaction of gas-phase NO_2 with water at the chamber walls (Finlayson-Pitts et al. 2003), or an unidentified source, which is strongly dependent on humidity (Rohrer et al. 2005). Another source of HONO in chamber experiments has recently been reported by Metzger et al. (Metzger et al. 2008) who proposed that a reaction involving the light-induced conversion of NO_2 to HONO at the chamber walls is responsible for much higher levels of HONO than those generated by dark reactions. Healy (Healy et al. 2009) therefore proposed that an increase in RH results in higher levels of HONO formation in the chamber which leads to increased OH concentration, a faster hydrocarbon decay rate and higher aerosol mass yields. A similar "rate effect" has also been observed in other studies when factors that affect the OH concentration, e.g., type of precursor (Song et al. 2007a; Shakya et al. 2010), light intensity and wavelength (Warren et al. 2008; Shakya et al. 2010), are varied.

The average OH radical concentration during each experiment was determined from the measured decay of naphthalene using a rate coefficient of 2.3×10^{-11} cm^3 $molecule^{-1}$ s^{-1} (Calvert et al. 2002). This approach assumes that OH is in a steady state and the resulting values, listed in Table 2.3, are therefore subject to a certain degree of uncertainty. Nevertheless, the values provide the best estimate of OH concentrations in the absence of direct measurements. The results show that a small increase in OH was observed as the RH was raised, indicating that the "rate effect" observed for *p*-xylene may also be operational in the naphthalene system. More information can also be gained from comparison of the SOA growth curves for experiments performed at different RH, **Figure 2.6**. The experiment performed under dry conditions (RH0_7) clearly shows that SOA formation is delayed and only occurs after a certain amount of naphthalene has reacted. This so-called "induction period" is a characteristic feature of classical photooxidation experiments on monocyclic aromatic hydrocarbons (Song et al. 2007a; Ng et al. 2007b). It is interesting to note, however, that an induction period is not observed in experiments at higher RH (**Figure 2.6**). Ng et al. (Ng et al. 2007b) showed that the induction period disappears when experiments are performed under very low NO_x levels (RO_2 + HO_2 reactions dominate) or when direct injection of HONO is used as the OH radical source. In the classical photooxidation experiments performed in this work SOA formation was observed even in the presence of high levels of NO_x and it therefore seems likely that the absence of an

induction period in the experiments performed at RH = 25% and 50% is due to: (i) increased formation of HONO at higher RH which caused a faster decay of naphthalene and hence more rapid formation of semivolatile products that result in SOA and/or (ii) the reaction of primary photooxidation products with water in the gas-phase yielding semivolatile products. However, such a rate effect on the SOA yields needs to be studied in more detail.

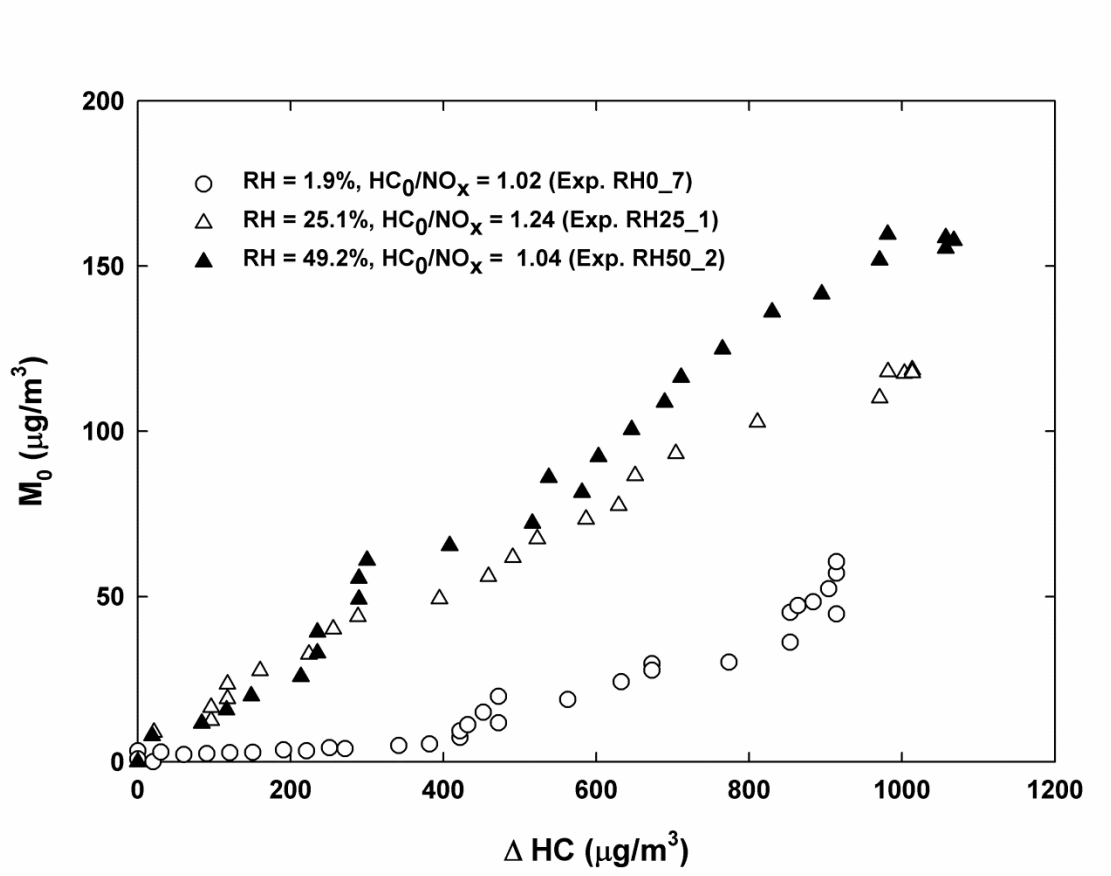


Figure 2.6 Growth curves for SOA formation during classical photooxidation experiments with similar hydrocarbon/NO_x levels but different RH.

In order to further investigate the effect of RH on SOA formation yields three additional experiments were performed using the direct injection of HONO as the OH radical precursor. While using HONO as OH radical precursor the contribution of the $NO_2 + H_2O$ reaction to the concentration of OH in the reaction system should be small and the 'rate effect' should be minimized. The experimental conditions are given in **Table 2.4**.

The two experiments performed under relatively dry conditions (5.0% and 6.2%)

were in good agreement and produced SOA yields of approximately 12%, whilst the experiment performed at higher RH gave a significantly higher yield of 19.8%. The OH levels produced during these three experiments were very similar (1.0-1.2 $\times 10^7$ molecule cm^{-3}), indicating that any additional OH produced from the reaction of NO_2 with water at the walls is smaller and does not significantly affect the photooxidation rate. This suggests that RH has another, more direct effect on SOA yields. One possibility is that water may promote the conversion of photooxidation products into semivolatile compounds in the gas or particle phase. One of the reaction products most likely to undergo this type of conversion is phthalic anhydride, which has been reported as one of the major products in the photooxidation of naphthalene under high NO_x conditions (Kautzman et al. 2010). It is known that gas- and particulate-phase water can hydrolyse phthalic anhydride to phthalic acid, which has a lower volatility and may therefore contribute to the SOA mass yields. A detailed investigation of the chemical composition of the SOA generated from the photooxidation of naphthalene would be needed to confirm this hypothesis.

Table 2.4 Experimental conditions and results for naphthalene/HONO reactions

Expt.	RH (%)	HC_0 [a] (ppbV)	NO [b] (ppbV)	ΔHC [c] ($\mu g/m^3$)	M_0 [d] ($\mu g/m^3$)	SOA yield[e] (%)
HONO_1	6.2	294	490	943	115	12.2
HONO_2	5.0	297	446	1027	118.2	11.5
HONO_3	51.1	291	488	1023	198.8	19.8

[a] Initial mixing ratio of hydrocarbon (naphthalene). [b] The Initial mixing ratio of NO, which includes a significant contribution from HONO. [c] Amount of parent hydrocarbon reacted, corrected for dilution and dark wall loss. [d] SOA mass concentration, determined at the time of measured maximum particle volume concentration, corrected for wall loss, assuming a density of 1.48 g cm^{-3}. [e] Calculated from $M_0/\Delta HC$.

Figure 2.7 shows the concentration-time-profiles obtained during the photooxidation of naphthalene with HONO as OH radical precursor under dry and humid conditions. It is noted that, similar to the classical photooxidation experiments performed under high RH, the 'induction period' is either not observed or very short. This is in contrast to the observations made by Chan et al. and Shakya et al. (Shakya et al. 2010) where the aerosol growth curves for naphthalene show an induction period when experiments were performed under high-NO_x conditions using HONO as the OH

precursor. The experiments were performed under relatively dry conditions (RH ca. 8%) and the effect of RH was not investigated. Chan et al. (Chan et al. 2009) proposed that the induction period may be due to the formation of relatively volatile photooxidation products from the RO_2 + NO reactions. This does not concur with the data obtained in this study where the observed formation of SOA at high NO_x levels indicates that the primary products of RO_2 + NO reactions during the photooxidation of naphthalene are able to undergo nucleation and condensation. Thus it seems that the very different reaction conditions employed in the studies may have influenced the yield and volatility of some of the first-generation oxidation products, and in turn, the rate of aerosol formation and growth.

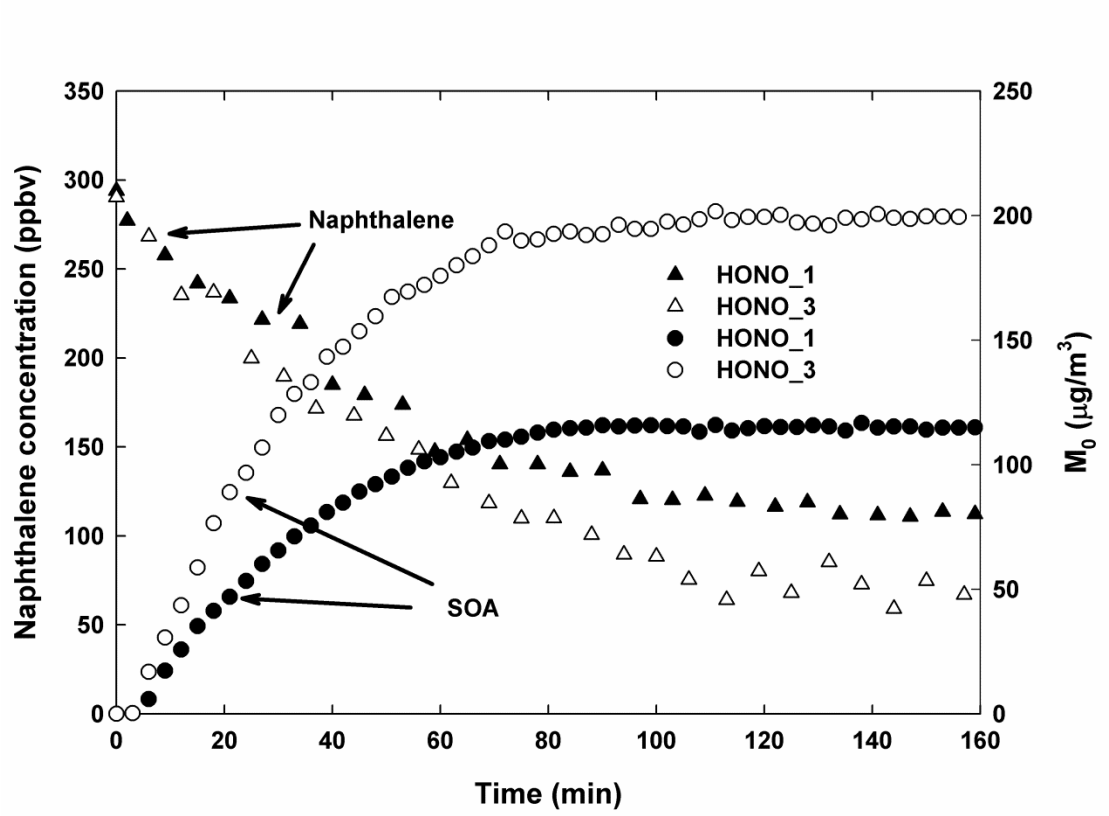


Figure 2.7 Concentration-time profiles for the naphthalene/HONO photooxidation experiments.

Black and white triangle means the concentration of naphthalene, and black and white circles means the SOA mass concentration.

There are a few important differences of note. Firstly, experiments by Chan et al. were conducted with seed aerosols and thus are not directly comparable to this study (Ng et al. 2007b). Secondly, the naphthalene concentrations employed in the present study are 600-1000 ppbV, which are much higher those used by Chan et al. (4.4-21.2

ppbV) and Shakya and Griffin (50-150 ppbV) and would lead to higher amounts of condensable oxidation products, making the induction period significantly shorter. Thirdly, the HC_0/NO_x ratio employed by Chan et al., (in the range 0.024-0.042) was much lower than in the present work and, as shown in **Table 2.2**, would be expected to result in a larger "induction period", while Shakya used similar HC_0/NO_x values to this study, leading to similar SOA yields. Finally, there are different levels of NO_2 present in the reaction systems. The initial OH-naphthalene adduct can react with O_2 to form peroxy radicals or NO_2 to produce nitronaphthalenes (Bunce et al. 1997; Calvert et al. 2002; Nishino et al. 2009b), which are relatively non-volatile species likely to influence SOA formation. The relative rates of the competing reactions for the OH-naphthalene adduct depend on the concentration of NO_2 and Nishino et al. (Nishino et al. 2008) recently reported that the reaction of the OH-naphthalene adduct with O_2 and NO_2 were comparable at an NO_2 mixing ratio of 60 ppbV. Chan et al. (Chan et al. 2009) used NO_2 mixing ratios in the range 50-100 ppbV in their experiments but did not observe nitronaphthalene as an oxidation product. The NO_2 levels in the present work typically reached a maximum of 150-250 ppbV and were even higher during the HONO experiments, which are slightly more favourable conditions for nitronaphthalene formation. The possible formation of non-volatile nitronaphthalenes may therefore help to explain, at least in part, some of the differences observed between the two studies. Finally the different light intensities and temperature in the chambers are other possible factors that may affect the SOA formation yields and volatility of the products in these three studies.

2.4 Conclusions

SOA formation yields from the photooxidation of naphthalene have been determined under a variety of reaction conditions. Experiments performed under classical photooxidation conditions in the absence of seed aerosol using nitrogen oxides (NO_x) as the OH radical precursor showed that SOA formation was observed even while the NO concentration was as high as 150-200 ppbV, indicating that the primary oxidation products can readily undergo gas-particle transfer via nucleation and condensation. By varying the initial NO_x and naphthalene concentrations, it was shown that reactions with a higher hydrocarbon to NO_x ratio generated particles more quickly and produced higher yields of SOA. The SOA yield was also found to increase by up to a factor of 1.5 over the relative humidity range 0-50%. A similar effect was also observed using HONO as the OH precursor. The results indicate that water may promote SOA formation and growth by conversion of photooxidation products into less volatile compounds via reaction in the gas or particle phase. However, detailed investigations of the chemical composition of the SOA generated under different reactions are required to confirm this possibility.

The results reported in the present work and in two other studies (Chan et al. 2009; Shakya et al. 2010) indicate that naphthalene is a potentially large source of SOA in urban areas and should be included in atmospheric SOA models. However, as chamber experiments are not truly representative of the real atmosphere, extrapolation of the results from the present work should be treated with caution. This work also highlights the need for further detailed investigations of SOA formation from naphthalene and other PAHs under a wide variety of reaction conditions.

2.5 References

Atkinson, R., S. M. Aschmann, J. Arey, B. Zielinska and D. Schuetzle (1989). "Gas-Phase Atmospheric Chemistry of 1-Nitronaphthalene and 2-Nitronaphthalene and 1,4-Naphthoquinone." Atmospheric Environment **23**(12): 2679-2690.

Baltensperger, U., M. Kalberer, J. Dommen, D. Paulsen, M. R. Alfarra, H. Coe, R. Fisseha, A. Gascho, M. Gysel, S. Nyeki, M. Sax, M. Steinbacher, A. S. H. Prevot, S. Sjogren, E. Weingartner and R. Zenobi (2005). "Secondary Organic Aerosols from Anthropogenic and Biogenic Precursors." Faraday Discussions **130**: 265-278.

Bunce, N. J., L. Liu, J. Zhu and D. A. Lane (1997). "Reaction of Naphthalene and Its Derivatives with Hydroxyl Radicals in the Gas Phase." Environmental Science & Technology **31**(8): 2252-2259.

Calvert, J. G., R. Atkinson, K. H. Becker, R. M. Kamens, J. H. Seinfeld, T. J. Wallington and G. Yarwood (2002). The Mechanisms of Atmospheric Oxidation of Aromatic Hydrocarbons. Oxford, Oxford University Press.

Chan, A. W. H., K. E. Kautzman, P. S. Chhabra, J. D. Surratt, M. N. Chan, J. D. Crounse, A. Karten, P. O. Wennberg, R. C. Flagan and J. H. Seinfeld (2009). "Secondary Organic Aerosol Formation from Photooxidation of Naphthalene and Alkylnaphthalenes: Implications for Oxidation of Intermediate Volatility Organic Compounds (IVOCs)." Atmospheric Chemistry and Physics **9**(9): 3049-3060.

Cocker III, D. R., B. T. Mader, M. Kalberer, R. C. Flagan and J. H. Seinfeld (2001). "The Effect of Water on Gas-particle Partitioning of Secondary Organic Aerosol: II. m-xylene and 1,3,5-trimethylbenzene Photooxidation Systems." Atmospheric Environment **35**(35): 6073-6085.

Edney, E. O., D. J. Driscoll, R. E. Speer, W. S. Weathers, T. E. Kleindienst, W. Li and D. F. Smith (2000). "Impact of Aerosol Liquid Water on Secondary Organic Aerosol Yields of Irradiated Toluene/propylene/NO_x/$(NH_4)_2SO_4$/air Mixtures." Atmospheric Environment **34**(23): 3907-3919.

Edney, E. O., D. J. Driscoll, W. S. Weathers, T. E. Kleindienst, T. S. Conver, C. D. McIver and W. Li (2001). "Formation of Polyketones in Irradiated Toluene/Propylene/NO_x/Air Mixtures." Aerosol Science and Technology **35**: 998-1008.

Finlayson-Pitts, B. J., L. M. Wingen, A. L. Sumner, D. Syomin and K. A. Ramazan (2003). "The Heterogeneous Hydrolysis of NO_2 in Laboratory Systems and in Outdoor and Indoor Atmospheres: An Integrated Mechanism." Physical Chemistry Chemical Physics **5**(2): 223-242.

Gao, S., N. L. Ng, M. Keywood, V. Varutbangkul, R. Bahreini, A. Nenes, J. He, K. Y. Yoo, J. L. Beauchamp, R. P. Hodyss, R. C. Flagan and J. H. Seinfeld (2004). "Particle Phase Acidity and Oligomer Formation in Secondary Organic Aerosol." Environmental Science & Technology **38**(24): 6582-6589.

Gómez-González, Y., J. D. Surratt, F. Cuyckens, R. Szmigielski, R. Vermeylen, M. Jaoui, M. Lewandowski, J. H. Offenberg, T. E. Kleindienst, E. O. Edney, F. Blockhuys, C. Van Alsenoy, W. Maenhaut and M. Claeys (2008). "Characterization of Organosulfates from the Photooxidation of Isoprene and Unsaturated Fatty Acids in Ambient Aerosol Using Liquid Chromatography/electrospray Ionization Mass Spectrometry." Journal of Mass Spectrometry **43**(3): 371-382.

Healy, R. M., B. Temime, K. Kuprovskyte and J. C. Wenger (2009). "Effect of Relative Humidity on Gas/Particle Partitioning and Aerosol Mass Yield in the Photooxidation of *p*-Xylene." Environmental Science & Technology **43**(6): 1884-1889.

Healy, R. M., J. C. Wenger, A. Metzger, J. Duplissy, M. Kalberer and J. Dommen (2008). "Gas/particle Partitioning of Carbonyls in the Photooxidation of Isoprene and 1,3,5-trimethylbenzene." Atmospheric Chemistry and Physics **8**(12): 3215-3230.

Henry, F., C. Coeur-Tourneur, F. Ledoux, A. Tomas and D. Menu (2008). "Secondary organic aerosol formation from the gas phase reaction of hydroxyl radicals with *m*-, *o*- and *p*-cresol." Atmospheric Environment **42**(13): 3035-3045.

Hurley, M. D., O. Sokolov, T. J. Wallington, H. Takekawa, M. Karasawa, B. Klotz, I. Barnes and K. H. Becker (2001). "Organic Aerosol Formation during the Atmospheric Degradation of Toluene." Environmental Science & Technology **35**(7): 1358-1366.

Johnson, D., M. E. Jenkin, K. Wirtz and M. Martin-Reviejo (2004). "Simulating the Formation of Secondary Organic Aerosol from the Photooxidation of Toluene." Environmental Chemistry **1**(3): 150-165.

Johnson, D., M. E. Jenkin, K. Wirtz and M. Martin-Reviejo (2005). "Simulating the Formation of Secondary Organic Aerosol from the Photooxidation of Aromatic Hydrocarbons." Environmental Chemistry **2**(1): 35-48.

Kautzman, K. E., J. D. Surratt, M. N. Chan, A. W. H. Chan, S. P. Hersey, P. S. Chhabra, N. F. Dalleska, P. O. Wennberg, R. C. Flagan and J. H. Seinfeld (2010). "Chemical Composition of Gas- and Aerosol-Phase Products from the Photooxidation of Naphthalene." Journal of Physical Chemistry A **114**(2): 913-934.

Kleindienst, T. E., D. F. Smith, W. Li, E. O. Edney, D. J. Driscoll, R. E. Speer and W. S. Weathers (1999). "Secondary Organic Aerosol Formation from the Oxidation of Aromatic Hydrocarbons in the Presence of Dry Submicron Ammonium Sulfate Aerosol." Atmospheric Environment **33**(22): 3669-3681.

Koch, R., R. Knispel, M. Elend, M. Siese and C. Zetzsch (2007). "Consecutive Reactions of Aromatic-OH adducts with NO, NO_2 and O_2: Benzene, Naphthalene, Toluene, *m*- and *p*-xylene, Hexamethylbenzene, Phenol, *m*-cresol and Aniline." Atmospheric Chemistry and Physics **7**(8): 2057-2071.

Kroll, J. H., A. W. H. Chan, N. L. Ng, R. C. Flagan and J. H. Seinfeld (2007). "Reactions of Semivolatile Organics and Their Effects on Secondary Organic Aerosol Formation." Environmental Science & Technology **41**(10): 3545-3550.

Kroll, J. H., N. L. Ng, S. M. Murphy, R. C. Flagan and J. H. Seinfeld (2006). "Secondary Organic Aerosol Formation from Isoprene Photooxidation." Environmental Science & Technology **40**(6): 1869-1877.

Kroll, J. H. and J. H. Seinfeld (2008). "Chemistry of secondary organic aerosol: Formation and evolution of low-volatility organics in the atmosphere." Atmospheric Environment **42**(16): 3593-3624.

Lane, D. A., S. S. Fielder, S. J. Townsend, N. J. Bunce, J. Zhu, L. Liu, B. Wiens and P. Pond (1996). "Atmospheric Photochemistry of Naphthalene: a Practical and Theoretical Approach." Polycyclic Aromatic Compounds **9**(1): 53 - 59.

Metzger, A., J. Dommen, K. Gaeggeler, J. Duplissy, A. S. H. Prevot, J. Kleffmann, Y. Elshorbany, A. Wisthaler and U. Baltensperger (2008). "Evaluation of 1,3,5 trimethylbenzene degradation in the detailed tropospheric chemistry mechanism, MCMv3.1, using environmental chamber data." Atmospheric Chemistry and Physics **8**(21): 6453-6468.

Mihele, C. M., H. A. Wiebe and D. A. Lane (2002). "Particle Formation and Gas/Particle Partition Measurements of the Products of the Naphthalene-OH Radical Reaction in a Smog Chamber." Polycyclic Aromatic Compounds **22**(3-4): 729-736.

Ng, N. L., P. S. Chhabra, A. W. H. Chan, J. D. Surratt, J. H. Kroll, A. J. Kwan, D. C. McCabe, P. O. Wennberg, A. Sorooshian, S. M. Murphy, N. F. Dalleska, R. C. Flagan and J. H. Seinfeld (2007a). "Effect of NO_x level on secondary organic aerosol (SOA) formation from the photooxidation of terpenes." Atmospheric Chemistry and Physics **7**(19): 5159-5174.

Ng, N. L., J. H. Kroll, A. W. H. Chan, P. S. Chhabra, R. C. Flagan and J. H. Seinfeld (2007b). "Secondary organic aerosol formation from m-xylene, toluene, and benzene." Atmospheric Chemistry and Physics **7**(14): 3909-3922.

Nishino, N., J. Arey and R. Atkinson (2009b). "Formation and Reactions of 2-Formylcinnamaldehyde in the OH Radical-Initiated Reaction of Naphthalene." Environmental Science & Technology **43**(5): 1349-1353.

Nishino, N., R. Atkinson and J. Arey (2008). "Formation of Nitro Products from the Gas-Phase OH Radical-Initiated Reactions of Toluene, Naphthalene, and Biphenyl: Effect of NO_2 Concentration." Environmental Science & Technology **42**(24): 9203-9209.

Odum, J. R., T. Hoffmann, F. Bowman, D. Collins, R. C. Flagan and J. H. Seinfeld (1996). "Gas/particle partitioning and secondary organic aerosol yields." Environmental Science & Technology **30**(8): 2580-2585.

Odum, J. R., T. P. W. Jungkamp, R. J. Griffin, R. C. Flagan and J. H. Seinfeld (1997a). "The atmospheric aerosol-forming potential of whole gasoline vapor." Science **276**(5309): 96-99.

Odum, J. R., T. P. W. Jungkamp, R. J. Griffin, H. J. L. Forstner, R. C. Flagan and J. H. Seinfeld (1997b). "Aromatics, reformulated gasoline, and atmospheric organic aerosol formation." Environmental Science & Technology **31**(7): 1890-1897.

Pöschl, U. (2005). "Atmospheric Aerosols: Composition, Transformation, Climate and Health Effects." Angewandte Chemie International Edition **44**(46): 7520-7540.

Rohrer, F., B. Bohn, T. Brauers, D. Broning, F. J. Johnen, A. Wahner and J. Kleffmann (2005). "Characterisation of the photolytic HONO-source in the

atmosphere simulation chamber SAPHIR." Atmospheric Chemistry and Physics **5**(8): 2189-2201.

Sasaki, J., S. M. Aschmann, E. S. C. Kwok, R. Atkinson and J. Arey (1997). "Products of the Gas-Phase OH and NO_3 Radical-Initiated Reactions of Naphthalene." Environmental Science & Technology **31**(11): 3173-3179.

Seinfeld, J. H., G. B. Erdakos, W. E. Asher and J. F. Pankow (2001). "Modeling the Formation of Secondary Organic Aerosol (SOA). 2. The Predicted Effects of Relative Humidity on Aerosol Formation in the *α*-Pinene-, *β*-Pinene-, Sabinene-, *Δ3*-Carene-, and Cyclohexene-Ozone Systems." Environmental Science & Technology **35**(9): 1806-1817.

Shakya, K. M. and R. J. Griffin (2010). "Secondary Organic Aerosol from Photooxidation of Polycyclic Aromatic Hydrocarbons." Environmental Science & Technology **44**(21): 8134-8139.

Song, C., K. Na and D. R. Cocker (2005). "Impact of the Hydrocarbon to NO_x Ratio on Secondary Organic Aerosol Formation." Environmental Science & Technology **39**(9): 3143-3149.

Song, C., K. Na, B. Warren, Q. Malloy and D. R. Cocker (2007a). "Secondary Organic Aerosol Formation from the Photooxidation of *p*- and *o*-Xylene." Environmental Science & Technology **41**(21): 7403-7408.

Song, C., K. Na, B. Warren, Q. Malloy and D. R. Cocker (2007b). "Secondary Organic Aerosol Formation from m-Xylene in the Absence of NO_x." Environmental Science & Technology **41**(21): 7409-7416.

Surratt, J. D., J. H. Kroll, T. E. Kleindienst, E. O. Edney, M. Claeys, A. Sorooshian, N. L. Ng, J. H. Offenberg, M. Lewandowski, M. Jaoui, R. C. Flagan and J. H. Seinfeld (2006). "Evidence for Organosulfates in Secondary Organic Aerosol." Environmental Science & Technology **41**(2): 517-527.

Temime, B., R. M. Healy and J. C. Wenger (2007). "A Denuder-Filter Sampling Technique for the Detection of Gas and Particle Phase Carbonyl Compounds." Environmental Science & Technology **41**(18): 6514-6520.

Tobias, H. J., K. S. Docherty, D. E. Beving and P. J. Ziemann (2000). "Effect of Relative Humidity on the Chemical Composition of Secondary Organic Aerosol Formed from Reactions of 1-Tetradecene and O_3." Environmental Science & Technology **34**(11): 2116-2125.

Warren, B., C. Song and D. R. Cocker (2008). "Light Intensity and Light Source Influence on Secondary Organic Aerosol Formation for the m-Xylene/NO_x Photooxidation System." Environmental Science & Technology **42**(15): 5461-5466.

Yu, Y., M. J. Ezell, A. Zelenyuk, D. Imre, L. Alexander, J. Ortega, B. D'Anna, C. W. Harmon, S. N. Johnson and B. J. Finlayson-Pitts (2008). "Photooxidation of α-pinene at high relative humidity in the presence of increasing concentrations of NO_x." Atmospheric Environment **42**(20): 5044-5060.

Chapter

3

On-line and Off-line Analysis of Products from the Photooxidation of Naphthalene

3.1 Introduction

3.1.1 Previous Product Studies on the Photooxidation of Naphthalene

The products of the atmospheric photooxidation of naphthalene have been determined in a number of studies. The first studies focussed on identification and quantification of gas-phase products using techniques such as GC-FID, HPLC, GC-MS, API-MS and FTIR spectroscopy (Bunce et al. 1997; Sasaki et al. 1997). More recent efforts in this area have led to improved quantification of certain products and hence refinements to the photooxidation mechanism (Lee et al. 2009; Nishino et al. 2009a; Nishino et al. 2009b; Kautzman et al. 2010; Nishino et al. 2010). A summary of the major gas-phase products and their reported yields is provided in **Table 3.1**

The gas/particle partitioning of oxidation products has also been investigated using denuder-filter sampling combined with off-line analysis by GC-MS (Mihele et al. 2002), and GC × GC-TOFMS (Lee et al. 2009). A range of photooxidation products were identified but not quantified. The results indicate that many products are distributed between both phases, with 1,4-naphthoquinone predominantly in the gas-phase and naphthols and nitronaphthalenes mainly in the particle phase. Finally, Kautzman et al. studied the chemical composition of both the gas- and aerosol-phase constituents produced from the OH-initiated photooxidation of naphthalene under low- and high-NO_x conditions (Kautzman et al. 2010). A range of gas-phase products were identified (but not quantified) using chemical ionisation mass spectrometry (CIMS) and GC/EI-TOFMS, while both online AMS and off-line high-resolution electrospray ionization time-of-flight mass spectrometry (HR-ESI-TOFMS) methods were used to characterise species in the particle phase. Oligomers, organosulfates (R-OSO_3), and other high-molecular-weight products were not observed in either the low- or high-NO_x conditions, but hydroxybenzene sulfonic acid, was observed in the SOA produced under both high- and low-NO_x conditions in the presence of $Al_2(SO_4)_3$ seed aerosol. Up to 68% of the SOA mass was chemically characterised in this comprehensive study.

Table 3.1 Major gas-phase products observed in the photooxidation of naphthalene.

Product	Molar Yield	Reference
2-Formylcinnamaldehyde	0.35 ± 0.10	(Sasaki et al. 1997)
	0.16	(Bunce et al. 1997)
	0.56 ± 0.15	(Nishino et al. 2009b)
2-Formylbenzaldehyde	0.027	(Sasaki et al. 1997)
	0.56 ± 0.15	(Nishino et al. 2009b)
1-Naphthol	0.029 ± 0.015	(Sasaki et al. 1997)
2-Naphthol	0.038 ± 0.011	(Sasaki et al. 1997)
1-Nitronaphthalene	0.012 ± 0.009	(Sasaki et al. 1997)
	0.07	(Bunce et al. 1997)
	0.0035	(Nishino et al. 2008)
2-Nitronaphthalene	0.013 ± 0.011	(Sasaki et al. 1997)
	0.006	(Nishino et al. 2008)
1-Hydroxy-2-nitronaphthalene	0.011 ± 0.011	(Sasaki et al. 1997)
1,4-Napthoquinone	0.010 ± 0.003	(Sasaki et al. 1997; Lee et al. 2009)
	0.06	(Bunce et al. 1997)
Phthalic anhydride	0.03	(Sasaki et al. 1997)
2-Formylcinnamic acid	0.018	(Bunce et al. 1997)
Phthaldialdehyde	0.045 ± 0.009	(Nishino et al. 2009a)
Glyoxal	0.052 ± 0.028	(Nishino et al. 2009a)

3.1.2 Photooxidation Mechanism for Naphthalene

Based on the identity of the observed reaction products, an overall reaction mechanism for the photooxidation of naphthalene can be proposed. As for the reactions of OH radicals with monocyclic aromatic hydrocarbons, the OH radical-initiated oxidation of naphthalene proceeds mainly by addition to form an OH-naphthalene adduct which subsequently reacts with O_2 or NO_2 (Atkinson et al. 2003; Atkinson et al. 2007; Koch et al. 2007):

$$\text{OH} + \text{aromatic} \rightarrow \text{OH-aromatic adduct} \quad (1)$$

$$\text{OH-aromatic adduct} + O_2 \rightarrow \text{products} \quad (2)$$

$$\text{OH-aromatic adduct} + NO_2 \rightarrow \text{products} \quad (3)$$

OH-naphthalene adducts react at equal rates with O_2 and NO_2 at $[NO_2] = 0.06$ ppmV (Nishino et al. 2008). Hence under typical atmospheric conditions the OH-monocyclic aromatic adducts mainly react with O_2, leading to the formation of 2-formylcinnamaldehyde in 56% yield (Nishino et al. 2009b), as shown in **Figure 3.1.** The formation of two other ring fragmentation products, phthaldialdehyde and glyoxal, observed with an approximate yield of 5% is attributed to a reaction pathway involving a bicyclic peroxy radical (Kautzman et al. 2010). Phthaldialdehyde and glyoxal can also be formed as secondary products via reaction of 2-formylcinnamaldehyde with OH or photolysis (Wang et al. 2007; Nishino et al. 2009b) and further reaction of phthaldialdehyde leads to the formation of phthalic anhydride and phthalide (Wang et al. 2006).

At NO_2 levels characteristic of polluted urban atmospheres, the OH-naphthalene adducts react to a significant extent with NO_2, forming ring-retaining products such as 2-nitronaphthalene and 1-naphthol. A proposed reaction mechanism for the formation of these species is shown in **Figure 3.2**. Here it should be noted that OH addition to the other position on the aromatic ring would produce the corresponding isomers, 1-nitronaphthalene and 2-naphthol (Sasaki et al. 1997; Kautzman et al. 2010). Mechanisms for the formation of other gas-phase products and the compounds detected in the particle phase are less certain (Kautzman et al. 2010).

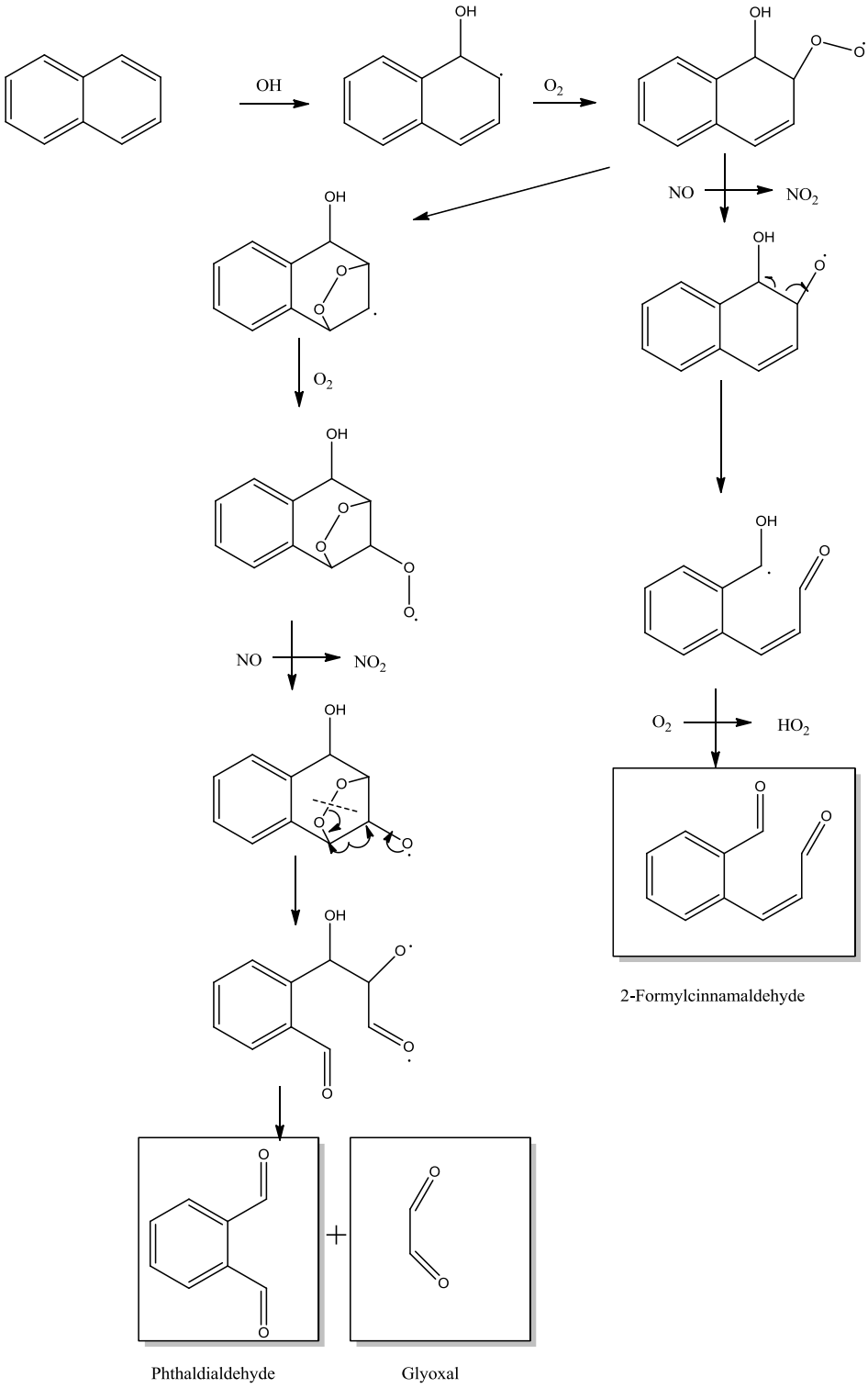


Figure 3.1 Proposed reaction pathways leading to formation of major ring-opening products from photooxidation of naphthalene (Nishino et al. 2009b).

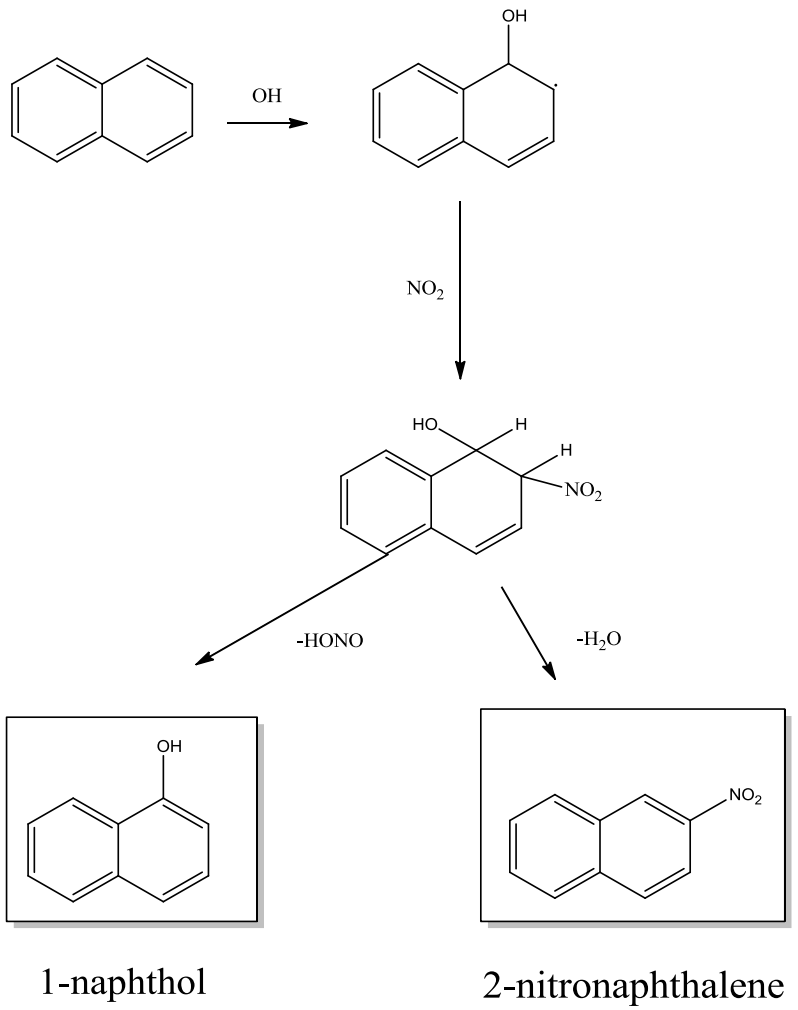


Figure 3.2 Proposed reaction pathways leading to formation of major ring-retaining products from photooxidation of naphthalene (Sasaki et al. 1997).

3.1.3 Denuder-Filter Sampling System

A combined denuder-filter sampling apparatus can be used to separate and simultaneously collect gas and particle phase compounds present in air. The denuder tube (coated with an appropriate adsorbent such as XAD-4 resin) traps the gas phase compounds, while particles, which diffuse about 1000 times more slowly than gaseous molecules, pass through the tube and may be collected on a filter downstream. The tube is short enough for particles to remain airborne but long enough for the gaseous molecules to be trapped. After sampling, the contents of the denuder and filter may be extracted and analysed by analytical techniques such as GC-MS, often with the use of derivatizing agents to aid the detection and identification of polar organic compounds.

Denuder-filter sampling has been employed in two previous studies of the photooxidation of naphthalene (Mihele et al. 2002; Lee et al. 2009). However, XAD-4 coated denuders typically have a low trapping efficiency for polar organic compounds such as carbonyls and carboxylic acids. In order to overcome this problem, the denuder may be coated with a derivatizing agent to enable polar organic compound to be converted to their derivatives on the surface of the denuder tube. For example, Temime et al. demonstrated that a multi-channel annular denuder coated with both XAD-4 and O-(1,2,3,4,5-pentafluorobenzyl)-hydroxylamine (PFBHA) was highly effective at trapping even the most volatile carbonyls and was later applied to simulation chamber studies of gas-particle partitioning (Healy et al. 2008; Healy et al. 2009). A similar approach has also recently been adopted for hydroxyl-containing compounds using pentafluorobenzyl bromide (PFBBr) as the derivatizing agent (Kuprovskyte 2010).

3.1.4 Aerosol Time-of-Flight Mass Spectrometer (ATOFMS)

The Aerosol Time of Flight Mass Spectrometer (ATOFMS, **Figure 3.3**) is one of the most technically advanced instruments available for determination of the chemical composition of aerosols. It can perform size and composition measurements for single particles in real-time and therefore provide valuable information on the chemical species present in aerosols in a variety of environments (Pratt et al. 2012b). Particle-laden air is sampled and accelerated into a sizing region where the aerodynamic diameter of individual particles is determined. The particles pass into a bipolar time-of-flight mass spectrometer and are desorbed and ionized using a UV laser operating at 266 nm. The resulting positive and negative ions generated from a single aerosol particle are detected by the spectrometer, thus generating two complete mass spectra from each individual particle.



Figure 3.3 Aerosol time-of-flight mass spectrometer model 3800, TSI.

The ATOFMS is portable and can measure particles in the size range 100-3000 nm and record mass spectra of species up to 800 Da. It is routinely used for analysing ambient atmospheric aerosols (Dall'Osto and Harrison 2006; Healy et al. 2009; Healy et al. 2010). The successful application of ATOFMS in probing the chemical composition of SOA produced in simulation chamber experiments was demonstrated for the first time by Gross (Gross et al. 2006) who performed measurements of the SOA generated from the photooxidation of 1,3,5-trimethylbenzene and α-pinene. This study showed that ATOFMS is not only capable of the on-line detection of oligomers in SOA, but also that the chemical evolution of these species can be followed in real-time.

3.1.5 Aim of this Study

The aim of this work was to employ a combination of off-line and on-line analytical methods to study the gas- and particle-phase photooxidation products of naphthalene. A denuder-filter sampling system combined with chemical derivatization and off-line analysis using GC-MS has been used to identify the products and investigate gas/particle partitioning. On-line analysis of the chemical composition of particles produced from naphthalene photooxidation under a variety of reaction conditions has been performed using ATOFMS. The results are used to gain further insights into the species and mechanisms involved in the formation, growth and evolution of SOA.

3.2 Experimental

3.2.1 Materials

The materials used in this work are listed in **Table 3.2**, used as received.

Table 3.2 Chemicals used in this work.

Material	Purity %	Manufacturers
Amberlite XAD-4 resin	n/a	Aldrich
Naphthalene	99	Aldrich
1-Nitronapthalene	N/A	Aldrich
Phthaldialdehyde	98	Aldrich
1,2-Naphthoquinone	97	Aldrich
1,4-Naphthoquinone	97	Aldrich
2-Formylcinnamic acid	97	Aldrich
Glyoxal	40% in water	Aldrich
Phthalide	98	Aldrich
Phthalic anhydride	99	Aldrich
PFBHA	98	Aldrich
PFBBr	99	Aldrich
BSTFA+TMCS(99:1)		SUPELCO
Potassium carbonate	≥98	Aldrich
Zinc	99	Aldrich
Acetic anhydride	99	Aldrich
Acetone	≥99.5	Fluka
Methanol	99.9	Aldrich
n-Pentane	HPLC grade	Aldrich
Dichloromethane	99.9	Aldrich
Methane	99.9999	Irish Oxygen
n-Hexane	HPLC grade	Aldrich
Sulfuric acid	98	Aldrich
Sodium nitrite	99	Aldrich
Acetonitrile	99	Aldrich
Hydrogen peroxide	50% in water solution	Aldrich

3.2.2 Off-line Analysis using GC-MS with Derivatization

A series of naphthalene photooxidation experiments was carried out in the 6.5 m^3 simulation chamber described in **Section 2.2.1**. HONO was used as the OH precursor and the experimental procedures were identical to those outlined in **Section 2.2.2**.

Details concerning the use of the denuder-filter sampling apparatus and GC-MS analysis are provided in the following sections.

3.2.2.1 Denuder-Filter Sampling System

The denuder-filter device is shown in **Figure 3.4** and has been described in detail in the literature (Possanzini et al. 1983; Ye et al. 1991; Turpin et al. 2000; Temime et al. 2007; Healy et al. 2008; Ortiz et al. 2009). Briefly, it consists of a 242 mm long annular denuder (University Research Glassware, North Carolina, USA, model URG-2000-30B) made of 5 concentric glass tubes, separated by an annular space of 1 mm giving a total surface area of 1,140 mm^2. When coated with a suitable adsorbent, the denuder can trap gas-phase compounds on the walls of the tube with a collection efficiency of 95-99% (Temime-Roussel et al. 2004a). Particles, which diffuse approximately 1000 times more slowly, pass through the exit of the tube and are trapped on the filter. The filter pack used in this device contains a fluorocarbon-coated glass fibre filter (Pallflex Fiberfilm, 47 mm diameter), cleaned before use by Soxhlet extraction for 24 h using dichloromethane and methanol.

The denuder tubes were coated with 0.4 g of finely ground XAD-4 resin (725 $m^2\ g^{-1}$) as an adsorbent. This was achieved by preparing a slurry of XAD-4 in approximately 10 cm^3 n-hexane. The mixture was sonicated for 1 min and applied to the walls of the denuder by inverting the tube (with end caps attached) end over end and pouring out the excess. The remaining n-hexane was then evaporated with a gentle flow of dry compressed air. The excess was poured back into the tube and the process was repeated (up to 4 times) until all of the resin had adhered to the denuder walls. If required, the XAD-4 coated denuder was also coated with a derivatizing agent (PFBHA or PFBBr) as described below. The denuder was sealed at both ends with polystyrene screw caps to prevent contamination from ambient air.

Typically, the denuder-filter sampling system was used twice during each experiment. The first was taken before the introduction of naphthalene to acquire “blank” samples, while the second was obtained when the particle mass concentration had reached a maximum. Sampling was performed for 30 min at a flow rate of 10 $dm^3\ min^{-1}$. The subsequent extraction, treatment and GC-MS method differed according to the type of derivatization reaction.

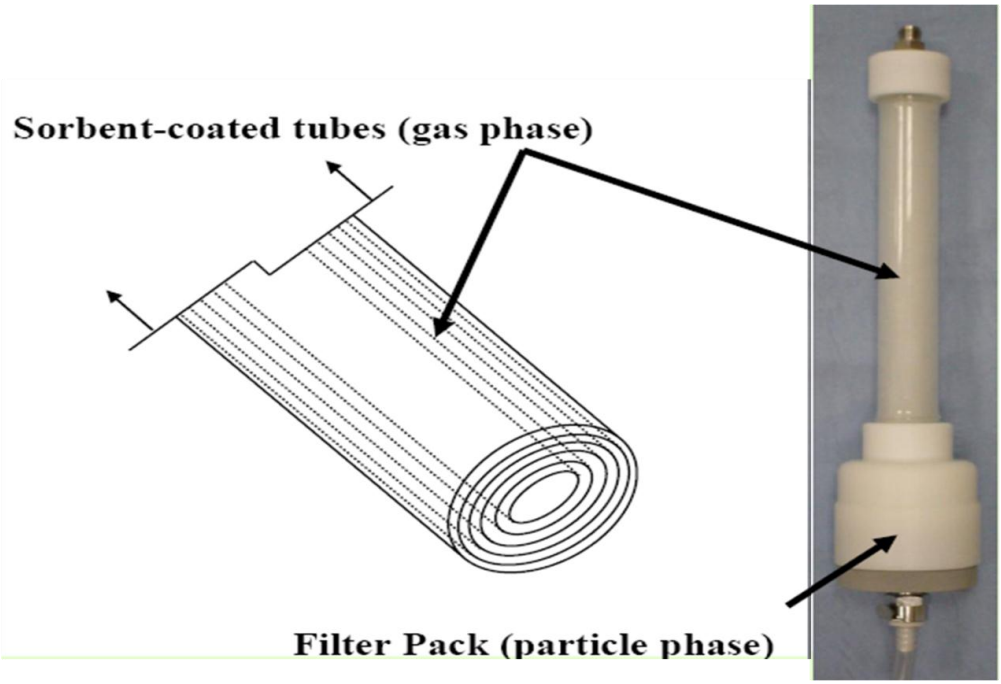


Figure 3.4 Denuder-filter system used in this study.

3.2.2.2 Derivatization with PFBHA

PFBHA is a very effective derivatizing agent for carbonyls. As shown in **Figure 3.5**, the carbonyl is converted to an oxime, which is less polar and more amenable to separation and detection by GC-MS (Temime et al. 2007; Healy et al. 2008). The oximes are relatively easy to synthesise and it is also possible to identify unknown compounds from interpretation of the mass spectrum. Carbonyl compounds are distinguished by the characteristic peak at *m/z* = 181 due to the ion fragment $C_6F_5CH_2^+$. Other common diagnostic ions include; *m/z* = molecular mass of the oxime (M), *m/z* = molecular mass of the carbonyl plus 195 (M + 195) for singly derivatized species and *m/z* = molecular mass of the carbonyl plus 390 (M + 390) for doubly derivatized species, *m/z* = molecular mass of the oxime minus 30 (M-30) corresponding to the loss of NO and *m/z* = molecular mass of the oxime minus 195 (M-195) from the loss of $C_6F_5CH_2N$ (Kuprovskyte 2010). It should be noted that some of the derivatives exist as geometric isomers consisting of *cis* and *trans* forms due to the restricted rotation of the carbon-nitrogen double bond. In addition, dicarbonyl compounds such as glyoxal and phthaldialdehyde can exist in both the mono- and di-derivatized forms. An excess of PFBHA and long derivatization times can help to ensure complete conversion to the double derivative.

In this work, PFBHA derivatization was performed on both denuder and filter samples. The contents of the denuder and filter were extracted using two 10 cm^3 portions of methanol. PFBHA (0.03 g) was added to the extracts and the samples were stored for 48 hours in the dark at room temperature to ensure that derivatization was complete (Healy et al. 2008). Then 1 cm^3 from each extract was filtered using a PTFE membrane filter (Cole-Palmer, pore size 0.45 μm) and reduced under a nitrogen stream almost to dryness and reconstituted with n-hexane (0.1 cm^3).

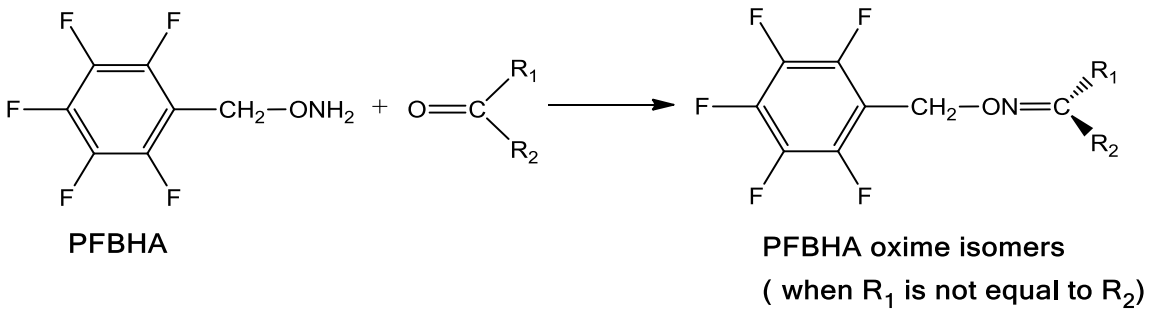


Figure 3.5 Derivatization of a carbonyl compound with PFBHA (Reisen et al. 2003)

A Varian GC-MS system (Saturn 2000) equipped with a split/splitless injector (Varian 1079) was used for chemical analysis. A 30 m CP-Sil-8CB (5% phenyl, 95% dimethylpolysiloxane) chromatographic column was installed. The derivatives were analysed using the following column oven temperature program: 60 ℃ held for 1 min, then ramped from 60 ℃ to 100 ℃ at 5 ℃ min^{-1}, from 100 ℃ to 280 ℃ at 10 ℃ min^{-1} and from 280 ℃ to 310 ℃ at 30 ℃ min^{-1}. The temperature was then held for 5 min. The injector temperature was held at 280 ℃ for 1 min and then ramped to 310 ℃ at 50 ℃ min^{-1}. The helium flow rate was 1.0 cm^3 min^{-1} and EI mass spectra were acquired over a mass range *m/z* 60-650 amu with electron energy of 70eV. Selected ion chromatograms (*m/z* 181) were used when analysing the PFBHA derivatives.

3.2.2.3 Derivatization of Quinones

Quinones were converted to their diacetyl derivatives by reaction with acetic anhydride following the method of Cho et al. (Cho et al. 2004). The denuder and filter samples were sonicated in dichloromethane for 15 minutes, reduced to 1 cm^3 by rotary evaporation and then reacted with 0.2 cm^3 acetic anhydride and 100 mg zinc as a catalyst at 80°C for 15 minutes followed by cooling to room temperature. The

heating was repeated for 15 minutes after adding a further 100 mg of zinc. The reaction was again cooled to room temperature and quenched by addition of 0.5 mL distilled water and 3 cm^3 *n*-pentane. Following centrifugation at 2000 rpm for 10 minutes, the *n*-pentane layer was filtered using PTFE membrane filters (0.45 μm pore size) and transferred to clean amber vials. The sample was evaporated until dry under a nitrogen stream, and then re-dissolved in 0.1 cm^3acetonitrile. GC-MS analysis was performed using the following column oven temperature program: 100 ℃ held for 5 min, then ramped from 100 ℃ to 280 ℃ at 5 ℃ min^{-1}, and the temperature was then held for 2 min, thus the total column time is 45 min (Valavanidis et al. 2006). The injector temperature was held at 250 ℃ for the duration of the analysis. The helium flow rate was 1.0 cm^3 min^{-1} and EI mass spectra were acquired over a mass range *m/z* 50-650 amu. Identification of the diacetyl derivatives of 1,2-naphthoquinine and 1,4-naphthoquinone was achieved by comparison with synthesized standards, **Figure 3.6**.

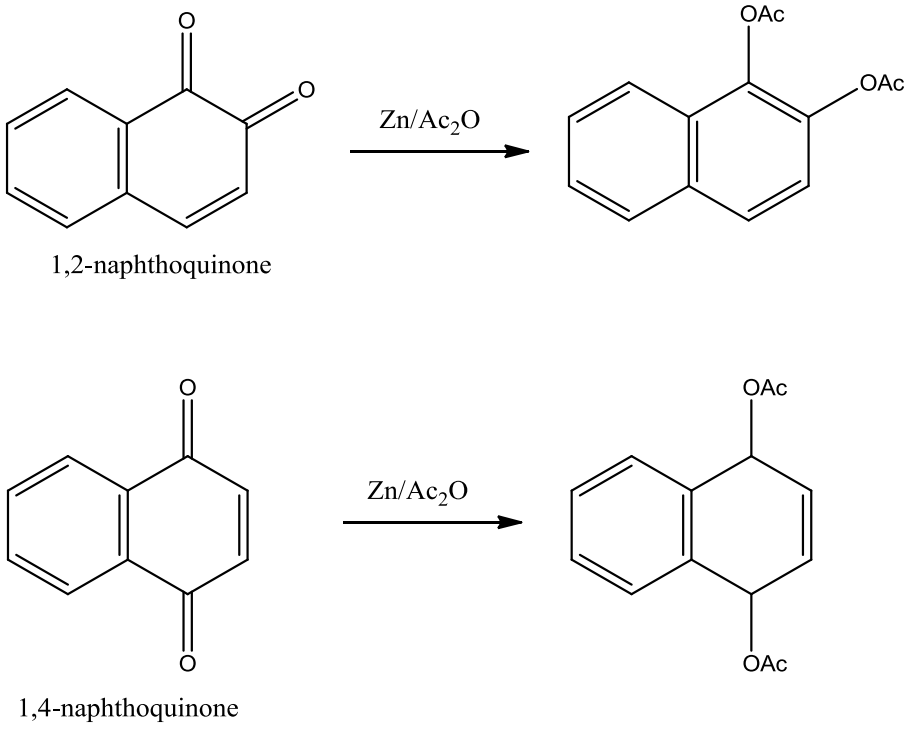


Figure 3.6 Conversion of naphthoquinones to their diacetyl derivatives following reaction with acetic anhydride using zinc as a catalyst (Cho et al. 2004).

3.2.2.4 Derivatization with BSTFA

N,O-bis(trimethylsilyl)-trifluoroacetamide (BSTFA) is a very effective derivatizing agent for hydroxyl-containing compounds such as carboxylic acids and alcohols. As shown in **Figure 3.7** the target compounds are converted to their trimethylsilyl (TMS)

derivatives, which are less polar and more amenable to separation and detection by GC-MS (Wenclawiak et al. 1993; Schummer et al. 2009). The derivatives are relatively easy to synthesise and it is also possible to identify unknown compounds from interpretation of the mass spectrum. Characteristic ions for TMS derivatives occur at *m/z* 73 due to $Si(CH_3)_3$, *m/z* 75 due to $HO=Si(CH_3)_2$, *m/z* 117 due to $COOSi(CH_3)_3$, *m/z* 147 due to $(CH_3)_2Si=OSi(CH_3)_3$. The latter ion, in particular, is indicative of a compound bearing more than one hydroxyl group.

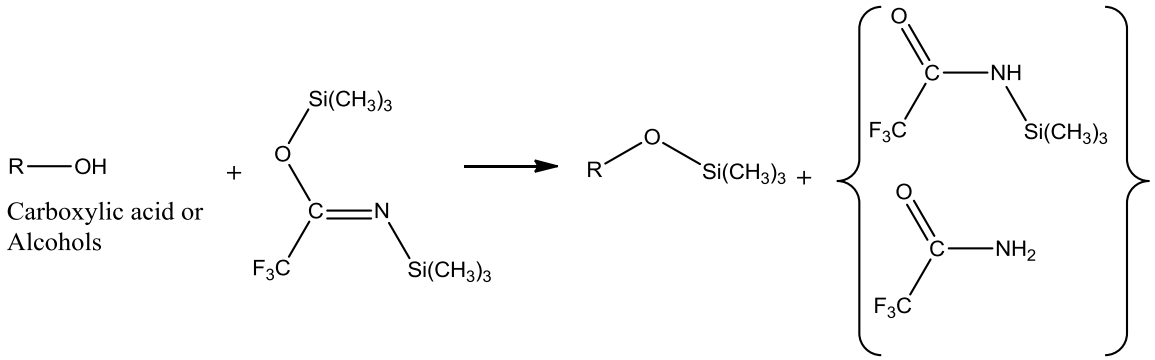


Figure 3.7 Derivatization of hydroxyl-containing compounds with BSTFA

The procedure for BSTFA derivatization was based on the method of Kourtchev et al. (Kourtchev et al. 2005). The contents of the denuder and filter were extracted three times with 20 cm^3 dichloromethane:methanol (80:20 v/v) under ultrasonic agitation for 30 min. Following reduction to approximately 1 cm^3 by rotary evaporation, the samples were transferred to 2 cm^3 amber vials and blown until dry using a pure nitrogen stream. The residues were reconstituted by adding 0.1 cm^3 dichloromethane:methanol (1:1) and derivatized by addition of 0.060 cm^3 of BSTFA containing 1% trimethylchlorosilane (BSTFA + 1% TMCS) and 0.030 cm^3 pyridine at 80°C for 1 hour (Chiappini et al. 2006). The derivative samples were cooled to room temperature, filtered and analysed by GC-MS using the following column oven temperature program: 50 ℃ held for 5 min, then ramped from 50 ℃ to 200 ℃ at 3.5 ℃ min^{-1}, from 200 ℃ to 310 ℃ at 30 ℃ min^{-1} and the temperature was then held for 2 min, thus the total column time was 53.52 min. The injector temperature was held at 250 ℃ for the duration of the analysis. The helium flow rate was 1.2 cm^3 min^{-1} and EI and CI mass spectra were acquired over the mass range *m/z* 50-650 amu.

3.2.2.5 Derivatization with PFBBr

Pentafluorobenzyl bromide (PFBBr) is an alternative derivatizing agent for hydroxyl-containing compounds. As shown in **Figure 3.8**, PFBBr reacts to form derivatives similar to those produced from PFBHA. Subsequent ionization of the derivative produces a characteristic fragment $C_6F_5CH_2^+$ with *m/z* 181. The interpretation of mass spectra is thus very similar to that described above for PFBHA derivatization. The procedure employed for PFBBr derivatization was based on the method developed by Kuprovskyte (Kuprovskyte 2010). The denuder tube was coated evenly with 0.4 g XAD-4 resin and allowed to dry thoroughly. It was then coated with 10 cm^3 PFBBr (10% w/v in acetone), allowed to dry and sealed at both ends with polyethylene screw caps to prevent water entering the tube (PFBBr is very reactive towards water). Following sample collection, the denuder was extracted twice with 10 cm^3 acetone. Extraction of the particles trapped on the filter was achieved by addition of 10 cm^3 of acetone and the derivatizing agent PFBBr (0.30 cm^3, 5% solution in acetone). The extracts (2 cm^3) were introduced into a conical vial (3 cm^3) and K_2CO_3 (20 mg) was added. 18-crown-6 (0.100 cm^3, 4000 ppmV in acetone) was used as a derivatization reaction catalyst. Samples were left to react in the dark at ambient temperature for 48 h and filtered using PTFE membrane filters. 1 cm^3 of each sample was blown to dryness using pure N_2, and then reconstituted in 0.1 cm^3 acetone for GC-MS analysis. The GC was programmed to maintain oven temperature at 60 ℃ for 1 min then progressively ramped from 60 ℃ to 100 ℃ at 5 ℃ min^{-1}, from 100 ℃ to 280 ℃ at 10 ℃ min^{-1} and from 280 ℃ to 310 ℃ at 30 ℃ min^{-1}. The temperature was then held for 5 min. The injector temperature was held at 280 ℃ for 1 min and then ramped to 310 ℃ at 50 ℃ min^{-1}. Helium was used as the carrier gas, at a flow rate of 1.5 cm^3 min^{-1}, and electron ionization (EI) mass spectra were acquired over the range *m/z* 60-650.

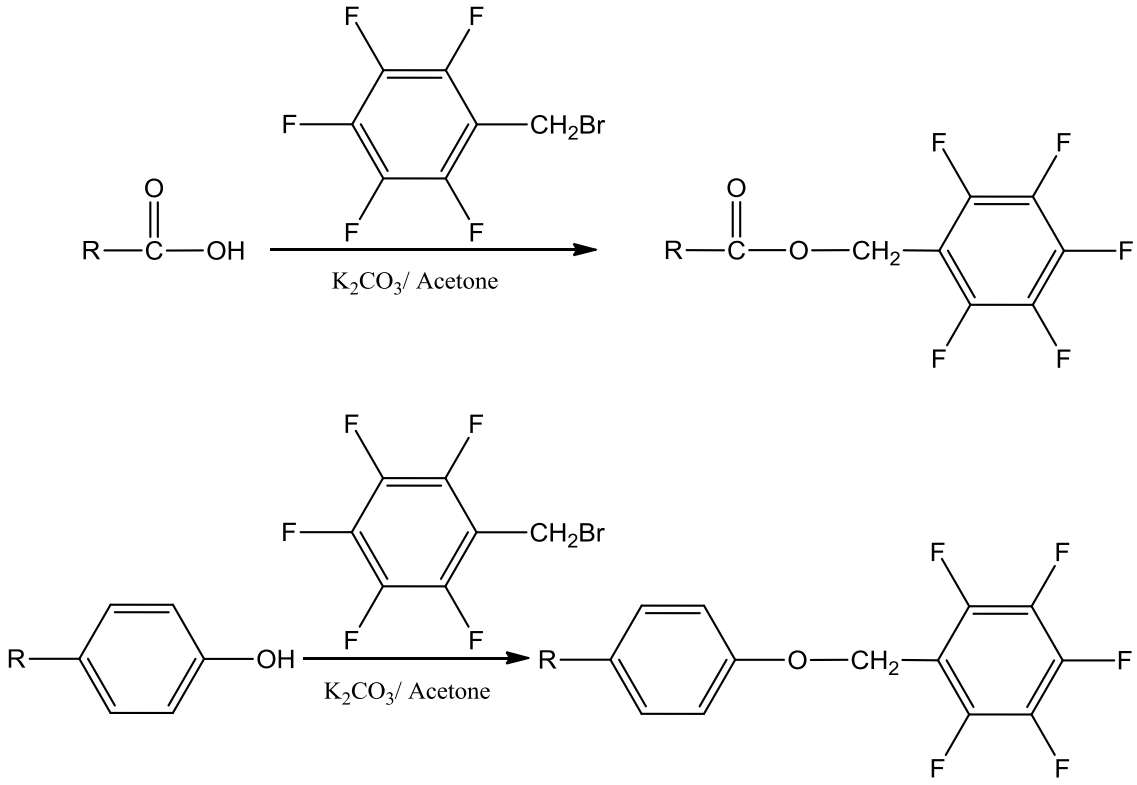


Figure 3.8 Derivatization of carboxylic acids and phenols by reaction with PFBBr.

3.2.3 On-line Analysis of SOA using ATOFMS

The on-line analysis of SOA from the photooxidation of naphthalene was studied using ATOFMS in a 3.9 m^3 simulation chamber located in the Chemistry Department, University College Cork.

3.2.3.1 Atmospheric Simulation Chamber

The chamber has been in operation since 2002 and is described in detail elsewhere (Thüner et al. 2004). It consists of a cylinder (4.1 m long, 1.1 m diameter) made of chemically inert FEP Teflon foil sealed at the ends by two aluminium endplates coated with FEP foil, **Figure 3.9**. The chamber has a sufficiently large volume (3.9 m^3) and volume-to-surface ratio (0.24 m) in order to minimise the role of surface reactions and the deposition of reactants and products with low volatility. The chamber is surrounded by 12 Philips TL05 (40 W) lamps (λ_{max}=360 nm) and 16 Philips TL12 (40 W) lamps (λ_{max}=310 nm). The chamber is operated using purified dry air at 0.1-1 mbar above atmospheric pressure as monitored by a differential pressure transducer (MKS instruments) located on one of the end-plate flanges. The

purified air is generated by an air purification system (Zander KMA 75) which runs on compressed air and reduces concentrations of NO_x and non-methane hydrocarbons to < 10 ppbV. The temperature and amount of water in the chamber is monitored by a dew point meter (Vaisala DM70). Between experiments the chamber is cleaned by flushing with purified air at a flow rate of 0.150 m^3 min^{-1} for a minimum of 4 hours and usually overnight. The chamber design has been recently modified to include fans, located at both ends of the cylinder, in order to promote rapid mixing of reactants. This reduces the mixing time of reactants to approximately 40 seconds and allows reliable concentrations to be measured earlier.

The end-plates, cylindrical foil and lamps are supported by a frame constructed of 60 mm aluminium profiles (Bosch) and covered with aluminium sheets to prevent light from escaping. Both end-plates are fitted with five symmetrically positioned removable flanges. The large central flanges are used to support the field and objective mirrors required for long path *in situ* FTIR spectroscopy, whilst the other flanges are used for the introduction and sampling of gases and for filling and flushing the chamber with air.

The optical arrangement for *in situ* FTIR spectroscopy consists of a White-type mirror system with two circular field mirrors (diameter 254 mm) and a rectangular objective mirror (200 mm × 406 mm) separated by (3.82 ± 0.01) m. The mirrors are made of Pyrex, gold-coated and mounted on adjustable screws to facilitate alignment of the optical system (Thüner et al. 2004). The infrared spectrometer (BioRad Excalibur) is interfaced to the chamber *via* a transfer optics arrangement consisting of 12 gold-coated mirrors. The infrared beam enters and leaves the chamber through KBr windows (50 mm diameter, 3 mm thickness, Moltech, Berlin) and passes through two cut-out edges in the objective mirror. The White system is typically operated at 60 traverses; this path length combined with twice the distance from the surface of the objective mirror to the wall of the chamber, gives a total optical path length of (229.6 ± 0.6) m.



Figure 3.9 The 3.9 m^3 atmospheric simulation chamber at University College Cork.

3.2.3.2 The Aerosol Time-of-Flight Mass Spectrometer (ATOFMS)

The aerosol time-of-flight mass spectrometer (TSI 3800, Shoreview, MN) is a single-particle mass spectrometer designed to sample individual aerosol particles in real time (Pratt et al. 2012b). A schematic diagram of the ATOFMS is shown in **Figure 3.10**. Particle laden-air is sampled at 0.1 cm^3 min^{-1} and enters an aerodynamic lens where the particles and air is accelerated, and the velocity of the particle depends on its aerodynamic diameter (D_a). Two continuous wave diode-pumped Nd:Yag lasers (532 nm, CrystaLaser, Reno, NV), located a known distance apart, are used to determine the D_a by measuring the time between pulses of scattered light when the particle passes through them. After the velocity of the particle is determined, it arrives at the bipolar time-of-flight mass spectrometer which uses the fourth harmonic of a Nd:YAG laser for desorption and ionization of the particles (λ = 266 nm, ~1 mJ/pulse, 1×10^8 W/cm^2, Big Sky Laser, Bozeman, MT). The resulting positive and negative gaseous ions are accelerated into the respective flight tubes of the instrument and positive and negative ion mass spectra of the chemical components contained in the particle are generated.

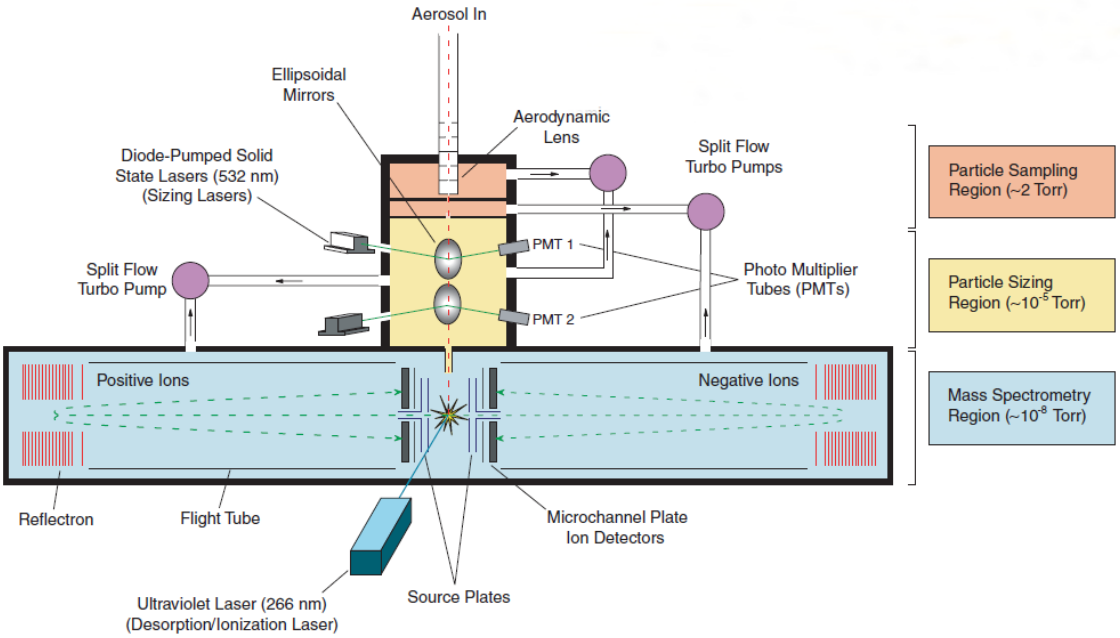


Figure 3.10 Scheme of aerosol time-of-flight mass spectrometer model 3800 (TSI).

3.2.3.3 Procedure

After flushing overnight with dry purified air, the chamber was further cleaned by performing several cycles of ozone addition, combined with photolysis and flushing to ensure that the background concentration of particles in the chamber was < 200 cm^{-3}. Experiments were performed at ambient temperature (295 ± 2 K) and atmospheric pressure. The inlet and outlet valves were closed and data collection was initiated on all instruments. The relative humidity (RH) in the chamber was typically less than 1%. Some experiments were carried out at a RH ~50% by adding water to the chamber by flowing purified air through the headspace of a heated impinger containing deionized (Milli-Q) water. Naphthalene was introduced to the chamber in the same manner and photooxidation was initiated using either HONO or H_2O_2 as the OH precursor. HONO was generated by adding a 1% $NaNO_2$ aqueous solution dropwise into a flask containing 30% sulfuric acid and then flushed into the chamber using dry purified air. H_2O_2 (50%) was added to the chamber by passing dry purified air over a heated impinger containing a known amount of the compound. Photolysis of the OH precursor was initiated by turning on all the lamps for several hours.

Several analytical instruments were used continuously throughout the experiments. The concentration of naphthalene was monitored using FTIR spectroscopy. The spectra were collected at a resolution of 1 cm^{-1} by co-adding 300 scans over

approximately 5 min. The concentrations of NO_x and O_3 were measured (1 minute time resolution) using a chemiluminescence NO_x analyser (Thermo model 42*i*) and UV photometric O_3 analyser (Thermo model 49*i*). The formation and evolution of particles in the range 10-470 nm was monitored with 3 min time resolution using a scanning mobility particle sizer (SMPS 3080, TSI). The sheath and aerosol sampling flow were 5.0 dm^3 min^{-1} and 0.5 dm^3 min^{-1}, respectively. The volume concentration of the particles was converted to mass concentration using a particle density of 1.48 g cm^{-1} (Chan et al. 2009). The wall loss rates of naphthalene and the SOA formed were determined after the lamps had been switched off and found to obey first order kinetics. The wall losses of both naphthalene and the SOA have been corrected in the data evaluation.

The ATOFMS was connected directly to the chamber with ¼″ stainless steel tubing. Particles generated in the simulation chamber from the photooxidation of naphthalene were expected to exhibit homogeneous composition. However, with long sampling times, some ambient particles entered the chamber through diffusion. Thus, when analysing the data, EDAM ENCHILADA (Environmental Chemistry through Intelligent Atmospheric Data Analysis, http://www.cs.carleton.edu/enchilada), was used to separate background particles from the SOA using the *K*-means algorithm (Gross et al. 2010). The spectra were averaged over 5 min and 1 h intervals. In all experiments described here, peak detection was carried out up to ± 800 Da using threshold values of peak height > 5 units, area > 6 square units and contribution more than 0.00001 of the total peak area (Gross et al. 2006).

3.3 Results and Discussion

Denuder and filter extracts were subjected to a number of derivatization procedures and analysed using GC-MS in order to identify the gas- and particle-phase photooxidation products of naphthalene. Wherever possible, the products were identified by comparing the retention times and mass spectra with those obtained from authentic standards. For reaction products that were not commercially available, identification was based upon careful interpretation of the mass spectra and the use of mass spectral libraries, whilst taking into account the results from previous studies (Bunce et al. 1997; Sasaki et al. 1997; Lee et al. 2009; Kautzman et al. 2010).

3.3.1 PFBHA Derivatization

PFBHA derivatization of denuder and filter extracts followed by GC-MS analysis was performed in an effort to identify carbonyls produced from the photooxidation of naphthalene. Typical selected ion chromatograms (*m/z* 181) for denuder (gas phase species) and filter (particle phase) extracts are shown in **Figure 3.11**.The six carbonyl products identified are listed in **Table 3.3**. Three of the main products - glyoxal, phthaldialdehyde and 2-formylcinnamaldehyde - were detected in both the gas- and particle-phases, while 1,4-naphthoquinone, 2-formylcinnamic acid, and 2,3-Epoxy-2,3-dihydro-1,4-naphthoquinone were only observed in the particle phase. All of these species have been detected in previous studies and mechanisms for their formation have been proposed (Lee et al. 2009; Kautzman et al. 2010). The observation of 2-formylcinnamic acid only in the particle phase is consistent with previous studies, and lends further support to the assertion that this product is generated via reaction of 2-formylcinnamaldehyde in the particle-phase (Kautzman et al. 2010). However, the observation of 1,4-naphthoquinone only in the particle phase is not in agreement with Mihele et al. (Mihele et al. 2002), who reported that this species, when underivatized, appeared predominantly in the gas-phase. Finally, although glyoxal has been previously observed in SOA generated from monoaromatic hydrocarbons (Temime et al. 2007; Healy et al. 2008), this is the first study to show that this volatile species undergoes partitioning to the particle-phase during naphthalene photooxidation. This observation suggests that glyoxal may be involved in the formation and growth of naphthalene SOA.

A large number of un-derivatized reaction products were also identified in the denuder and filter extracts. Typical total ion chromatograms for denuder (gas phase species) and filter (particle phase) extracts are shown in **Figure 3.11**. A total of 9 products were identified including the un-derivatized carbonyls, 1,4-naphthoquinone, and 2-formylcinnamaldehyde, along with a range of phenolic and nitro compounds, listed in **Table 3.4**. All of these products have been detected in previous studies of naphthalene photooxidation. Phthalic acid, which is probably produced from hydrolysis of phthalic anhydride in either the gas- or particle-phase, was only detected in the particle-phase. The observation of 2-naphthol only in the particle-phase is also consistent with the results of Mihele et al. (Mihele et al. 2002) who reported that phenolic compounds were found mainly in the particle-phase.

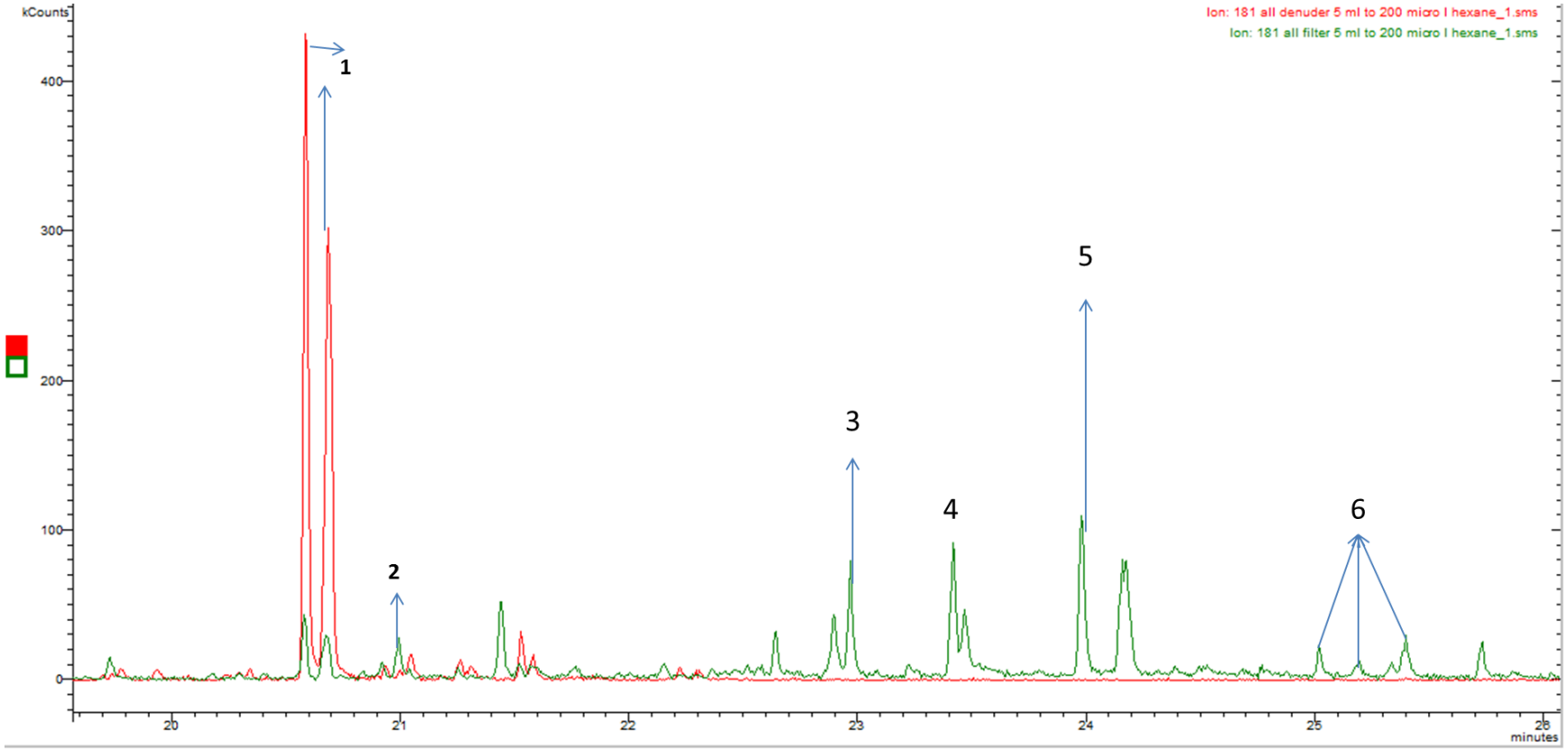
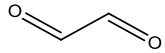
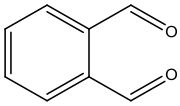
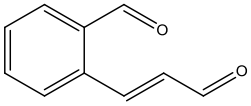
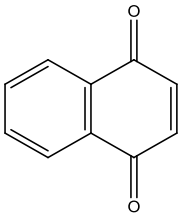
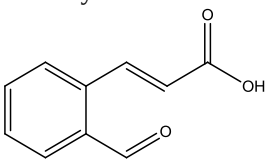
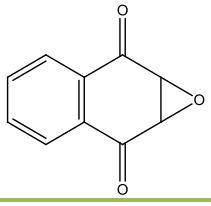


Figure 3.11 Selected ion chromatograms (*m/z* 181) of denuder (red) and filter (green) extracts obtained during the photooxidation of naphthalene and derivatized by PFBHA.

1) glyoxal, 2) phthaldialdehyde, 3) 2-formylcinnamaldehyde, 4) 1,4-naphthoquinone, 5) 2-formylcinnamic acid, 6) 2,3-Epoxy-2,3-dihydro-1,4-naphthoquinone.

Table 3.3 Gas- and particle phase carbonyl products identified by PFBHA derivatization GC-MS (*m/z* 181) during the photooxidation of naphthalene.

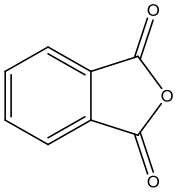
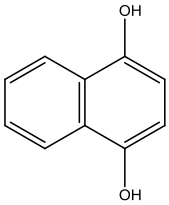
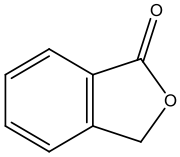
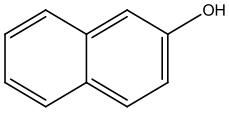
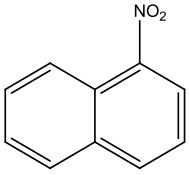
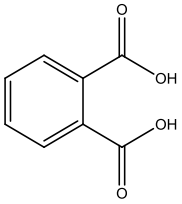
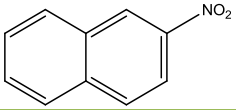
Compound	RT (min)	M*	Peaks	Phase#	Reference
Glyoxal 	20.99	448	448(M), 181	G/P	f
Phthaldialdehyde 	20.58	329	77, 105, 132, 329 (M)	G/P	a, c, d, e, f
2-Formylcinnamaldehyde 	22.96, 23.97	355	77, 103, 133, 181, 160, 327, 355(M)	P	a, b, c, d, e
1,4-Naphthoquinone 	23.42	353	353(M), 324, 181	P	a, b, c, d, e
2-Formylcinnamic acid 	24.05	371	181, 148, 133, 371(M)	P	a, c, e
2,3-Epoxy-2,3-dihydro-1,4-naphthoquinone 	25.01, 25.19, 25.40	369	133, 181, 325, 369(M)	P	a, d, e

** M. is the molecular weight of the oxime derivative*

 # G:gas-phase, P:particle-phase

References: (a) Bunce et al. 1997,(b) Sasaki et al. 1997, (c) Mihele et al. 2002, (d) Lee et al. 2009,(e) Kautzman et al. 2010,(f) Nishino et al. 2009a.

Table 3.4 Gas- and particle-phase products identified by GC-MS (total ion chromatogram) during the photooxidation of naphthalene.

Compound	RT(min)	M*	Peaks	Phase#	Reference
Phthalic anhydride 	13.38	148	76, 104, 148(M)	P	a,b,e
1,4-Naphthalenediol 	13.78	160	103, 116, 146, 159(M-1)	G/P	
Phthalide 	13.86	134	133(M-1), 105, 77	G/P	a,d
2-Naphthol 	16.10	144	144(M), 115, 89	P	a,b,c,d,e
1-Nitronaphthalene 	17.38	173	127, 146, 173(M)	G/P	a,b,c,d,e
Phthalic acid 	17.53	166	77, 105, 133, 147(M-17)	P	a,e
2-Nitronaphthalene 	19.83	173	173, 143, 158(M)	G/P	a,b,c,d,e

** M. is the molecular weight; # G:gas-phase, P:particle-phase*

References: (a) Bunce et al. 1997,(b) Sasaki et al. 1997, (c) Mihele et al. 2002, (d) Lee et al. 2009,(e) Kautzman et al. 2010,(f) Nishino et al. 2009a.

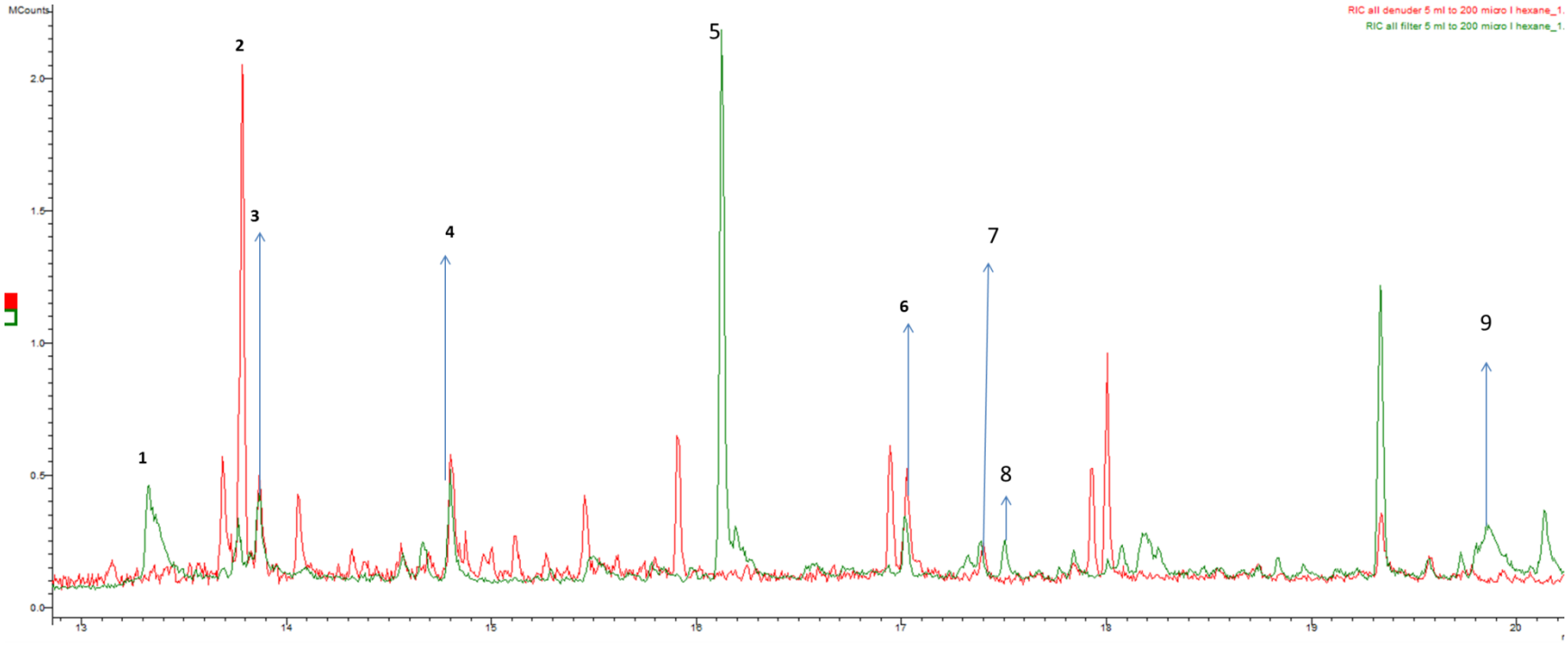


Figure 3.12 Total ion chromatograms of denuder (red) and filter (green) extracts obtained during the photooxidation of naphthalene. The products are not derivatized by PFBHA.

1) phthalic anhydride, 2) 1,4-naphthalenediol, 3) phthalide, 4) 1,4-naphthoquinone, 5) 2-naphthol, 6) 2-formylcinnamaldehyde, 7) 1-nitronaphthalene, 8) phthalic acid, 9) 2-nitronaphthalene.

3.3.2 Quinone Derivatization

Denuder and filter extracts were analysed for the presence of 1,2-naphthoquinone and 1,4-naphthoquinone using the derivatization method of Cho et al. (Cho et al. 2004). Mechanisms for the formation of these quinones have been proposed by Lee and Lane (Lee et al. 2009), who identified them as naphthalene oxidation products in both gas- and particle-phases. The results obtained in this study are shown in **Figure 3.13** and indicate that 1,2-naphthoquinone and 1,4-naphthoquinone are produced with similar abundance in the gas-phase, but the latter compound undergoes a greater amount of transfer to the particle phase. This observation is consistent with the vapour pressure calculations of Jakober (Jakober et al. 2007) who determined values of 1.4×10^{-3} Torr for 1,2-naphthoquinone and 1.8×10^{-4} Torr for 1,4-naphthoquinone. However, the results are in contrast to the findings of Lee and Lane who reported a greater abundance of 1,2-naphthoquinone in the particle phase. Both quinones have been identified and quantified in diesel exhaust and ambient air (Cho et al. 2004; Chung et al. 2006; Valavanidis et al. 2006; Eiguren-Fernandez et al. 2008) with 1,2-naphthoquinone generally exhibiting greater partitioning to the particle phase. In view of the known toxicity of the naphthoquinones (Kumagai et al. 2012), it is suggested that additional work should be carried out to resolve the apparent discrepancies concerning their gas-particle partitioning.

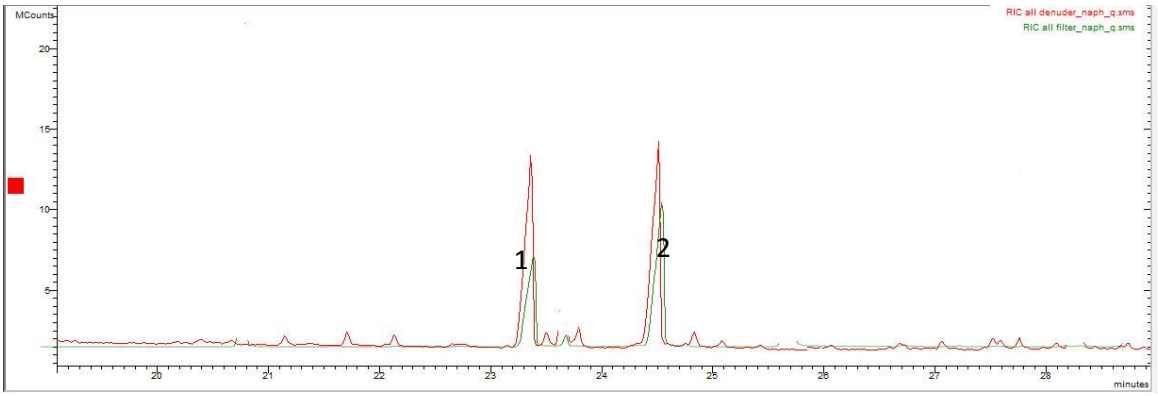


Figure 3.13 Total ion chromatograms of denuder (red) and filter (green) extracts obtained during the photooxidation of naphthalene and derivatized by the method of Cho et al. (Cho et al. 2004). *1) 1,2-naphthoquinone, 2) 1,4-naphthoquinone.*

3.3.3 PFBBr Derivatization

PFBBr derivatization of denuder and filter extracts followed by GC-MS analysis was

performed in an effort to identify hydroxyl-containing species produced from the photooxidation of naphthalene. Typical selected ion chromatograms (*m/z* 181) for denuder (gas phase species) and filter (particle phase) extracts are shown in **Figure 3.14**. A total of 8 species were identified and are listed in **Table 3.5**. The products include a number of phenols and carboxylic acids, which apart from nitrobenzoic acid have all been detected in previous studies of naphthalene photooxidation (Lee et al. 2009; Kautzman et al. 2010). Benzoic acid is present as a large peak in the denuder extract, but was also detected in denuder blanks and is likely a contaminant in the XAD-4 or generated in the derivatization process. Nitrobenzoic acid was not observed in previous studies and it is also likely that this species is an artefact, possibly produced from the nitration of benzoic acid during the sampling and/or derivatization process.

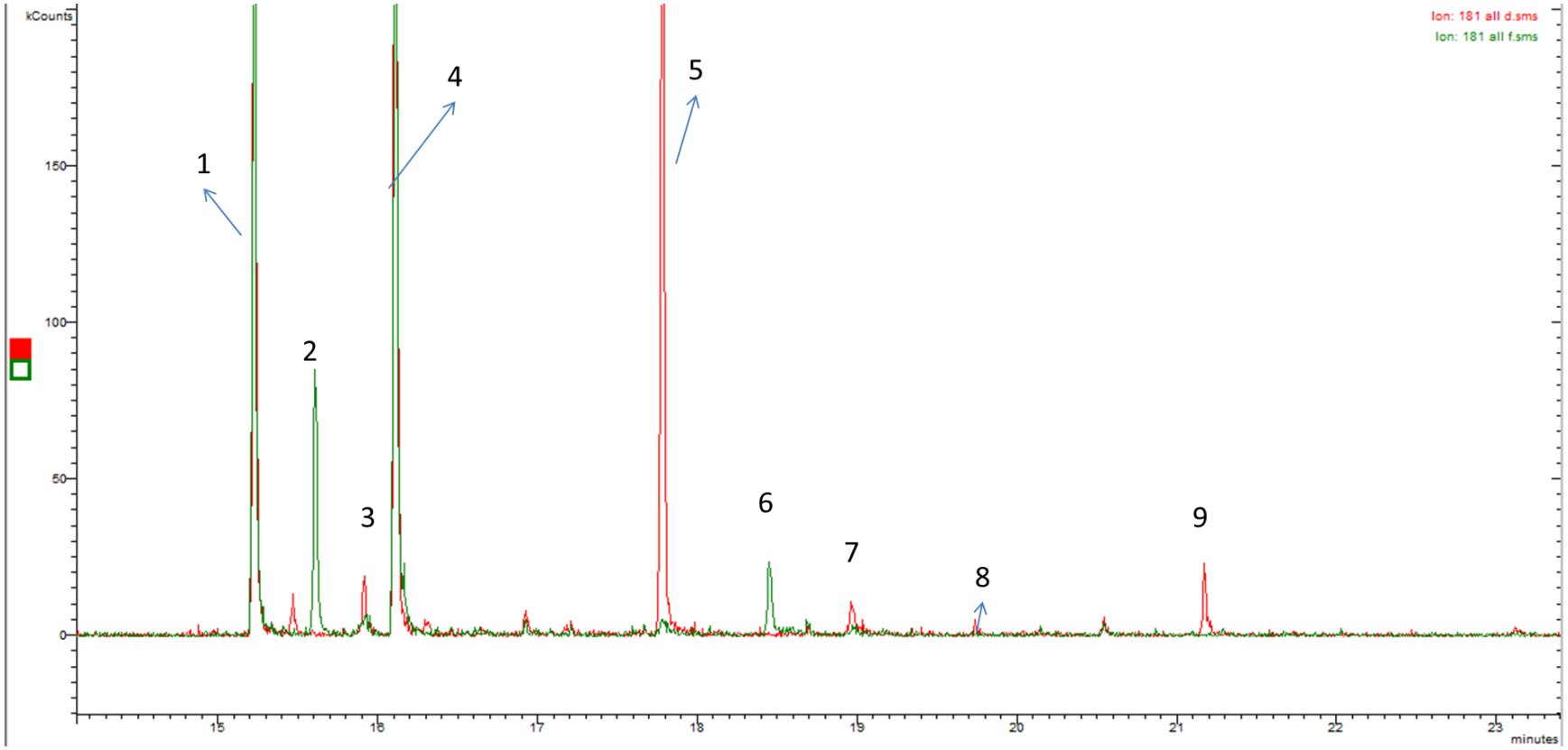
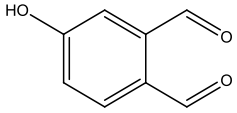
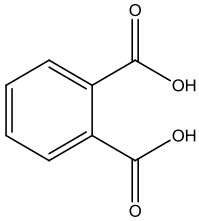
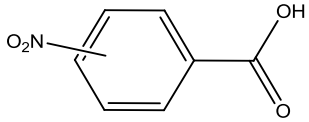
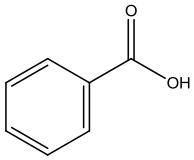
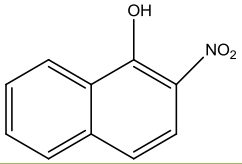


Figure 3.14 Selected ion chromatograms (*m/z* 181) of denuder (red) and filter (green) extracts obtained during the photooxidation of naphthalene and derivatized by PFBBr.

1) unreacted PFBBr, 2) hydroxyphthaldialdehyde, 3) phthalic acid, 4) nitrobenzoic acid, 5) benzoic acid, 6) 2-nitro-1-naphthol, 7) o-carboxycinnamic acid, 8) 2-formylcinnamic acid, 9) 1-naphthol.

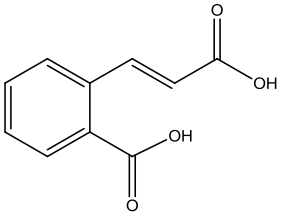
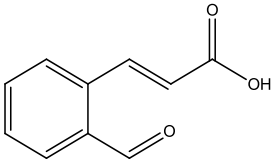
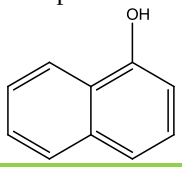
Table 3.5 Gas- and particle-phase products identified by PFBBr derivatization GC-MS (*m/z* 181) during the photooxidation of naphthalene.

Compound	RT (min)	M*	Peaks	Phase[#]	Reference
Hydroxyphthaldialdehyde 	15.60	330	329 (M-1), 297, 181	P	e
Phthalic acid 	15.91	347(single), 528(double)	346(M-1), 181, 133, 107	G/P	a,e
Nitrobenzoic acid 	16.07	347	181, 285(M-62), 347 (M)	G/P	
Benzoic acid 	17.78	302	77, 105, 302(M)	P	e
2-Nitro-1-naphthol 	18.50	370	369(M-1), 327, 181	P	a,b,d,e

** M. is the molecular weight of the derivative; # G:gas-phase, P:particle-phase*

References: (a) Bunce et al. 1997,(b) Sasaki et al. 1997, (c) Mihele et al. 2002, (d) Lee et al. 2009,(e) Kautzman et al. 2010,(f) Nishino et al. 2009a.

(Continued) Table 3.5 Gas- and-particle phase products identified by PFBBr derivatization GC-MS (*m/z* 181) during the photooxidation of naphthalene.

Compound	RT (min)	M*	Peaks	Phase#	Reference
o-Carboxycinnamic acid 	18.96	373(single), 554(double)	181, 356, 372(M-1)	G/P	e
2-Formylcinnamic acid 	19.75	357	356(M-1), 329(M-28), 301, 181, 133, 105	G	a,c,e
1-Naphthol 	21.17	324	324(M), 181, 143	P	a,b,c,d,e

** M. is the molecular weight of the derivative; # G:gas-phase, P:particle-phase*

References: (a) Bunce et al. 1997,(b) Sasaki et al. 1997, (c) Mihele et al. 2002, (d) Lee et al. 2009,(e) Kautzman et al. 2010,(f) Nishino et al. 2009a.

3.3.4 BSTFA Derivatization

BSTFA derivatization of denuder and filter extracts followed by GC-MS analysis was performed in an effort to identify hydroxyl-containing products from the photooxidation of naphthalene. Typical selected ion chromatograms (*m/z* 73) for denuder (gas phase species) and filter (particle phase) extracts are shown in **Figure 3.11**. The fifteen products identified are listed in **Table 3.6**. Apart from phthalic acid methyl ester, all of these products have been identified in previous studies (Lee et al. 2009; Kautzman et al. 2010). The products detected by BSTFA derivatization are mainly acids derived from the principal carbonyl products, 2-formylcinnamaldehyde and phthaldialdehyde. The formation mechanisms for these compounds remain somewhat speculative but are basically oxidation reactions that may occur in both gas and particle phases (Kautzman et al. 2010).The identification of these species is potentially useful since they can be used as markers for naphthalene SOA in ambient organic aerosol. Kautzman et al. (Kautzman et

al. 2010) compared laboratory and urban aerosol samples and concluded that phthalic acid, hydroxyphthalic acid and 4-nitro-1-naphthol could all be considered as potential markers for naphthalene SOA in ambient particles.

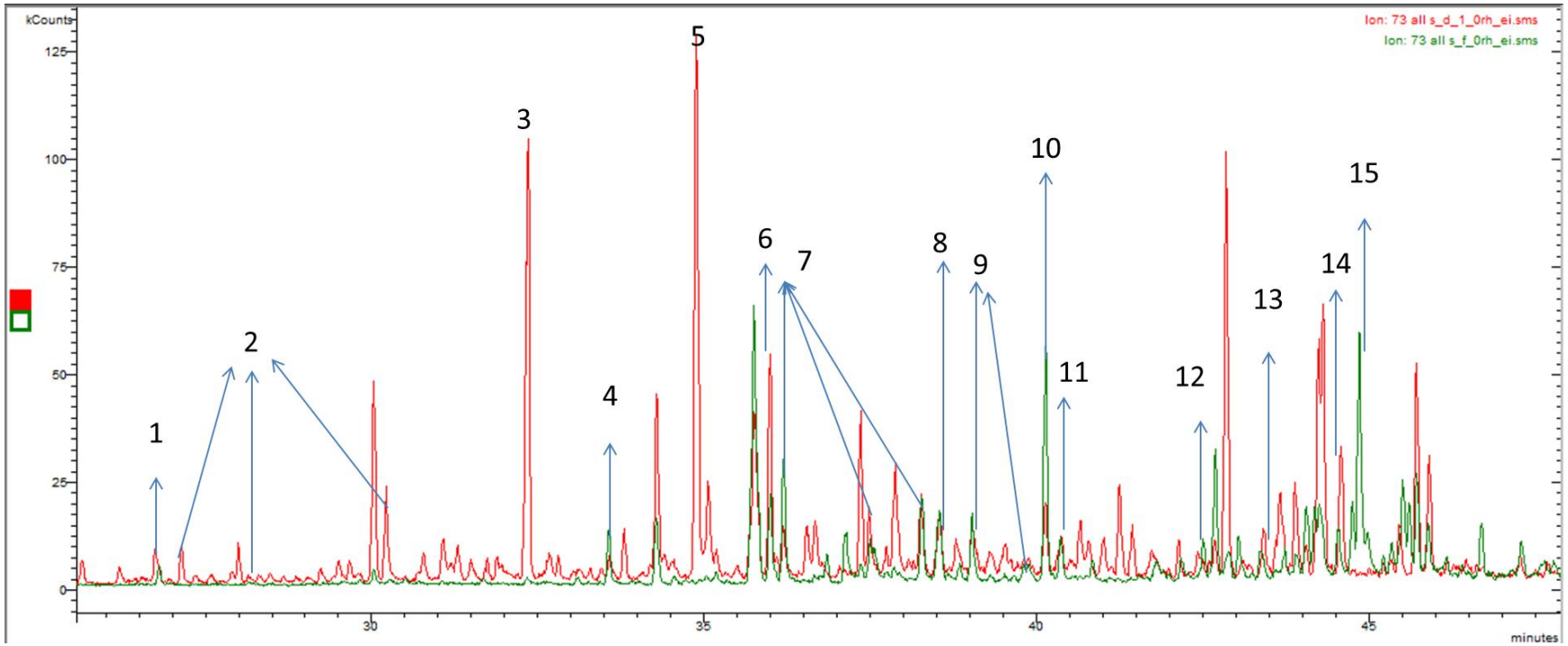
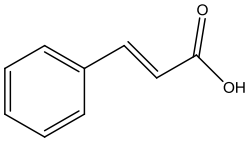
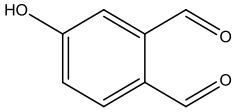
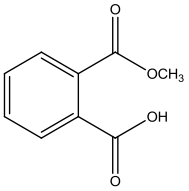
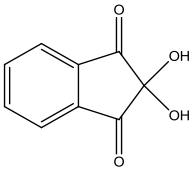
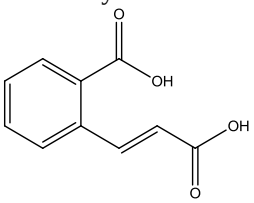
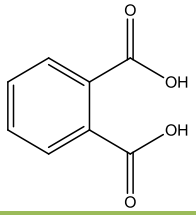


Figure 3.15 Selected ion chromatograms (*m/z* 73) of denuder (red) and filter (green) extracts obtained during the photooxidation of naphthalene and derivatized by BSTFA.

1) Cinnamic acid, 2) hydroxyphthaldialdehyde, 3) phthalic acid methanol ester, 4) 1,2,3-indantrione, 5) o-carboxycinnamic acid (single derivative), 6) Phthalic acid, 7) 2-formylcinnamic acid, 8) dihydroxyphthalic acid, 9) 4-hydroperoxynaphthalen-1-ol, 10) 4-hydroxy-4,4a-dihydronaphthalen-1(8aH)-one, 11) dihydroxynitrobenzene, 12) 2,3-dihydroxy-1,4-naphthoquinone, 13) o-carboxycinnamic acid (double derivative), 14) 2-nitro-1-naphthol (isomer), 15) 2,5-dihydroxycinnamic acid.

Table 3.6 Gas- and particle-phase products identified by BSTFA derivatization GC-MS (*m/z* 73) during the photooxidation of naphthalene.

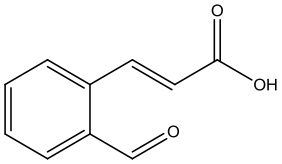
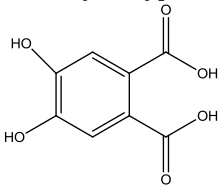
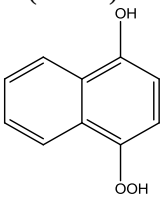
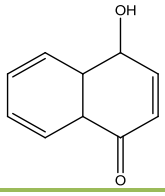
Compound	R.T.	M*	Peaks	Phase[#]	Reference
Cinnamic acid 	26.75	220	77, 103, 131, 161, 205, 220(M)	G/P	a,b,e
Hydroxyphthaldialdehyde 	27.13, 28.00, 30.23	222	73, 77, 105, 133, 163, 207, 222(M)	G/P	e
Phthalic acid methanol Ester 	32.31	252	73, 77, 133, 163, 237, 252(M)	G/P	
1,2,3-Indantrione 	33.72	250	73, 147, 193, 223, 250(M)	G/P	d
o-Carboxycinnamic acid 	34.80	264(single)	73, 131, 161, 220, 233, 249, 264 (M)	P	e
Phthalic acid 	36.02	238(single) 310(double)	73, 91, 105, 147, 221, 237, 251, 265, 295(M-15), 310(M)	G/P	a,e

** M. is the molecular weight of the TMS derivative*

[#] G:gas-phase, P:particle-phase

References: (a) Bunce et al. 1997,(b) Sasaki et al. 1997, (c) Mihele et al. 2002, (d) Lee et al. 2009,(e) Kautzman et al. 2010,(f) Nishino et al. 2009a.

(continued) Table 3.6 Gas- and particle phase products identified by BSTFA derivatization GC-MS (*m/z* 73) during the photooxidation of naphthalene.

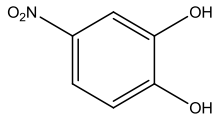
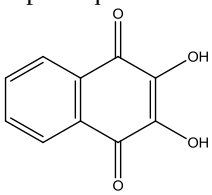
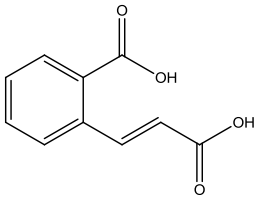
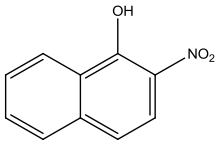
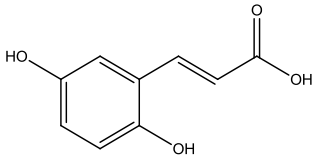
Compound	R.T	M*	Peaks	Phase[#]	Reference
2-Formylcinnamic acid 	36.20, 38.20	248	73, 103, 131, 159, 177, 248 (M)	G/P	a,c,e
4,5-Dihydroxyphthalic acid 	38.60	270(single), 342 (double),414 (triple), 486	73, 147, 193, 221, 265, 295, 383(M-103), 486(M-30)	G/P	e
4-hydroperoxynaphthalen-1-ol (isomer) 	39.00, 39.70	248	73, 115, 147, 217, 232, 248(M)	G/P	e
4-Hydroxy-4,4a-dihydronaphthalen-1(8aH)-one 	40.20	234	73, 75, 147, 217, 233(M-1)	G/P	e

** M. is the molecular weight of the TMS derivative*

[#] G:gas-phase, P:particle-phase

References: (a) Bunce et al. 1997,(b) Sasaki et al. 1997, (c) Mihele et al. 2002, (d) Lee et al. 2009,(e) Kautzman et al. 2010,(f) Nishino et al. 2009a.

(continued) Table 3.6 Gas- and particle phase products identified by BSTFA derivatization GC-MS (*m/z* 73) during the photooxidation of naphthalene.

Compound	R.T.	M*	Peaks	Phase[#]	Reference
4-Nitrobenzene-1,2-diol 	40.43	299	73, 75, 206, 262, 285, 299(M-1)	G/P	e
2,3-Dihydroxy-1,4-naphthoquinone 	42.63	334	73, 217, 262, 289, 307, 334(M)	G/P	e
o-Carboxycinnamic acid 	43.52	336 (double)	147, 191, 221, 280, 321, 336(M)	G/P	e
2-nitro-1-naphthol 	44.51, 44.62	261	73, 199, 229, 246, 261(M)	G/P	a,b,c,d,e
2,5-dihydroxyphenyl acrylic acid 	44.92	396	191, 203, 218, 232, 246, 321, 336, 351(M-45),381, 396(M)	P	e

** M. is the molecular weight of the TMS derivative*

[#] G:gas-phase, P:particle-phase

References: (a) Bunce et al. 1997,(b) Sasaki et al. 1997, (c) Mihele et al. 2002, (d) Lee et al. 2009,(e) Kautzman et al. 2010,(f) Nishino et al. 2009a.

As indicated in Chapter 2, higher yields of naphthalene SOA were observed as the relative humidity was increased. The results indicated that water may promote SOA formation and growth by conversion of photooxidation products into less volatile compounds via reaction in the gas or particle phase. In order to investigate this further, BSTFA derivatization was performed on filter extracts obtained from photooxidation experiments performed using virtually identical starting concentrations of naphthalene and NO_x but with the relative humidity at <1% and ca. 50%. The resulting chromatograms are shown in **Figure 3.16** and resemble each other very closely. However, the intensity of most of the peaks attributed to carboxylic acids appear to be slightly higher in the particles collected at RH 50%, suggesting that enhanced formation of carboxylic acids may contribute to the observed increase in SOA yields at higher RH. Further tests, including on-line chemical analysis, should be performed to confirm this hypothesis.

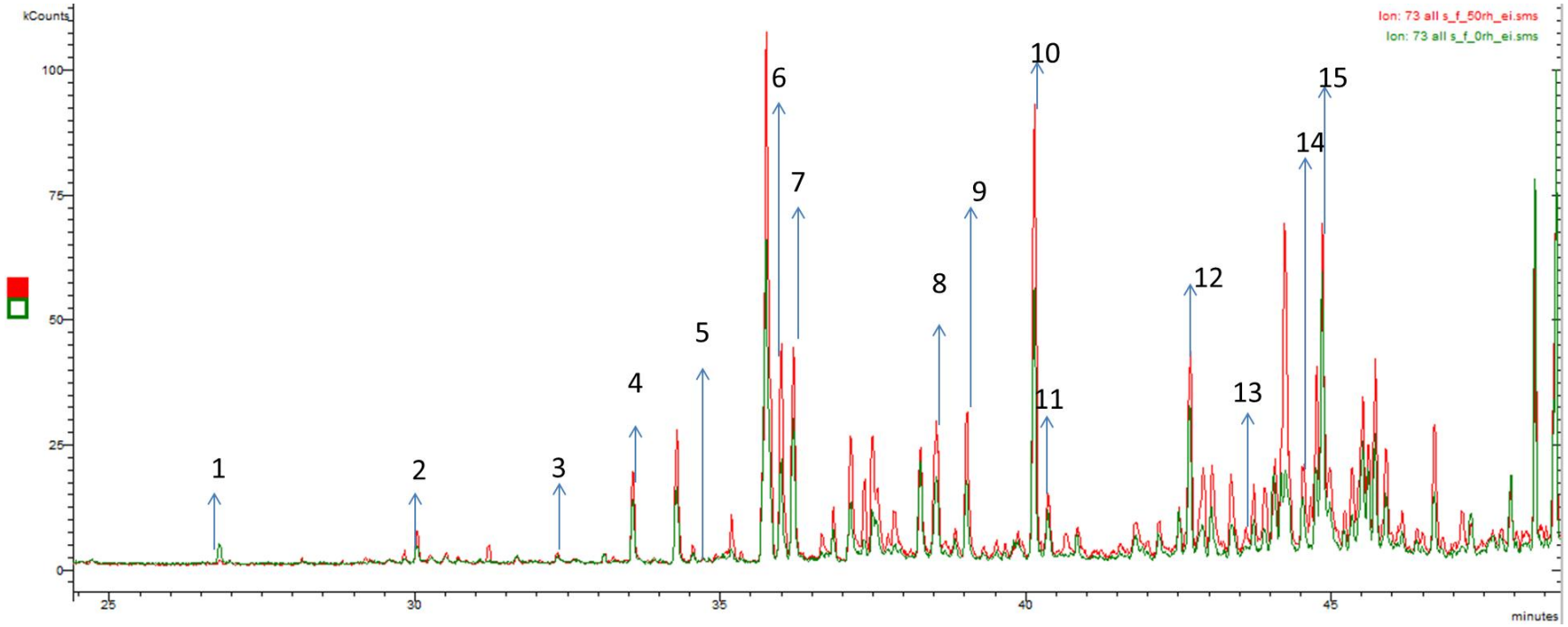


Figure 3.16 Selected ion chromatograms (*m/z* 73) of filter extracts obtained during the photooxidation of naphthalene at RH <1% (green) and RH 50% (red) and derivatized by BSTFA.

1) Cinnamic acid, 2) hydroxyphthaldialdehyde, 3) phthalic acid methanol ester, 4) 1,2,3-indantrione, 5) o-carboxycinnamic acid (single derivative), 6) Phthalic acid, 7) 2-formylcinnamic acid, 8) dihydroxyphthalic acid, 9) 4-hydroperoxynaphthalen-1-ol, 10) 4-hydroxy-4,4a-dihydronaphthalen-1(8aH)-one, 11) 4-Nitrobenzene-1,2-diol, 12) 2,3-dihydroxy-1,4-naphthoquinone, 13) o-carboxycinnamic acid (double derivative), 14) 2-nitro-1-naphthol (isomer), 15) 2,5-dihydroxycinnamic acid.

3.3.5 On-line Analysis of SOA using ATOFMS

The composition of naphthalene SOA was further investigated using ATOFMS for on-line analysis in a series of photooxidation experiments in the 3.9 m^3 simulation chamber at University College Cork. Experiments were performed in the absence of seed aerosol using different OH radical precursors and at different relative humidity, **Table 3.7**. A lower laser power density was explored to minimise fragmentation and thus retain as much molecular information as possible (Fang et al. 2011).

Table 3.7 Experimental conditions and results from the photooxidation of naphthalene using ATOFMS.

Conc.(ppbV)	OH precursor	HC/NO_x	RH(%)	SOA yield (%)
300	H_2O_2	-	~50	11.4
300	H_2O_2	-	0-5	8.0
300	HONO	2.95	0-5	9.1
300	HONO	3.10	~50	12.3

3.3.5.1 Effect of OH Precursor

Average mass spectra of naphthalene SOA formed using H_2O_2 and HONO as OH precursors are shown in **Figure 3.17** and **Figure 3.18**, respectively. The ions, possible structures and parent species are summarized in **Table 3.8**. These peaks indicate that the major products include 2-formylcinnamaldehydye, phthaldialdehyde and nitronaphthalenes (Kautzman et al. 2010).

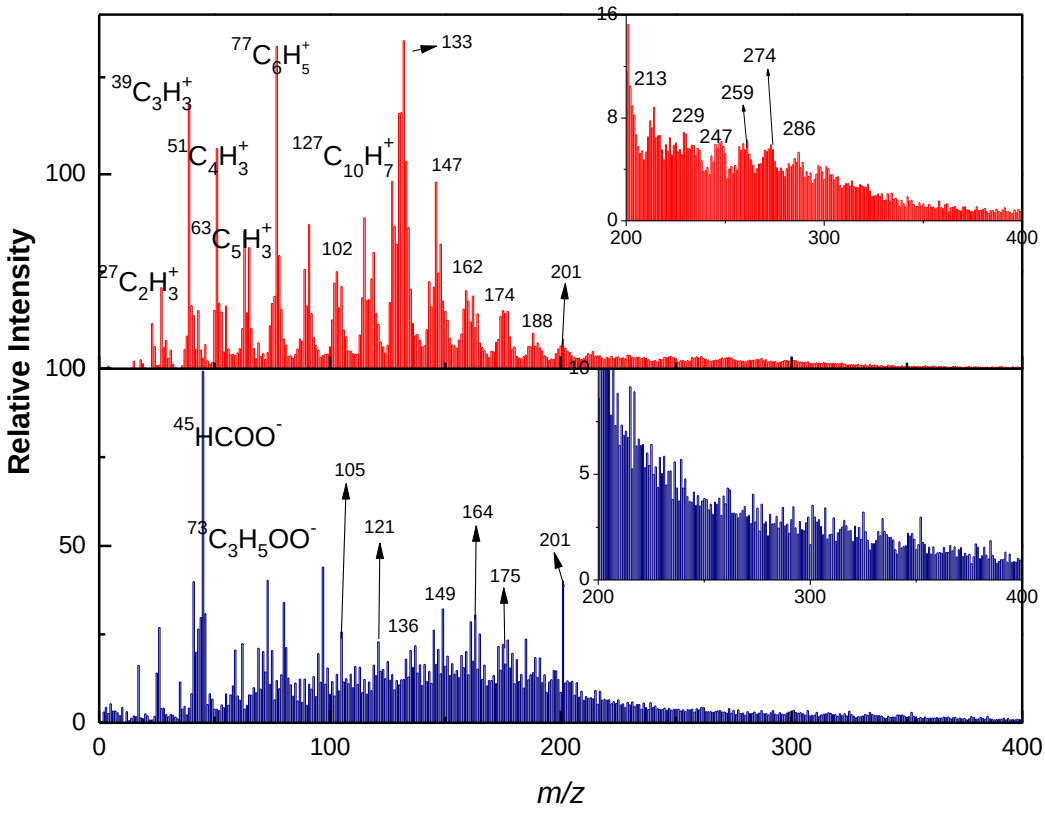


Figure 3.17 Average positive (top) and negative (bottom) ion mass spectra of SOA formed from the photooxidation of naphthalene using H_2O_2 as OH precursor at RH <5%.

The positive ion mass spectra obtained using the different precursors are very similar, exhibiting signals for hydrocarbon fragments and a molecular ion for naphthalene (*m/z* 128). The ions observed at *m/z* 39, 51, 77 are aromatic fragments, while peaks larger than *m/z* 133 can be attributed to products such as phthaldialdehyde, phthalide, 2-formylcinnamaldehyde, nitronaphthalenes and naphthols, as well as their derivatives. The larger fragments with *m/z* over 200 could possibly be due to oligomers.

The negative ion mass spectra obtained using the two OH precursors are noticeably different. The spectra obtained during the H_2O_2 experiments are dominated by the oxidized organic fragment at *m/z* -45, assigned to $HCOO^-$ and also contain peaks that may be attributed to a number of possible oxidation products, **Table 3.8**. In contrast, the

negative ion spectra obtained during the HONO experiments contain strong signals due to nitrate (*m/z* -46, -62), sulfate (*m/z* -80, -97) and carbon-nitrogen adducts (*m/z* -26, -42), indicating that the nitrogen oxides and sulfuric acid present in the chamber due to HONO generation are involved in aerosol formation and quickly become internally mixed with the naphthalene SOA shortly after nucleation. The peaks in the range -100 to -200 are not as strongly clustered as in the positive ion mass spectra and exhibit a more continuous pattern, making the identification of individual oxidation products difficult. The larger fragments with *m/z* over 200 could possibly be due to oligomers.

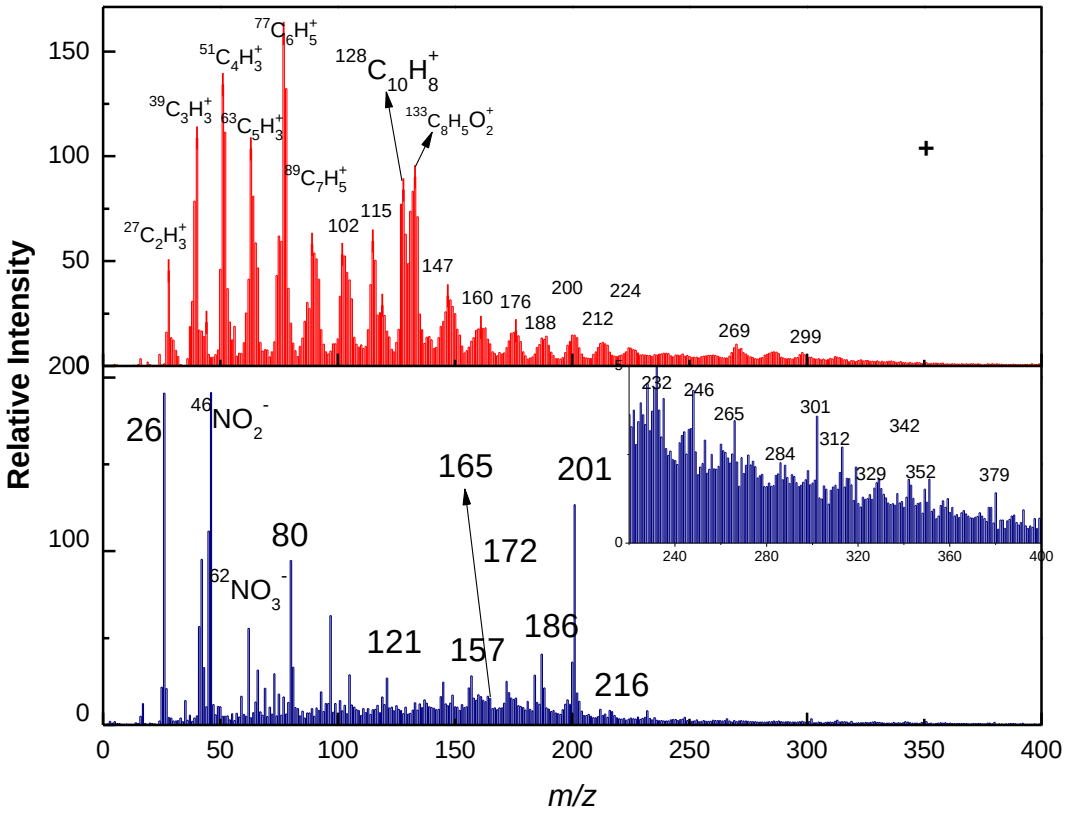
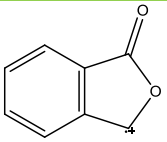
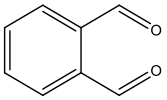
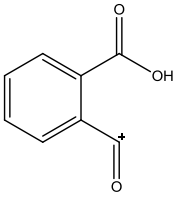
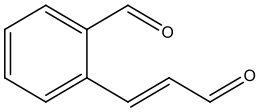
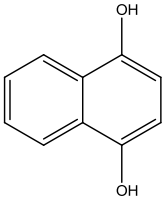
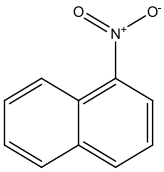
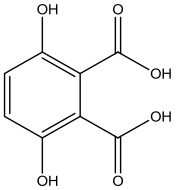
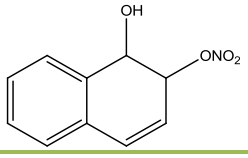
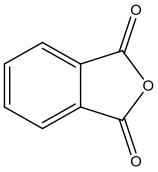
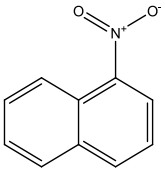
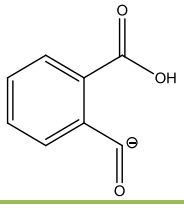


Figure 3.18 Average positive (top) and negative (bottom) ion mass spectra of SOA formed from the photooxidation of naphthalene using HONO as OH precursor at RH <5%.

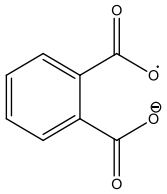
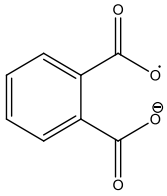
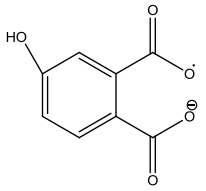
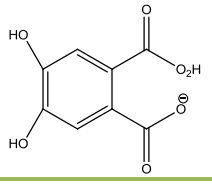
Table 3.8 Positive Ions and possible oxidation products observed by ATOFMS during the photooxidation of naphthalene.

m/z	Formula	Possible Structure	Possible Parent Molecule
133	$C_8H_5O_2^+$,		Phthalide
	$C_8H_5O_2^+$		Phthaldialdehyde
149	$C_8H_5O_3^+$		Phthalic acid
160	$C_{10}H_8O_2^+$		2-Formylcinnamaldehyde
	$C_{10}H_8O_2^+$		1,4-Naphthalenediol
173	$C_{10}H_8NO_2^+$		Nitronaphthalene (isomer)
197	$C_8H_6O_6$		Dihydroxyphthalic acid (isomer)
207	$C_{10}H_9NO_4$		2-Nitrate ester-1-naphthol

(Continued)Table 3.8 Negative ions and possible oxidation products observed by ATOFMS during the photooxidation of naphthalene.

m/z	Formula	Possible Structure	Possible Parent Molecule
-26	$C_2H_2^-$		Aromatic species
	CN^-		Nitrogenated product
-42	CNO^-		Nitrogenated product
-45	$HCOO^-$		Oxygenated product
-46	NO_2^{--}		Nitrate
-62	NO_3^{--}		Nitrate
-77	$C_6H_5^-$		Aromatic species
-80	SO_3^-		Sulfate
-97	HSO_4^-		Sulfate
-147	$C_8H_3O_3^-$		Phthalic anhydride
-157	$C_{10}H_7NO^-$		1-Nitronaphthalene (isomer)
-149	$C_8H_5O_3^-$		Phthalic acid

(Continued)Table 3.8 Negative ions and possible oxidation products observed by ATOFMS during the photooxidation of naphthalene.

m/z	Formula	Possible Structure	Possible Parent Molecule
-164	$C_8H_4O_4^-$		Phthalic acid
-165	$C_8H_5O_4^-$		Phthalic acid
-181	$C_8H_5O_5^-$		Hydroxyphthalic acid (isomer)
-213	$C_8H_5O_7^-$		4,5-dihydroxyphthalic acid (isomer)

3.3.5.2 Effect of Relative Humidity

Average mass spectra of naphthalene SOA formed using H_2O_2 and HONO as OH precursors at a relative humidity ca. 50% are shown in **Figure 3.19** and **Figure 3.20**, respectively. The spectra contain similar features as those obtained under dry conditions, except that the peak at *m/z* -45 exhibits a much higher relative intensity. This peak is attributed to $HCOO^-$, which is most likely produced from fragmentation of oxidised products such as carboxylic acids. A number of carboxylic acids have been identified in naphthalene SOA, including phthalic acid, 2-formylcinnamic acid and their hydroxylated derivatives (Kautzman et al. 2010). The results presented in the preceding section indicated that larger amounts of these species were present in naphthalene SOA formed at RH 50%, suggesting that enhanced formation of carboxylic acids may contribute to the observed increase in SOA yields at higher RH. The ATOFMS spectra thus provide further evidence to support this hypothesis.

The presence of oligomers in the SOA is confirmed by the appearance of peaks at almost every *m/z* in the range 200-500 in the negative ion mode. Oligomers are detected primarily in the negative ion mode because they are oxidised organics that readily undergo deprotonation during ionization (Denkenberger et al. 2007). The oligomeric peaks are much more prominent when H_2O_2 was used as the OH precursor and appear very quickly after the onset of nucleation. Signals at *m/z* > 200 in the negative ion mass spectra are much lower for the HONO system, indicating that oligomers might be formed less effectively in that case. Another possible explanation is that the presence of ions with low ionization energies, such as alkali metals or inorganic acids introduced during HONO generation, can suppress the detection of ions with higher ionization efficiencies, such as organic compounds during the desorption/ionization step (Reinard et al. 2008). This may cause a suppression of the signal intensity for oligomers in the HONO system. The relative intensity for the oligomer fragment ions (*m/z* >200) do not increase for either system, even after 6-7 hours of aging in the chamber. This is in contrast to the formation of oligomers in the 1,3,5-trimethylbenzene-NO_x system at PSI, which developed slowly but consistently over a period of 6-7 hours (Gross et al. 2006).

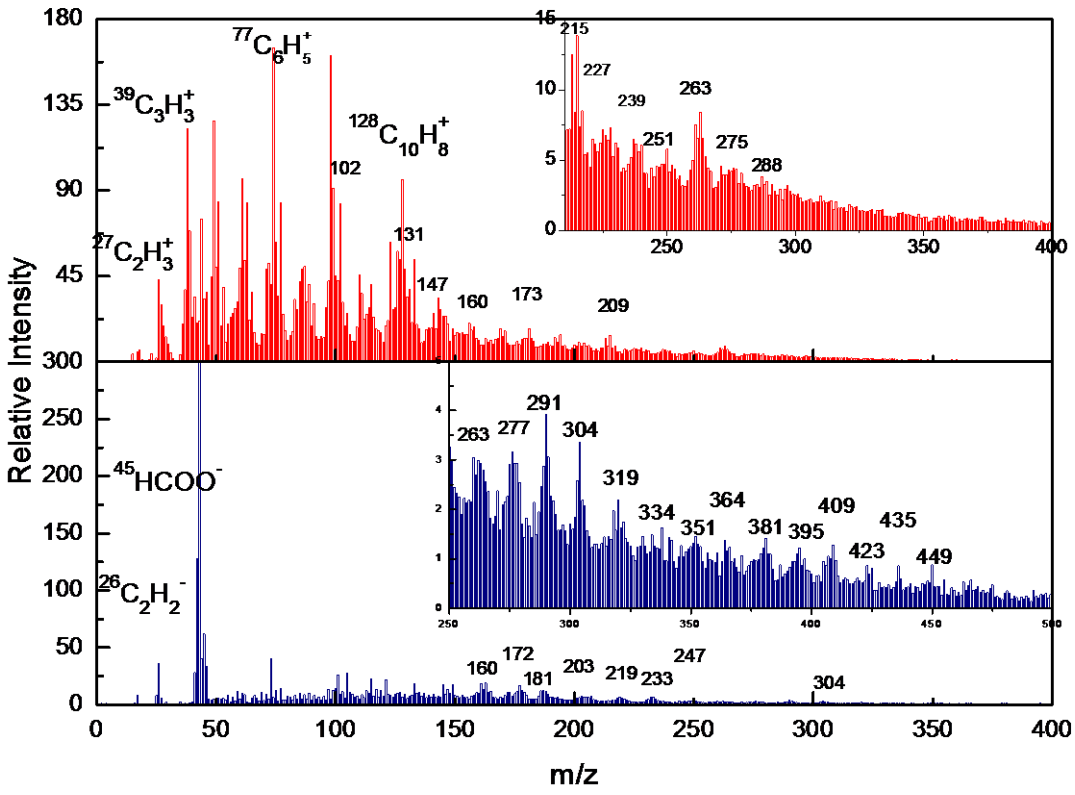


Figure 3.19 Average positive (top) and negative (bottom) ion mass spectra of SOA formed from the photooxidation of naphthalene using H_2O_2 as OH precursor at RH ca. 50%.

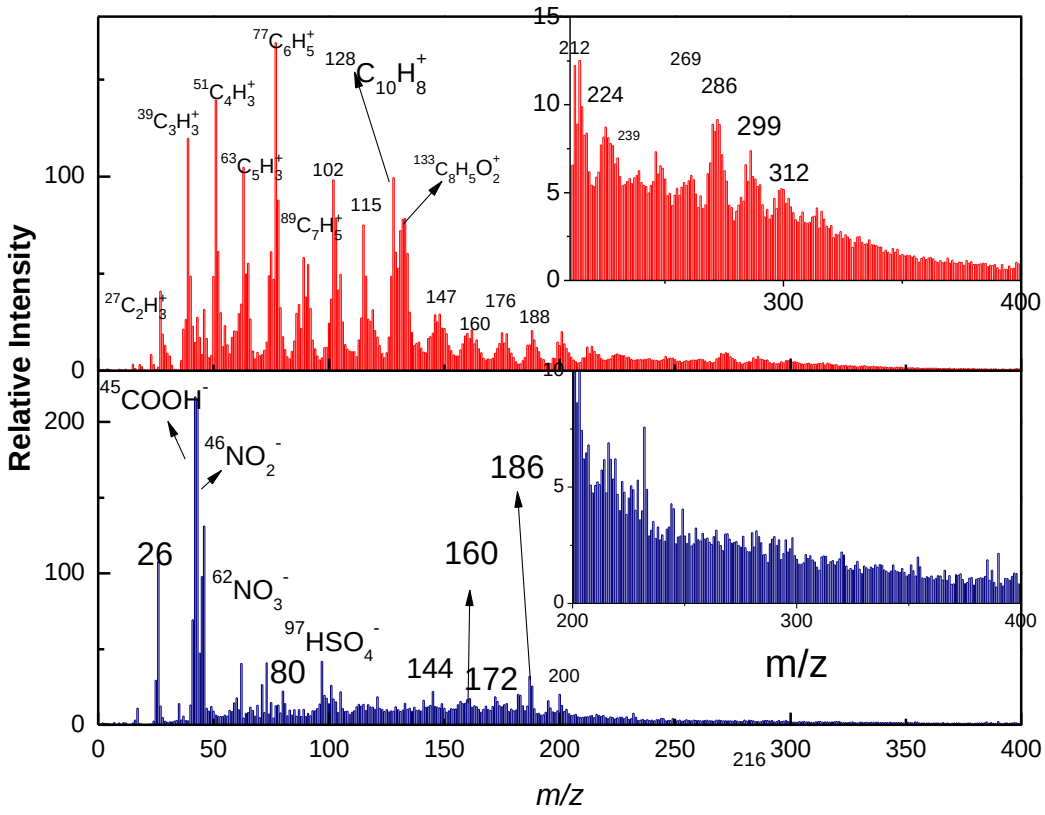


Figure 3.20 Average positive (top) and negative (bottom) ion mass spectra of SOA formed from the photooxidation of naphthalene using HONO as OH precursor at RH ca. 50%.

3.3.5.3 Chemical Evolution of SOA in the Photooxidation of Naphthalene

Due to a high temporal resolution, the ATOFMS is able to monitor the chemical evolution of SOA in chamber photooxidation experiments. Typical data obtained during the experiments performed using HONO as the OH precursor at different RH are shown **Figure 3.21** and **Figure 3.22**. In most cases, the relative ion intensity for the organic fragment ions does not change very much, indicating that the organic components of the aerosol do not change significantly from the time it was formed. However, there is a small and gradual increase observed for the peak at *m/z* -45 due to $HCOO^-$, even in the dark, suggesting that the amount of carboxylic acids in the SOA is slowly increasing with time. The peaks at *m/z* -46 and -62, due to nitrate, also appear to increase after the lights are turned off, possibly due to uptake of NO_2 or nitric acid by the SOA particles.

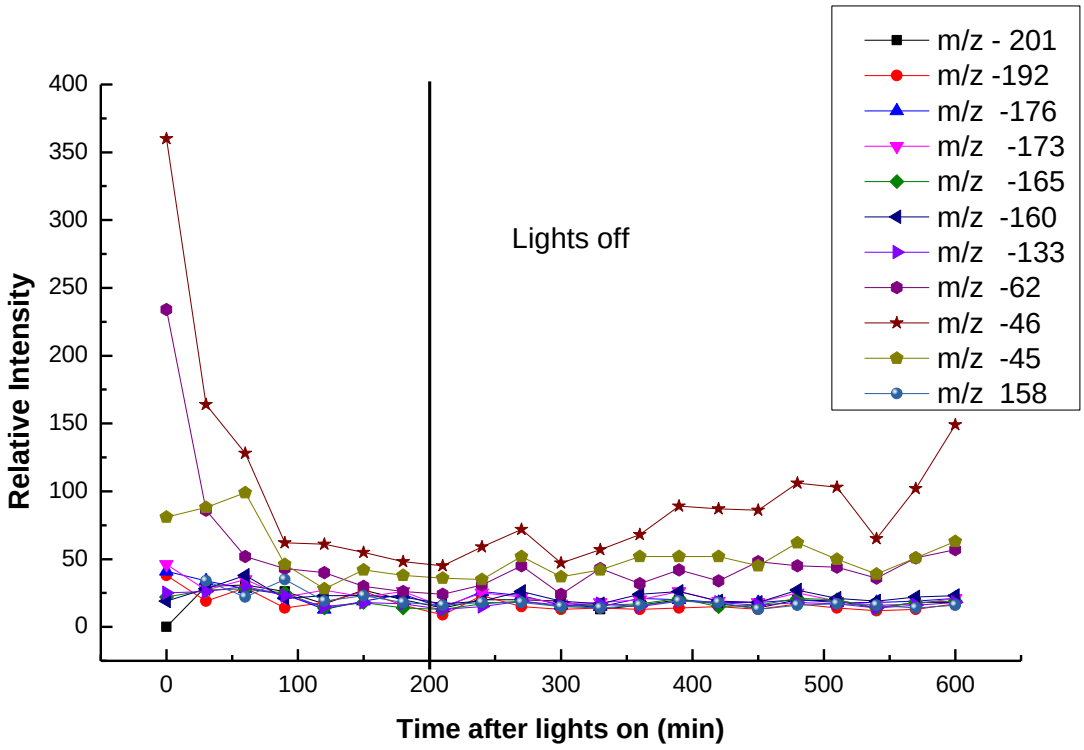


Figure 3.21 Temporal trend for selected ions observed by ATOFMS during the photooxidation of naphthalene using HONO as a precursor at RH <5%.

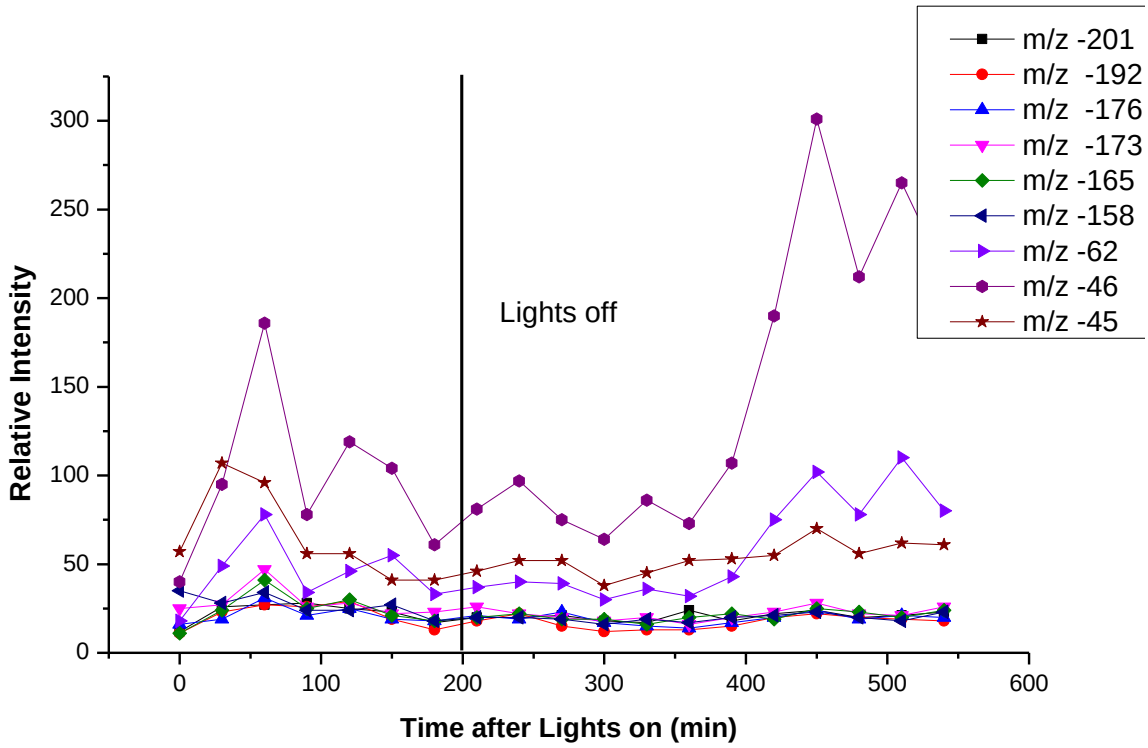


Figure 3.22 Temporal trend for selected ions observed by ATOFMS during the photooxidation of naphthalene using HONO as a precursor at RH ca. 50%.

3.4 Conclusions

A combination of off-line and on-line analytical methods has been employed to study the gas- and particle-phase photooxidation products of naphthalene. A denuder-filter sampling system combined with chemical derivatization and off-line analysis using GC-MS has been used to identify the products and investigate gas/particle partitioning. A wide range of carbonyls, nitro-compounds, phenols, carboxylic acids and quinones have been identified and the results are generally in agreement with previous studies. On-line analysis of the chemical composition of naphthalene SOA has been performed using ATOFMS for the first time. The mass spectra contained ions that could possibly be attributed to some of the major photooxidation products generated using both HONO and H_2O_2 as the OH precursor. There is also evidence for the formation of oligomers with MW in the range 200-500. The results of the off-line and on-line analyses indicate that larger amounts of carboxylic acids were present in naphthalene SOA formed at RH 50%, suggesting that enhanced formation of carboxylic acids may contribute to the observed increase in SOA yields at higher RH.

3.5 References

Atkinson, R. and J. Arey (2003). "Gas-phase tropospheric chemistry of biogenic volatile organic compounds: a review." Atmospheric Environment **37, Supplement 2**(0): 197-219.

Atkinson, R. and J. Arey (2007). "Mechanisms of the gas-phase reactions of aromatic hydrocarbons and PAHs with OH and NO_3 radicals." Polycyclic Aromatic Compounds **27**(1): 15-40.

Bunce, N. J., L. Liu, J. Zhu and D. A. Lane (1997). "Reaction of Naphthalene and Its Derivatives with Hydroxyl Radicals in the Gas Phase." Environmental Science & Technology **31**(8): 2252-2259.

Chan, A. W. H., K. E. Kautzman, P. S. Chhabra, J. D. Surratt, M. N. Chan, J. D. Crounse, A. Kurten, P. O. Wennberg, R. C. Flagan and J. H. Seinfeld (2009). "Secondary organic aerosol formation from photooxidation of naphthalene and alkylnaphthalenes: implications for oxidation of intermediate volatility organic compounds (IVOCs)." Atmospheric Chemistry and Physics **9**(9): 3049-3060.

Chiappini, L., E. Perraudin, R. Durand-Jolibois and J. Doussin (2006). "Development of a supercritical fluid extraction–gas chromatography–mass spectrometry method for the identification of highly polar compounds in secondary organic aerosols formed from biogenic hydrocarbons in smog chamber experiments." Analytical and Bioanalytical Chemistry **386**(6): 1749-1759.

Cho, A. K., E. Di Stefano, Y. You, C. E. Rodriguez, D. A. Schmitz, Y. Kumagai, A. H. Miguel, A. Eiguren-Fernandez, T. Kobayashi, E. Avol and J. R. Froines (2004). "Determination of Four Quinones in Diesel Exhaust Particles, SRM 1649a, and Atmospheric PM2.5 Special Issue of Aerosol Science and Technology on Findings from the Fine Particulate Matter Supersites Program." Aerosol Science and Technology **38**(sup1): 68-81.

Chung, M. Y., R. A. Lazaro, D. Lim, J. Jackson, J. Lyon, D. Rendulic and A. S. Hasson (2006). "Aerosol-Borne Quinones and Reactive Oxygen Species Generation by Particulate Matter Extracts." Environmental Science & Technology **40**(16): 4880-4886.

Denkenberger, K. A., R. C. Moffet, J. C. Holecek, T. P. Rebotier and K. A. Prather (2007). "Real-Time, Single-Particle Measurements of Oligomers in Aged Ambient Aerosol Particles." Environmental Science & Technology **41**(15): 5439-5446.

Eiguren-Fernandez, A., A. H. Miguel, E. Di Stefano, D. A. Schmitz, A. K. Cho, S. Thurairatnam, E. L. Avol and J. R. Froines (2008). "Atmospheric Distribution of Gas- and Particle-Phase Quinones in Southern California." Aerosol Science and Technology **42**(10): 854-861.

Fang, W., L. Gong, X. Shan, F. Liu, Z. Wang and L. Sheng (2011). "Thermal Desorption/Tunable Vacuum–Ultraviolet Time-of-Flight Photoionization Aerosol Mass Spectrometry for Investigating Secondary Organic Aerosols in Chamber Experiments." Analytical Chemistry **83**(23): 9024-9032.

Gross, D. S., R. Atlas, J. Rzeszotarski, E. Turetsky, J. Christensen, S. Benzaid, J. Olson, T. Smith, L. Steinberg, J. Sulman, A. Ritz, B. Anderson, C. Nelson, D. R. Musicant, L. Chen, D. C. Snyder and J. J. Schauer (2010). "Environmental chemistry through intelligent atmospheric data analysis." Environmental Modelling & Software **25**(6): 760-769.

Gross, D. S., M. E. Galli, M. Kalberer, A. S. H. Prevot, J. Dommen, M. R. Alfarra, J. Duplissy, K. Gaeggeler, A. Gascho, A. Metzger and U. Baltensperger (2006). "Real-Time Measurement of Oligomeric Species in Secondary Organic Aerosol with the Aerosol Time-of-Flight Mass Spectrometer." Analytical Chemistry **78**(7): 2130-2137.

Healy, R. M., B. Temime, K. Kuprovskyte and J. C. Wenger (2009). "Effect of Relative Humidity on Gas/Particle Partitioning and Aerosol Mass Yield in the Photooxidation of *p*-Xylene." Environmental Science & Technology **43**(6): 1884-1889.

Healy, R. M., J. C. Wenger, A. Metzger, J. Duplissy, M. Kalberer and J. Dommen (2008). "Gas/particle Partitioning of Carbonyls in the Photooxidation of Isoprene and 1,3,5-trimethylbenzene." Atmospheric Chemistry and Physics **8**(12): 3215-3230.

Jakober, C. A., S. G. Riddle, M. A. Robert, H. Destaillats, M. J. Charles, P. G. Green and M. J. Kleeman (2007). "Quinone Emissions from Gasoline and Diesel Motor Vehicles." Environmental Science & Technology **41**(13): 4548-4554.

Kautzman, K. E., J. D. Surratt, M. N. Chan, A. W. H. Chan, S. P. Hersey, P. S. Chhabra, N. F. Dalleska, P. O. Wennberg, R. C. Flagan and J. H. Seinfeld (2010). "Chemical Composition of Gas- and Aerosol-Phase Products from the Photooxidation of Naphthalene." Journal of Physical Chemistry A **114**(2): 913-934.

Koch, R., R. Knispel, M. Elend, M. Siese and C. Zetzsch (2007). "Consecutive Reactions of Aromatic-OH adducts with NO, NO_2 and O_2: Benzene, Naphthalene, Toluene, *m*- and *p*-xylene, Hexamethylbenzene, Phenol, *m*-cresol and Aniline." Atmospheric Chemistry and Physics **7**(8): 2057-2071.

Kourtchev, I., T. Ruuskanen, W. Maenhaut, M. Kulmala and M. Claeys (2005). "Observation of 2-methyltetrols and related photo-oxidation products of isoprene in boreal forest aerosols from Hyyti, Finland." Atmos. Chem. Phys. **5**(10): 2761-2770.

Kumagai, Y., Y. Shinkai, T. Miura and A. K. Cho (2012). "The Chemical Biology of Naphthoquinones and Its Environmental Implications." Annual Review of Pharmacology and Toxicology **52**(1): 221-247.

Kuprovskyte, K. (2010). Laboratory and Field Measurment of Gas and Particle Phase Oxygenated Hydrocarbons. Ph.D., University College Cork.

Lee, J. Y. and D. A. Lane (2009). "Unique products from the reaction of naphthalene with the hydroxyl radical." Atmospheric Environment **43**(32): 4886-4893.

Mihele, C. M., H. A. Wiebe and D. A. Lane (2002). "Particle Formation and Gas/Particle Partition Measurements of the Products of the Naphthalene-OH Radical Reaction in a Smog Chamber." Polycyclic Aromatic Compounds **22**(3-4): 729-736.

Nishino, N., J. Arey and R. Atkinson (2009a). "Yields of Glyoxal and Ring-Cleavage Co-Products from the OH Radical-initiated Reactions of Naphthalene and Selected Alkylnaphthalenes." Environmental Science & Technology **43**(22): 8554-8560.

Nishino, N., J. Arey and R. Atkinson (2009b). "Formation and Reactions of 2-Formylcinnamaldehyde in the OH Radical-Initiated Reaction of Naphthalene." Environmental Science & Technology **43**(5): 1349-1353.

Nishino, N., J. Arey and R. Atkinson (2010). "Formation of Nitro-Products from the Gas-Phase OH Radical-Initiated Reactions of Toluene, Naphthalene and Biphenyl: Effect of NO2 Concentration (vol 42, pg 9203, 2008)." Environmental Science & Technology **44**(9): 3644-3645.

Nishino, N., R. Atkinson and J. Arey (2008). "Formation of Nitro Products from the Gas-Phase OH Radical-Initiated Reactions of Toluene, Naphthalene, and Biphenyl: Effect of NO_2 Concentration." Environmental Science & Technology **42**(24): 9203-9209.

Ortiz, R., K. Enya, K. Sekiguchi and K. Sakamoto (2009). "Experimental testing of an annular denuder and filter system to measure gas-particle partitioning of semivolatile bifunctional carbonyls in the atmosphere." Atmospheric Environment **43**(2): 382-388.

Possanzini, M., A. Febo and A. Liberti (1983). "New design of a high-performance denuder for the sampling of atmospheric pollutants." Atmospheric Environment (1967) **17**(12): 2605-2610.

Pratt, K. A. and K. A. Prather (2012b). "Mass spectrometry of atmospheric aerosols—Recent developments and applications. Part II: On-line mass spectrometry techniques." Mass Spectrometry Reviews **31**(1): 17-48.

Reinard, M. S. and M. V. Johnston (2008). "Ion Formation Mechanism in Laser Desorption Ionization of Individual Nanoparticles." Journal of the American Society for Mass Spectrometry **19**(3): 389-399.

Sasaki, J., S. M. Aschmann, E. S. C. Kwok, R. Atkinson and J. Arey (1997). "Products of the Gas-Phase OH and NO_3 Radical-Initiated Reactions of Naphthalene." Environmental Science & Technology **31**(11): 3173-3179.

Schummer, C., O. Delhomme, B. M. R. Appenzeller, R. Wennig and M. Millet (2009). "Comparison of MTBSTFA and BSTFA in derivatization reactions of polar compounds prior to GC/MS analysis." Talanta **77**(4): 1473-1482.

Temime-Roussel, B., A. Monod, C. Massiani and H. Wortham (2004a). "Evaluation of an annular denuder tubes for atmospheric PAH partitioning studies1: evaluation of the trapping efficiency of gaseous PAHS." Atmospheric Environment **38**(13): 1913-1924.

Temime, B., R. M. Healy and J. C. Wenger (2007). "A Denuder-Filter Sampling Technique for the Detection of Gas and Particle Phase Carbonyl Compounds." Environmental Science & Technology **41**(18): 6514-6520.

Thüner, L. P., P. Bardini, G. J. Rea and J. C. Wenger (2004). "Kinetics of the Gas-Phase Reactions of OH and NO_3 Radicals with Dimethylphenols." The Journal of Physical Chemistry A **108**(50): 11019-11025.

Turpin, B. J., P. Saxena and E. Andrews (2000). "Measuring and simulating particulate organics in the atmosphere: problems and prospects." Atmospheric Environment **34**(18): 2983-3013.

Valavanidis, A., K. Fiotakis, T. Vlahogianni, V. Papadimitriou and V. Pantikaki (2006). "Determination of Selective Quinones and Quinoid Radicals in Airborne Particulate Matter and Vehicular Exhaust Particles." Environmental Chemistry **3**(2): 118-123.

Wang, D. L., S. Atkinson, A. Hoover-Miller and Q. X. Li (2007). "Polychlorinated naphthalenes and coplanar polychlorinated biphenyls in tissues of harbor seals (Phoca vitulina) from the northern Gulf of Alaska." Chemosphere **67**(10): 2044-2057.

Wang, L., J. Arey and R. Atkinson (2006). "Kinetics and products of photolysis and reaction with OH radicals of a series of aromatic carbonyl compounds." Environmental Science & Technology **40**(17): 5465-5471.

Wenclawiak, B. W., T. E. Jensen and J. F. O. Richert (1993). "GC/MS-FID analysis of BSTFA derivatized polar components of diesel particulate matter (NBS SRM-1650) extract." Fresenius' Journal of Analytical Chemistry **346**(6): 808-812.

Ye, Y., C. Tsai, D. Y. H. Pui and C. W. Lewis (1991). "Particle Transmission Characteristics of an Annular Denuder Ambient Sampling System." Aerosol Science and Technology **14**(1): 102 - 111.

Chapter

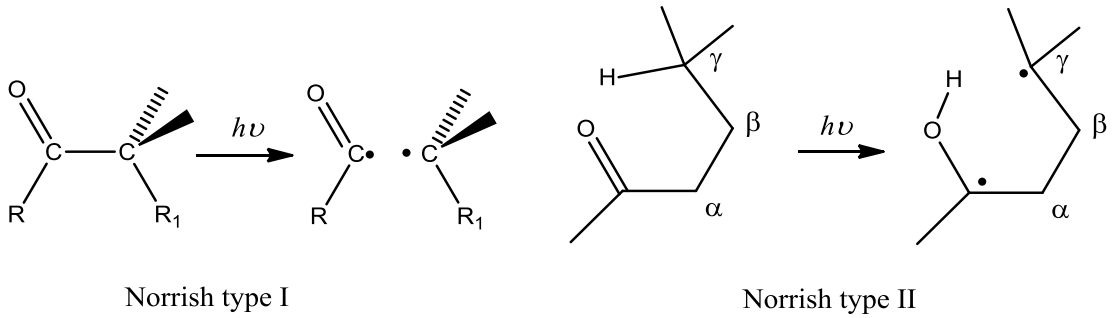
4

Photolysis of Phthaldialdehyde

4.1 Introduction

In the troposphere, the maximum energy available from solar radiation is 412 kJ mol^{-1} (at λ= 290 nm). The aromatic C-H bond energy is approximately 464 kJ mol^{-1} and naphthalene therefore cannot directly undergo photolysis in the atmosphere (Calvert et al. 2002). However, the introduction of a carbonyl or NO_2 group can shift the absorption to longer wavelengths which coincide with the solar radiation that reaches the lower atmosphere. For example, aldehydes typically show absorption in the range 220-370 nm, due to the dipole forbidden n $\rightarrow\pi^*$ electronic transition of the carbonyl group (Martinez et al. 1992). As a result, several naphthalene photooxidation products, including 2-formylcinnamaldehyde, 1- and 2-nitronaphthalenes, and phthaldialdehyde can undergo photolysis under atmospheric conditions (Atkinson et al. 1989; Feilberg et al. 1999b; Wang et al. 2006).

Photolysis of carbonyl compounds, and aldehydes in particular, is therefore an important removal process which effectively competes with OH-initiated oxidation (Finlayson-Pitts et al. 2000). The principal reactions in the atmospheric photolysis of ketones and aldehydes are Norrish type I and Norrish type II (Laue et al. 2005), **Figure 4.1**. In Norrish type I reactions, the carbonyl group accepts a photon and is excited to a photochemical singlet or triplet state, which undergoes carbon-carbon bond cleavage to form two free radicals. In Norrish type II reactions, a H atom in the γ-position can be abstracted by the excited carbonyl compound to produce a 1,4-biradical, which can also undergo further reaction to yield molecular products (Laue et al. 2005). The generation of free radicals from photolysis of carbonyls plays an important role in tropospheric chemistry and can influence local and regional ozone formation and may also contribute to SOA formation (Clifford et al. 2011).



Norrish type I Norrish type II

Figure 4.1 Photochemical Norrish type I and Norrish type II reactions.

4.1.1 Photolysis in the Troposphere

It is possible for a compound in the troposphere to photolyse if it has absorption at wavelengths ≥ 290 nm. The photolysis rate coefficient, *j*, is given by equation (I):

$$j = \int \sigma_T(\lambda)\Phi(\lambda)F(\lambda)d\lambda \quad \text{(I)}$$

where σ is the absorption cross section at temperature T (cm^2 $molecule^{-1}$), F is the solar actinic flux (photon cm^{-2} s^{-1}), and Φ is the quantum yield of photolysis (molecule $photon^{-1}$). The integral is carried out from 290 nm to some wavelength at which either the quantum yield or absorption cross-section becomes negligible (Finlayson-Pitts et al. 2000). Calculation of *j* requires the values of σ and φ to be known. While the experimental determination of absorption cross-sections is fairly straightforward, the measurement of quantum yields is not, mainly due to the rapid secondary reactions of radicals. In fact, there is no quantum yield data available for the vast majority of aldehydes. As a result, calculations of photolysis rates are often carried out in which it is assumed that Φ(λ) = 1. This, of course, only produces a value for the *maximum* photolysis rate. In addition, because the actinic flux depends on many factors, including geographical location, time and season, photolysis rates are normally calculated for certain conditions; *e.g.* at noon on a cloudless day at a location 40°N on the Earth's surface on July 1st.

The problems associated with calculating photolysis rates can be overcome by the experimental determination of *j* values in outdoor simulation chambers, such as the European Photoreactor (EUPHORE), in Valencia, Spain (Wenger et al. 2004).

Photolysis by sunlight follows first order kinetics:

$$A + h\upsilon \xrightarrow{j} products \quad \text{(II)}$$

The rate of removal of the compound is given by:

$$-dA/dt = j\,[A] \quad \text{(III)}$$

Thus

$$\ln([A]_t/[A]_0) = -jt \quad \text{(IV)}$$

where the 0 and *t* refer to the concentrations of compound *A* at initial time, t_0 and elapsed time *t*, respectively. Therefore a plot in the form of equation (IV) should be a straight line with zero intercept and slope of $-j$. The importance of photolysis relative to other loss processes such as reaction with OH, O_3 or NO_3 can be determined by comparison of the rates of all the competing degradation pathways.

4.1.2 Previous Studies of the Photolysis of Aromatic Aldehydes

Previous studies on the photochemical behaviour of aromatic aldehydes have mainly focussed on the determination of UV absorption cross-section values. Gas-phase data are available for benzaldehyde (Chen et al. 2011), tolualdehydes (Clifford et al. 2011) and dimethylbenzaldehydes (El Dib et al. 2008). Wang et al. (2006) measured absorption spectra for phthaldialdehyde and several other aromatic carbonyls in solution and also investigated their photolysis in an indoor simulation chamber using blacklamps as the light source. The UV absorption coefficients for phthaldialdehyde in *n*-hexane solution are plotted in **Figure 4.2**. A *j* value of $(2.7 \pm 0.6) \times 10^{-4}$ s^{-1} was determined for phthaldialdehyde under the experimental conditions, where $j(NO_2) = 8.9 \times 10^{-3}$ s^{-1}, giving $j(\text{phthaldialdehyde})/j(NO_2) = 0.030$. The average quantum yield over the range 290-400 nm was calculated to be Φ_{av}=0.19. The major gas-phase photolysis products of phthaldialdehyde identified by GC-MS were phthalide and phthalic anhydride, with yields of (53 ±14) % and (35 ±10) %, respectively. Wang et al (Wang et al. 2006) proposed that phthalic anhydride could be formed through a photoisomerization pathway, **Figure 4.3**.

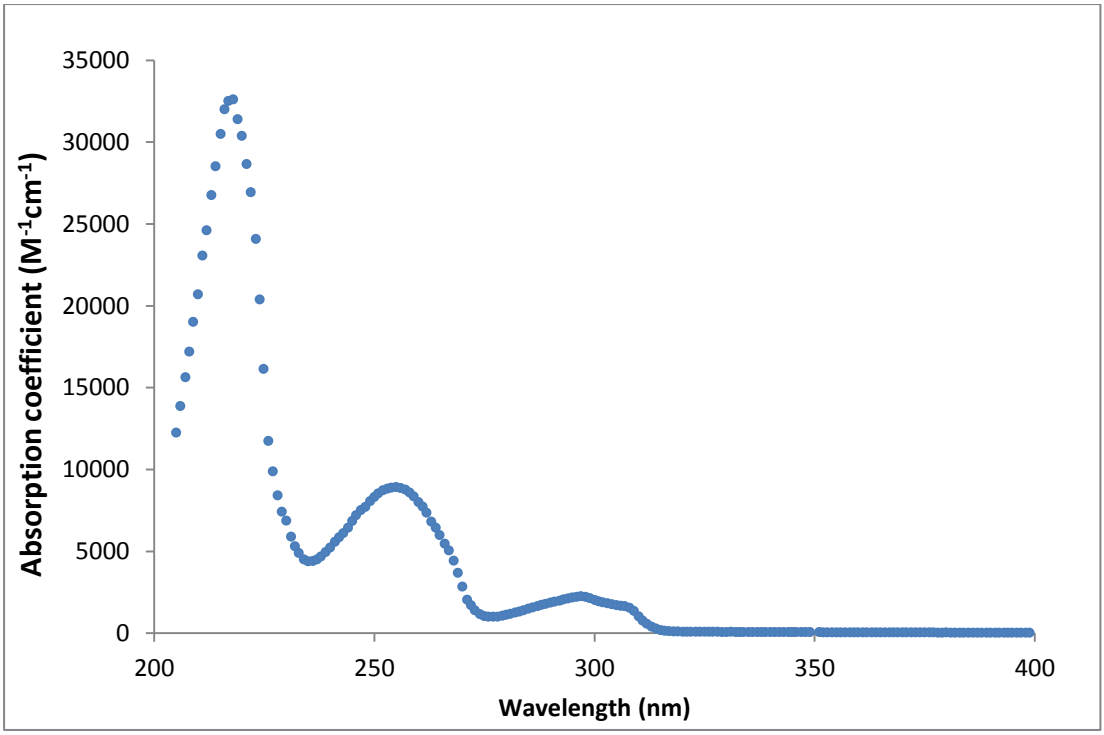


Figure 4.2. UV absorption coefficient for phthaldialdehyde measured in *n*-hexane over the wavelength range 200−400 nm (Wang et al. 2006).

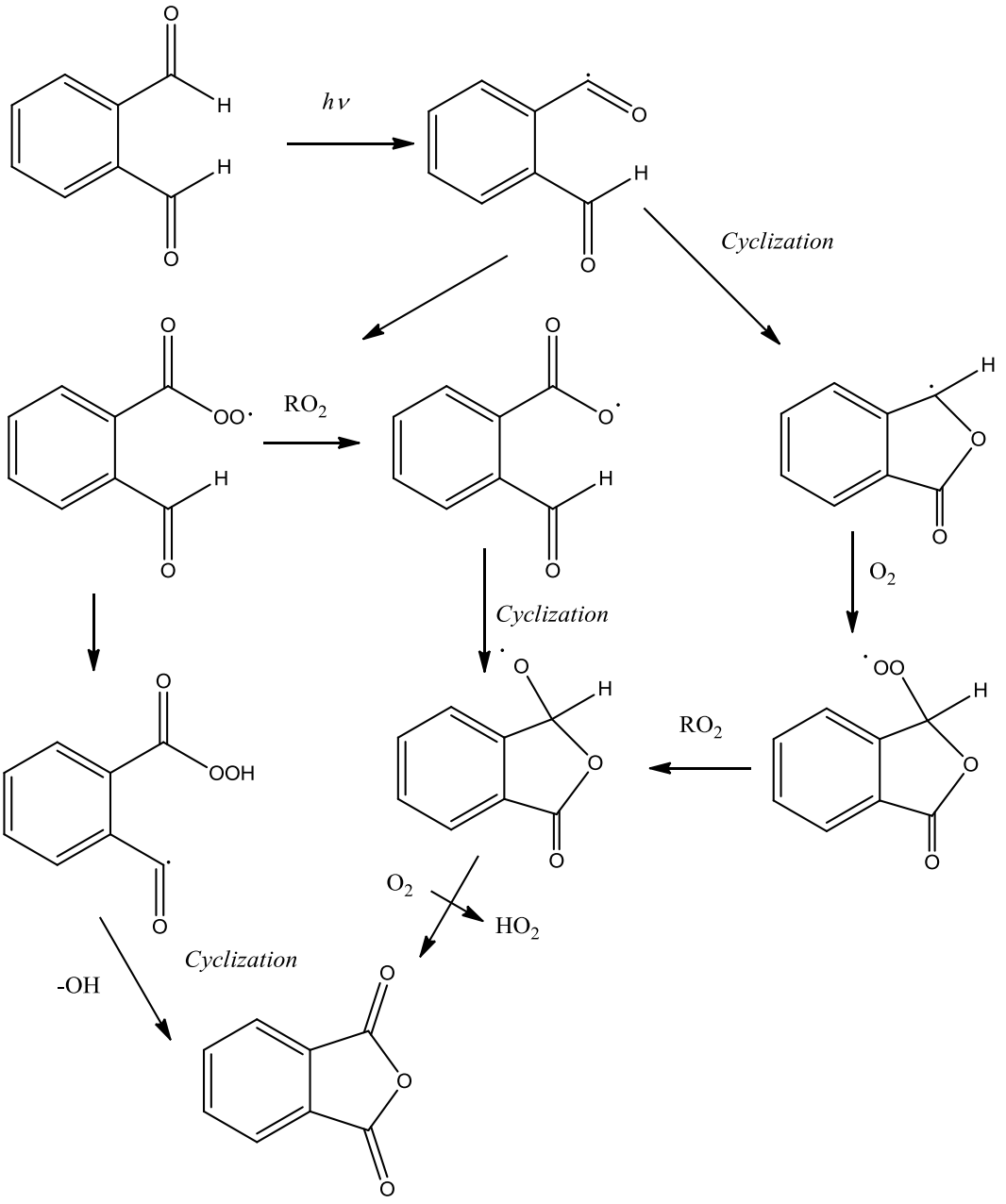


Figure 4.3 Proposed mechanism for the formation of phthalic anhydride from the photolysis of phthaldialdehyde (Wang et al. 2006).

There has only been one reported study of the photolysis of an aromatic aldehyde using natural sunlight, in which Clifford et al (Clifford et al. 2011) performed a detailed investigation of the photolysis of *o*-tolualdehyde by natural sunlight at the European Photoreactor (EUPHORE) in Valencia, Spain. The photolysis rate coefficient was determined, with a value of j(*o*-tolualdehyde) = (1.62-2.15) $\times 10^{-4}$ s^{-1}, yielding an average value of j(*o*-tolualdehyde)/$j(NO_2)$ = (2.53 ± 0.25) $\times 10^{-2}$. A similar value for j(*o*-tolualdehyde)/$j(NO_2)$ was also obtained from experiments performed in an indoor chamber using blacklamps. UV absorption cross-section data (Thiault et al. 2004) were used to derive an effective quantum yield (290 – 400 nm) close to unity. The principal reaction products were identified, as benzocyclobutenol and phthaldialdehyde, possibly generated via the photoisomerization pathway shown in **Figure 4.4**. Appreciable yields of secondary organic aerosol (SOA) were also observed in the photolysis experiments.

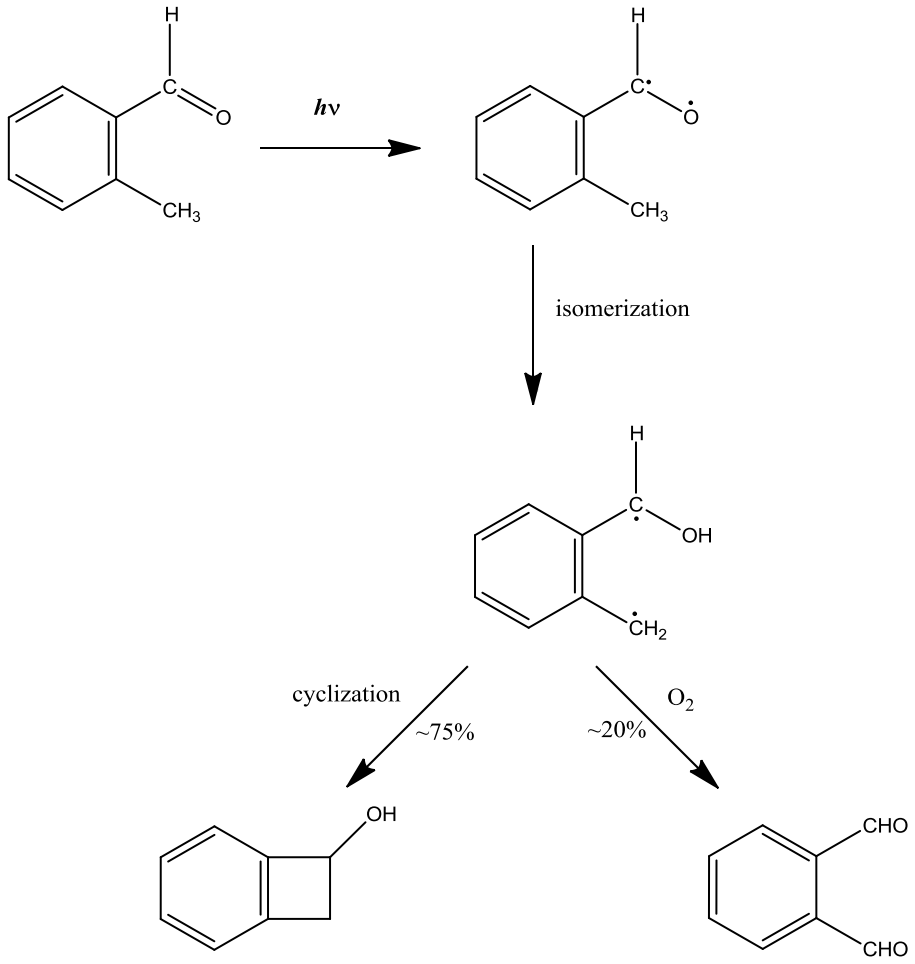


Figure 4.4 Proposed reaction scheme for the photolysis of o-tolualdehyde (Clifford et al. 2011).

4.1.3 Aim of this work

The aim of the work presented in this chapter was to investigate the atmospheric photolysis of phthaldialdehyde. Experiments have been performed at the European Photoreactor (EUPHORE) in Valencia, Spain using natural sunlight to measure the photolysis rate coefficient and thus calculate the atmospheric lifetime due to photolysis. The main reaction products have been identified to provide information on the reaction mechanism and the formation of SOA observed. A series of supplementary experiments have also been performed in an indoor simulation chamber using an artificial light source. A key feature of these experiments was the use of ATOFMS to measure the chemical composition of the SOA produced from direct photolysis of phthaldialdehyde.

4.2 Experimental

The photolysis of phthaldialdehyde was studied using natural sunlight in EUPHORE and artificial light in an indoor chamber at University College Cork. The materials used in this work are listed in **Table 4.1**, used as received.

Table 4.1 Materials used in this study.

Material	Purity %	Manufacturer
Phthaldialdehyde	99	Sigma-Aldrich
Phthalide	99	Sigma-Aldrich
Phthalic anhydride	99	Sigma-Aldrich
Acetone	HPLC grade	Sigma-Aldrich
1,3,5-Trimethylbenzene	99	Sigma-Aldrich
CO	99.99	Irish Oxygen
SF_6	99	Sigma-Aldrich
BSTFA+TMCS(99:1)		SUPELCO
Methanol	99.9	Sigma-Aldrich
Dichloromethane	99.9	Sigma-Aldrich
n-Hexane	HPLC grade	Sigma-Aldrich

4.2.1 Experiments in EUPHORE Chamber

4.2.1.1 Apparatus

The photolysis of phthaldialdehyde by sunlight was investigated at the European PhotoReactor (EUPHORE) in July 2009 (**Figure 4.5**). The facility consists of two large outdoor simulation chambers, A and B, in the Centro de Estudios Ambientales del Mediterraneo (CEAM), Valencia, Spain. The experiments were performed in Chamber B, **Figure 4.5**. Full details concerning the operation of the chamber and associated instruments are available in the literature (Wenger et al. 2004; O'Connor et al. 2006; Clifford et al. 2011), hence, only a brief description of the features particularly relevant to the photolysis experiments are given here.

The chamber consists of a hemispherical reactor made of FEP Teflon foil, with a volume of 177 m^3 (July 2009). The FEP Teflon foil is highly transparent; the transmission through the chamber walls is 85–90% for wavelengths 500–320 nm, and around 75% at 290 nm. A retractable steel housing surrounds the chamber and is used to control the time of exposure to sunlight. The floor consists of several aluminium panels covered by FEP foil and cooled by water to reduce the effects of heating from exposure to sunlight. A number of ports situated on the floor of the chamber are available for the introduction and sampling of reaction mixtures. The chamber is operated using dry purified air from a purification air system and is equipped with powerful fans to ensure homogeneous mixing of the reactants.



Figure 4.5 European PhotoReactor (EUPHORE) chamber in CEAM, Valencia, Spain.

Temperature and humidity inside the chamber is measured continuously using PT-100 thermocouples and a dew-point mirror system (Walz TS-2), respectively. A variety of instruments are attached to the chamber for chemical and physical analysis.

4.2.1.2 Procedure and Analysis

The chamber was cleaned by flushing with purified air overnight and filled to atmospheric pressure. All the analytical instruments were set up for data collection. Phthaldialdehyde was introduced into the chamber by flowing dry purified air over a heated glass impinger containing a known amount of the compound. Mixing ratios ranging from 169-425 ppbV of phthaldialdehyde were used in different experiments. The reactant was allowed to mix for at least 30 min while its loss to the chamber walls was measured. In one experiment, a large excess of CO (ca. 500 ppmV) was added as a scavenger for OH radicals, while in another experiment, 1,3,5-trimethylbenzene (400 ppbV) was used as a reactive tracer for OH radicals. Photolysis was initiated by opening the protective housing around midday to expose the contents of the chamber to sunlight for 2-3 h. The temperature inside the chamber increased slightly as the experiments progressed but was always within the range 298-307 K. Relative humidity remained below 3% in all experiments.

The solar flux intensity was measured using two different instruments. A calibrated spectroradiometer (Bentham DM300) provided solar flux intensity over the range of 290-520 nm with a spectral resolution of 1 nm. The flux data was used along with recommended values for the absorption cross-section and photolysis quantum yield (DeMore 1997) to calculate $j(NO_2)$ with a time resolution of 420-430 s (Wenger et al. 2004). $j(NO_2)$ values were also obtained directly using an independently calibrated filter radiometer (Schmitt Glashütten, Germany), with a time resolution of 1 min.

Chemical analysis was performed throughout the experiments. A White mirror system installed inside the chamber and aligned with an optical path length of 553.5 m was used for *in situ* measurements by Fourier Transform Infrared (FTIR) spectroscopy. The FTIR spectrometer (Nicolet Magna 550) was positioned on a platform beneath the chamber and operated using a broad-band MCT detector. The background FTIR spectrum was recorded before the compound was introduced by co-adding 600 interferograms. Infrared spectra in the range 600-4000 cm^{-1} were obtained at a resolution of 1 cm^{-1} and derived from the co-addition of 270 scans collected over 5 minutes. The reactants and products were quantified using calibrated reference infrared spectra obtained by introducing known volumes of pure materials into the chamber. Since gas molecules are known to diffuse through tiny holes in the FEP foil,

the leak rate was determined in each experiment by adding about 20 ppbV of the unreactive tracer gas SF_6 to the chamber and measuring its loss by FTIR spectroscopy throughout the course of the photolysis experiments. The derived correction factors were applied to determine the amounts of reactants consumed and products formed. Due to the slight variation in temperature and pressure during the experiments, additional correction factors, based on the ideal gas equation ($PV=nRT$), were applied to the concentrations determined by FTIR spectroscopy.

The formation of second organic aerosol during the photolysis experiments was monitored using a Scanning Mobility Particle Sizer (SMPS) system, which is capable of recording the particle size distribution, particle number and volume concentrations with a time resolution of 3 min. The system consisted of a condensation particle counter (TSI 3022A) and a differential mobility analyser (DMA, TSI 3081). Sheath and aerosol sampling flow rates were 5.0 dm^3 min^{-1} and 0.5 dm^3 min^{-1} respectively. The instrument was started prior to the introduction of reactants to confirm that no particles were present in the chamber before photolysis was initiated and also operated for several hours after the chamber was closed to measure the loss of particles to the chamber walls. The SOA particles were collected onto a filter (PallFlex 47 mm quartz fibre) at a flow rate of 10 dm^3 min^{-1} for 30 min. The filters were stored in a freezer and later shipped to University College Cork for off-line analysis using GC-MS. One quarter of each filter was used for derivatization with PFBHA, a second quarter was used for derivatization with BSTFA and a third quarter simply extracted into a dichloromethane:methanol (1:1) mixture. Details of the procedures for derivatization and subsequent GC-MS analysis are provided in **Section 3.2**.

4.2.2 Experiments in the Indoor Chamber

4.2.2.1 Apparatus

Experiments were performed in 3.91 m^3 atmospheric simulation chamber located at University College Cork. Details are provided in S**ection 3.2.3** in **Chapter 3**. As part of this work, the distribution and intensity of the light provided by the lamps was measured and used to determine a value for $j(NO_2)$. A calibrated portable spectroradiometer (LiCor-LI 1800) was used to measure the radiation flux inside the

chamber. The instrument was placed inside the centre of the chamber and oriented in 6 different directions to obtain the light intensity as a function of wavelength in the range 300-850 nm. The total flux, shown in **Figure 4.6**, was obtained by adding the measured flux values obtained when the instrument was receiving light from two opposite directions (above and below). The total flux was used in combination with recommended values for the NO_2 absorption cross-section (Voigt et al. 2001) and the quantum yield (DeMore 1997). $j(NO_2)$ was calculated using equation (I) and found to be $(6.6 \pm 0.6) \times 10^{-3}$ s^{-1}.

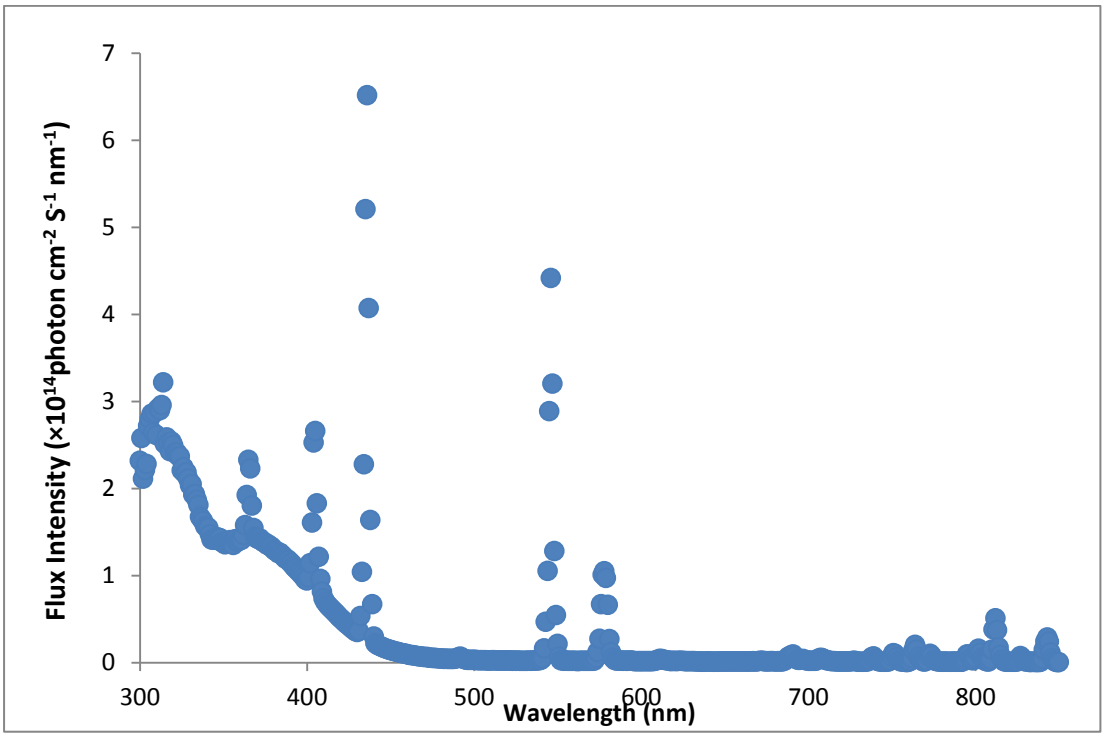


Figure 4.6 Measured total flux intensity in the 3.91 m^3 atmospheric simulation chamber (using 16 TL05 lamps and 12 TL12 lamps).

4.2.2.2 Procedure and Analysis

After flushing overnight with dry purified air, the chamber was further cleaned by performing several cycles of ozone addition, combined with photolysis and flushing to ensure that the background concentration of particles in the chamber was < 150 cm^{-3}. Experiments were performed at ambient temperature (295 ± 2 K) and atmospheric pressure. The inlet and outlet valves were closed and data collection was initiated on all instruments. The relative humidity (RH) in the chamber was typically less than 1%. Some experiments were carried out at RH ~50% by adding water to the

chamber by flowing purified air through the headspace of a heated impinger containing deionized (Milli-Q) water. Phthaldialdehyde was introduced to the chamber in the same manner and photolysis was initiated by turning on all of the lamps (16 TL05 and 12 TL12) for several hours. In some experiments, an excess amount of CO (500 ppmV) was added as an OH radical scavenger.

Several analytical instruments were used continuously throughout the experiments. The concentration of phthaldialdehyde was monitored using FTIR spectroscopy. The spectra were collected at a resolution of 1 cm^{-1} by co-adding 300 scans over approximately 5 min. The reactant and photolysis products were quantified by successive subtraction of calibrated reference spectra. The formation and evolution of particles in the range 10-470 nm was monitored with 3 min. time resolution using a scanning mobility particle sizer (SMPS 3080, TSI). The sheath and aerosol sampling flow were 5.0 dm^3 min^{-1} and 0.5 dm^3 min^{-1}, respectively. The volume concentration of the particles was converted to mass concentration using a particle density of 1.4 g cm^{-1} (Hallquist et al. 2009). The wall loss rates of phthaldialdehyde and SOA were determined before the lamps were switched on and after they were switched off respectively. The loss rates were found to obey first order kinetics and the derived rate coefficients were used to correct the reactant and particle concentrations. Additional information on the identity of gas- and particle-phase products was obtained using a denuder-filter sampling system coupled with GC-MS analysis. Samples were collected at the end of some of the experiments using a flow rate of 10 dm^3 min^{-1} for 30 min. The denuder and filter samples were either derivatized with BSTFA or simply extracted into a dichloromethane:methanol (1:1) mixture. Details of the procedures for derivatization and subsequent GC-MS analysis are provided in **Section 3.2**.

The chemical composition of the SOA was measured on-line using the ATOFMS, which was connected directly to the chamber with ¼″ stainless steel tubing. Particles generated in the simulation chamber from the photolysis of phthaldialdehyde are expected to exhibit homogeneous composition. However, with long sampling times, some ambient particles can enter the chamber through diffusion. Thus, when analysing the data, EDAM ENCHILADA (Environmental Chemistry through Intelligent Atmospheric Data Analysis, http://www.cs.carleton.edu/enchilada), was used to separate background particles from the SOA using the *K*-means algorithm

(Gross et al. 2010). The spectra were averaged over 5 min and 1 h intervals. In all experiments described here, peak detection was carried out up to ± 800 Da using threshold values of peak height > 5 units, area > 6 square units and contribution more than 0.00001 of the total peak area.

4.3 Results and Discussion

4.3.1 Photolysis Rate Coefficient

The photolysis rate coefficient, *j*(phthal), can be determined from the measured decay of the compound in the EUPHORE and indoor chambers. Other loss processes for phthaldialdehyde include deposition to the walls of the chambers and reaction with OH radicals, present in the background or produced as a result of the photolysis process itself. The measured rate coefficients for wall loss and reaction with OH, k_{wall} and $k_{OH}[OH]$ respectively, can be incorporated into equation (IV) to yield the following;

$$\ln \frac{[phthaldialdehyde]_t}{[phthaldialdehyde]_0} = -k_{total}t = -(j + k_{wall} + k_{OH}[OH])t \qquad \text{(V)}$$

Although dilution was also observed during the EUPHORE experiments, the rate determined by measuring the loss of SF_6 from the chamber, k_{SF6}, was lower than the wall loss and is therefore already incorporated into k_{wall}. Thus a plot in the form of Equation (V) should yield a straight line with gradient $-k_{total}$. The wall loss was measured during each experiment, while $k_{OH}[OH]$ could be determined from experiments where 1,3,5-trimethylbenene was used as a tracer. In some experiments an excess of CO was used to scavenge all OH radicals and $k_{OH}[OH]$ was therefore eliminated, giving k_{total}-k_{wall} =*j*(phthal).

4.3.1.1 EUPHORE Chamber

Concentration–time profiles and kinetic plots in the form of Equation (V) were generated for all experiments. The concentration-time profiles and the corresponding photolysis rate plots are shown in **Figure 4.7**-**Figure 4.14**. The reaction conditions and results are summarized in **Table 4.2.** The decay of phthaldialdehyde was similar in all experiments and started immediately after opening the chamber to sunlight. The kinetic plots exhibited good linearity and near-zero intercepts, yielding values of k_{total}

in the range (1.09- 1.89) $\times 10^{-4}$ s^{-1}, following correction for wall loss. The experiments performed on 1st and 2nd July 2009 were performed under almost identical sunlight conditions and yielded very similar results, indicating a high degree of reproducibility. However, an OH tracer or scavenger was not used and the values for j(phthal) obtained from these experiments are therefore upper limits. In the experiment conducted on 10th July 2009, an excess of CO was added as a scavenger and the possible loss of phthaldialdehyde by reaction with OH was thus eliminated. The value for j(phthal) obtained in this experiment was lower than k_{total} in the first two experiments thereby confirming that reaction with OH was contributing to the loss of phthaldialdehyde. In order to make direct comparisons between experiments with different light intensity, j(phthal) was normalized by dividing by $j(NO_2)$. The resulting value of $j(\text{phthal})/j(NO_2) = 0.020 \pm 0.003$ obtained on 10th July 2009 is lower than that obtained in the experiments without scavenger. The contribution of the OH reaction, i.e. the value of $k_{OH}[OH]$, in the experiments performed on 1st and 2nd July 2009 can be estimated by assuming that $j(\text{phthal})/j(NO_2) = 0.020$, rather than 0.023. This would yield values of j(phthal) = 1.65×10^{-4} s^{-1} and $k_{OH}[OH] = 2.4 \times 10^{-5}$ s^{-1} for both experiments, indicating that 12.7% of the loss of phthaldialdehyde was due to reaction with OH radicals.

Table 4.2 Experimental conditions and results for the photolysis of phthaldialdehyde by natural sunlight in the EUPHORE chamber.

Date	**1st July 2009**	**2nd July 2009**	**03rd July 2009[1]**	**10th July 2009[2]**
Initial conc.(ppbV)	261	169	425	406
Irradiation time	2 h 47 min	2 h 21 min	2 h 57 min	3 h 3 min
$j(NO_2)$ ($\times 10^{-3}$ s^{-1})	8.26 ± 0.50	8.22 ± 0.50	5.07 ± 0.40	8.04 ± 0.50
k_{SF6} ($\times 10^{-6}$ s^{-1})	5.50 ± 0.30	7.00 ± 0.40	5.70 ± 0.60	4.50 ± 0.30
k_{wall} ($\times 10^{-5}$ s^{-1})	1.55 ± 0.20	2.30 ± 0.40	1.93 ± 0.20	1.9 ± 0.30
k_{total} ($\times 10^{-4}$ s^{-1})	1.89 ± 0.05	1.86 ± 0.04	1.09 ± 0.02	1.59 ± 0.02
k_{OH}[OH] ($\times 10^{-6}$ s^{-1})	-	-	8.05	0
j(phthal) ($\times 10^{-4}$ s^{-1})	1.89 ± 0.01	1.86 ± 0.04	1.01 ± 0.02	1.59 ± 0.02
j(phthal)/$j(NO_2)$	0.023 ± 0.005	0.023 ± 0.004	0.020 ± 0.004	0.020 ± 0.003
SOA yield (%)	2.8	3.2	10.0	10.5
Phthalide (%)	15 ± 0.4	17 ± 0.4	44 ± 0.7	42 ± 0.4
Phthalic anhydride (%)	42 ± 0.4	43 ± 0.8	33 ± 1	24 ± 0.6

[1] In this experiment, 1,3,5-trimethylbenzene (400 ppbV) was as an OH radical tracer.[2] In this experiment CO (500 ppmV) used as an OH radical scavenger. Errors are twice the standard deviation. The yield of SOA was corrected with the measured wall loss value of (2-7) × 10^{-5} s^{-1} on each day, and the yield on 10th July 2009 was calculated from the net growth of SOA.

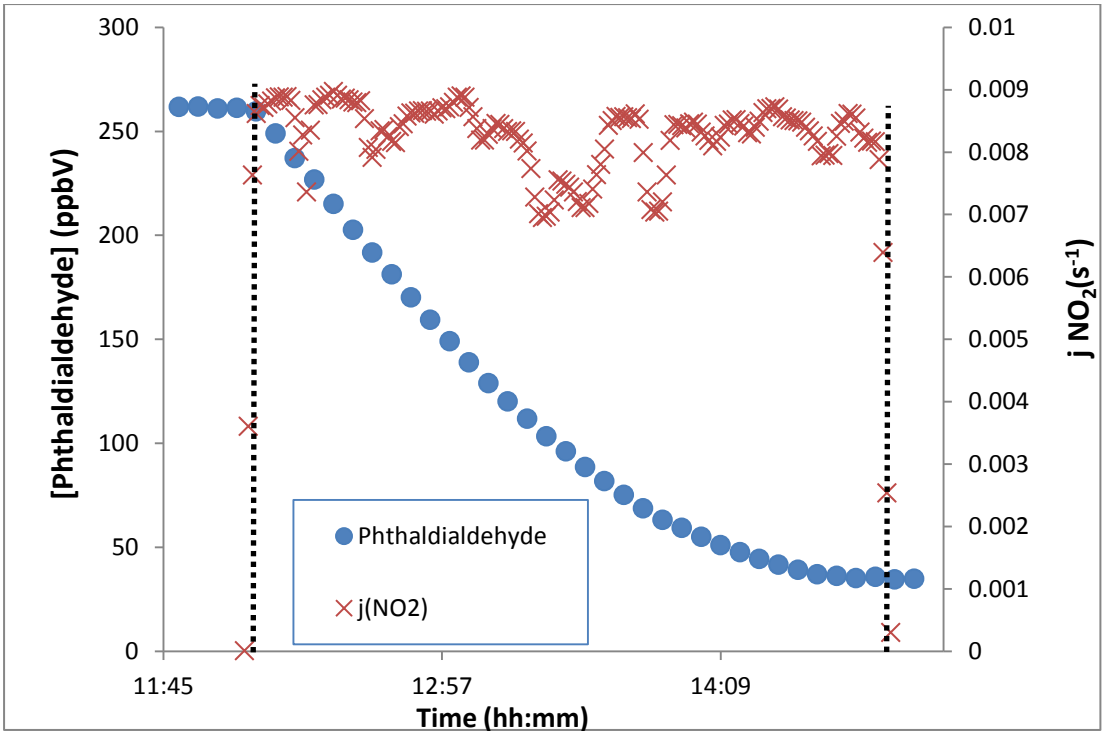


Figure 4.7 Concentration-time profile and $j(NO_2)$ during the photolysis of phthaldialdehyde at EUPHORE on 1st July 2009. The vertical dotted lines indicate the time the chamber was opened (12:06) and closed (14:53).

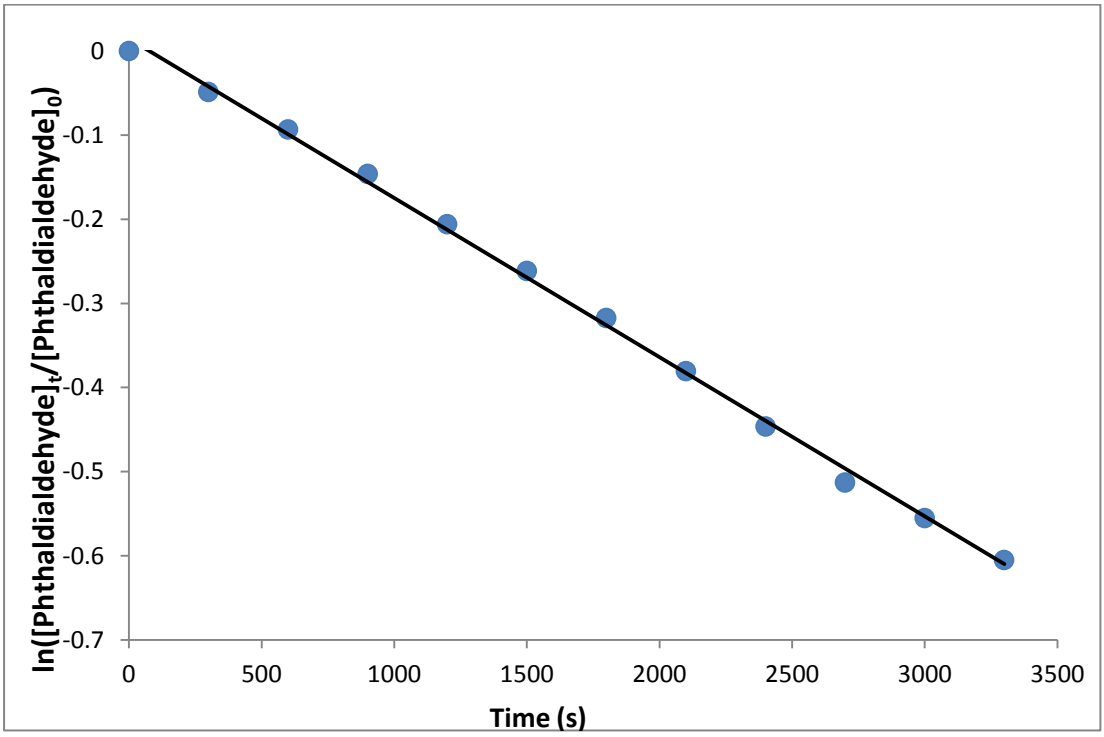


Figure 4.8 Photolytic loss of phthaldialdehyde (corrected for wall loss) during the experiment performed at EUPHORE on 1st July 2009.

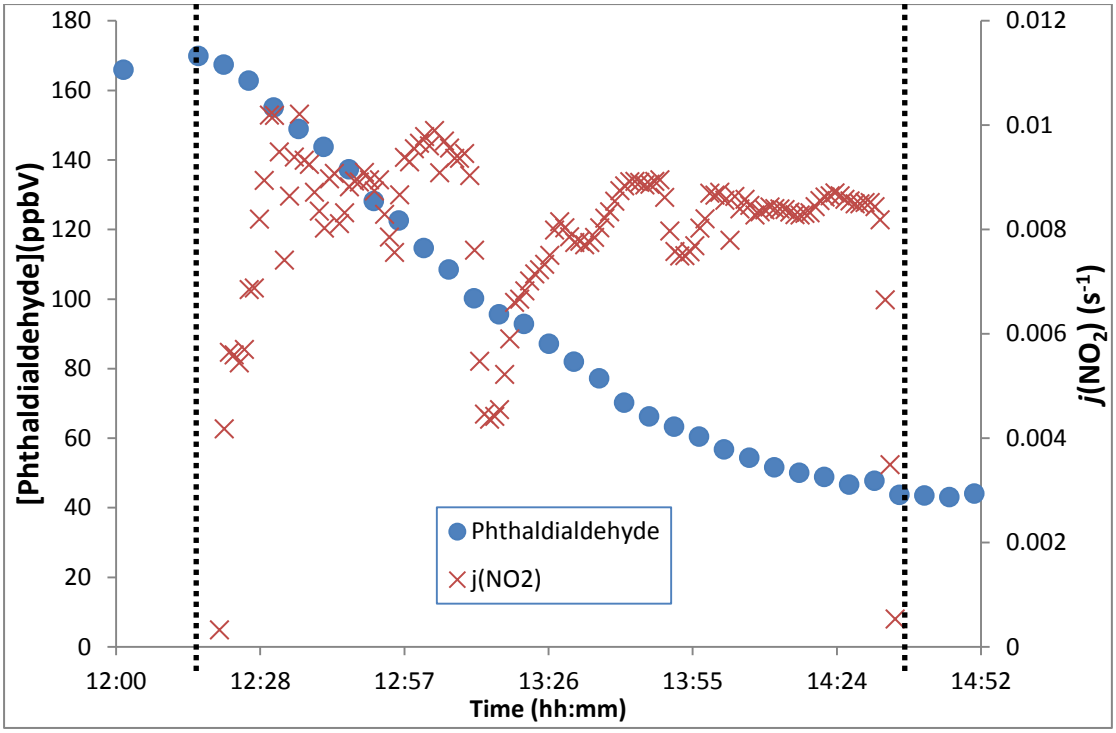


Figure 4.9 Concentration-time profile and $j(NO_2)$ during the photolysis of phthaldialdehyde at EUPHORE on 2nd July 2009. The vertical dotted lines indicate the time the chamber was opened (12:14) and closed (14:35).

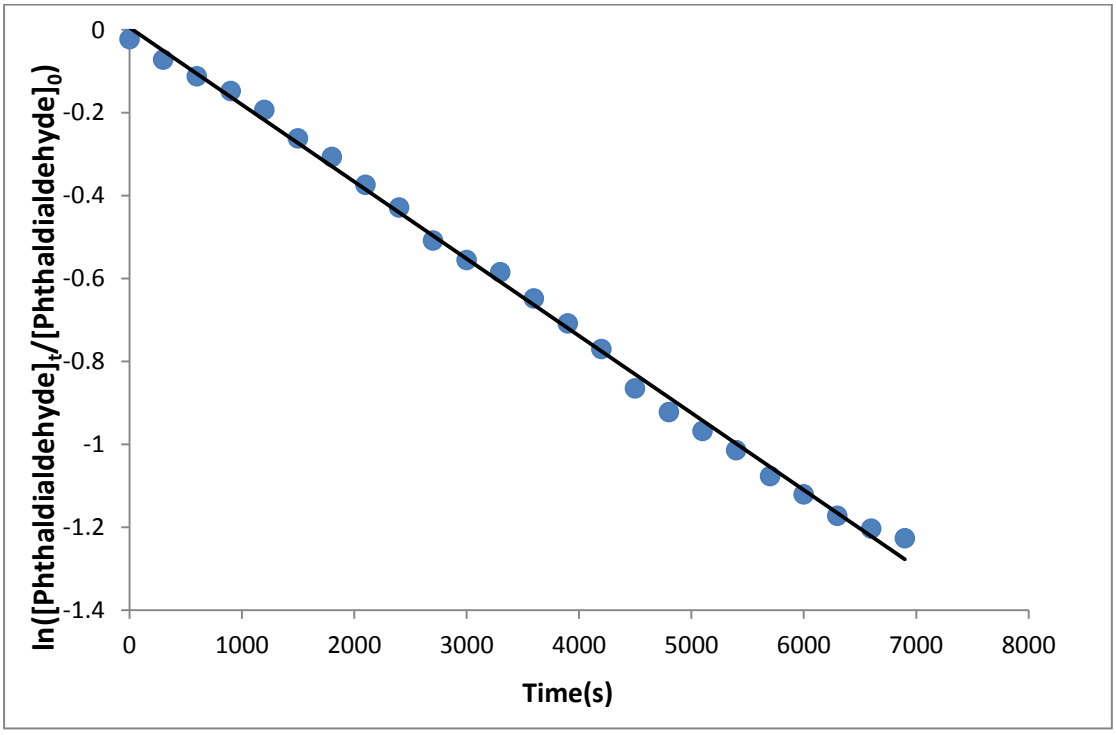


Figure 4.10 Photolytic loss of phthaldialdehyde (corrected for wall loss) during the experiment performed at EUPHORE on 2nd July 2009.

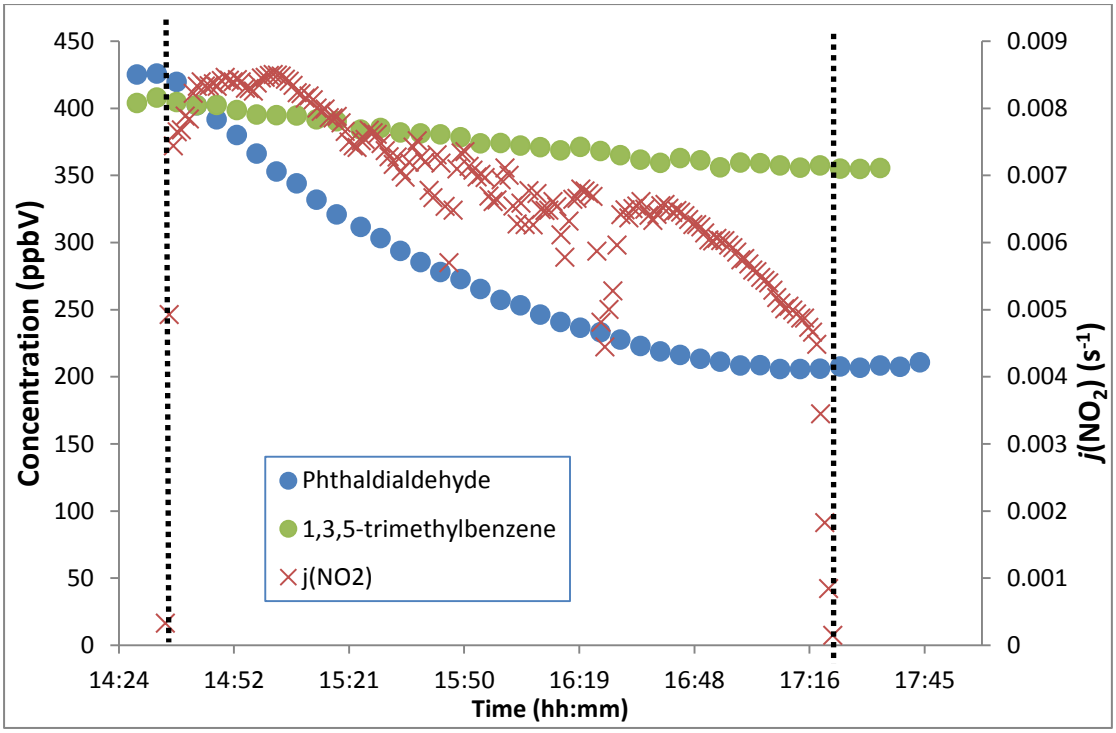


Figure 4.11 Concentration-time profile and $j(NO_2)$ during the photolysis of phthaldialdehyde at EUPHORE on 3rd July 2009. The vertical dotted lines indicate the time the chamber was opened (14:35) and closed (17:22).

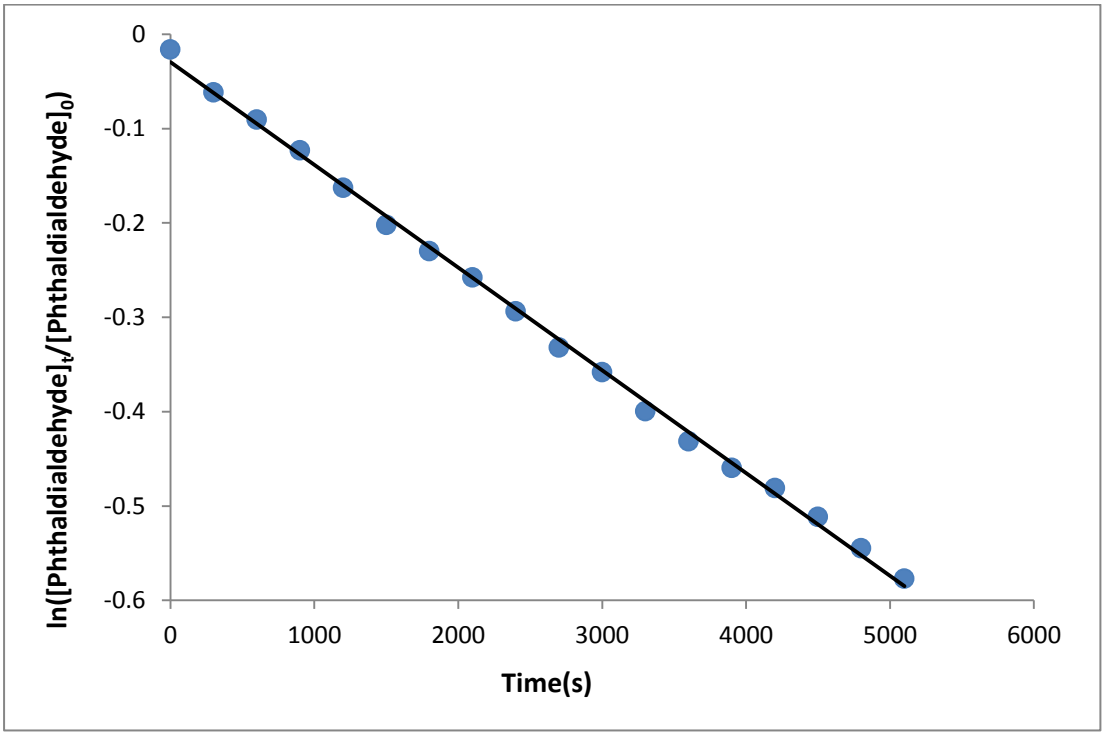


Figure 4.12 Photolytic loss of phthaldialdehyde (corrected for wall loss) during the experiment performed at EUPHORE on 3rd July 2009.

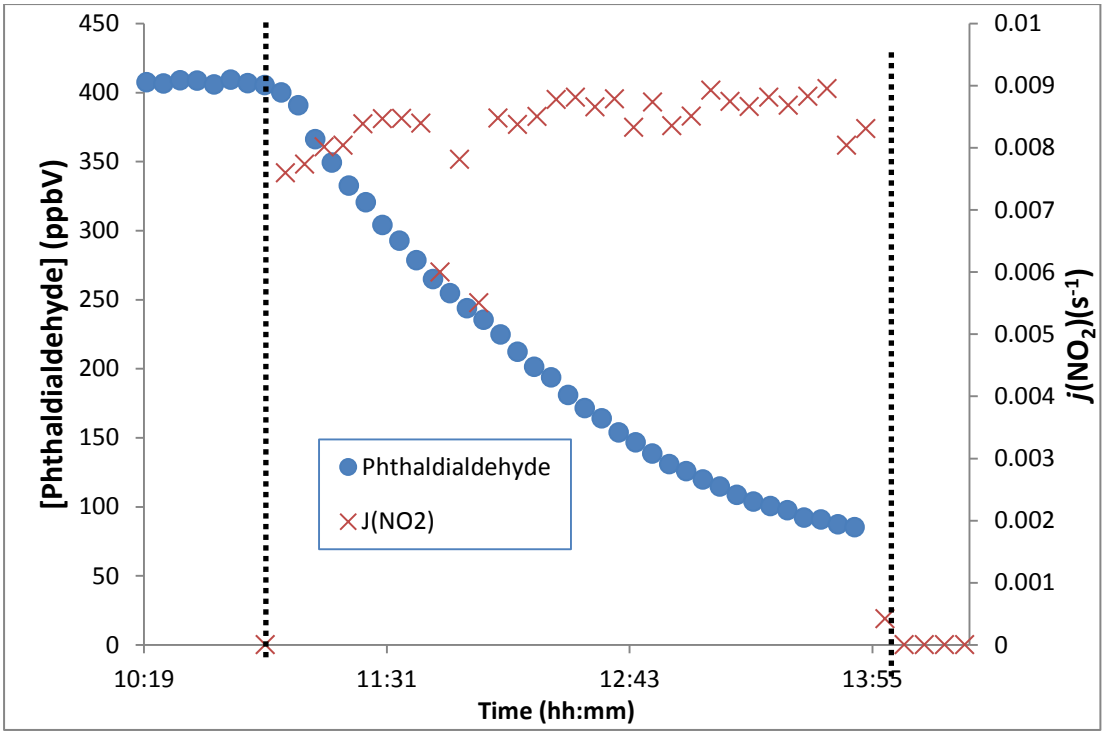


Figure 4.13 Concentration-time profile and $j(NO_2)$ during the photolysis of phthaldialdehyde at EUPHORE on 10th July 2009 The vertical dotted lines indicate the time the chamber was opened (10:55) and closed (13:58).

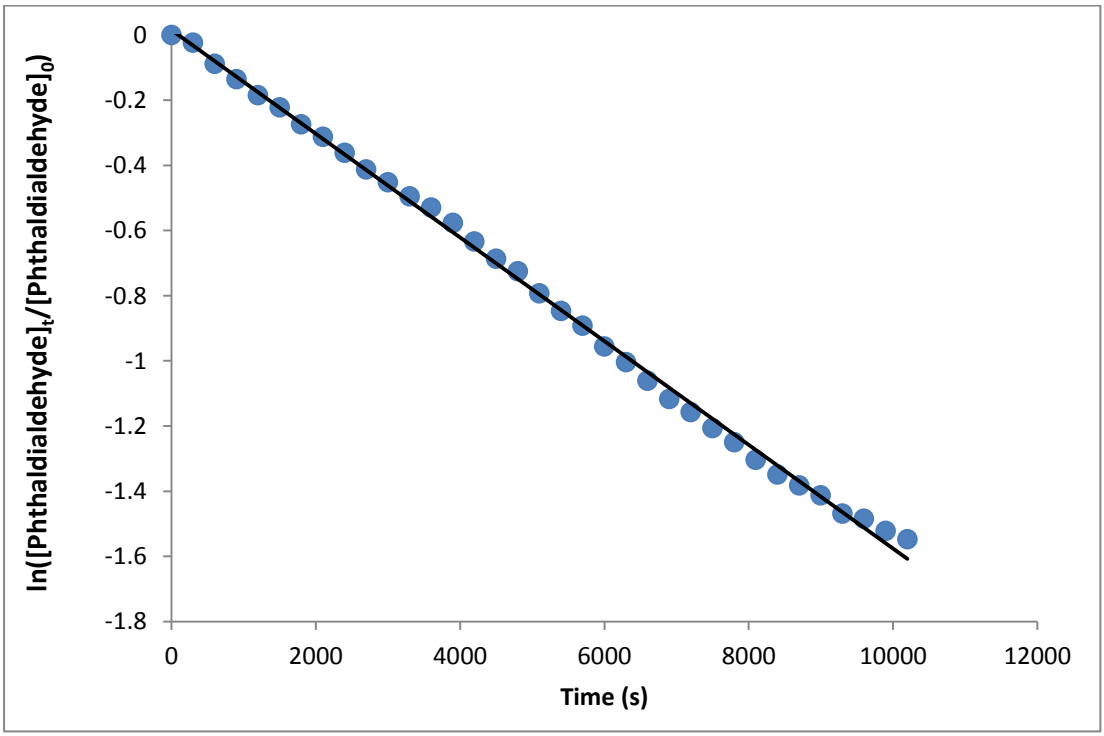


Figure 4.14 Photolytic loss of phthaldialdehyde (corrected for wall loss) during the experiment performed at EUPHORE on 10th July 2009.

In the experiment performed on 3rd July 2009, 400 ppbV of 1,3,5-trimethylbenzene (TMB) was introduced to the chamber to act as a tracer for OH radicals. As a result, any OH generated during the experiment reacted with both 1,3,5-trimethylbenzene and phthaldialdehyde. The OH concentration can be estimated from the measured decay of TMB:

$$\frac{-d[TMB]}{dt} = k_0[TMB][OH] \qquad \text{(VI)}$$

where k_0 is the rate coefficient for reaction of OH with TMB. Assuming that the concentration of OH is in a steady state, the reaction is occurring under pseudo-first order conditions:

$$\frac{-d[TMB]}{dt} = k_1[TMB] \qquad \text{(VII)}$$

where $k_1 = k_0[OH]$ and integrating from the time t=0, when the initial concentration of TMB is $[TMB]_0$ to the time t when the concentration of TMB is $[TMB]_t$ gives:

$$ln\frac{[TMB]_t}{[TMB]_0} = -k_1 t \qquad \text{(VIII)}$$

A plot in the form of this equation is shown in **Figure 4.15** and yields a value of $k_1 = (2.0 \pm 0.1) \times 10^{-5}$ s^{-1}. Using a value of $k_0 = 5.73 \times 10^{-11}$ cm^3 $molecue^{-1}$ s^{-1} (Kramp et al. 1998) yields [OH] = 0.35×10^6 molecule cm^{-3}. This value for the OH steady state concentration can be used to calculate $k_{OH}[OH]$, which represents the loss of phthaldialdehyde due to reaction with OH. Using a value of $k_{[OH]} = 2.3 \times 10^{-11}$ cm^3 $molecue^{-1}$ s^{-1} (Wang et al. 2006) gives $k_{OH}[OH] = 8.05 \times 10^{-6}$ s^{-1}, indicating that 7.4% of the loss of phthaldialdehyde was due to reaction with OH radicals. The resulting value for the photolysis rate coefficient is j(phthal) = $(1.01 \pm 0.02) \times 10^{-4}$ s^{-1}, yielding a value of $j(phthal)/j(NO_2) = 0.020 \pm 0.004$, in excellent agreement with the result obtained in the experiment performed with the OH scavenger.

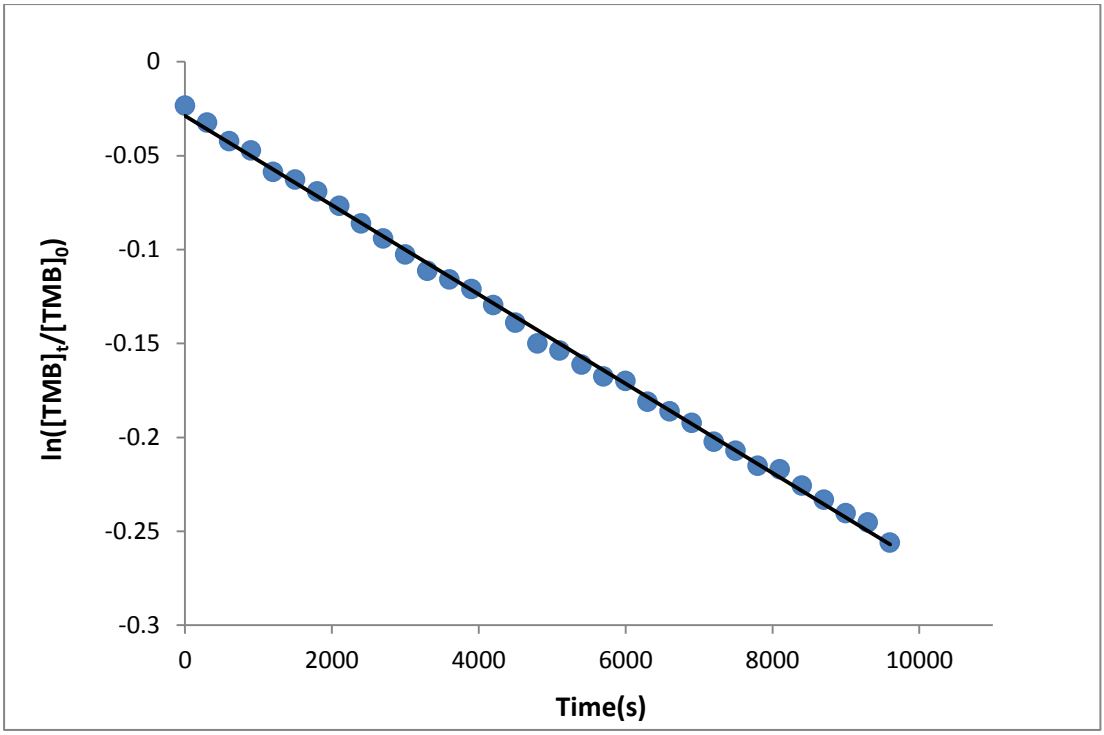


Figure 4.15 Decay rate of 1,3,5-trimethylbenzene (TMB) (corrected for wall loss) during the photolysis of phthaldialdehyde at EUPHORE on 3rd July 2009.

4.3.1.2 Indoor Chamber

A series of phthaldialdehyde photolysis experiments was conducted in the indoor simulation chamber in order to compare the photolysis rate with that obtained using sunlight at EUPHORE and by Wang et al. (2006) using blacklamps. Some experiments were performed using 1,3,5-trimethylbenzene and CO as an OH radical tracer and scavenger respectively. The effect of relative humidity was investigated by repeating the set of experiments at RH ~50%. Concentration–time profiles and kinetic plots in the form of Equation (V) were generated for all experiments. The kinetic plots exhibited good linearity and near-zero intercepts as shown in **Figure 4.16**. The reaction conditions and results are summarized in **Table 4.2.**

The results are similar to those obtained in the EUPHORE experiments, with the loss of phthaldialdehyde observed to be slightly lower in the presence of the OH radical scavenger or tracer. The average value of j(phthal) determined from experiments performed with tracer and scavenger is $(3.79 \pm 0.70) \times 10^{-4}$ s^{-1}, with $j(\text{phthal})/j(NO_2) = 0.056 \pm 0.008$. Some variations in the photolysis rate were observed when the relative humidity was increased to 50%. However, these variations are small and

inconsistent and are probably due to random errors in the analysis. It is therefore concluded that relative humidity does not affect the photolysis rate of phthaldialdehyde. The use of the tracer to determine the steady state OH radical concentration during the experiments was again successful, as indicated in **Figure 4.17**, and gave values of [OH] = 0.17×10^6 and 0.35×10^6 molecule cm^{-3} in experiments 16122010 and 14012011 respectively. These values indicate that reaction with OH radicals account for a maximum of 2% of the loss of phthaldialdehyde in these experiments, somewhat lower than in the EUPHORE chamber.

Table 4.3 Conditions and results for the photolysis of phthaldialdehyde in the indoor simulation chamber.

Date	**10122010**	**22122010**[2]	**16122010**[1]	**21122010**[2]	**13012011**	**17012011**[2]	**14012011**[1]
Relative humidity (%)	<5%	<5%	<5%	<5%	47	49	51
Initial conc.(ppbV)	397	486	546	546	500	600	600
Irradiation time	50 min	55 min	90 min	25 min	42 min	25 min	35 min
k_{wall} ($\times 10^{-4}$ s^{-1})	1.40 ±0.30	1.40 ±0.20	1.40 ±0.20	1.40 ±0.20	2.00 ±0.30	2.00 ±0.30	2.00 ±0.30
$j(NO_2)$ ($\times 10^{-3}$ s^{-1})	6.7 ±0.6	6.7 ±0.6	6.7 ±0.6	6.7 ±0.6	6.7 ±0.6	6.7 ±0.6	6.7 ±0.6
k_{total} ($\times 10^{-4}$ s^{-1})	4.6 ±0.13	3.90 ±0.70	3.76 ±0.20	4.0 ±0.25	4.10 ±0.16	3.50 ±0.40	3.91 ±0.12
k_{OH}[OH] ($\times 10^{-6}$ s^{-1})	-	-	3.91 ±0.20	0	-	0	8.03 ±0.13
j(phthal) ($\times 10^{-4} s^{-1}$)	4.6 ±0.13	3.90 ±0.70	3.72 ±0.20	4.0 ±0.25	4.10 ±0.16	3.50 ±0.40	3.83 ±0.12
j(phthal)/$j(NO_2)$	0.068 ±0.004	0.058 ±0.007	0.056 ±0.002	0.059 ±0.003	0.061 ±0.001	0.052 ±0.004	0.057 ±0.003
SOA (%)	2.00	6.50	2.40	7.00	2.80	11.10	1.20
Phthalide (%)	56 ±1.2	48 ±3.2	51 ±1.6	42 ±3.2	35 ±1.6	40 ±6	50 ±8
Phthalic anhydride (%)	35 ±0.9	26 ±1.6	20 ±2.0	21 ±2	18 ±2.3	26 ±3	32 ±10

[1] In this experiment 1,3 5-trimethylbenzene (300 ppbV) was as an OH radical tracer. [2] In this experiment CO (500 ppmV) used as an OH radical scavenger. Phthaldialdehyde and SOA mass concentration was corrected for wall loss. Errors are twice the standard deviation.

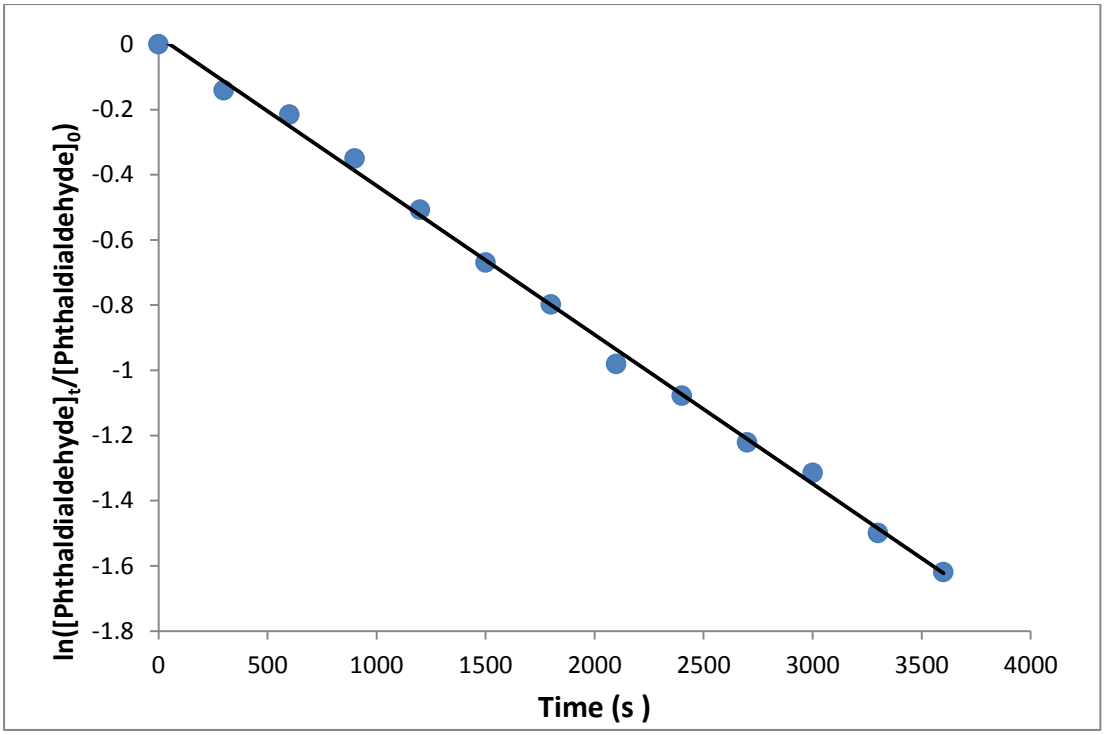


Figure 4.16 Photolytic loss of phthaldialdehyde (corrected for wall loss) in experiment 10122010 performed in the indoor chamber.

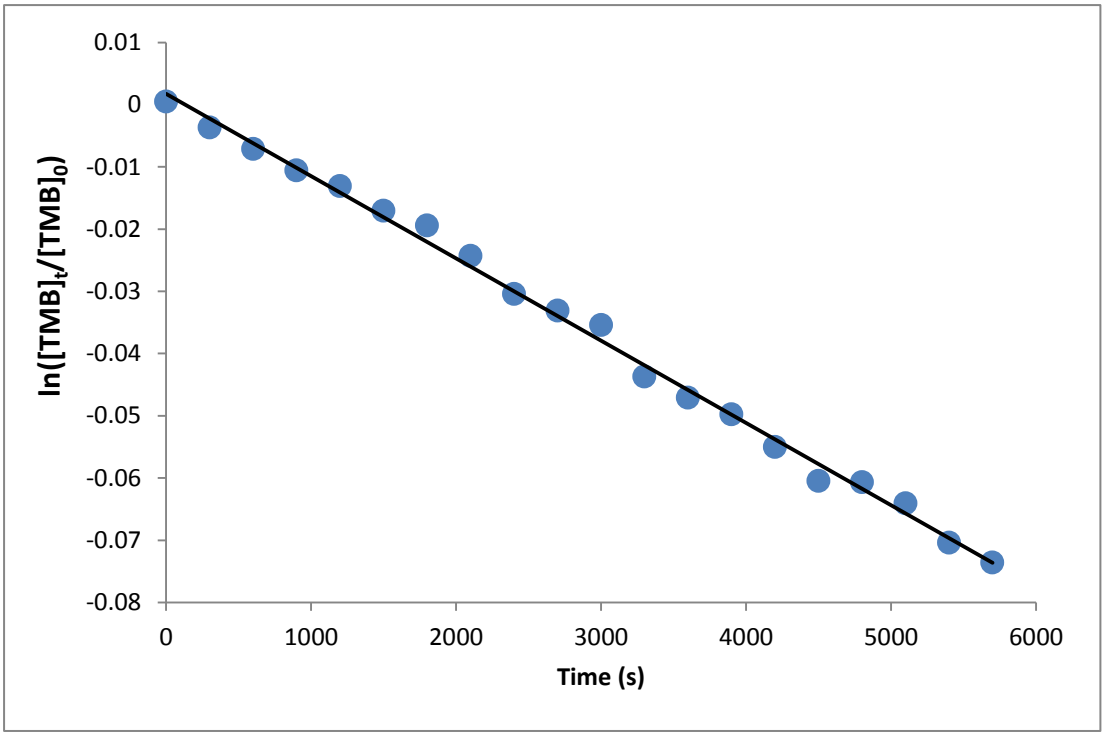


Figure 4.17 Decay rate of 1,3,5-trimethylbenzene (TMB, corrected for wall loss) during the photolysis of phthaldialdehyde in experiment 16122010 performed in the indoor chamber.

4.3.1.3 Comparison with Previous Studies

The photolysis rates measured in the indoor experiments are compared to those obtained at EUPHORE and by Wang et al. (2006) in **Table 4.4**. The values for *j*(phthal) and *j*(phthal)/*j*(NO_2) are quite different, indicating that the wavelength distribution and intensity of the light sources has a significant effect. The blacklamps used by Wang et al. have a peak emission around 360 nm, similar to the Philips TL05 lamps used in this work. However, the presence of the Philips TL12 lamps, with an emission maximum around 310 nm, creates a different light distribution in the indoor chamber used in this work, **Figure 4.6**. The poor agreement between the *j*(phthal)/*j*(NO_2) values obtained from the indoor chamber experiments highlights the need for such measurements to be performed using natural sunlight.

Table 4.4 Comparison of the photolysis rates of phthaldialdehyde measured in different atmospheric simulation chamber studies.

***j*(phthal)** **($\times 10^{-3}$ s^{-1})**	***j*(NO_2)** **($\times 10^{-3}$ s^{-1})**	***j*(phthal)/*j*(NO_2)**	**Light source**	**Reference**
0.38 ± 0.070*	6.7 ± 0.3	0.056 ± 0.008*	Philips TL05 lamps (λ_{max}=360 nm) and Philips TL12 lamps (λ_{max}=310 nm)	This work
0.101 ± 0.002 0.159 ± 0.002	5.07 ± 0.40 8.0 ± 0.6	0.020 ± 0.004*	Natural light	This work
0.265 ± 0.003	8.9 ± 0.9	0.030 ± 0.004	Black lamps (λ_{max}=360 nm)	(Wang et al. 2006)

** Average value obtained from experiments performed using OH scavenger and tracer*

There has only been one previous study of the photolysis of an aromatic aldehyde using natural sunlight, in which Clifford et al. (Clifford et al. 2011) performed a detailed investigation of the photolysis of *o*-tolualdehyde by natural sunlight at the European Photoreactor (EUPHORE) in Valencia, Spain. The photolysis rate coefficient was determined, with a value of *j*(*o*-tolualdehyde) = (1.62-2.15) $\times 10^{-4}$ s^{-1}, yielding an average value of *j*(*o*-tolualdehyde)/*j*(NO_2) = (2.53 ± 0.25) $\times 10^{-2}$. The

corresponding values of j(phthal) and j(phthal)/j(NO_2) obtained in this work for the photolysis of phthaldialdehyde at EUPHORE are very similar, **Table 4.4**. This is not surprising given that *o*-tolualdehyde and phthaldialdehyde have similar chemical structures.

4.3.2 Photolysis Products

Gas-phase products arising from the photolysis of phthaldialdehyde were determined by FTIR spectroscopy. Two main products were identified; phthalide and phthalic anhydride, in agreement with Wang et al. (Wang et al. 2006). Quantification of the reactant and products was achieved by careful subtraction of calibrated FTIR spectra, as indicated in **Figure 4.18**. The yield of the products was determined using the following relationship:

$$yield = \frac{\Delta[product](ppbV)}{\Delta[phthaldialdehyde](ppbV)} \times 100\% \quad \text{(IX)}$$

Where $\Delta[product]$ is the amount of product generated and $\Delta[phthaldialdehyde]$ is the amount of phthaldialdehyde consumed. These concentration terms were corrected for wall loss since phthaldialdehyde, phthalide and phthalic anhydride were all observed to undergo deposition to the walls of the chambers.

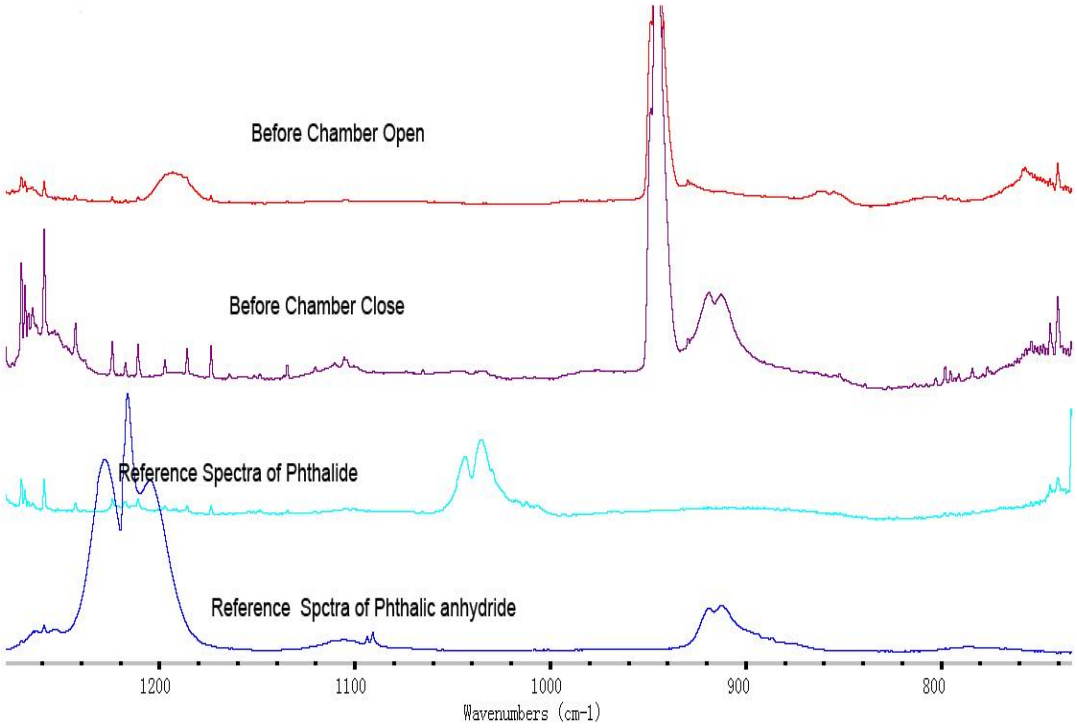


Figure 4.18 FTIR spectra obtained during the photolysis of phthaldialdehyde in the EUPHORE chamber, along with calibrated reference spectra of the reaction products. The strong peak present at ca. 950 cm^{-1} is due to the inert tracer SF_6.

4.3.2.1 EUPHORE Chamber

Concentration–time profiles and product yield plots in the form of **Equation (IX)** were generated for all experiments and are shown in **Figure 4.19**-**Figure 4.26**. The yield plots for both phthalide and phthalic anhydride are linear indicating that these compounds are primary products of the reaction and are not removed to any significant extent during the timescale of the experiments. Product yields were determined from a linear least squares fit of the data in the plots and are listed in **Table 4.2.** The yields of both products show some variation between experiments and is attributed to interference from the reaction of phthaldialdehyde with OH radicals, which is known to produce phthalic anhydride with a yield of (85 ± 20)% , but no phthalide (Wang et al. 2006). However, the experiment performed on 10th July 2009 employed an excess of CO to scavenge OH radicals and the products can only be attributed to direct photolysis. The yields of (42 ± 0.4)% for phthalide and (24 ± 0.6)% for phthalic anhydride are slightly lower than those reported by Wang et al. in their indoor chamber study (Wang et al. 2006). In the experiment performed on 3rd July

2009, a value of [OH] = 0.35 × 10^6 molecule cm^{-3} was measured, indicating that the OH radical reaction accounts for ca. 2% of the loss of phthaldialdehyde. The higher yield of phthalic anhydride obtained in this experiment is consistent with this observation. In the experiments performed on 1st July 2009 and 2nd July 2009, no scavenger or tracer was used and it was estimated that [OH] = 1.05 × 10^6 molecule cm^{-3}. The higher concentration of OH in these latter experiments results in approximately 12.7% loss of phthaldialdehyde due to reaction with OH. As expected, this results in a reduced yield of phthalide and an increased yield of phthalic anhydride.

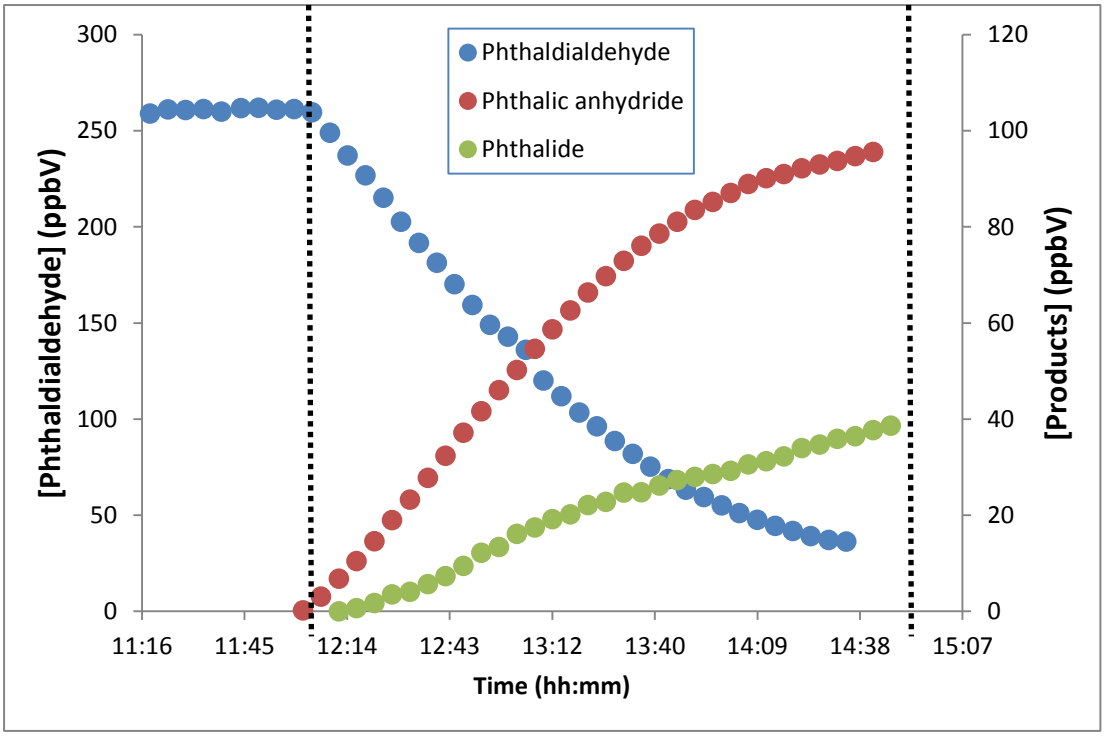


Figure 4.19 Concentration-time profiles for phthaldialdehyde and its photolysis products at EUPHORE on 1st July 2009. The vertical dotted lines indicate the time the chamber was opened (12:06) and closed (14:53).

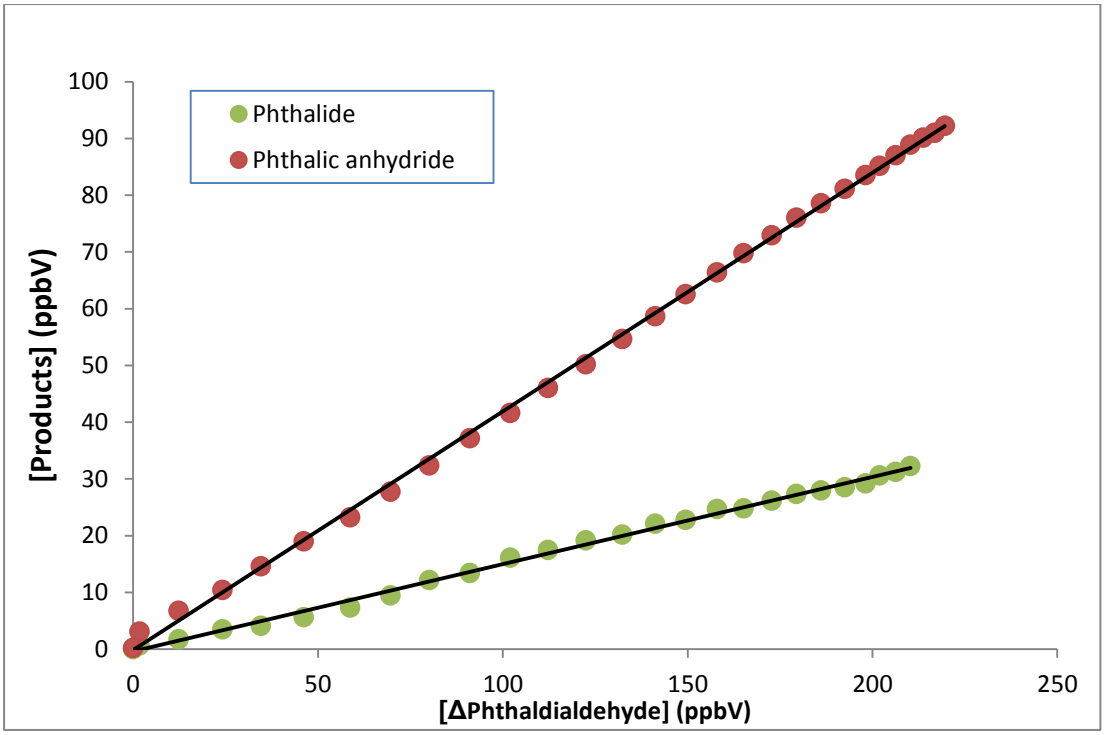


Figure 4.20 Product yield plot for phthalide and phthalic anhydride during the photolysis of phthaldialdehyde at EUPHORE on 1st July 2009.

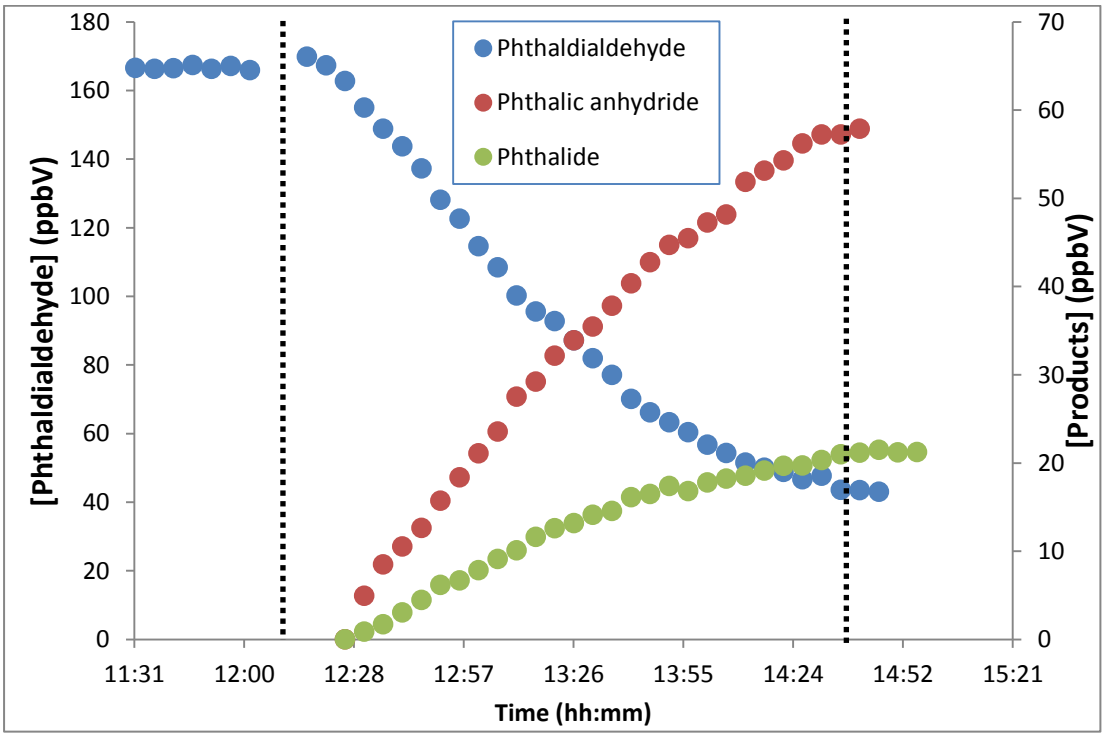


Figure 4.21 Concentration-time profiles for phthaldialdehyde and its photolysis products at EUPHORE on 2nd July 2009. The vertical dotted lines indicate the time the chamber was opened (12:20) and closed (14:35).

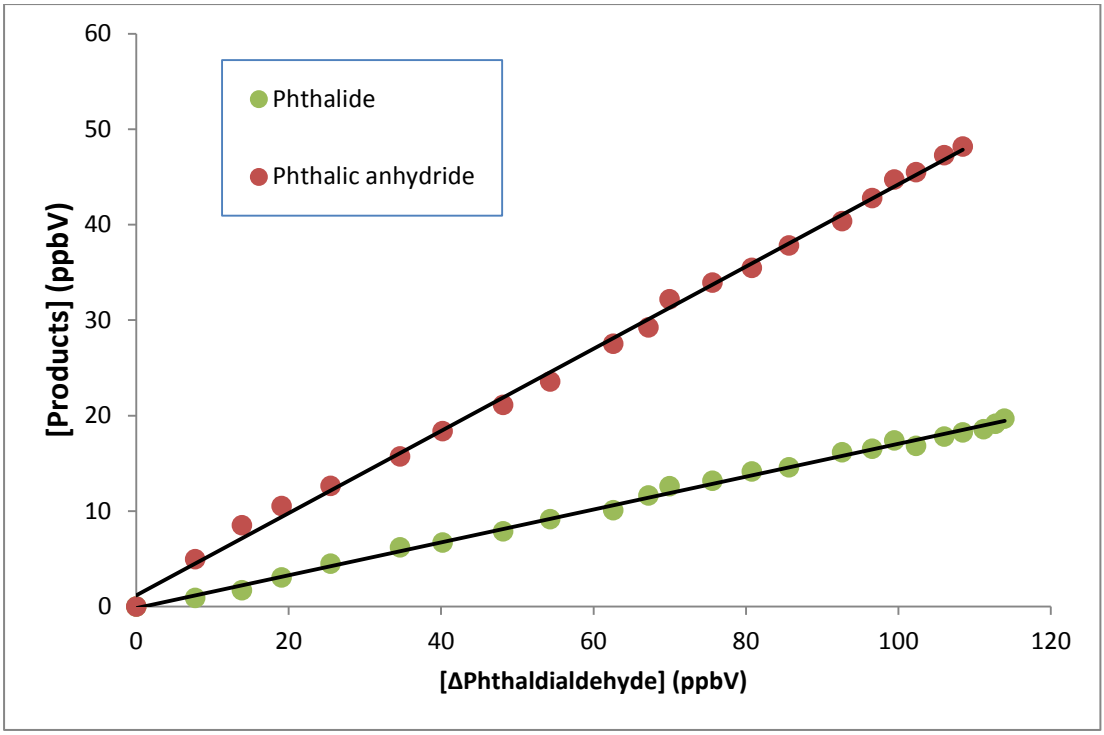


Figure 4.22 Product yield plot for phthalide and phthalic anhydride during the photolysis of phthaldialdehyde at EUPHORE on 2nd July 2009.

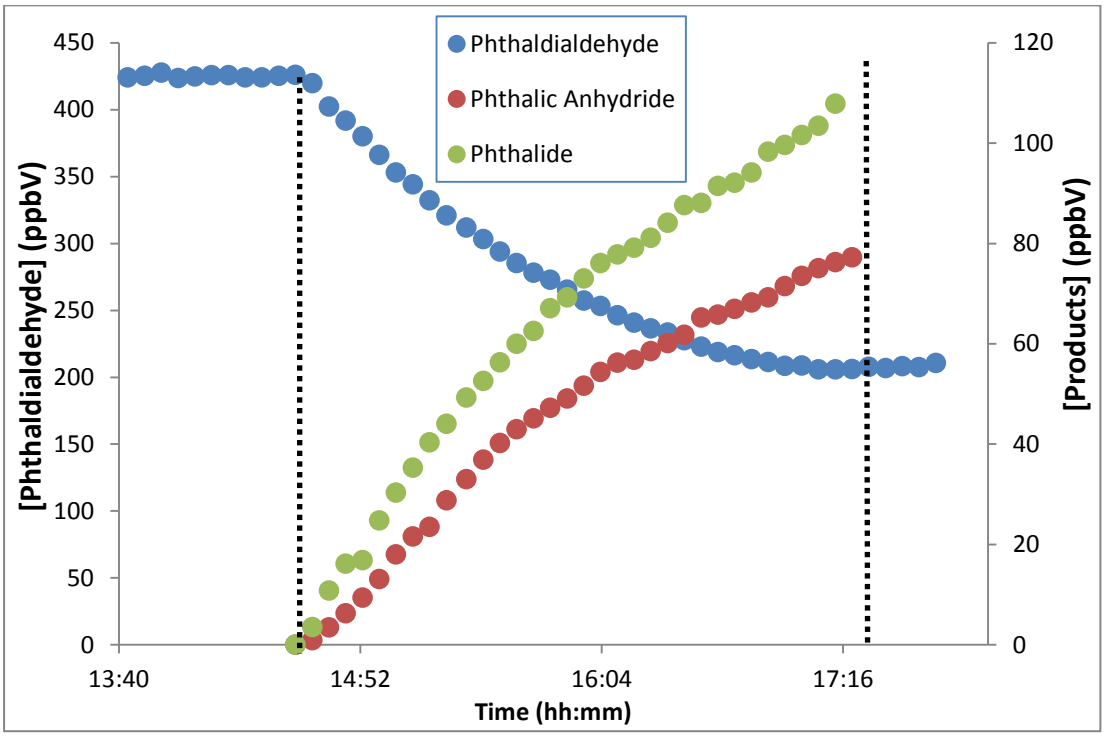


Figure 4.23 Concentration-time profiles for phthaldialdehyde and its photolysis products at EUPHORE on 3rd July 2009. The vertical dotted lines indicate the time the chamber was opened (14:35) and closed (17:22).

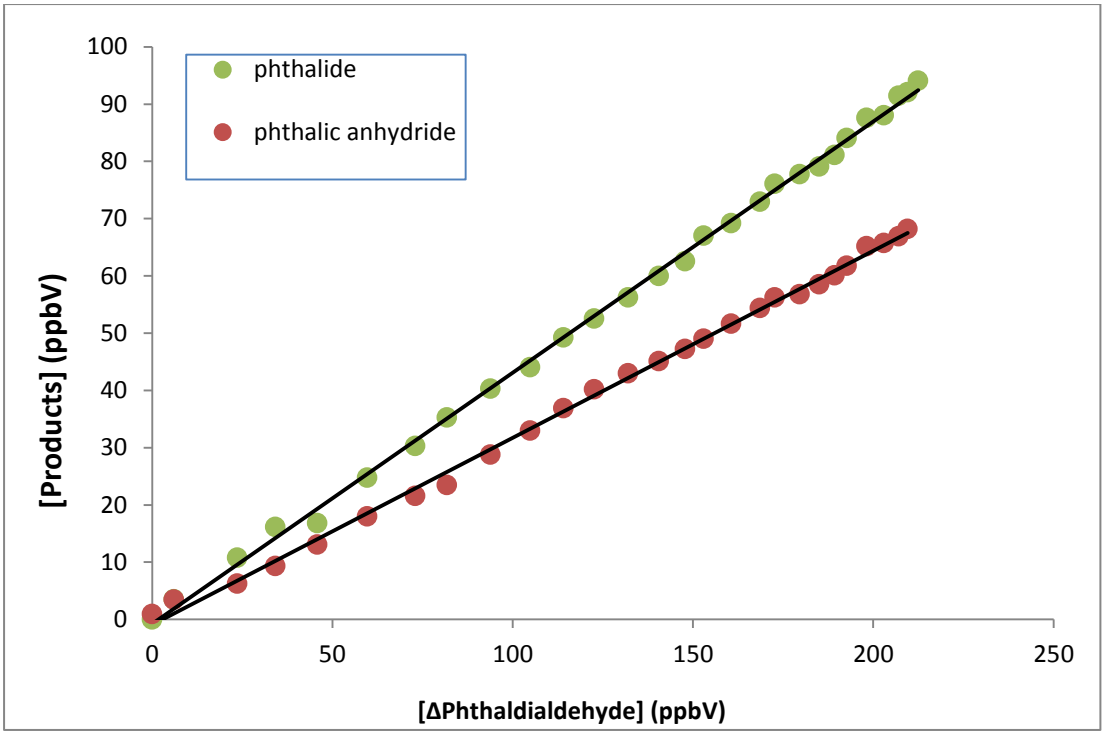


Figure 4.24 Product yield plot for phthalide and phthalic anhydride during the photolysis of phthaldialdehyde at EUPHORE on 3rd July 2009.

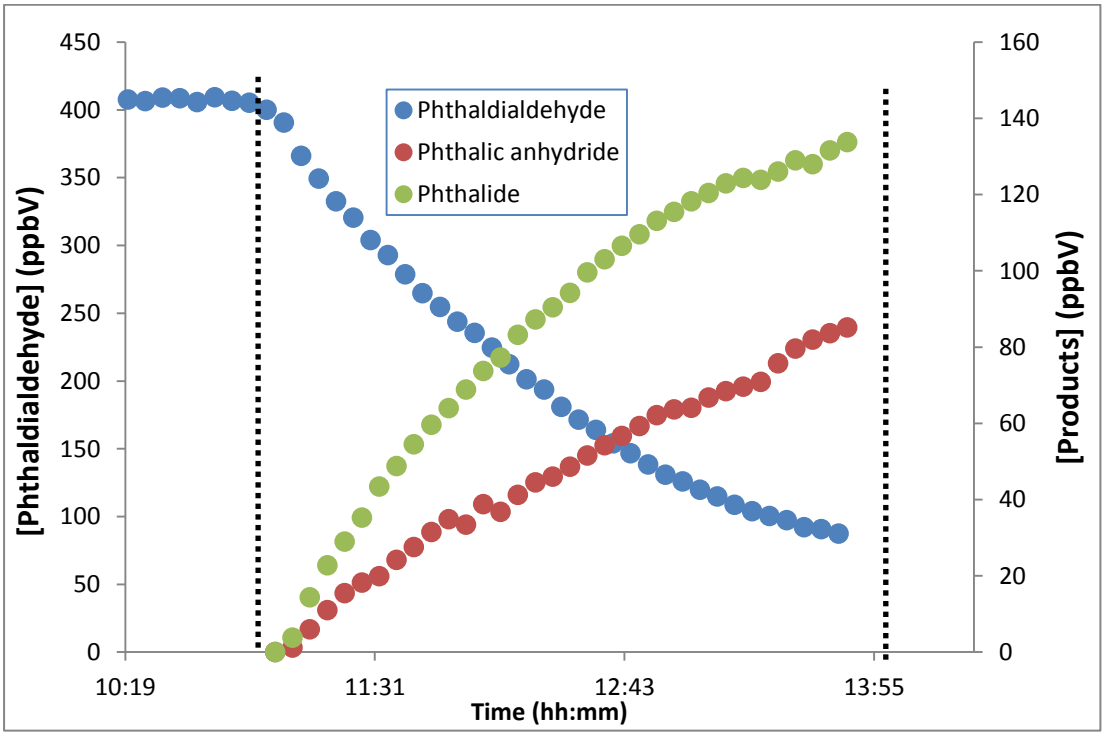


Figure 4.25 Concentration-time profiles for phthaldialdehyde and its photolysis products at EUPHORE on 10th July 2009. The vertical dotted lines indicate the time the chamber was opened (10:55) and closed (13:58).

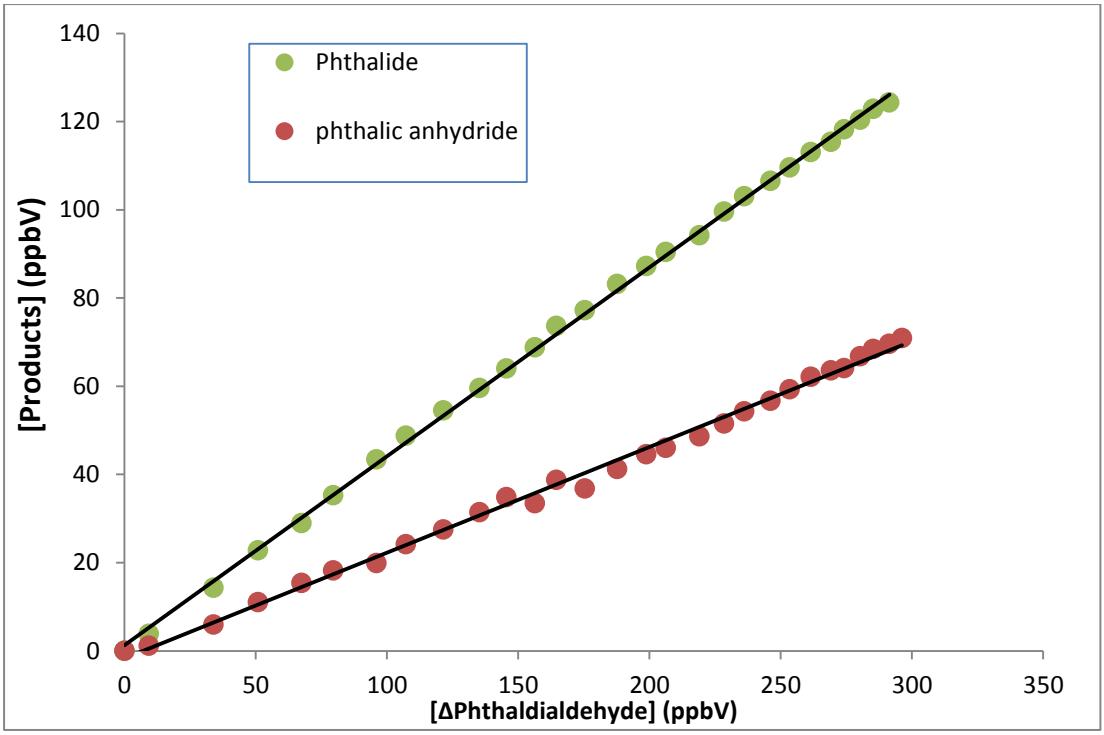


Figure 4.26 Product yield plot for phthalide and phthalic anhydride during the photolysis of phthaldialdehyde at EUPHORE on 10th July 2009.

4.3.2.2 Indoor Chamber

Concentration–time profiles and product yield plots in the form of Equation (IX) were generated for all experiments performed in the indoor chamber. Representative data from one of the experiments are shown in **Figures 4.27** and **Figure 4.28**. The plots for both phthalide and phthalic anhydride were linear and the product yields were determined from a linear least squares fit of the data. The product yields are summarized in **Table 4.3**, along with details of the experimental conditions. As in the EUPHORE experiments, the yields of both products showed some variation between the experiments. However, the variation is much smaller and the yield of phthalide was always higher than that of phthalic anhydride, indicating that the OH reaction only had a very minor influence on the reactive loss of phthaldialdehyde. This is consistent with the observation from kinetic measurements that reaction with OH only accounts for ca. 2% of the loss of phthaldialdehyde in the tracer experiments. The product yields were not affected significantly when the relative humidity was increased to ~50%.

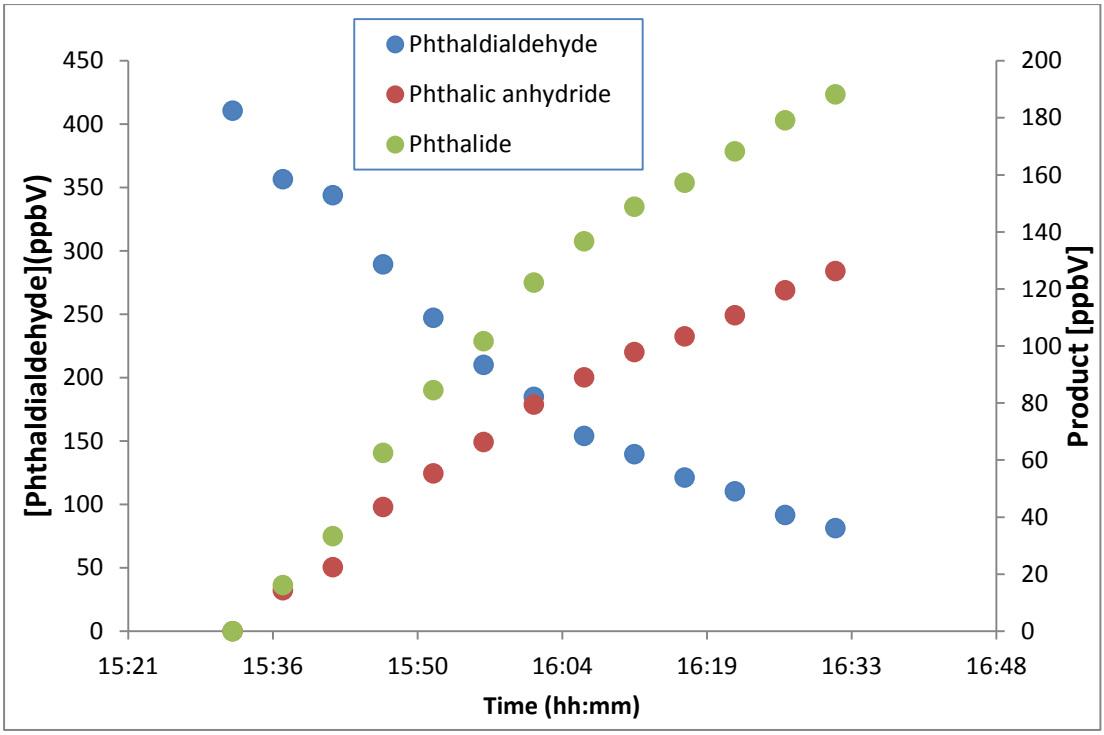


Figure 4.27 Concentration-time profiles for phthaldialdehyde and its photolysis products in experiment 10122010 performed in the indoor chamber.

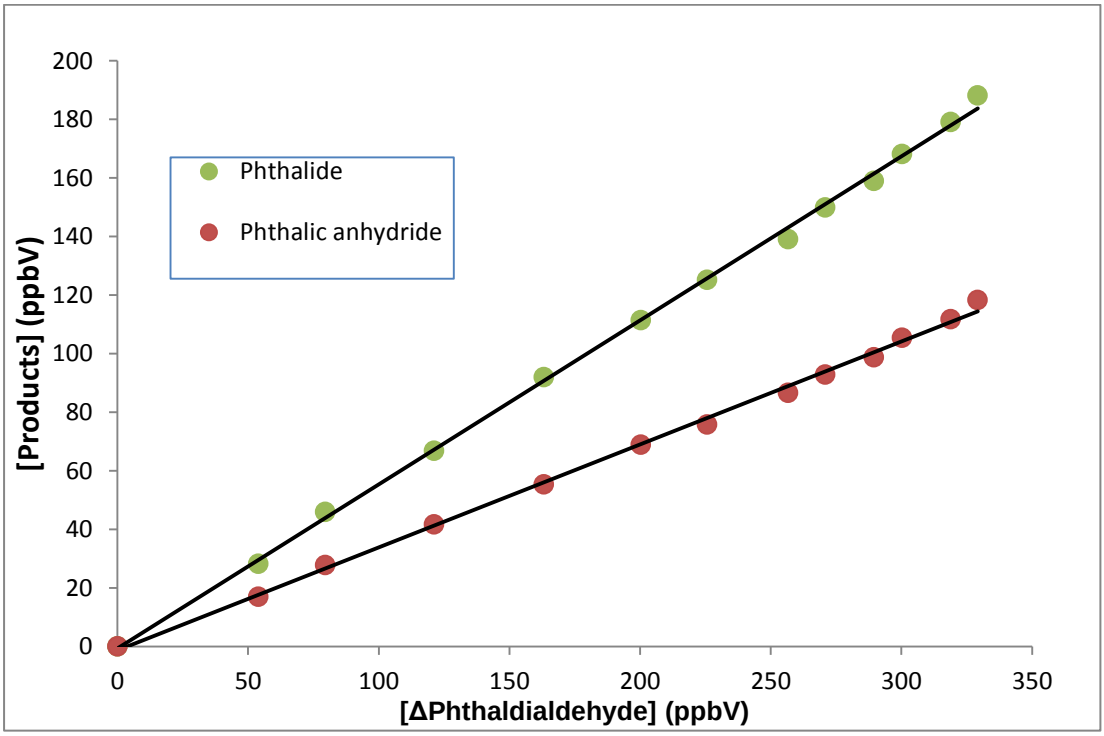


Figure 4.28 Product yield plot for phthalide and phthalic anhydride during the photolysis of phthaldialdehyde in experiment 10122010 performed in the indoor chamber.

4.3.2.3 Comparison with Previous Studies

In the only previous study of the photolysis of phthaldialdehyde, Wang et al. (Wang et al. 2006) reported yields of (53 ± 14) % and (35 ± 10) % for phthalide and phthalic anhydride respectively in the presence of cyclohexane as the OH radical scavenger. As indicated in **Table 4.2** and **Table 4.3**, the yields determined in this work are generally in good agreement with those of Wang et al., particularly for experiments where a scavenger or tracer was used. In the absence of scavenger, higher yields of phthalic anhydride were obtained, due to reaction of phthaldialdehyde with OH radicals. The highest yields of phthalic anhydride were obtained in EUPHORE experiments conducted without a scavenger or tracer. However, this effect was not observed in the indoor chamber, indicating that less OH radicals are produced, either during the photolysis process itself or from chamber artefacts such as wall reactions. The overall product yields were in the range 53-91%, with the variations being ascribed to variable contributions of OH reaction and aerosol formation, as well as experimental error. It is interesting to note that the lowest overall yields were generally obtained when CO was used as the scavenger. The reaction of OH with CO produces HO_2 radicals with unit yield and it is possible that the relatively large amounts of these radicals may increase the efficiency of reaction pathways, e.g. RO_2 + HO_2 reactions, that result in different products.

4.3.2.4 Photolysis Mechanism

The information obtained from the product studies can be used to propose a mechanism for the atmospheric photolysis of phthaldialdehyde. In general, the principal reactions in the atmospheric photolysis of aldehydes are Norrish type I and Norrish type II reactions. The cleavage of a C-C bond via the Norrish Type I reaction would release the HCO radical which subsequently oxidizes to produce CO in unit yield. Since carbon monoxide was not detected in any of the experiments performed in this work, this pathway can be ruled out. A possible reaction scheme arising from a Norrish type II process is presented in **Figure 4.29**. It is based on analogous mechanisms proposed to explain photocyclization reactions during the photochemical synthesis of organic compounds (Wagner et al. 1991; Moorthy et al. 2001), and was also used to explain the cyclic products arising from the atmospheric photolysis of o-tolualdehyde (Clifford et al. 2011). The initial step in the mechanism is

photoexcitation of the aldehyde through the n→π* electronic transition followed by intramolecular hydrogen abstraction to produce a 1,4-biradical species. Yang cyclization to form a benzocyclobutenol derivative is possible, but this species was not observed by FTIR spectroscopy or GC-MS study. It is possible that the formation of this species is unfavourable due to excessive ring strain. It is therefore proposed that the main pathway for the 1,4-biradical species is cyclization to form a 5-membered ring radical species which rearranges to form phthalide or reacts with O_2 to form phthalic anhydride. An alternative mechanism, involving direct cyclization of the photoexcited species, is shown in **Figure 4.30**.

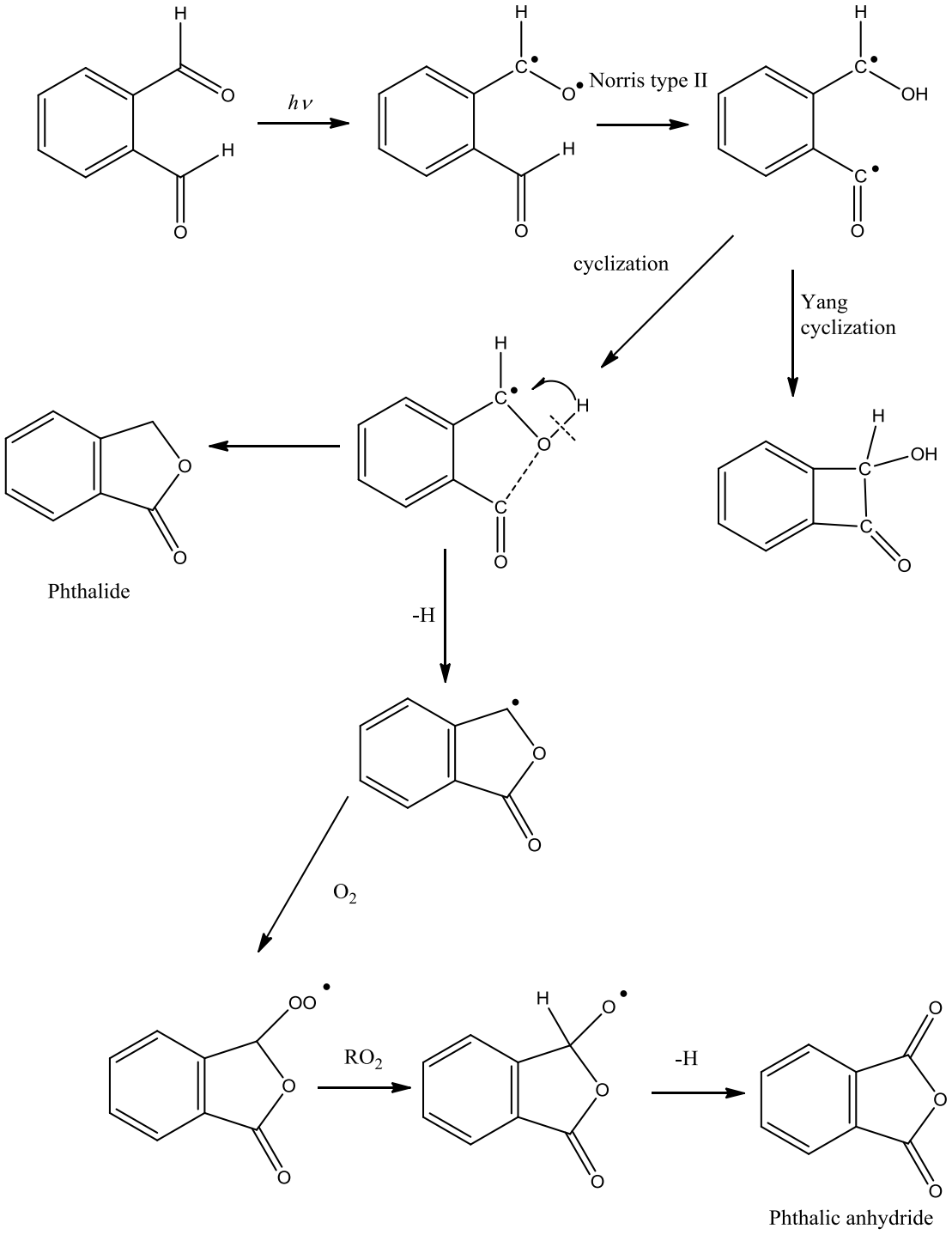


Figure 4.29 Possible reaction mechanism for the atmospheric photolysis of phthaldialdehyde via the formation of a 1,4-biradical.

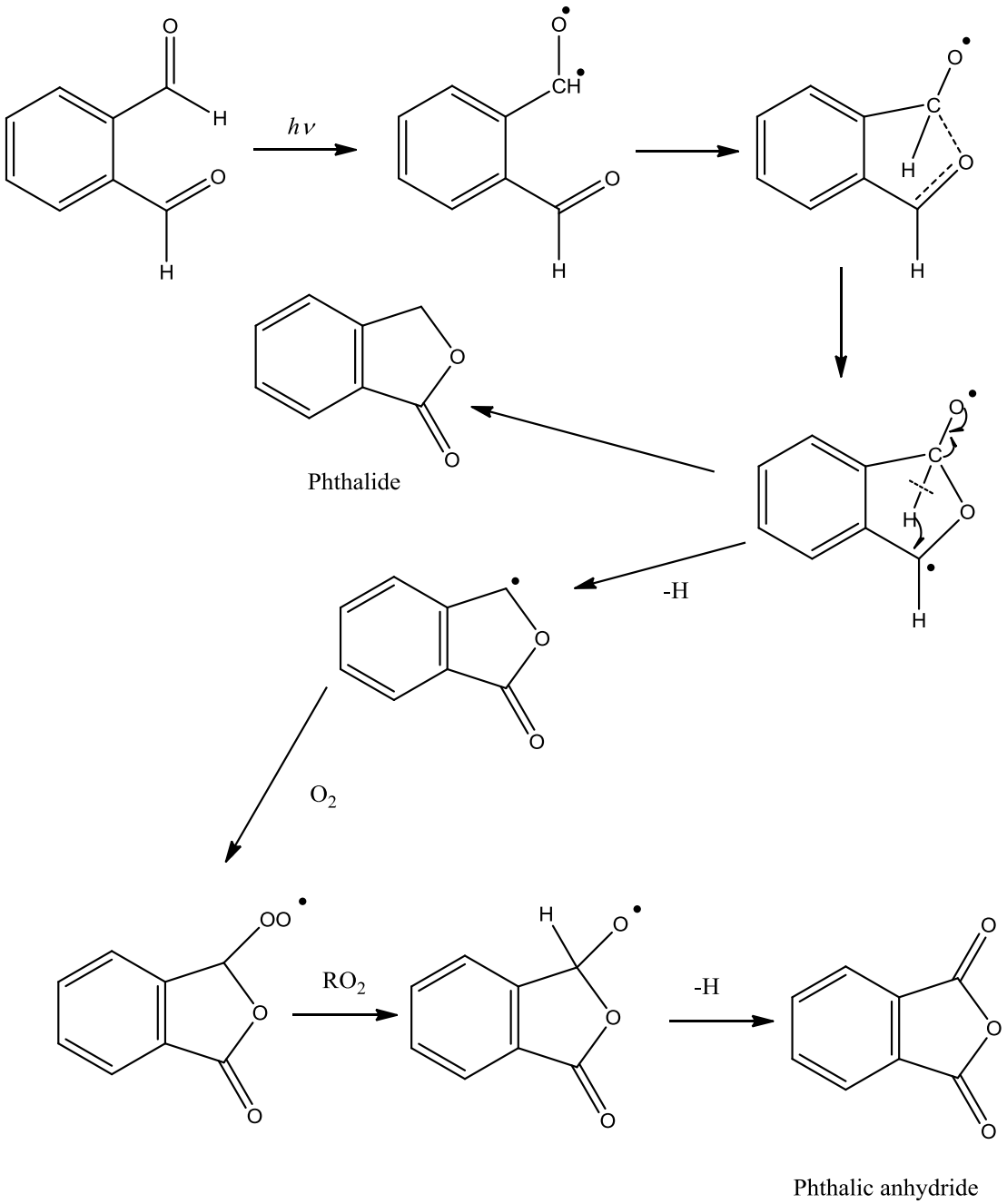


Figure 4.30 Possible reaction mechanism for the atmospheric photolysis of phthaldialdehyde via direct cyclization of the photoexcited molecule.

4.3.3 Secondary Organic Aerosol (SOA) Formation

The formation of secondary organic aerosol (SOA) was observed in all experiments performed in both chambers. The experiments were carried out in the absence of seed aerosol, which favoured the formation of new particles by nucleation. The volume concentration of the particles measured by the SMPS was converted to mass

concentration by assuming a density of 1.4 g cm^{-3} (Hallquist et al. 2009). The loss of particles to the chamber walls was determined by monitoring their decay in the dark at the end of each experiment. A first-order rate coefficient for wall loss was derived and used to correct the measured concentration data. The concentration of phthaldialdehyde was also corrected for wall loss as outlined previously.

4.3.3.1 EUPHORE Chamber

Concentration-time profiles showing the decrease of phthaldialdehyde and increase in aerosol mass were generated for each experiment and are shown in **Figures 4.31**, **Figure 4.33**, **Figure 4.35** and **Figure 4.37**. Wall loss correction factors in the range 4-8% and 8-14% were applied to the concentrations of phthaldialdehyde and aerosol mass respectively. The concentration-time profiles show that aerosol formation was observed immediately after opening the chamber and continued to rise until all of the phthaldialdehyde had reacted or the chamber was closed. The yield of aerosol produced in the experiments was determined from the following expression:

$$yield = \frac{\Delta[SOA](\mu g\ m^{-3})}{\Delta[phthaldialdehyde](\mu g\ m^{-3})} \times 100\% \qquad (X)$$

where Δ[SOA] is the mass concentration of particles produced and Δ[phthaldialdehyde] is the amount of phthaldialdehyde consumed at the end of the experiment, corrected for wall loss. The calculated aerosol yields are listed in **Table 4.2.** SOA yields were lowest (2.8% and 3.2%) in the experiments performed without a scavenger or tracer. The addition of 1,3,5-trimethylbenzene as a tracer resulted in a considerable increase in SOA yield to 10.0%. This was expected since the reaction of OH radicals with 1,3,5-trimethylbenzene is known to produce SOA with yields up to 8% (Healy et al. 2008). The SOA produced in this experiment will therefore be a mixture of products arising from three different processes; direct photolysis of phthaldialdehyde, OH reaction with 1,3,5-trimethylbenzene and OH reaction with phthaldialdehyde. The experiment conducted with CO as the OH scavenger produced the highest aerosol yield. It should be noted that some aerosol of unknown composition was generated in the chamber during the addition of CO and that the SOA yield was determined from the net increase of particle mass as a result of photolysis. Carbon monoxide has previously been used as an OH radical scavenger

during ozonolysis experiments, where it was shown to increase SOA yields via the efficient production of HO_2 radicals which combine with RO_2 to produce condensable products (Keywood et al. 2004).

The evolution of the aerosol particle and size distribution during the photolysis experiments is shown in **Figure 4.32**, **Figure 4.34**, **Figure 4.36**, and **Figure 4.42**. The aerosol formation is most clearly illustrated in the experiments performed without scavenger or tracer, **Figures 4.32** and **Figure 4.34**. A large number of particles with a mean diameter of approximately 20-30 nm were observed in the first 3 min of photolysis. This initial "burst" of particles also corresponded to the greatest number present during the reaction. As photolysis continued, there was a gradual reduction in the particle number and increase in average particle diameter due to coagulation. Particles with a mean diameter in the range 60-100 nm were present at the end of the experiments.

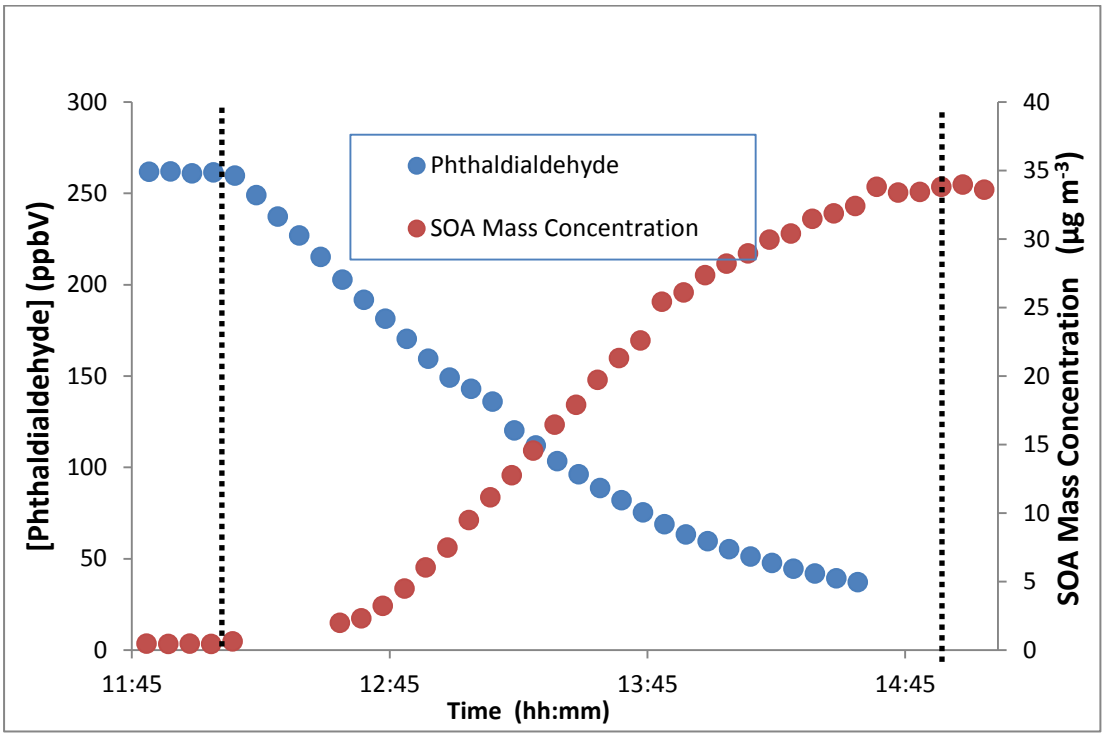


Figure 4.31 Concentration-time profile showing SOA formation during the photolysis of phthaldialdehyde at EUPHORE on 1st July 2009. The vertical dotted lines indicate the time the chamber was opened (12:06) and closed (14:53).

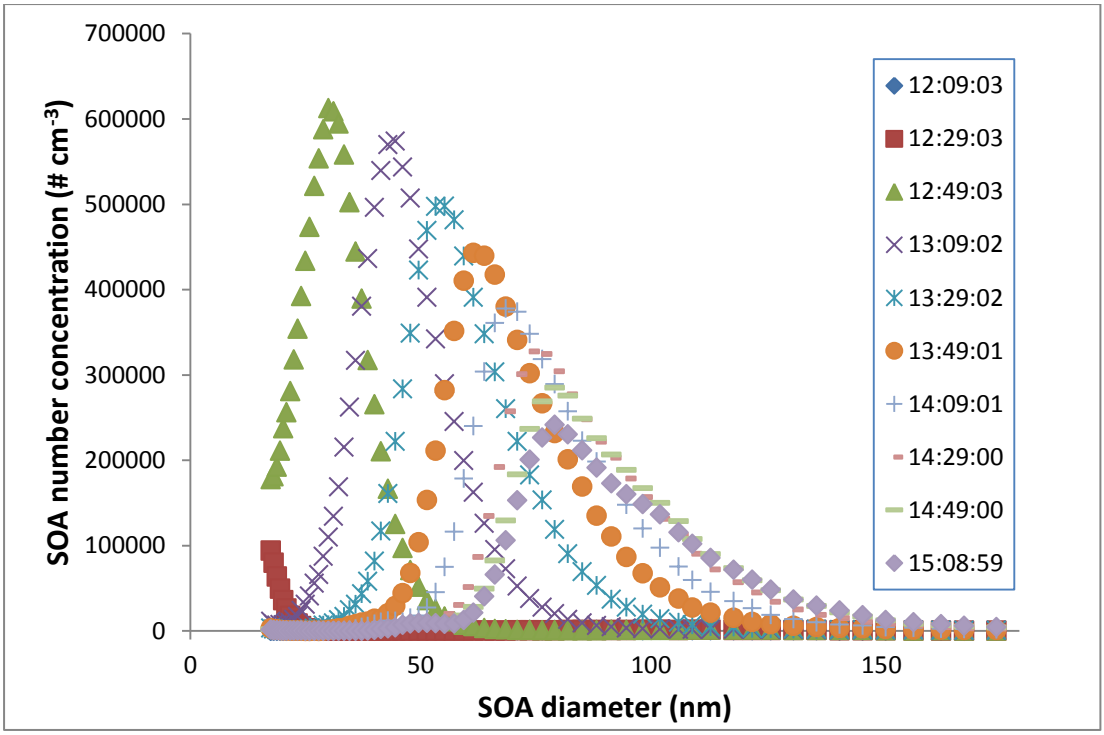


Figure 4.32 Number and size distribution of SOA particles formed during the photolysis of phthaldialdehyde at EUPHORE on 1st July 2009.

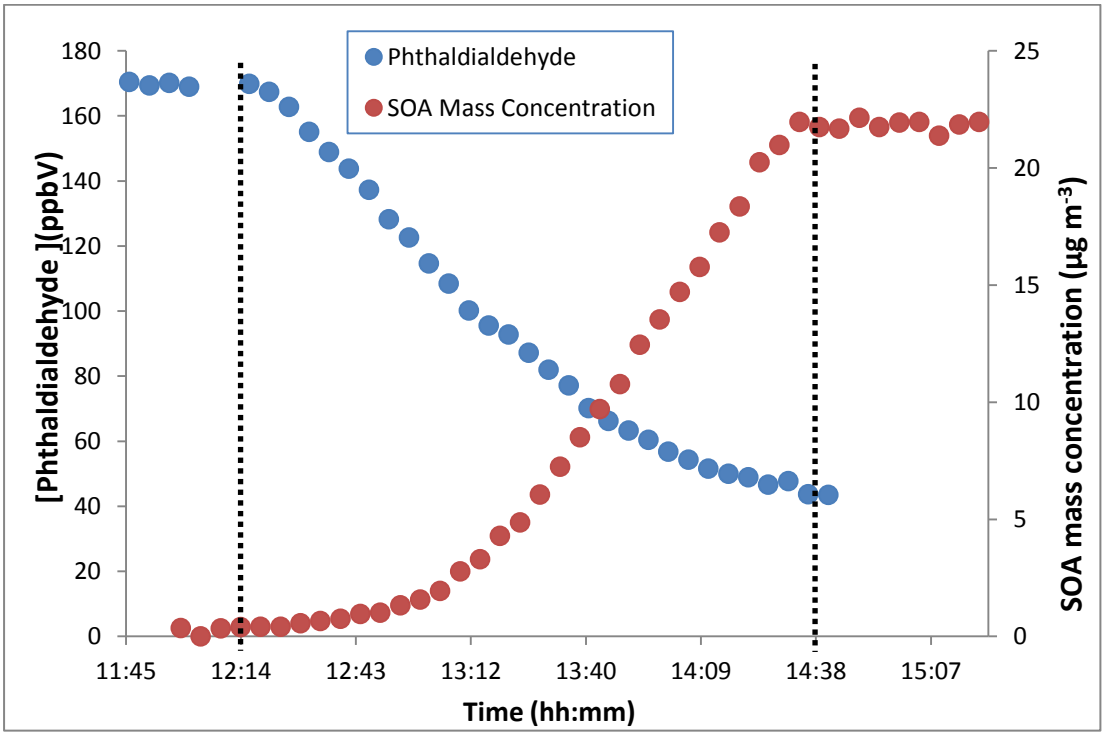


Figure 4.33 Concentration-time profile showing SOA formation during the photolysis of phthaldialdehyde at EUPHORE on 2nd July 2009. The vertical dotted lines indicate the time the chamber was opened (12:14) and closed (14:35).

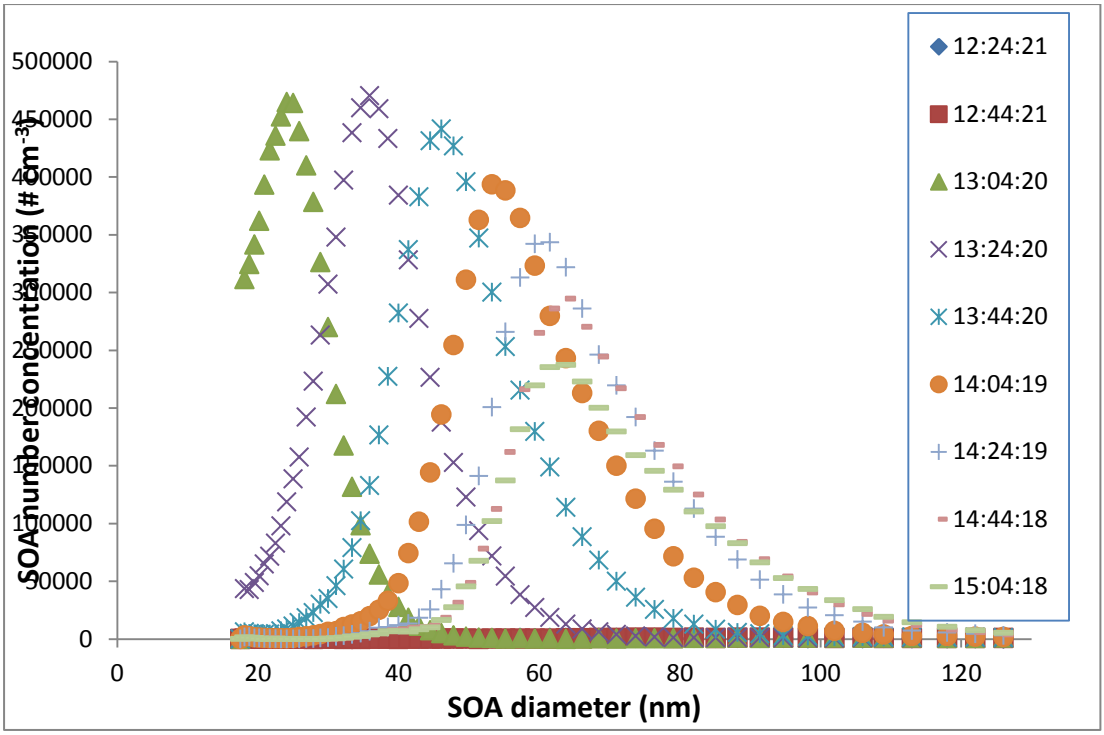


Figure 4.34 Number and size distribution of SOA particles formed during the photolysis of phthaldialdehyde at EUPHORE on 2nd July 2009.

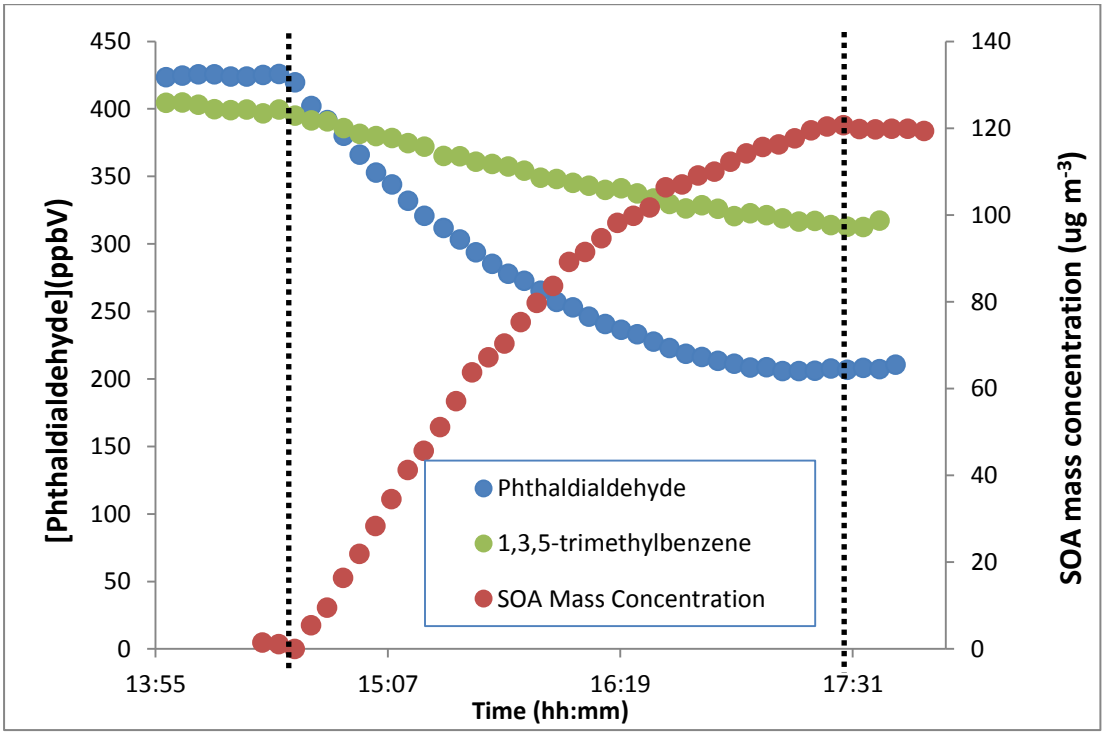


Figure 4.35 Concentration-Time profile showing SOA formation during the photolysis of phthaldialdehyde at EUPHORE on 3rd July 2009. The vertical dotted lines indicate the time the chamber was opened (14:35) and closed (17:22).

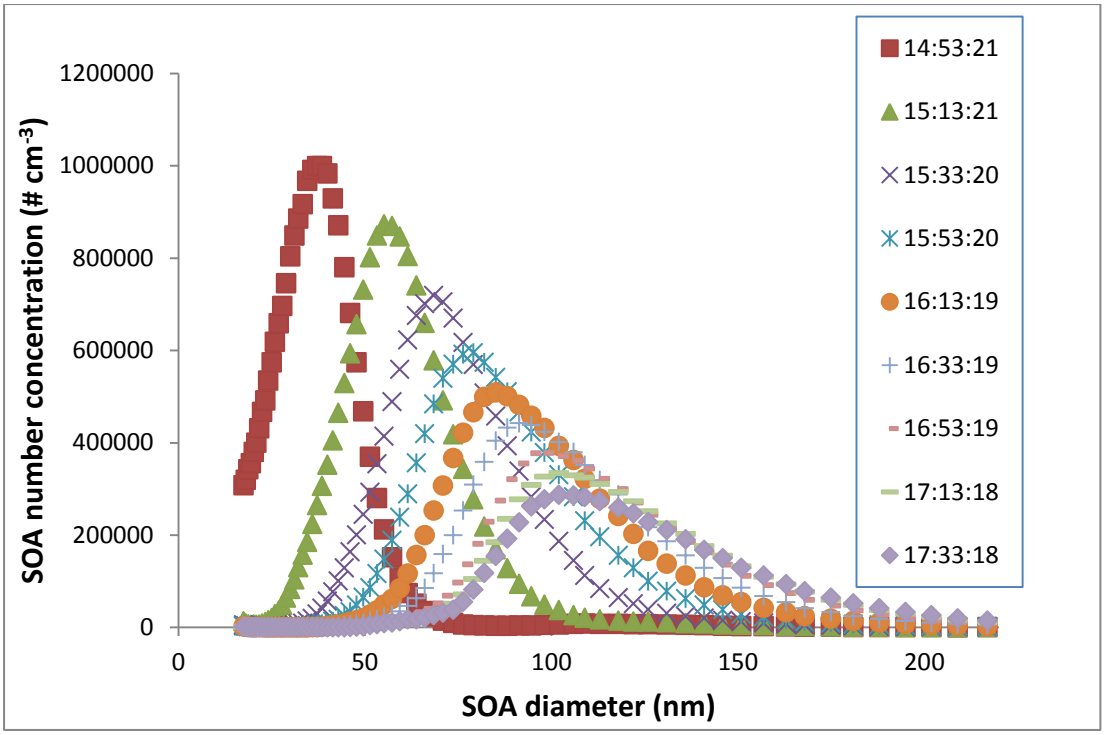


Figure 4.36 Number and size distribution of SOA particles formed during the photolysis of phthaldialdehyde at EUPHORE on 3rd July 2009.

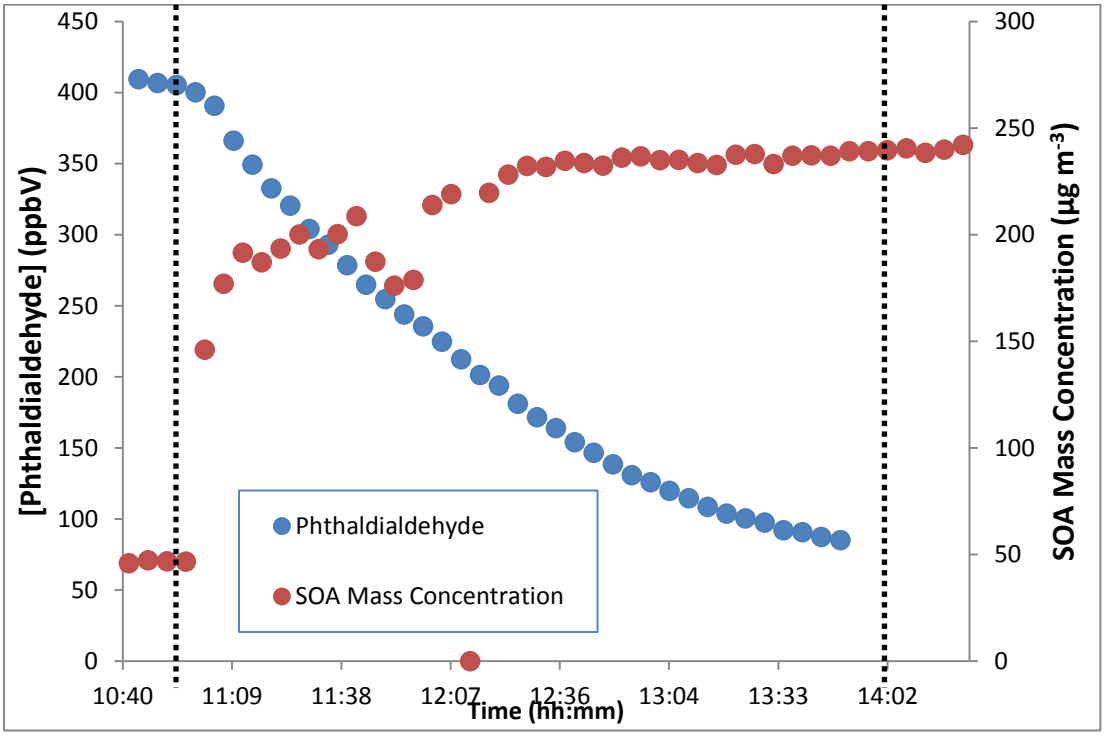


Figure 4.37 Concentration-Time profiles showing SOA formation during the photolysis of phthaldialdehyde at EUPHORE on 10th July 2009. The vertical dotted lines indicate the time the chamber was opened (10:55) and closed (13:58).

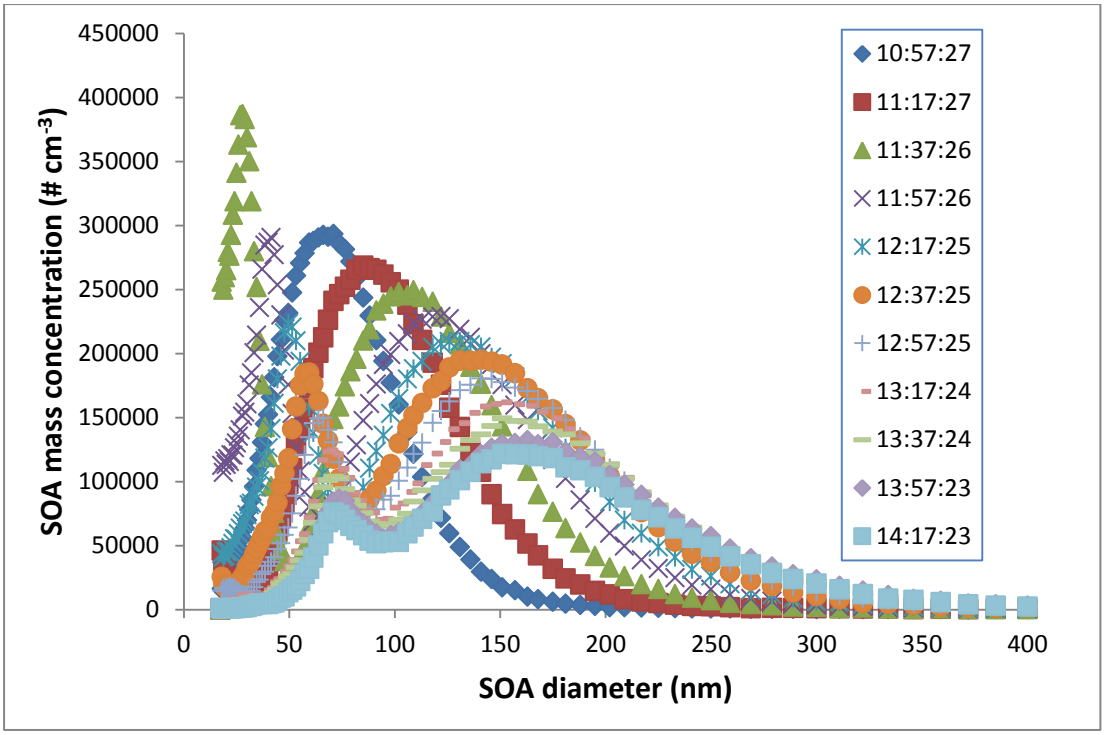


Figure 4.38 Number and size distribution of SOA particles formed during the photolysis of phthaldialdehyde at EUPHORE on 10th July 2009.

The composition of SOA arising from photolysis of phthaldialdehyde without tracer or scavenger was analysed by GC-MS. Filter samples collected at the end of the experiment were treated in three different ways: extracted into a solvent and analysed by a direct injection method, derivatized by PFBHA in order to identify any carbonyls, derivatized by BSTFA to identify hydroxyl-containing products. There were no carbonyl products detected using PFBHA derivatization and the only products observed using the direct injection method were phthalide and phthalic anhydride. The total ion chromatogram obtained from BSTFA derivatization of the filter extracts is shown in **Figure 4.39**. Six products were identified and are listed in **Table 3.5**. Apart from salicylic acid, all of these products have been identified in previous studies of naphthalene photooxidation (Kautzman et al. 2010). The dominant species is dihydroxyphthalic acid, which may be formed from successive oxidation of phthalic acid (Kautzman et al. 2010; Nakao et al. 2011), as shown in **Figure 4.39**. The first step in this process is hydrolysis of phthalic anhydride, either in the gas or particle phase, to produce phthalic acid which will exist predominantly in the particle phase. Over time, phthalic acid may undergo oxidation in the particle phase to yield hydroxyl derivatives or decarboxylation to produce benzoic acid, which may also oxidise further to produce salicylic acid.

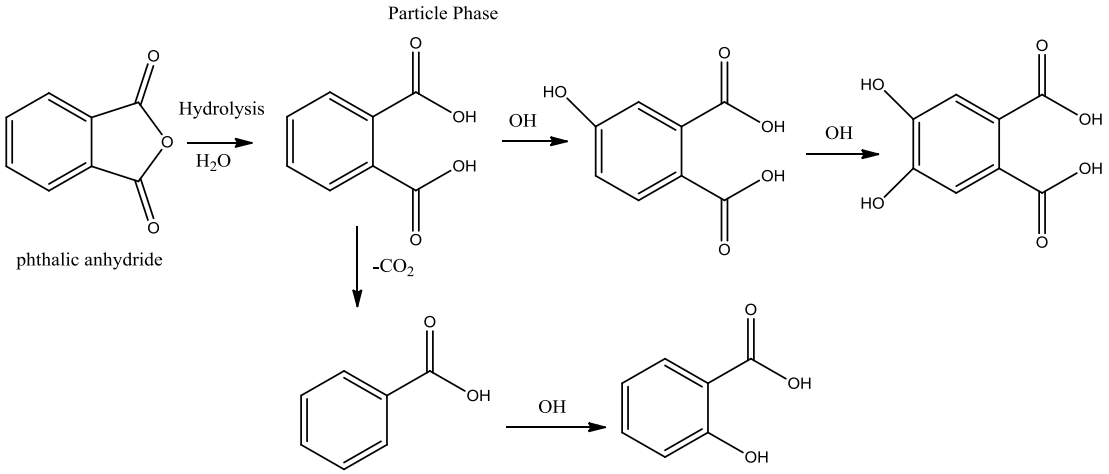


Figure 4.39 Possible reaction pathways leading to the formation of carboxylic acids detected by GC-MS with BSTFA derivatization.

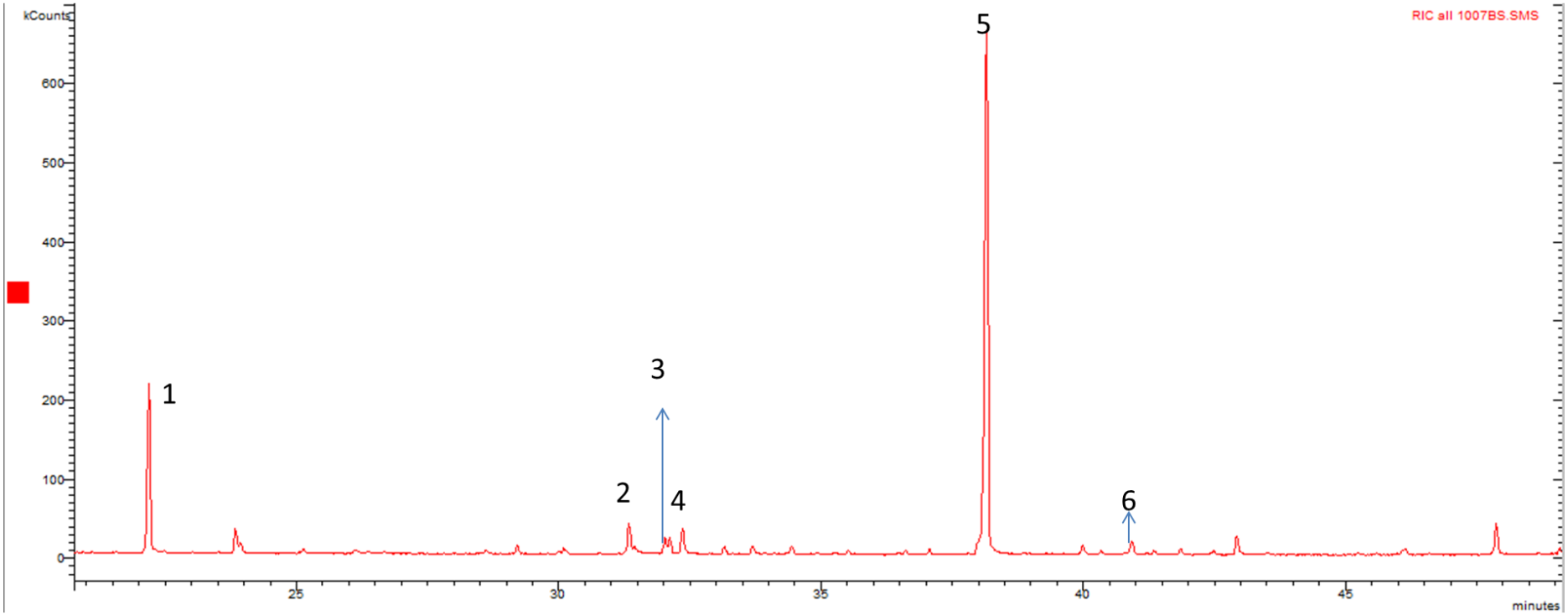
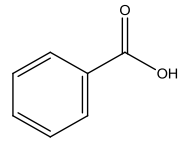
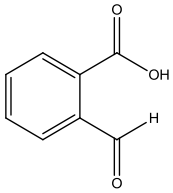
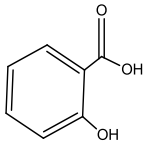
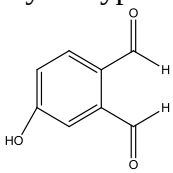
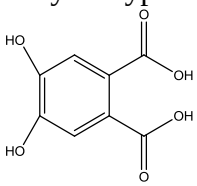
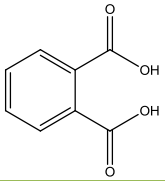


Figure 4.40 Total ion chromatogram of filter extracts obtained during the photolysis of phthaldialdehyde at EUPHORE and derivatized by BSTFA.

1) benzoic acid, 2) 2-formylbenzoic acid, 3) salicylic acid, 4) hydroxyphthaldialdehyde, 5) dihydroxyphthalic acid 6) phthalic acid.

Table 4.5 Particle phase products identified by BSTFA derivatization GC-MS (*m/z* 73) during the photolysis of phthaldialdehyde by natural sunlight in the EUPHORE chamber.

Compound	RT(min)	M*	Peaks	Reference
Benzoic acid 	22.12	194	51, 73, 77, 105, 135, 179, 194(M)	b, c
2-formylbenzoic acid 	31.34	222	73, 77, 105, 133, 179, 207, 222(M)	b
Salicylic acid 	32.25	267	73, 135, 267(M)	
Hydroxyphthaldialdehyde 	32.36	222	73, 77, 105, 133, 179, 207, 222(M)	b
Dihydroxyphthalic acid 	38.13	486	73, 119, 147, 193, 221, 265, 295, 383, 456(M-30).	b
Phthalic acid` 	40.90	310	73, 103, 207, 221, 251, 295, 310(M)	b, c

** M. is the molecular weight of the TMS derivative. References: (a) Lee and Lane 2009, (b) Kautzman et al. 2010, (c) Bunce et al.1997.*

4.3.3.2 Indoor Chamber

Concentration-time profiles showing the decrease of phthaldialdehyde and increase in aerosol mass were generated for all experiments performed in the indoor chamber. Representative data from one of the experiments is shown in **Figure 4.41**. Wall loss correction factors in the range 6-11% and 6-20% were applied to the concentrations of phthaldialdehyde and aerosol mass respectively. The concentration-time profiles were similar to those obtained in the EUPHORE experiments: aerosol formation was observed immediately after initiating photolysis and continued to rise until all of the phthaldialdehyde had reacted or the lights were turned off. However, aerosol formation was observed more rapidly in the indoor chamber experiments, probably due to the higher photolysis rate of phthaldialdehyde. The typical evolution of aerosol particle and size distribution during one of the photolysis experiments is shown in **Figure 4.42.** The pattern is very similar to that observed in the EUPHORE chamber, except that the mean particle diameters at the beginning and end of the experiments were slightly larger, again possibly due to the higher photolysis rate.

The calculated aerosol yields are listed in **Table 4.3** and are in the same range as those measured in the EUPHORE experiments. The highest yields were again obtained when using CO as a scavenger, further highlighting the importance of HO_2 chemistry in SOA formation and growth. The addition of 1,3,5-trimethylbenzene as OH radical tracer did not result in any noticeable increase in SOA. This finding is consistent with the results obtained from kinetics and products analysis which indicate that only small amounts of OH radicals were generated in the indoor chamber. Two out of three of the experiments performed at ~50% relative humidity produced higher SOA yields indicating that, as for naphthalene, aerosol formation and growth may be enhanced by the presence of additional water vapour. However, the results from these experiments are not conclusive and further investigation is required.

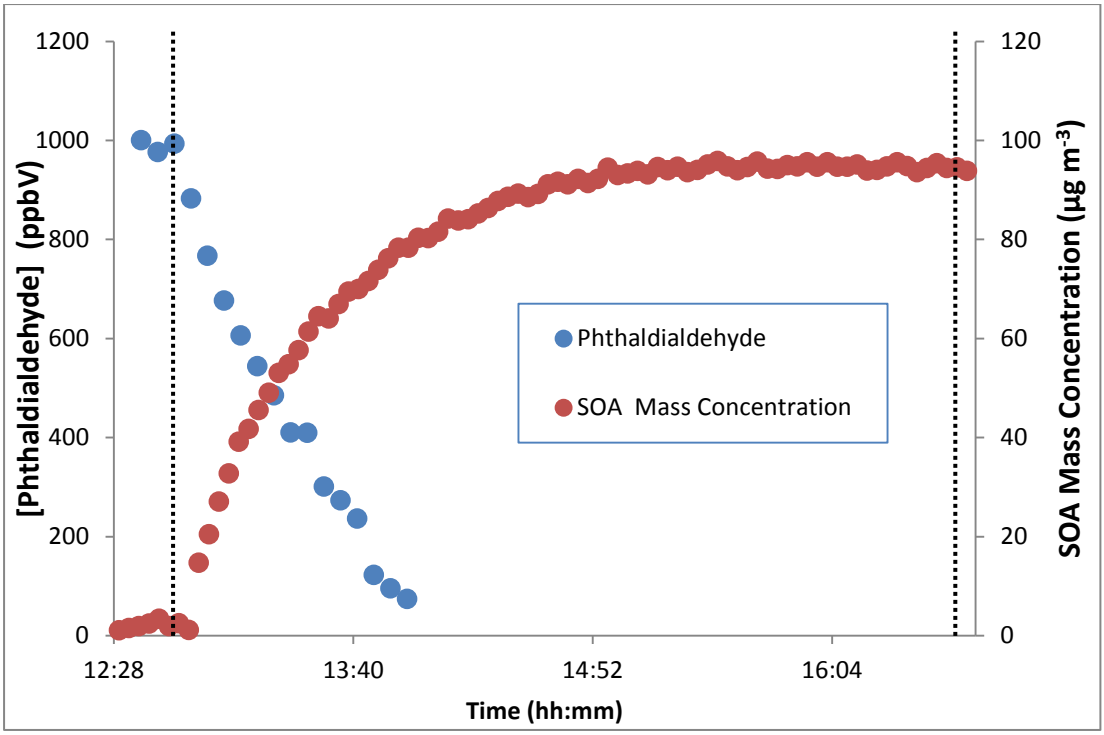


Figure 4.41 Concentration-time profile showing SOA formation during the photolysis of phthaldialdehyde in experiment 22122010. The vertical dotted lines indicate the time the lamps were turned on (12:42) and off (16:39).

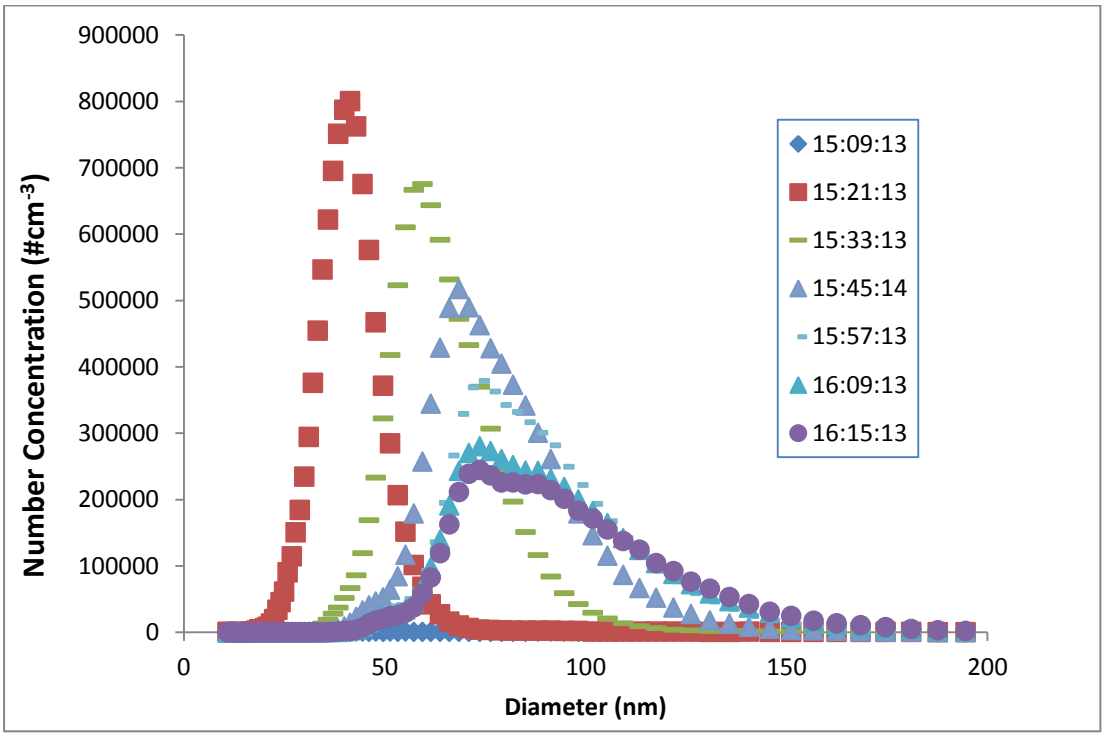


Figure 4.42 Number and size distribution of SOA particles formed during the photolysis of phthaldialdehyde in experiment 13012011.

Further investigation of the gas- and particle-phase photolysis products was performed by collecting denuder and filter samples during the indoor chamber experiments. The samples collected at the end of the experiment were treated in three different ways: extracted into a solvent and analysed by a direct injection method, derivatized by PFBHA in order to identify any carbonyls, derivatized by BSTFA to identify hydroxyl-containing products. There were no carbonyl products detected using PFBHA derivatization and the only products observed using the direct injection method were phthalide and phthalic anhydride. The selected ion chromatograms (*m/z* 73) for denuder (gas phase species) and filter (particle phase) extracts following BSTFA derivatization are in **Figure 4.43**. The six products identified were the same as those observed in the filter samples collected in the EUPHORE experiments. The major species identified in the gas phase were benzoic acid and salicylic acid. The dominant products found in the particle phase were phthalic acid and dihydroxyphthalic acid.

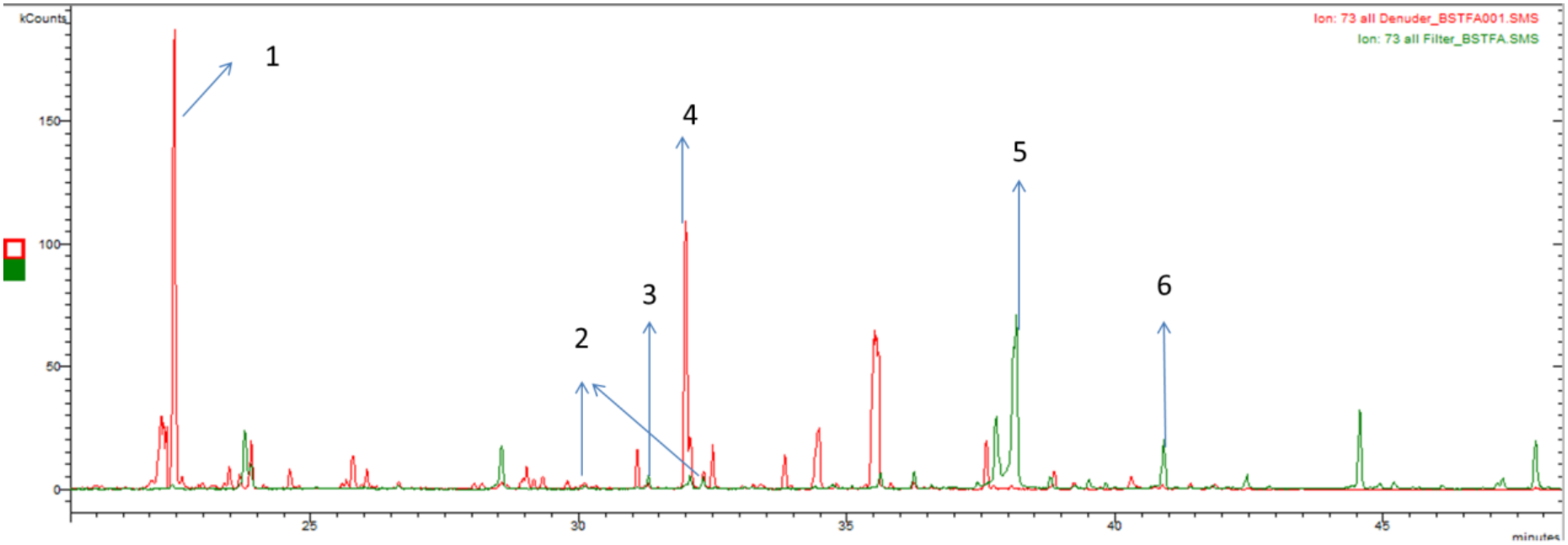


Figure 4.43 Selected ion chromatograms (*m/z* 73) of denuder (red) and filter (green) extracts obtained during the photolysis of phthaldialdhyde in the indoor chamber. .

1) benzoic acid, 2) 2-formylbenzoic acid, 3) salicylic acid, 4) Hydroxyphthaldialdehyde, 5) Dihydroxyphthalic acid 6) phthalic acid.

4.3.4 On-line Analysis of SOA using ATOFMS

The composition of SOA from photolysis of phthaldialdehyde was further investigated using ATOFMS for on-line analysis in a series of photooxidation experiments in the 3.91 m^3 simulation chamber. Experiments were performed using 300-500 ppbV of phthaldialdehyde in the absence of seed aerosol at different relative humidity and under different operating conditions. Spectra were collected only after the SOA number size distribution reached high enough diameters to be detected by the PMT detectors in the sizing region of the instrument (>200 nm). The irradiation time was approximately 4 hours in the experiments. A typical plot showing SOA growth monitored using the SMPS during one of the experiments is shown in **Figure 4.44**.

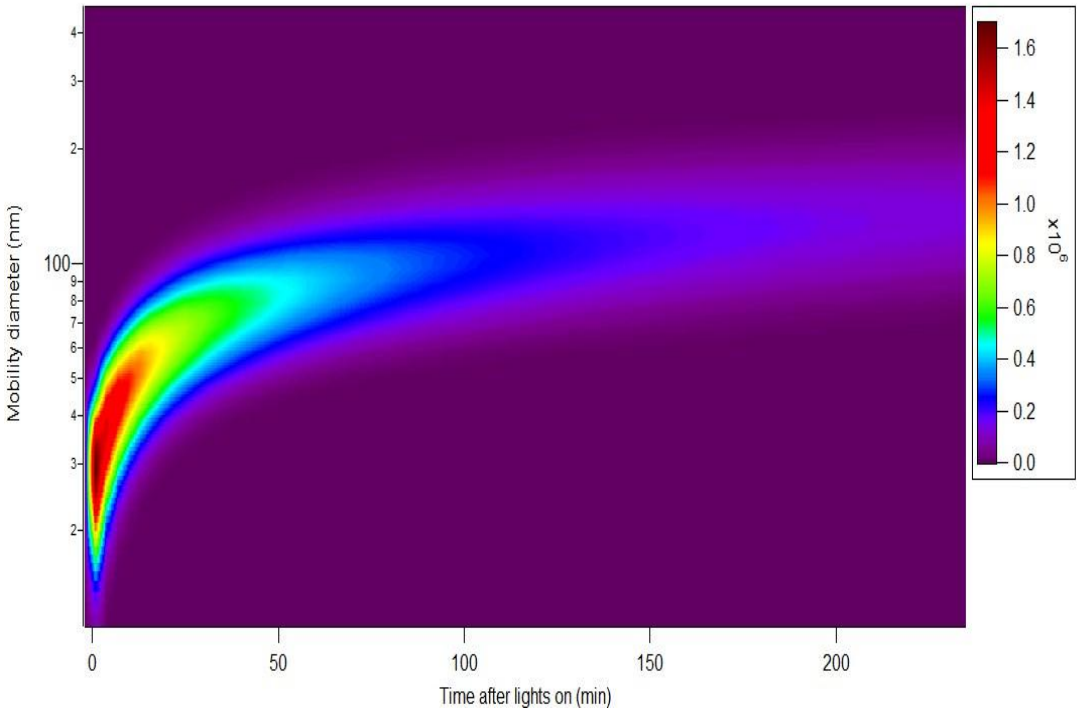


Figure 4.44 Contour plot of number and size distribution of SOA formed from the photolysis of phthaldialdehyde at 50% relative humidity. SOA growth proceeds for 120 min before reaching a maximum mass concentration of 96 μg m^{-3} and a mean diameter of ~100 nm.

Fang et al. have demonstrated that mass spectra can be obtained at different laser power densities in the thermal desorption/tunable vacuum–ultraviolet photoionization time-of-flight aerosol mass spectrometer (TD-VUV-TOF-PIAMS) (Fang et al. 2011). Lower power densities were also used in this work to increase the signal for molecular ions and thus aid product identification. The average dual ion mass spectra obtained using the laser power density at 15% of the maximum value (~0.20 mJ) are shown in **Figure 4.45**.

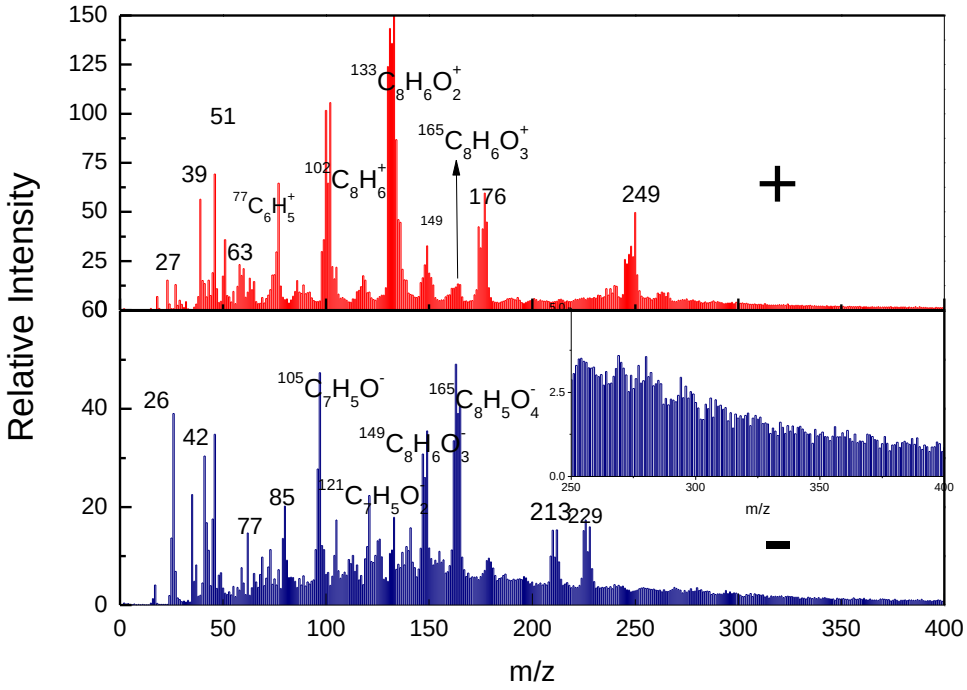


Figure 4.45 Average dual ion mass spectra of phthaldialdehyde SOA under dry conditions and lower laser power density (0.2 mJ).

The most abundant positive and negative ions in **Figure 4.45** are summarised in **Table 4.6** and **Table 4.7**. The peaks at *m/z* 27 ($C_2H_3^+$), 39($C_3H_3^+$), 51($C_4H_3^+$), 63 ($C_5H_3^+$) and 77 ($C_6H_5^+$) are aromatic fragment ions arising from phthaldialdehyde or any of the photolysis products. The higher mass ions, such as *m/z* 85($C_6H_6O^+$) 90($C_7H_6^+$), 102($C_8H_6^+$) are expected to be fragments of phthalide. The major peak at *m/z* 133 ($C_8H_5O_2^+$) is most likely a fragment ion of phthaldialdehyde or phthalide, which both have MW 134. In the negative mode, the peak at *m/z* 43 is probably due to the oxygen-containing organic fragment ion ($C_2H_3O^-$). Another relatively intense peak

at *m/z* 105 ($C_7H_5O^-$), is assigned as a fragment ion of the parent compound, phthaldialdehyde, losing a CHO group during ionisation. The peaks at *m/z* 105 in the negative ion mode and *m/z* 133 in the positive ion mode suggest that phthaldialdehyde may transfer from the gas phase to the particle phase during SOA formation. It is notable that *m/z* 149 ($C_8H_5O_3^+$) and 165 ($C_8H_5O_4^-$) are expected to be fragment ions from phthalic acid, MW 166, which was also determined in the off-line analysis of SOA.

Table 4.6 Positive Ions detected by ATOFMS during the photolysis of phthaldialdehyde.

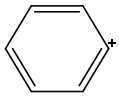
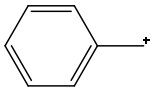
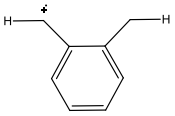
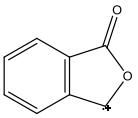
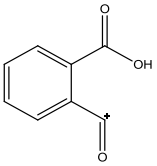
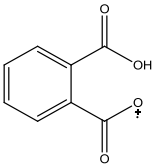
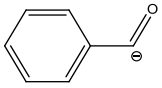
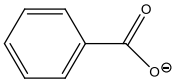
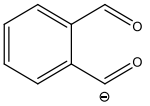
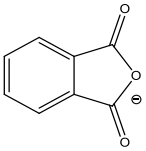
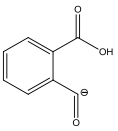
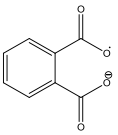
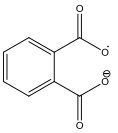
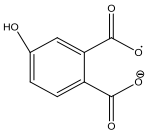
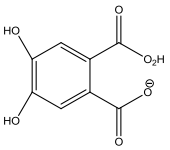
m/z	**Formula**	**Proposed structure**
27	$C_2H_3^+$	
39	$C_3H_3^+$	
51	$C_4H_3^+$	
63	$C_5H_3^+$	
77	$C_6H_5^+$	
90	$C_7H_6^+$,	
102	$C_8H_6^+$	
133	$C_8H_5O_2^+$,	
149	$C_8H_5O_3^+$	
165	$C_8H_5O_4^+$	

Table 4.7 Negative Ions detected by ATOFMS during the photolysis of phthaldialdehyde.

m/z	Formula	Proposed structure
26	$C_2H_2^-$	
46	$C_2H_2O_2^-$	
77	$C_6H_5^-$	
105	$C_7H_5O^-$	
121	$C_7H_5O_2^-$	
133	$C_8H_5O_2^-$	
148	$C_8H_4O_3^-$	
149	$C_8H_5O_3^-$	
164	$C_8H_4O_4^-$	
165	$C_8H_5O_4^-$	
181	$C_8H_5O_5^-$	
213	$C_8H_5O_7^-$	

As noted in **Chapter 3**, the ATOFMS was able to identify some differences in the chemical composition of naphthalene SOA formed at different relative humidity. The effect of relative humidity on the composition of SOA from photolysis of phthaldialdehyde was also investigated. The average dual ion mass spectra obtained during an experiment conducted at a relative humidity ~50% are shown in **Figure 4.46**. The spectra contain similar features as those obtained under dry conditions, **Figure 4.45**, indicating that the composition of the SOA formed at different RH is similar. The only noticeable difference is that the peak at *m/z* -43($C_2H_3O^-$) is much higher in the RH 50% spectra than in the RH 0%, suggesting that there are more oxidised compounds generated in the higher RH experiment.

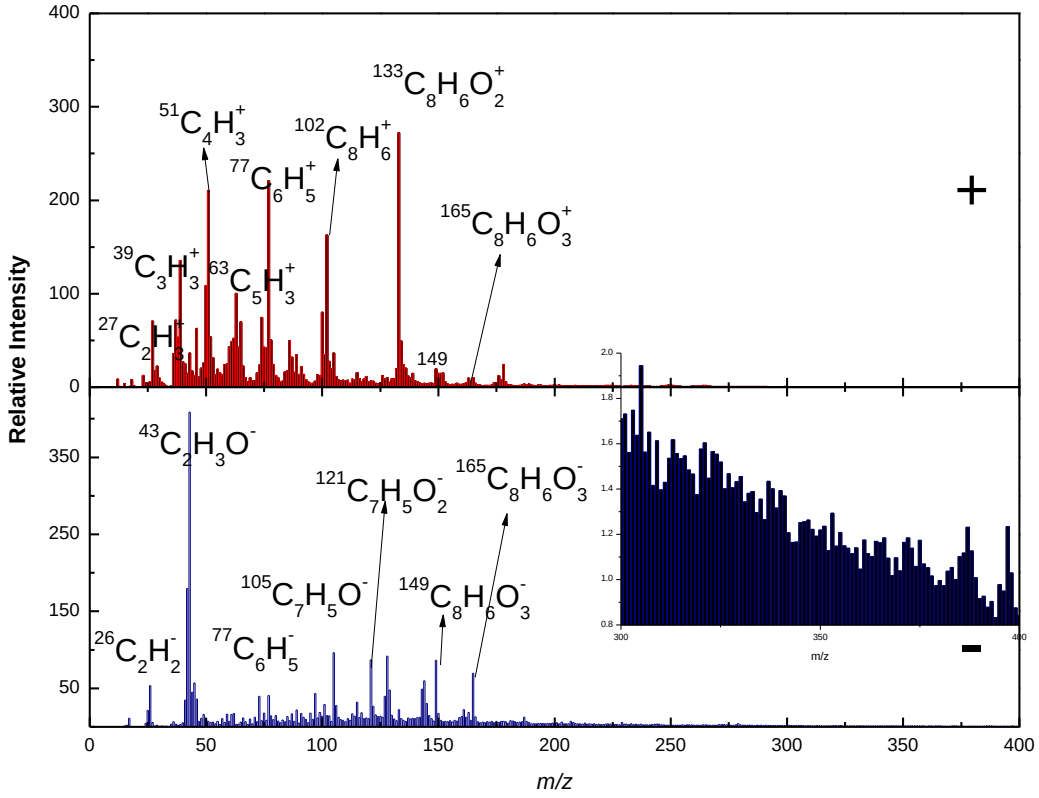


Figure 4.46 Average ATOFMS dual ion mass spectra from the photolysis of phthaldialdehyde at ~50% relative humidity.

The chemical evolution of SOA during the experiments was also investigated. The average mass spectra obtained during the first hour and 4th hour of an experiment conducted at RH 50% are shown in **Figure 4.47**. The lower mass positive ions, such as *m/z* 27, *m/z* 39 and *m/z* 51 increased in the later stage, while the *m/z* 133 ion

decreased. This latter ion is most likely due to phthaldialdehyde or phthalide and the observed decrease in intensity suggests that these species could be undergoing some form of chemical conversion, e.g. oxidation or hydrolysis, in the particle phase.

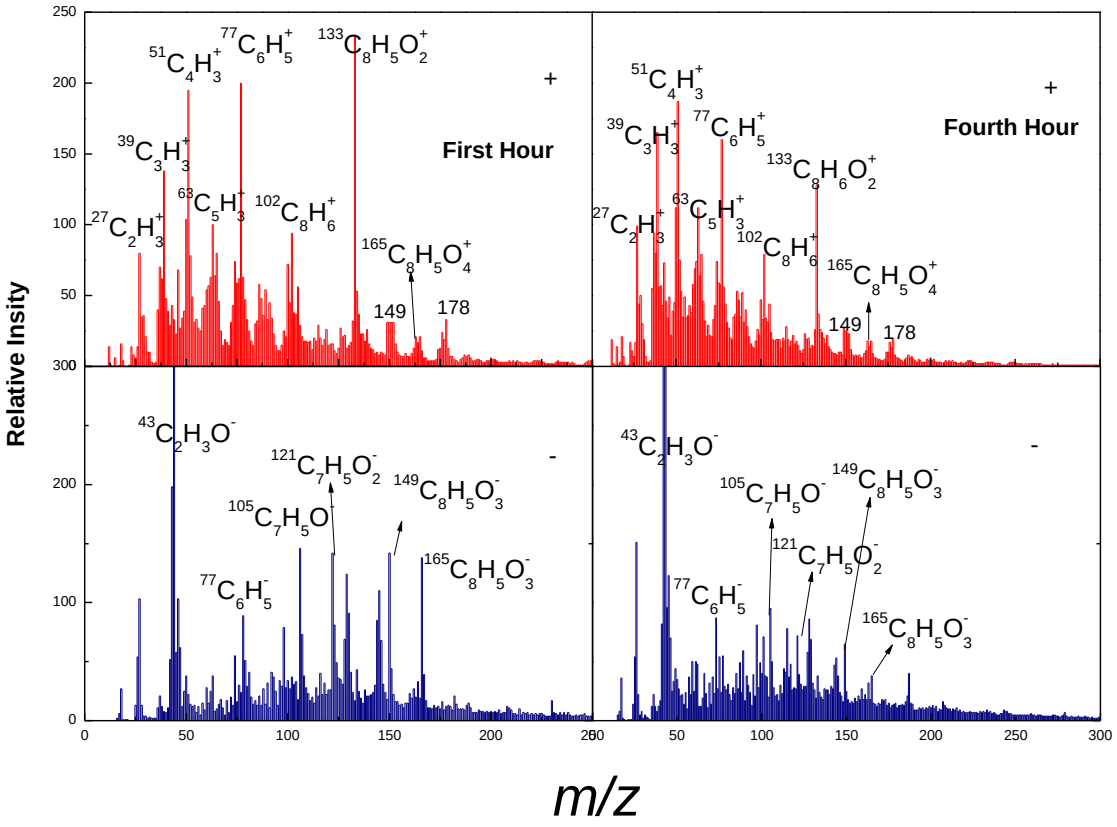


Figure 4.47 Average ATOFMS dual ion mass spectra from the photolysis of phthaldialdehyde at ~50% relative humidity obtained in the first hour and fourth hour.

The average mass spectra obtained during the first hour and fourth hour of an experiment conducted at RH 0% are shown in **Figure 4.48**. No significant changes are observed in the positive ion mass spectrum. However, the relative intensity of the following peaks increased noticeably in the negative ion spectrum: *m/z* -26, *m/z* -43 ($C_2H_3O^-$), *m/z* -73 ($C_3H_5O_2^-$), *m/z* -89 ($COOHCOO^-$). These ions clearly originate from oxidized species and their observed increase is a strong indication that oxidation reactions are taking place in the particle phase as time progresses.

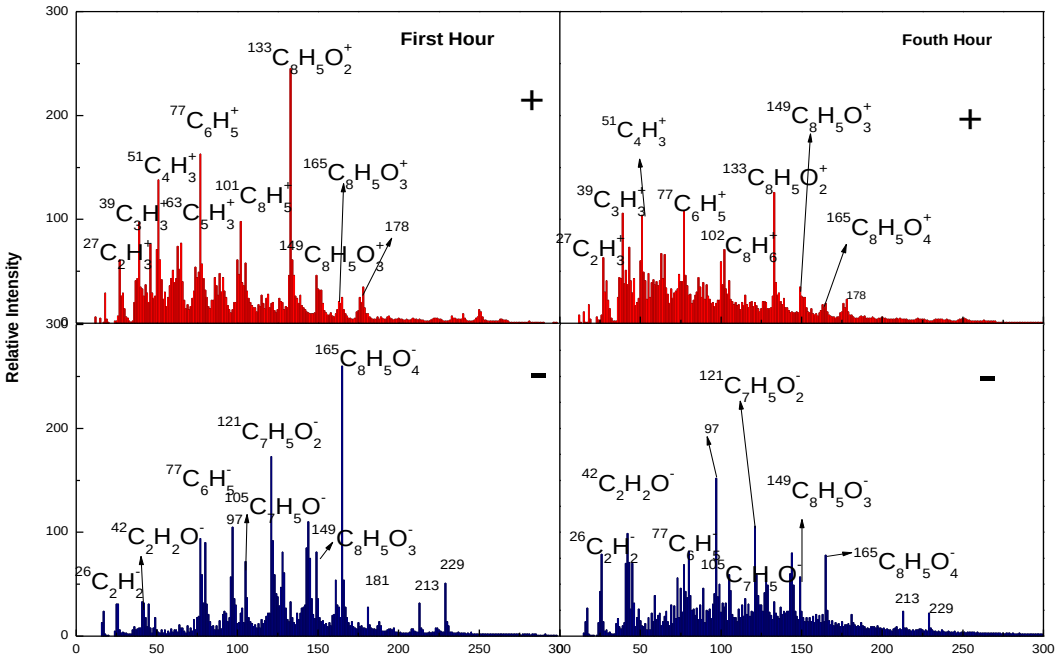


Figure 4.48 Average ATOFMS dual ion mass spectra from the photolysis of phthaldialdehyde under dry conditions obtained in the first hour and fourth hour.

4.4 Conclusions

The photolysis of phthaldialdehyde has been investigated using natural light at EUPHORE and artificial light in an atmospheric simulation chamber in University College Cork. The photolysis rate coefficient was measured directly and values in the range j(phthal) = (1.01 – 1.89) $\times 10^{-4}$ s^{-1} were observed under natural light, yielding an average value of j(phthal)/$j(NO_2)$ = 0.020±0.004. The corresponding lifetime due to photolysis is 1-3 hours, confirming that photolysis is the major atmospheric loss process for phthaldialdehyde (Wang et al. 2006). The main photolysis products identified in the gas-phase were phthalide and phthalic anhydride with average yields ca. 45% and 30% respectively. A mechanism has been proposed to explain the formation of these products. The formation of SOA was observed in the experiments, with yields in the range 1-11% highly dependent on the presence of an OH radical tracer or scavenger. The major particle-phase products identified using off-line GC-MS analysis were phthalic acid and dihydroxyphthalic acid. On-line analysis of the chemical composition of the SOA generated in the indoor chamber was performed using ATOFMS. The mass spectra contained ions that could possibly be attributed to some of the acids identified by GC-MS. The composition of the SOA was slightly different when produced at higher relative humidity and some evidence was found to indicate that species in the particle phase were slowly oxidized over a timescale of 4 hours.

4.5 References

Atkinson, R., S. M. Aschmann, J. Arey, B. Zielinska and D. Schuetzle (1989). "Gas-Phase Atmospheric Chemistry of 1-Nitronaphthalene and 2-Nitronaphthalene and 1,4-Naphthoquinone." Atmospheric Environment **23**(12): 2679-2690.

Calvert, J. G., R. Atkinson, K. H. Becker, R. M. Kamens, J. H. Seinfeld, T. J. Wallington and G. Yarwood (2002). The Mechanisms of Atmospheric Oxidation of Aromatic Hydrocarbons. Oxford, Oxford University Press.

Chen, J., J. C. Wenger and D. S. Venables (2011). "Near-Ultraviolet Absorption Cross Sections of Nitrophenols and Their Potential Influence on Tropospheric Oxidation Capacity." The Journal of Physical Chemistry A **115**(44): 12235-12242.

Clifford, G. M., A. Hadj-A ïssa, R. M. Healy, A. Mellouki, A. Mu ñoz, K. Wirtz, M. Mart ín Reviejo, E. Borr ás and J. C. Wenger (2011). "The Atmospheric Photolysis of *o*-Tolualdehyde." Environmental Science & Technology **45**(22): 9649-9657.

DeMore, W. B. S., S. P.; Golden, D. M.; Hampson, R. F.; Kurylo, M. J.; Howard, C. J.; Ravishankara, A. R.; Kolb, C. E.;Molina, M. J. (1997). In Chemical Kinetics and Photochemical Data for Use in Stratospheric Modelling. Pasadena, CA, JPL Publication.

El Dib, G., A. Chakir and A. Mellouki (2008). "UV Absorption Cross-Sections of a Series of Dimethylbenzaldehydes." The Journal of Physical Chemistry A **112**(37): 8731-8736.

Fang, W., L. Gong, X. Shan, F. Liu, Z. Wang and L. Sheng (2011). "Thermal Desorption/Tunable Vacuum–Ultraviolet Time-of-Flight Photoionization Aerosol Mass Spectrometry for Investigating Secondary Organic Aerosols in Chamber Experiments." Analytical Chemistry **83**(23): 9024-9032.

Feilberg, A., R. M. Kamens, M. R. Strommen and T. Nielsen (1999b). "Photochemistry and partitioning of semivolatile nitro-PAH in the atmosphere." Polycyclic Aromatic Compounds **14**: 151-160.

Finlayson-Pitts, B. J. and J. N. Pitts (2000). Chemistry of the upper and lower atmosphere: Theory, experiments, and applications, Academic Press.

Gross, D. S., R. Atlas, J. Rzeszotarski, E. Turetsky, J. Christensen, S. Benzaid, J. Olson, T. Smith, L. Steinberg, J. Sulman, A. Ritz, B. Anderson, C. Nelson, D.

R. Musicant, L. Chen, D. C. Snyder and J. J. Schauer (2010). "Environmental chemistry through intelligent atmospheric data analysis." Environmental Modelling & Software **25**(6): 760-769.

Hallquist, M., J. C. Wenger, U. Baltensperger, Y. Rudich, D. Simpson, M. Claeys, J. Dommen, N. M. Donahue, C. George, A. H. Goldstein, J. F. Hamilton, H. Herrmann, T. Hoffmann, Y. Iinuma, M. Jang, M. E. Jenkin, J. L. Jimenez, A. Kiendler-Scharr, W. Maenhaut, G. McFiggans, T. F. Mentel, A. Monod, A. S. H. Pravit, J. H. Seinfeld, J. D. Surratt, R. Szmigielski and J. Wildt (2009). "The formation, properties and impact of secondary organic aerosol: current and emerging issues." Atmospheric Chemistry and Physics **9**(14): 5155-5236.

Healy, R. M., J. C. Wenger, A. Metzger, J. Duplissy, M. Kalberer and J. Dommen (2008). "Gas/particle Partitioning of Carbonyls in the Photooxidation of Isoprene and 1,3,5-trimethylbenzene." Atmospheric Chemistry and Physics **8**(12): 3215-3230.

Kautzman, K. E., J. D. Surratt, M. N. Chan, A. W. H. Chan, S. P. Hersey, P. S. Chhabra, N. F. Dalleska, P. O. Wennberg, R. C. Flagan and J. H. Seinfeld (2010). "Chemical Composition of Gas- and Aerosol-Phase Products from the Photooxidation of Naphthalene." Journal of Physical Chemistry A **114**(2): 913-934.

Keywood, M. D., J. H. Kroll, V. Varutbangkul, R. Bahreini, R. C. Flagan and J. H. Seinfeld (2004). "Secondary Organic Aerosol Formation from Cyclohexene Ozonolysis: Effect of OH Scavenger and the Role of Radical Chemistry." Environmental Science & Technology **38**(12): 3343-3350.

Kramp, F. and S. E. Paulson (1998). "On the Uncertainties in the Rate Coefficients for OH Reactions with Hydrocarbons, and the Rate Coefficients of the 1,3,5-Trimethylbenzene and m-Xylene Reactions with OH Radicals in the Gas Phase." The Journal of Physical Chemistry A **102**(16): 2685-2690.

Laue, T. and A. Plagens (2005). Named organic reactions, John Wiley & Sons.

Martinez, R. D., A. A. Buitrago, N. W. Howell, C. H. Hearn and J. A. Joens (1992). "The near U.V. absorption spectra of several aliphatic aldehydes and ketones at 300 K." Atmospheric Environment. Part A. General Topics **26**(5): 785-792.

Moorthy, J. N., P. Mal and R. Natarajan (2001). "Efficient photocyclization of o-alkylbenzaldehydes in the solid state: direct observation of E-xylylenols en

route to benzocyclobutenols." Journal of Organic Chemistry **66**(21): 7013-7019.

Nakao, S., C. Clark, P. Tang, K. Sato and D. Cocker III (2011). "Secondary organic aerosol formation from phenolic compounds in the absence of NO_x." Atmospheric Chemistry and Physics **11**: 10649-10660.

O'Connor, M. P., J. C. Wenger, A. Mellouki, K. Wirtz and A. Munoz (2006). "The atmospheric photolysis of E-2-hexenal, Z-3-hexenal and E,E-2,4-hexadienal." Physical Chemistry Chemical Physics **8**(44): 5236-5246.

Thiault, G., A. Mellouki, G. Le Bras, A. Chakir, N. Sokolowski-Gomez and D. Daumont (2004). "UV-absorption cross sections of benzaldehyde, *ortho*-, *meta*-, and *para*-tolualdehyde." Journal of Photochemistry and Photobiology A: Chemistry **162**(2-3): 273-281.

Voigt, S., J. Orphal, K. Bogumil and J. P. Burrows (2001). "The temperature dependence (203-293 K) of the absorption cross sections of O_3 in the 230-850 nm region measured by Fourier-transform spectroscopy." Journal of Photochemistry and Photobiology A: Chemistry **143**(1): 1-9.

Wagner, P. J., D. Subrahmanyam and B. S. Park (1991). "The mechanism for the photocyclization of ortho-alkyl ketones to cyclobutenols." Journal of the American Chemical Society **113**(2): 709-710.

Wang, L., J. Arey and R. Atkinson (2006). "Kinetics and products of photolysis and reaction with OH radicals of a series of aromatic carbonyl compounds." Environmental Science & Technology **40**(17): 5465-5471.

Wenger, J. C., S. Le Calve, H. W. Sidebottom, K. Wirtz, M. M. Reviejo and J. A. Franklin (2004). "Photolysis of chloral under atmospheric conditions." Environmental Science & Technology **38**(3): 831-837.

Chapter

5

Photolysis of 1-nitronaphthalene

5.1 Introduction

Nitro-polycyclic aromatic hydrocarbons (nitro-PAHs) are one of the most important classes of environmental pollutants, found in air, aquatic systems and sediments (Arey et al. 1987; Arey et al. 1989; Dimashki et al. 2000; Reisen et al. 2003; Albinet et al. 2007; Ozaki et al. 2010). They are released into the atmosphere directly from combustion sources such as diesel exhaust (Yu et al. 1984; Feilberg et al. 1999a; Feilberg et al. 1999b) and cigarette smoke (Havey et al. 2009) and are also formed *in situ* via the atmospheric degradation of PAHs (Arey et al. 1989; Reisen et al. 2004; Atkinson et al. 2007; Nishino et al. 2008). Many nitro-PAHs have been identified as mutagenic and carcinogenic (Tokiwa et al. 1981; Landvik et al. 2007) and there is concern over the potential risk that they pose to human health. Information on their atmospheric reactivity is required in order to understand their lifetimes and persistence in the environment.

5.1.1 Previous studies of atmospheric chemistry of 1-Nitronaphthalene

1-Nitronaphthalene (1-NN) is a primary pollutant (Feilberg et al. 1999a; Feilberg et al. 1999b) and also a minor product of the photooxidation of naphthalene (Bunce et al. 1997; Sasaki et al. 1997; Mihele et al. 2002; Lee et al. 2009; Kautzman et al. 2010). It has been regularly detected in ambient air (Arey et al. 1987; Arey et al. 1989; Dimashki et al. 2000; Reisen et al. 2003; Albinet et al. 2007) and Feilberg et al. performed a comprehensive experimental and modelling study which showed that it exists mainly in the gas-phase (Feilberg et al. 1999a; Feilberg et al. 1999b).

The first study of the atmospheric reactivity of 1-NN was performed by Atkinson et al. (Atkinson et al. 1989) who investigated the gas phase reactions with OH and NO_3 radicals and also carried out photolysis experiments using both natural sunlight and blacklamps. The photolysis rate coefficient, j(1-NN), was found to be $(1.37 \pm 0.10) \times 10^{-4}$ s^{-1} using natural sunlight with $j(NO_2) = 4.3 \times 10^{-3} s^{-1}$, and around an order of magnitude higher using the artificial light source. 1,4-Naphthoquinone and 2-nitro-1-naphthol were identified among the photolysis products. Rate coefficients were determined for the reaction of 1-NN with OH and NO_3 radicals, with the results indicating that photolysis is the dominant loss process under atmospheric conditions.

Feilberg et al. studied gas-particle partitioning and photochemistry of 1-NN in a 190 m^3 outdoor smog chamber in the presence and absence of diesel exhaust particles (Feilberg et al. 1999a, Feilberg et al. 1999b). The results from several experiments were used to derive a value of j(1-NN)/j(NO_2) = 0.07. Phousongphouang et al. investigated the photolysis rates of 1-NN, 2-NN, and a series of methylnitronaphthalenes using blacklamp irradiation and also in an outdoor chamber using natural sunlight (Phousongphouang et al. 2003).The photolysis rate coefficient, j(1-NN), was found to be $(2.52 \pm 0.30) \times 10^{-4}$ s^{-1} using natural sunlight with $j(NO_2) = 4.57 \times 10^{-3} s^{-1}$, and about a factor of 3 higher using the artificial light source.

The UV absorption cross-section values for 1-NN have not been reported in the literature. However, Zugazagoitia et al. measured the steady-state absorption spectrum of 1-NN in methanol (Zugazagoitia et al. 2008), **Figure 5.1**. The spectrum shows a strong absorption band between 300 and 400 nm, which can interact with UV solar radiation.

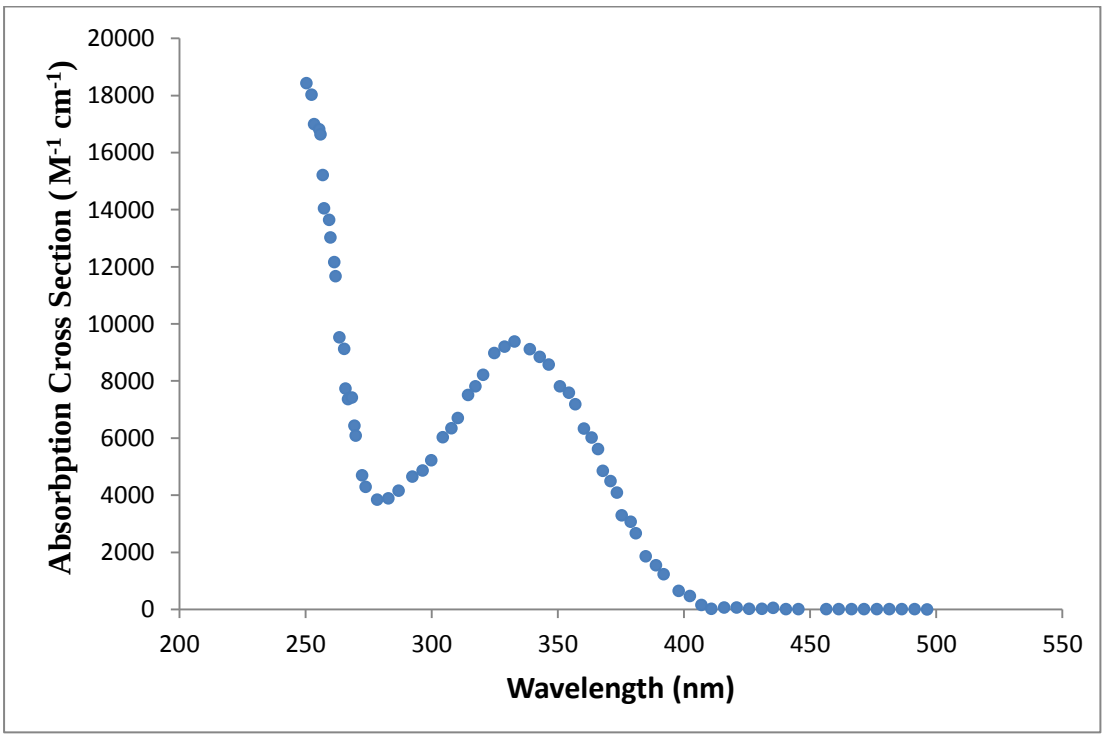


Figure 5.1 Steady-state UV absorption cross section of 1-NN in methanol (Zugazagoitia et al. 2008).

5.1.2 Aim of this Work

The aim of this work was to investigate the photolysis of 1-NN in an outdoor chamber using natural sunlight to measure the photolysis rate coefficient and thus calculate the atmospheric lifetime due to photolysis. The formation of SOA was observed and off-line chemical analysis was performed to identify the particle-phase products. Supplementary experiments have also been performed in an indoor simulation chamber using an artificial light source. A key feature of these experiments was the use of ATOFMS for on-line measurements of the chemical composition of the SOA produced from direct photolysis of 1-NN.

5.2 Experimental

5.2.1 Materials

All the materials used in this work are listed in **Table 5.1**, used as received.

Table 5.1 Materials used in this study.

Material	Purity %	Manufacturer
1-NN	99	Sigma-Aldrich
Acetone	HPLC grade	Sigma-Aldrich
1,3,5-Trimethylbenzene	99	Sigma-Aldrich
CO	99.99	Irish Oxygen
SF_6	99	Sigma-Aldrich
BSTFA+TMCS	(99:1)	SUPELCO
Methanol	99.9	Sigma-Aldrich
Dichloromethane	99.9	Sigma-Aldrich
n-Hexane	HPLC grade	Sigma-Aldrich
n-Butyl ether	99.9	Sigma-Aldrich
Nitrobenzene	99	Sigma-Aldrich
Nitric oxide	99	Sigma-Aldrich

5.2.2 Experiments in EUPHORE Chamber

The photolysis of 1-NN by sunlight was investigated at the European PhotoReactor (EUPHORE) in July 2009. Details of the chamber, associated instrumentation and experimental procedure are provided in **Section 4.2.1**. Mixing ratios ranging from 146-283 ppbV of 1-NN were used in four different experiments. The reactant was allowed to mix for at least 30 min while its loss to the chamber walls was measured. In one experiment, a large excess of CO (ca. 500 ppmV) was added as a scavenger for OH radicals, while in another experiment, 1,3,5-trimethylbenzene (150 ppbV) was used as a reactive tracer for OH radicals. Photolysis was initiated by opening the

protective housing around midday to expose the contents of the chamber to sunlight for 1-3 h. FTIR spectroscopy was used to follow the decay of 1-NN and OH tracer, while automated analysers were used to monitor NO_x (ECO-Physics CLD 770 with PLC 760 photolytic converter) and ozone (Monitor Labs 9810). At the end of one of the experiments, SOA particles were collected onto a filter (PallFlex 47 mm quartz fibre) at a flow rate of 10 dm^3 min^{-1} for 30 min. The filters were stored in a freezer and later shipped to University College Cork for off-line analysis using GC-MS. One quarter of each filter was used for derivatization with PFBHA, a second quarter was used for derivatization with BSTFA and a third quarter simply extracted into a dichloromethane:methanol (1:1) mixture. Details of the procedures for derivatization and subsequent GC-MS analysis are provided in **Section 3.2**.

5.2.3 Experiments in the Indoor Chamber

Two different sets of experiments were also carried out in the 3.91 m^3 atmospheric simulation chamber located at University College Cork. Details concerning the apparatus and experimental procedure are provided in S**ection 3.2.3 and Section 4.2.2.**

The first set of experiments was performed to measure the photolysis rate, SOA yield and collect particle-phase products for analysis by GC-MS. Mixing ratios ranging from 300-350 ppbV of 1-NN were used in the experiments. The reactant was allowed to mix for at least 30 min while its loss to the chamber walls was measured. In one experiment, a large excess of CO (ca. 500 ppmV) was added as a scavenger for OH radicals, while in another experiment, 1,3,5-trimethylbenzene (350 ppbV) was used as a reactive tracer for OH radicals. Photolysis was initiated by turning on the lamps (16 TL05 lamps and 12 × TL12 lamps) for 30-40 min. SOA particles were collected onto a filter (PallFlex 47 mm quartz fibre) at a flow rate of 10 dm^3 min^{-1} for 30 min and stored in a freezer awaiting GC-MS analysis. One quarter of each filter was used for derivatization with PFBHA, a second quarter was used for derivatization with BSTFA and a third quarter simply extracted into a dichloromethane:methanol (1:1) mixture. Details of the procedures for derivatization and subsequent GC-MS analysis are provided in **Section 3.2**.

In the second set of experiments, ATOFMS was used for on-line measurements of the chemical composition of the SOA produced from direct photolysis of 1-NN. Mixing ratios ca. 100 ppbV of 1-NN were used in the experiments. In one experiment, n-butyl ether (ca. 10 ppmV) was added as a scavenger for OH radicals, while other experiments, an excess of nitric oxide (ca. 0.8 ppmV) and nitrobenzene (ca. 10 ppmV) was added to influence the radical chemistry during photolysis.

5.3 Results and Discussion

5.3.1 Photolysis Rate Coefficient

The photolysis rate coefficient, j(1-NN), can be determined from the measured decay of the compound in the EUPHORE and indoor chambers. Other loss processes for 1-NN include deposition to the walls of the chambers and reaction with OH radicals, present in the background or produced as a result of the photolysis process itself. The measured rate coefficients for wall loss and reaction with OH, k_{wall} and k_{OH}[OH] respectively, can be incorporated into the kinetic equation as follows;

$$ln\frac{[1-NN]_t}{[1-NN]_0} = -k_{total}t = -(j + k_{wall} + k_{OH}[OH])t \qquad \text{(I)}$$

Although dilution was also observed during the EUPHORE experiments, the rate determined by measuring the loss of SF_6 from the chamber, k_{SF6}, was lower than the wall loss and is therefore already incorporated into k_{wall}. Thus a plot in the form of Equation (I) should yield a straight line with gradient $-k_{total}$. The wall loss was measured during each experiment, while k_{OH}[OH] could be determined from experiments where 1,3,5-trimethylbenene was used as a tracer. In some experiments an excess of CO was used to scavenge all OH radicals and k_{OH}[OH] was therefore eliminated, giving k_{total}-k_{wall} =j(1-NN).

5.3.1.1 EUPHORE Chamber

Concentration–time profiles and kinetic plots in the form of Equation (I) were generated for all experiments. The concentration-time profiles and the corresponding photolysis rate plots are shown in **Figure 5.2** to **Figure 5.9**. The reaction conditions and results are summarized in **Table 5.2.** The decay of 1-NN was very rapid in all experiments and started immediately after opening the chamber to sunlight. The kinetic plots exhibited good linearity and near-zero intercepts, yielding values of k_{total} in the range (0.70 – 1.20) × 10^{-3} s^{-1}, following correction for wall loss. The experiments on 6th and 14th July 2009 were performed without an OH tracer or scavenger and the values for j(1-NN) should therefore be considered as upper limits. In the experiment conducted on 13rd July 2009, an excess of CO was added as a scavenger and the possible loss of 1-NN by reaction with OH was thus eliminated.

The value for j(1-NN) obtained in this experiment was lower than k_{total} in the first two experiments thereby confirming that reaction with OH was contributing to the loss of 1-NN. In order to make direct comparisons between experiments with different light intensity, j(1-NN) was normalized by dividing by $j(NO_2)$. The resulting value of j(1-NN)/$j(NO_2)$ = 0.09 ± 0.01 obtained on 13rd July 2009 is lower than that obtained in the experiments without scavenger. The contribution of the OH reaction, i.e. the value of k_{OH}[OH], in the experiments performed on 6th and 14th July 2009 can be estimated by assuming that j(1-NN)/$j(NO_2)$ = 0.09, rather than 0.14. This would yield values of j(1-NN) = 0.76 × 10^{-3} s^{-1} and k_{OH}[OH] = 0.44 × 10^{-3} s^{-1} for 6th July 2009, indicating that ca. 36% of the loss of 1-NN was due to reaction with OH radicals. The corresponding values for the experiment performed on 14th July 2009 are j(1-NN) = 0.63 × 10^{-3} s^{-1} and k_{OH}[OH] = 0.37 × 10^{-3} s^{-1}, with 37% of the loss of 1-NN attributed to reaction with OH radicals.

In the experiment performed on 7th July 2009, 150 ppbV of 1,3,5-trimethylbenzene (TMB) was introduced to the chamber to act as a tracer for OH radicals. As a result, any OH generated during the experiment reacted with both 1,3,5-trimethylbenzene and 1-NN. The OH concentration can be estimated from the measured decay of TMB:

$$\frac{-d[TMB]}{dt} = k_0[TMB][\mathbf{OH}] \qquad \text{(I)}$$

where k_0 is the rate coefficient for reaction of OH with TMB. Assuming that the concentration of OH is in a steady state, the reaction is occurring under pseudo-first order conditions:

$$\frac{-d[TMB]}{dt} = k_1[TMB] \qquad \text{(III)}$$

where $k_1 = k_0$[OH] and integrating from the time t=0, when the initial concentration of TMB is $[TMB]_0$ to the time t when the concentration of TMB is $[TMB]_t$ gives:

$$ln\frac{[TMB]_t}{[TMB]_0} = -k_1 t \qquad \text{(IV)}$$

A plot in the form of this equation is shown in **Figure 5.10** and yields a value of k_1 = (5.2 ± 0.2) × 10^{-4} s^{-1}. Using a value of k_0 = 5.73 × 10^{-11} cm^3 $molecue^{-1}$ s^{-1} (Kramp et al. 1998), yields [OH] = 9.08 × 10^6 molecule cm^{-3}. This value for the OH steady state concentration can be used to calculate k_{OH}[OH], which represents the loss of 1-NN

due to reaction with OH. Using a value of $k_{[OH]} = 5.4 \times 10^{-12}$ cm^3 molecule^{-1} s^{-1} (Atkinson et al. 1989) gives $k_{OH}[OH] = 0.49 \times 10^{-4}$ s^{-1}, indicating that 5.4% of the loss of 1-NN was due to reaction with OH radicals. The resulting value for the photolysis rate coefficient is j(1-NN) = (0.85 ± 0.06) × 10^{-3} s^{-1}, yielding a value of j(1-NN)/j(NO_2) = 0.09 ± 0.01, in excellent agreement with the result obtained in the experiment performed with the OH scavenger.

Table 5.2 Experimental conditions and results for the photolysis of 1-NN by natural sunlight in the EUPHORE chamber.

Date	**6th July 2009**	**7th July [1]**	**13rd July [2]**	**14th July 2009**
Initial conc. (ppbV)	283	146	166	205
Irradiation time	154 min	90 min	51 min	126 min
$j(NO_2)$ ($\times 10^{-3} s^{-1}$)	8.4 ± 0.60	9.10 ± 0.80	7.4 ± 0.40	7.0 ± 0.50
k_{SF6} ($\times 10^{-6} s^{-1}$)	7.2 ± 0.90	7.0 ± 0.60	17 ± 0.60	8.6 ± 0.80
k_{wall} ($\times 10^{-5} s^{-1}$)	5.0 ± 1.0	2.0 ± 0.7	4.0 ± 0.4	5.0 ± 0.40
k_{total} ($\times 10^{-3} s^{-1}$)	1.20 ± 0.10	0.90 ± 0.06	0.70 ± 0.02	1.00 ± 0.02
k_{OH}[OH] ($\times 10^{-4} s^{-1}$)	-	0.50 ± 0.04	0	-
j(1-NN) ($\times 10^{-3} s^{-1}$)	1.20 ± 0.10	0.85 ± 0.06	0.70 ± 0.02	1.00 ±0.02
j(1-NN)/$j(NO_2)$	0.14 ± 0.02	0.09 ± 0.01	0.09 ± 0.01	0.14 ± 0.01
$[NO]_{max}$ (ppbV)	106 ± 7	46 ± 3	32 ± 2	67 ± 4
$[O_3]_{max}$ (ppbV)	12.7 ± 0.9	173 ± 11	302 ± 21	5 ± 0.5
SOA yield (%)	65	57	71	67

[1] In this experiment, 1,3,5-trimethylbenzene (150 ppbV) was used as an OH radical tracer. [2] In this experiment CO (500 ppmV) was used as an OH radical scavenger. Errors are twice the standard deviation. The yield of SOA was corrected with the measured wall loss value of (2-5) × 10^{-5} s^{-1} on each day. Estimated errors for ozone and NO measurements are 7%.

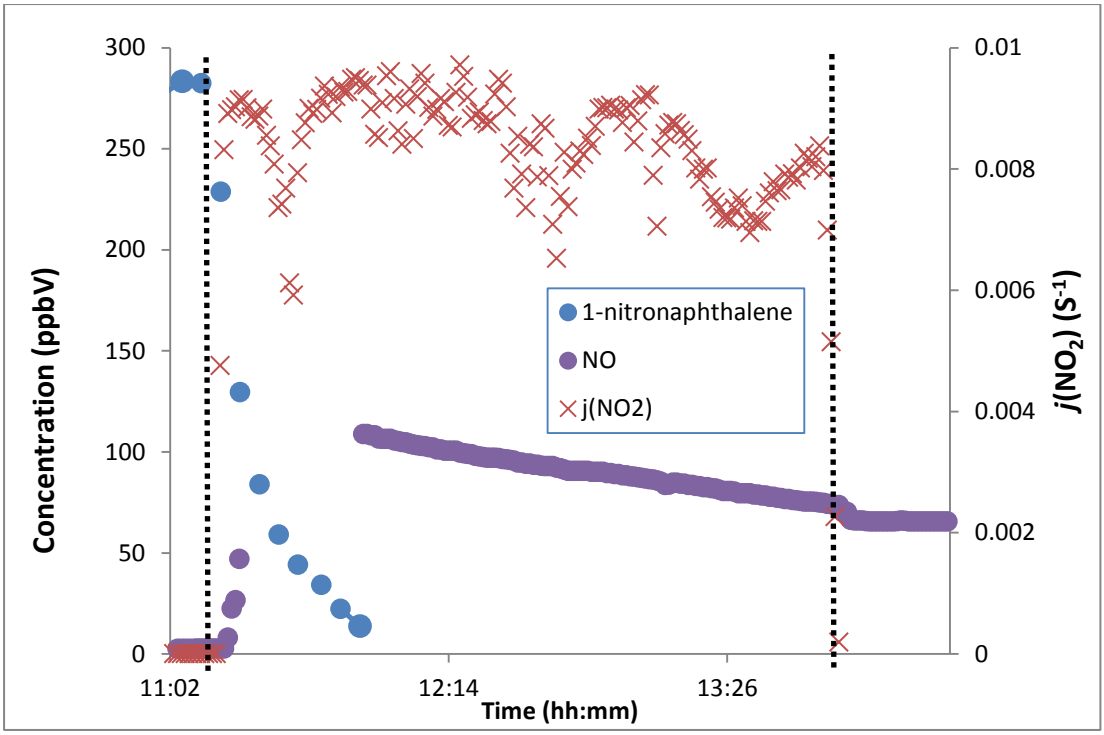


Figure 5.2 Concentration-time profile and $j(NO_2)$ during the photolysis of 1-NN at EUPHORE on 6th July 2009. The vertical dotted lines indicate the time the chamber was fully opened (11:11) and closed (13:55). Several NO data points were missed.

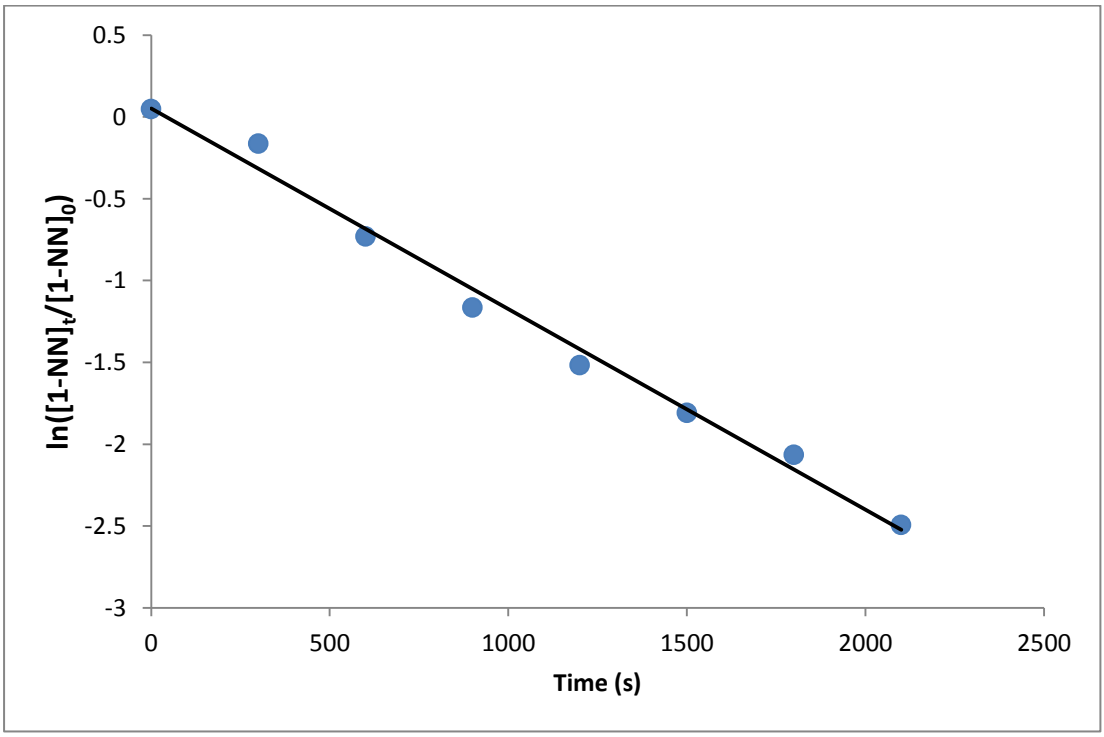


Figure 5.3 Decay of 1-NN (corrected for wall loss) during the experiment performed at EUPHORE on 6th July 2009.

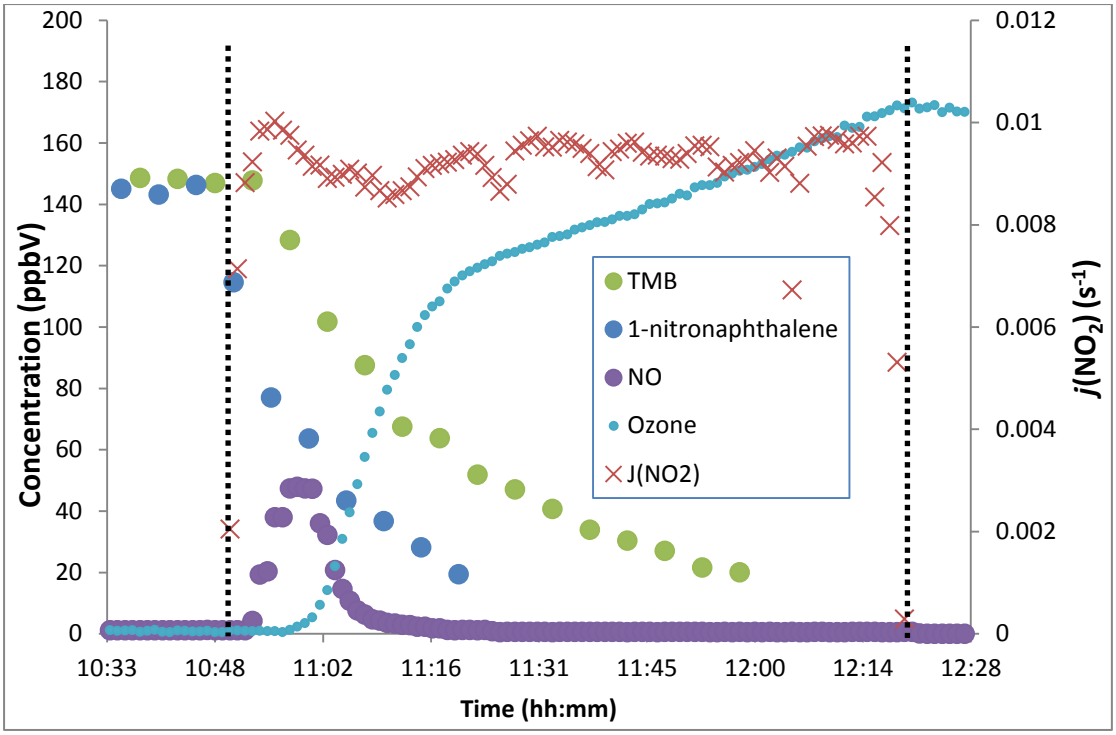


Figure 5.4 Concentration-time profile and $j(NO_2)$ during the photolysis of 1-NN at EUPHORE on 7th July 2009. The vertical dotted lines indicate the time the chamber was fully opened (10:50) and closed (12:20).

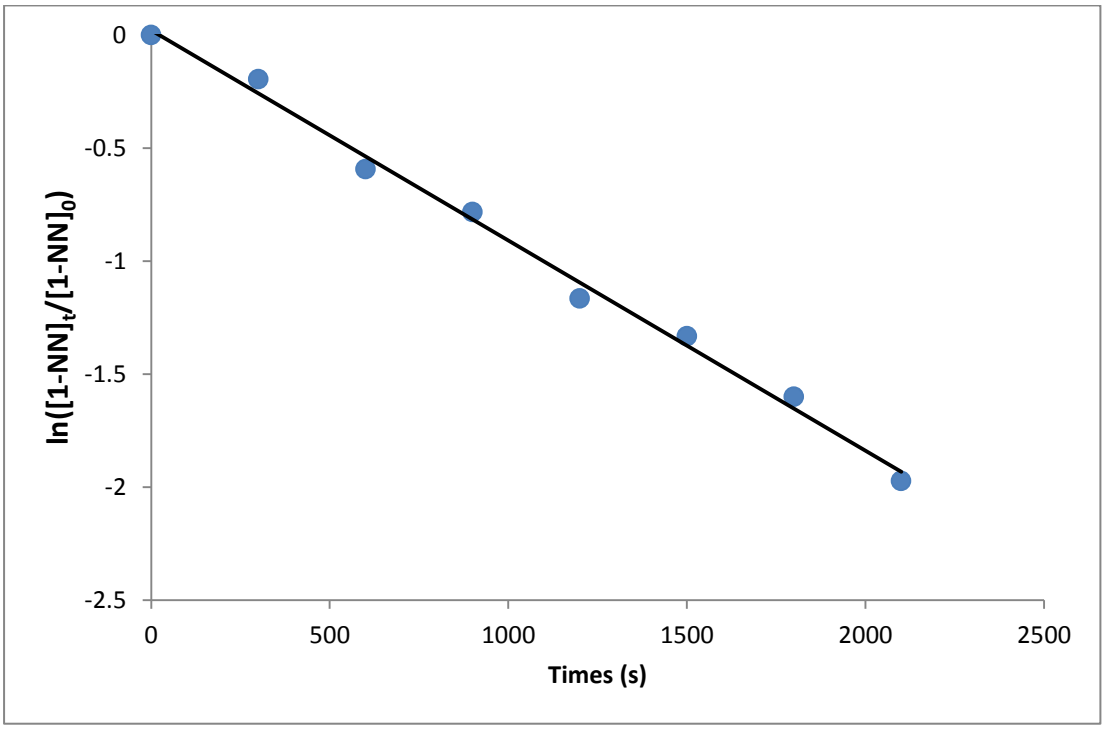


Figure 5.5 Decay of 1-NN (corrected for wall loss) during the experiment performed at EUPHORE on 7th July 2009.

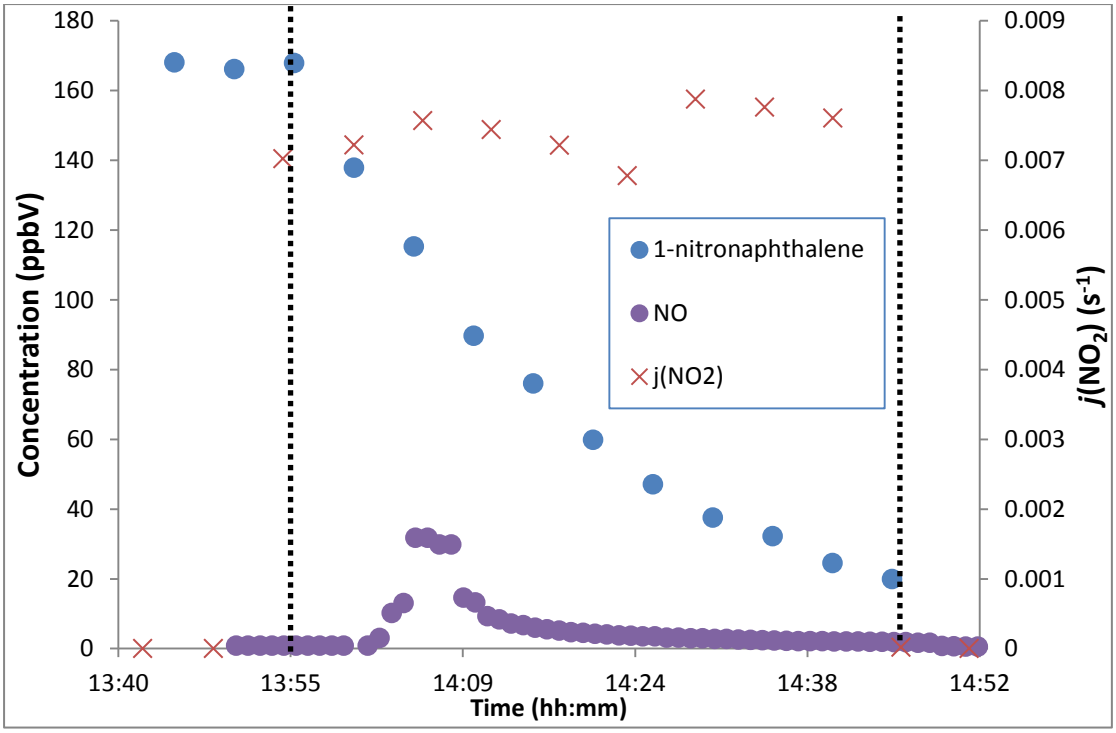


Figure 5.6 Concentration-time profile and $j(NO_2)$ during the photolysis of 1-NN at EUPHORE on 13rd July 2009. The vertical dotted lines indicate the time the chamber was fully opened (13:55) and closed (14:46).

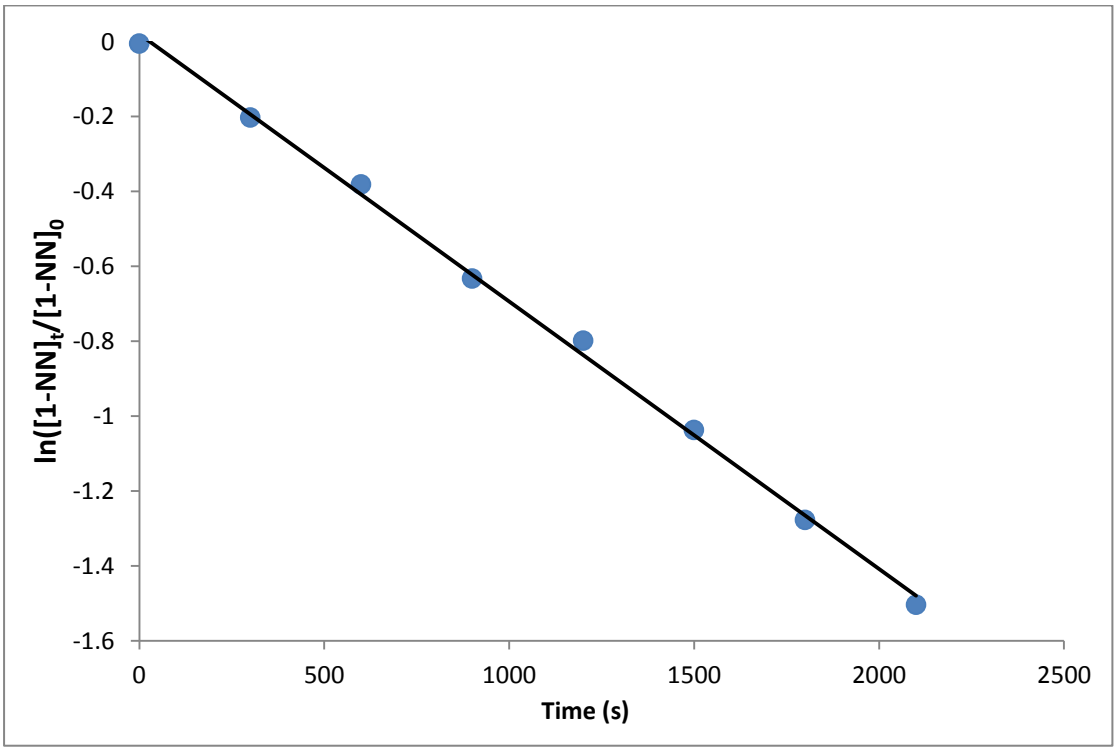


Figure 5.7 Decay of 1-NN (corrected for wall loss) during the experiment performed at EUPHORE on 13rd July 2009.

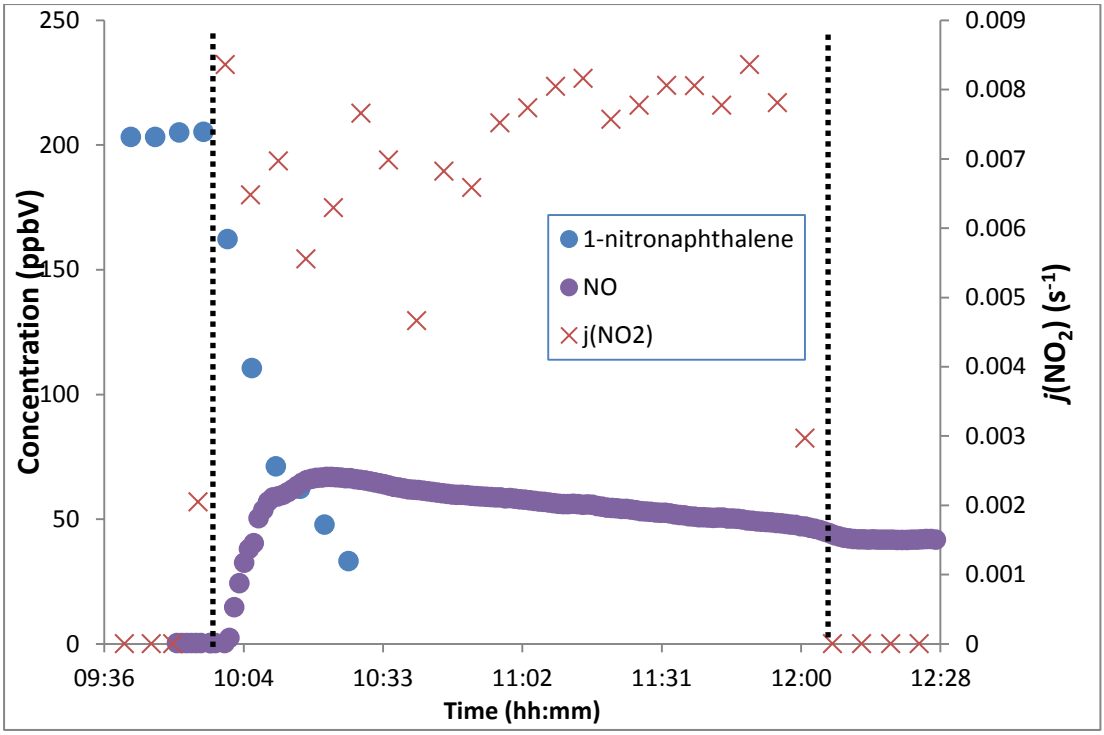


Figure 5.8 Concentration-time profile and $j(NO_2)$ during the photolysis of 1-NN at EUPHORE on 14th July 2009. The vertical dotted lines indicate the time the chamber was fully opened (10:00) and closed (12:06).

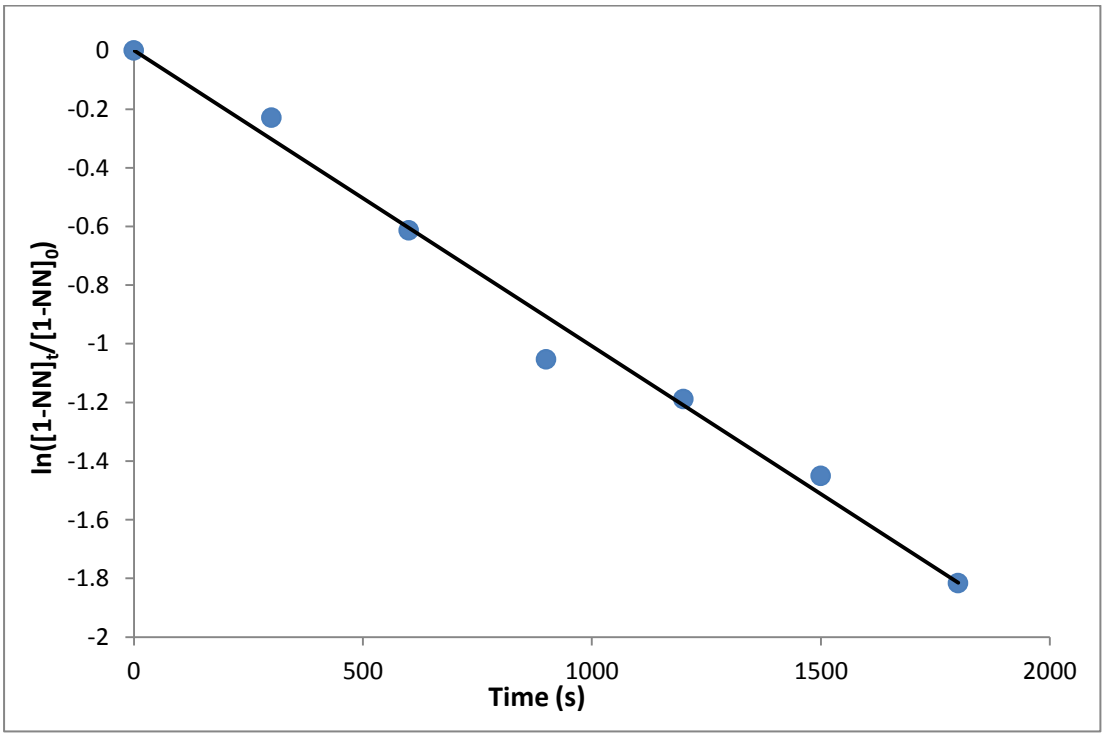


Figure 5.9 Decay of 1-NN (corrected for wall loss) during the experiment performed at EUPHORE on 14th July 2009.

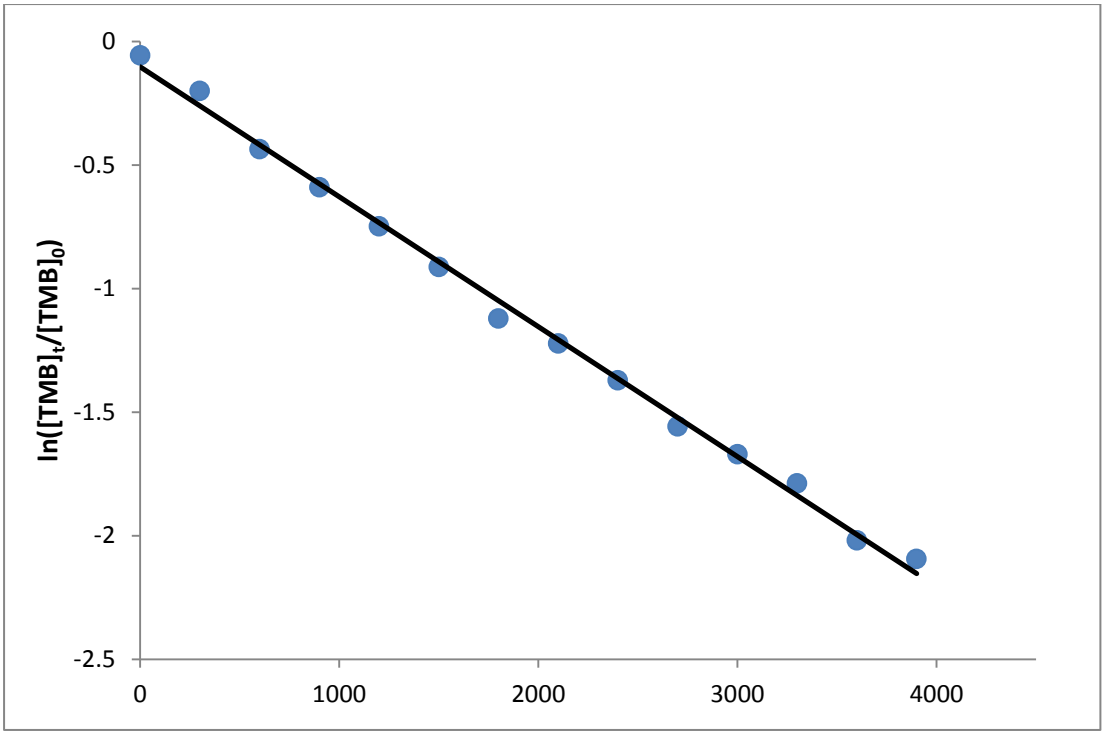


Figure 5.10 First order decay rate of 1,3,5-trimethylbenzene (TMB, corrected for wall loss) during the experiment performed at EUPHORE on 7th July 2009.

5.3.1.2 Indoor Chamber

Three experiments were conducted in the indoor simulation chamber in order to compare the photolysis rate with that obtained using sunlight at EUPHORE and with the previous studies (Atkinson et al. 1989; Feilberg et al. 1999b; Phousongphouang et al. 2003). One experiment was performed using 1,3,5-trimethylbenzene and CO as an OH radical tracer and scavenger respectively. Concentration–time profiles and kinetic plots in the form of Equation (I) were generated for all experiments. The kinetic plots exhibited good linearity and near-zero intercepts. The reaction conditions and results are summarized in **Table 5.3**.

The results are similar to those obtained in the EUPHORE experiments, with the decay of 1-NN observed to be slightly lower in the presence of the OH radical scavenger or tracer. The average value of j(1-NN) determined from experiments performed with tracer and scavenger is $(0.95 \pm 0.10) \times 10^{-3}$ s^{-1}, with j(1-NN)/j(NO_2) = 0.13 ± 0.03. The steady state OH radical concentration calculated during the tracer experiment was [OH] = 1.6×10^6 molecule cm^{-3}. These values indicate that reaction with OH radicals account for 9% of the loss of 1-NN in this experiment.

Table 5.3 Experimental conditions and results for the photolysis of 1-NN in the indoor simulation chamber.

Date	**27122009**	**28122009[2]**	**29122009[1]**
Initial conc.(ppbV)	353	350	346
Irradiation time	37 min	37 min	32 min
$j(NO_2)$ ($\times 10^{-3} s^{-1}$)	6.7 ± 0.6	6.7 ± 0.6	6.7 ± 0.6
k_{wall} ($\times 10^{-4} s^{-1}$)	5.5 ± 0.5	4.0 ± 0.7	5.0 ± 0.4
k_{total} ($\times 10^{-3} s^{-1}$)	1.20 ± 0.14	0.90 ± 0.10	1.00 ± 0.09
k_{OH}[OH] ($\times 10^{-3} s^{-1}$)	-	0	0.09 ± 0.04
j(1-NN) ($\times 10^{-3} s^{-1}$)	1.20 ± 0.14	0.90 ± 0.10	0.90 ± 0.05
j(1-NN)/$j(NO_2)$	0.18 ± 0.03	0.13 ± 0.01	0.13 ± 0.03
SOA yield (%)	65	53	66

[1] In this experiment, 1,3,5-trimethylbenzene (350 ppbV) was as an OH radical tracer. [2] In this experiment CO (500 ppmV) used as an OH radical scavenger. Errors are twice the standard deviation. The yield of SOA was corrected with the measured wall loss value of (2-5) × 10^{-5} s^{-1} on each day.

5.3.1.3 Comparison with Previous Studies

The photolysis rates determined in this work are compared to those obtained in previous studies in **Table 5.4**. The values obtained using natural sunlight show some variation, even when normalized for $j(NO_2)$. Although the experiments were performed under slightly different conditions, it seems that difficulties associated with accurate measurements of 1-NN also contribute to the observed variation. Atkinson et al. (Atkinson et al. 1989) and Phousongphouang and Arey (Phousongphouang et al. 2003) both used cyclohexane as an OH radical scavenger and off-line GC-FID for measuring 1-NN. However, problems associated with adsorption and desorption at the chamber walls were cited in both studies. In the experiments performed by Feilberg et al (Feilberg et al. 1999b), photolysis of 1-NN was studied in the presence of 0.8 mg m^{-3} of diesel exhaust particles. Although the reported value for $j(1\text{-NN})/j(NO_2)$ is in good agreement with the results from the EUPHORE experiments, it is not known how the particles affect the photolysis rate.

The values of $j(1\text{-NN})/j(NO_2)$ obtained from the indoor chamber studies show less variation and there is good agreement with the results obtained in this work and those of Phousongphouang and Arey (Phousongphouang et al. 2003). This is in contrast to phthaldialdehyde, where large differences were observed. This difference in behaviour may be ascribed to the fact that the maximum output of the blacklamps at 360 nm coincides with the absorption band in 1-NN but not for phthaldialdehyde.

Table 5.4 Comparison of the photolysis rates of 1-NN measured in different atmospheric simulation chamber studies.

j(1-NN) ($\times 10^{-4}$ s^{-1})	$j(NO_2)$ ($\times 10^{-3}$ s^{-1})	j(1-NN)/ $j(NO_2)$	Light source	Reference
0.70 ± 0.02	7.4 ± 0.40	0.09 ± 0.01*	Natural light	This work
1.37 ± 0.10	4.3	0.032 ± 0.02	Natural light	a
-	-	0.07	Natural light	b
8.3 ± 3.5	4.6 ± 1.3	0.18 ± 0.07	Natural light	c
0.90 ± 0.10	6.7 ± 0.6	0.13 ± 0.01*	Philips TL05 lamps (λ_{max}=360 nm) Philips TL12 lamps (λ_{max}=310 nm)	This work
15.9 ± 1.1	7.8	0.20 ± 0.03	Blacklamps (290<λ<470 nm)	a
2.5 ± 0.3	1.9	0.13 ± 0.02	Blacklamps	c

** Average value obtained from experiments performed using OH scavenger and tracer.*

References: (a) Atkinson et al. (1989), (b) Feilberg et al. (1999b), (c) Phousongphouang et al. (2003).

5.3.2 Photolysis Products and Mechanism

In the first study of the atmospheric photolysis of 1-NN, Atkinson et al. (Atkinson et al. 1989) identifed 1,4-naphthoquinone and 2-nitro-1-naphthol as products with estimated yields of 22% and 8% respectively. Efforts were made to quantify these products in the gas-phase using the FTIR spectra obtained in the EUPHORE experiments. However, this was not successful since considerable difficulties were encountered while introducing these compounds into the chamber. However, the formation of NO, NO_x and O_3 was observed in all chamber experiments.

The formation profiles of NO, NO_x and O_3 varied considerably in the EUPHORE experiments, **Figure 5.2**, **Figure 5.4**, **Figure 5.6**, and **Figure 5.8**. In the absence of scavenger or tracer, the formation of NO was initially very rapid and after reaching a maximum, the mixing ratio declined slowly for the remainder of the experiment. In photooxidation systems, NO is normally removed rapidly due to reactions with HO_2 and RO_2 radicals and the very slow decay of NO in these experiments indicates that the concentrations of the radicals was very low during the photolysis of 1-NN. As a result there was minimal conversion to NO_2 and O_3 in these experiments. In contrast large amounts of NO_2 and O_3 were formed in experiments conducted in the presence of tracer or scavenger, as the newly formed NO was found to undergo a very rapid decay via reaction with HO_2 and/or RO_2 generated from the OH-initiated oxidation of the tracer or scavenger. Product yield plots for NO could not be constructed for the EUPHORE experiments due to an insufficient number of data points collected by FTIR spectroscopy during the fast photolytic decay of 1-NN.

The results obtained in this work help to confirm that the initial step in the UV photolysis of 1-NN is the production of a naphthoxy radical and NO (Reichardt et al. 2009). Experimental and theoretical evidence indicates that this process can occur via a dissociation-combination mechanism or an intramolecular rearrangement where the NO_2 group on the photoexcited 1-NN molecule could rotate to a position, which is vertical to the naphthalene ring (Platz et al. 1998), as shown in **Figure 5.11** , followed by C-N bond scission while an oxygen atom forms a new bond to the aromatic ring. A similar process has also been proposed in the photolysis of nitrobenzene (Galloway et al. 1993; Osterheld et al. 1993) and other nitro-PAHs (Crespo-Hernández et al. 2008).

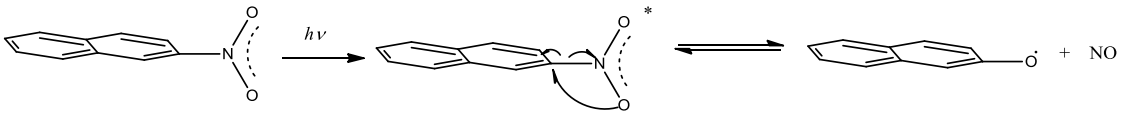


Figure 5.11 Proposed mechanism for the initial step in the photolysis of 1-NN.

Subsequent reactions of the naphthoxy radical are proposed in **Figure 5.12** which explain the formation of 1,4-naphthoquinone and 2-nitro-1-naphthol, which were observed as reaction products by Atkinson et al. (Atkinson et al. 1989).

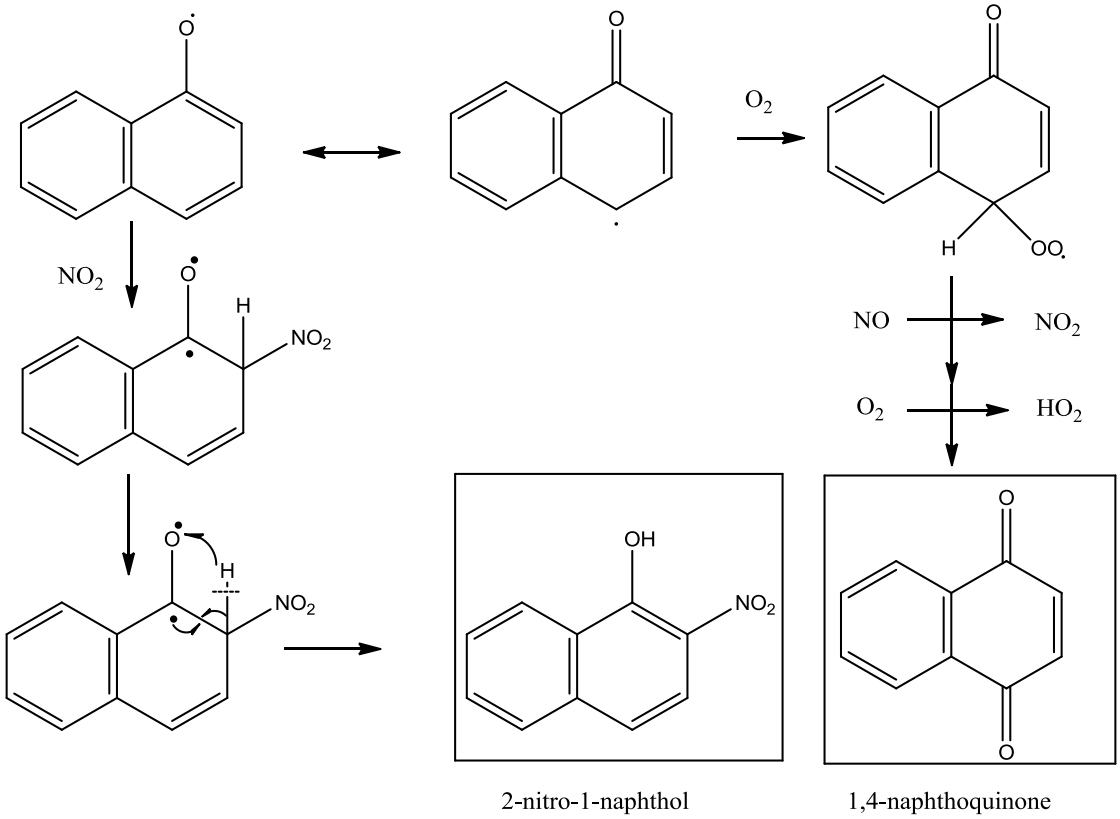


Figure 5.12 Proposed mechanisms for the formation of 1,4-naphthoquinone and 2-nitro-1-naphthol from the naphthoxy radical.

5.3.3 Secondary organic aerosol (SOA) Formation

The formation of secondary organic aerosol (SOA) was observed in all experiments performed in both chambers. The experiments were carried out in the absence of seed aerosol, which favoured the formation of new particles by nucleation. The volume

concentration of the particles measured by the SMPS was converted to mass concentration by assuming a density of 1.4 g cm^{-3} (Hallquist et al. 2009). The loss of particles to the chamber walls was determined by monitoring their decay in the dark at the end of each experiment. A first-order rate coefficient for wall loss was derived and used to correct the measured concentration data. The concentration of 1-NN was also corrected for wall loss as outlined previously.

5.3.3.1 EUPHORE Chamber

Concentration-time profiles showing the decrease of 1-NN and increase in aerosol mass were generated for each experiment and are shown in **Figures 5.13**, **Figure 5.15**, **Figure 5.17** and **Figure 5.19**. Wall loss correction factors in the range 5-13% and 7-18% were applied to the concentrations of 1-NN and aerosol mass respectively. The concentration-time profiles show that aerosol formation was observed immediately after opening the chamber and continued to rise until all of the 1-NN had reacted or the chamber was closed. The yield of aerosol produced in the experiments was determined from the following expression:

$$yield = \frac{\Delta[SOA](\mu g\ m^{-3})}{\Delta[1-NN](\mu g\ m^{-3})} \times 100\% \qquad \text{(II)}$$

where Δ[SOA] is the mass concentration of particles produced and Δ[1-NN] is the amount of 1-NN consumed at the end of the experiment, corrected for wall loss. The calculated aerosol yields are listed in **Table 5.2.** SOA yields were very high, in the range 57-71%. Unlike during phthaldialdehyde photolysis, the yields did not show a particular dependence on the presence of OH radical scavenger or tracer. The yields are considerably higher than those obtained for direct photolysis of phthaldialdehyde (2-11%) and o-tolualdehyde (5-11%) (Clifford et al. 2011). The evolution of the aerosol particle and size distribution during the photolysis experiments is shown in **Figure 5.14**, **Figure 5.16**, **Figure 5.18** and **Figure 5.20.** A large number of particles were observed in the first 3 min of photolysis. This initial "burst" of particles also corresponded to the greatest number present during the reaction. As photolysis continued, there was a gradual reduction in the particle number and increase in average particle diameter due to coagulation. In the absence of scavenger or tracer, particles with an initial mean diameter in the range 195-220 nm formed (**Figure 5.14**

and **Figure 5.20)** and grew up to ~250 nm when all the 1-NN decayed. Using TMB as a tracer, the initial particles were slightly larger (**Figure 5.16**) and when CO was used as a scavenger, aerosol formation appeared to be slightly slower (**Figure 5.18**).

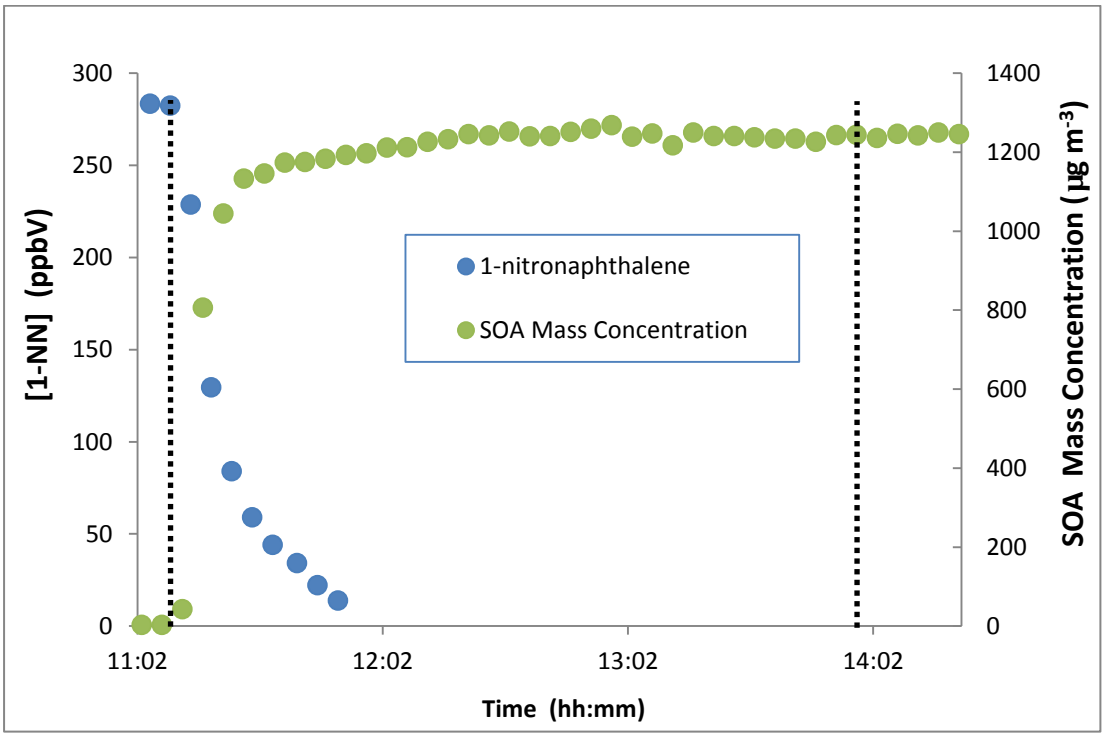


Figure 5.13 Concentration-time profile and SOA formation during the photolysis of 1-NN at EUPHORE on 6th July 2009. The vertical dash line indicating the time of chamber fully opened (11:11) and closed (13:55).

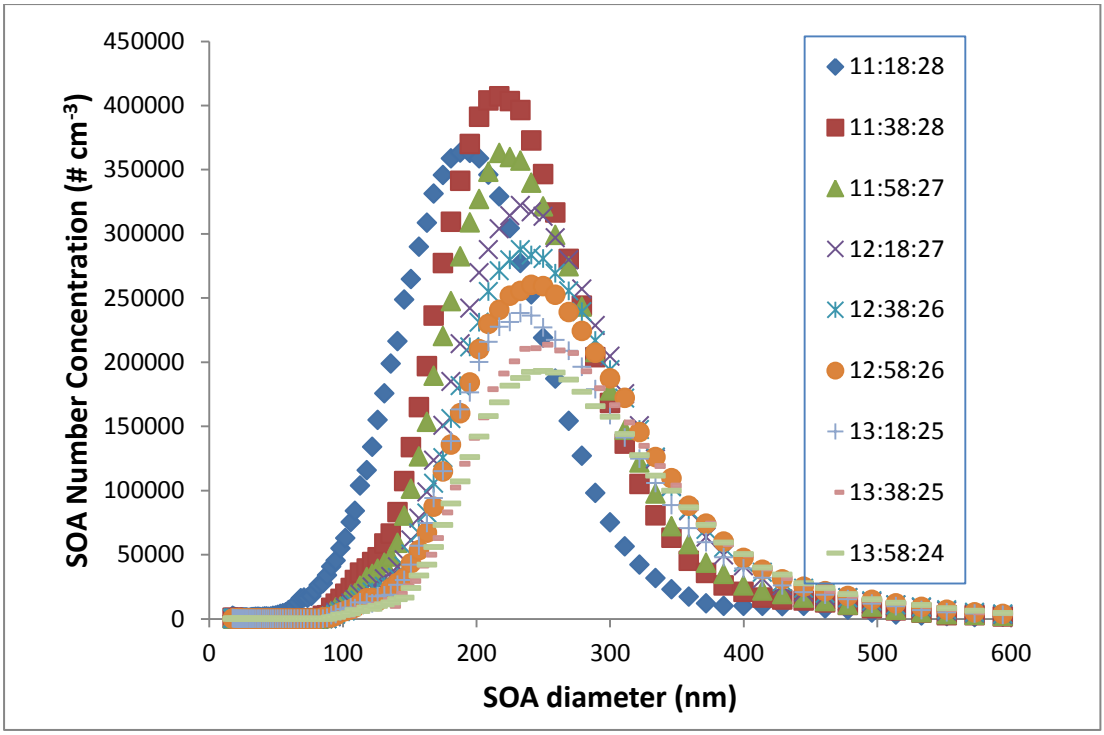


Figure 5.14 Number and size distribution of SOA in the photolysis of 1-NN on 6th July 2009 at EUPHORE chamber.

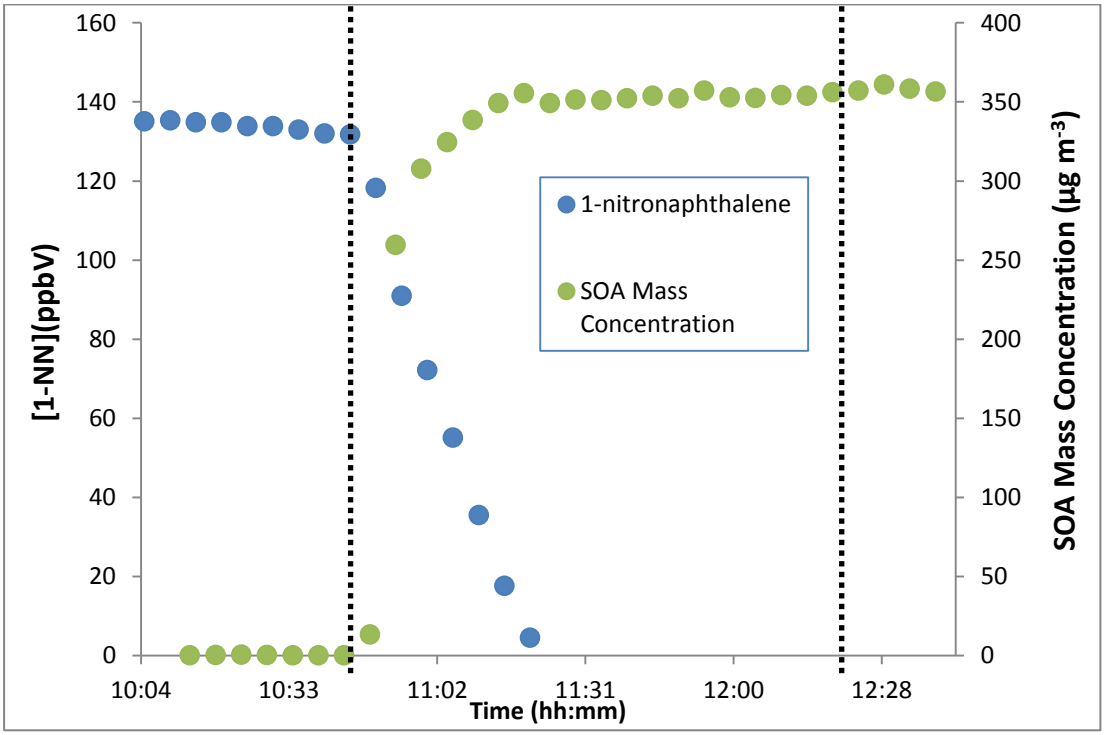


Figure 5.15 Concentration-time profile and SOA formation during the photolysis of 1-NN at EUPHORE on 7th July 2009. The vertical dash line indicating the time of chamber fully open (10:50) and chamber closed (12:20).

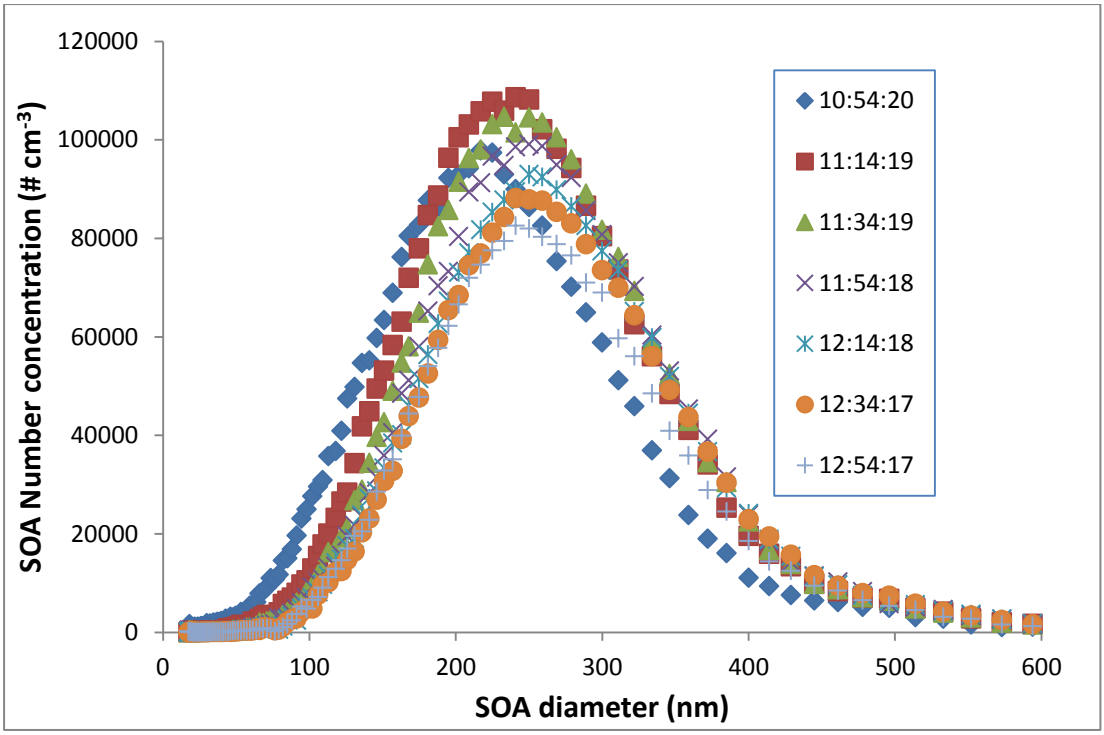


Figure 5.16 Number and size distribution of SOA generated at EUPHORE on 7th July 2009.

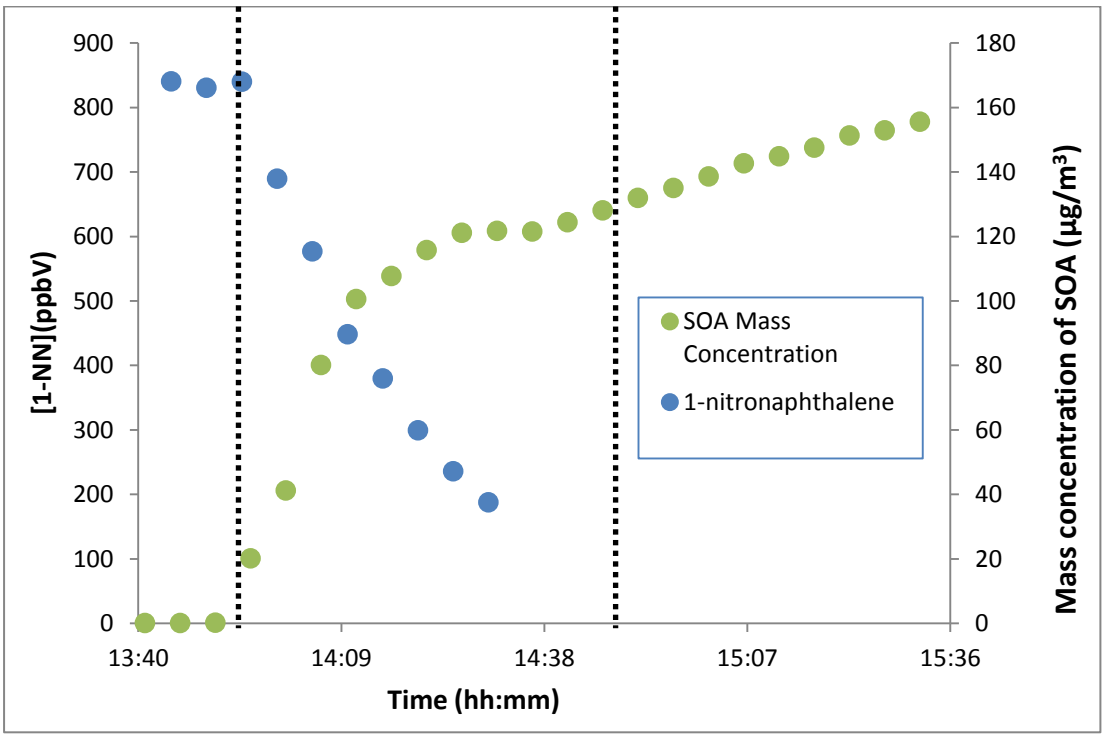


Figure 5.17 Concentration-Time profile and SOA formation during the photolysis of 1-NN at EUPHORE on 13rd July 2009. The vertical dash line indicating the time of fully chamber open (13:55) and chamber closed (14:46).

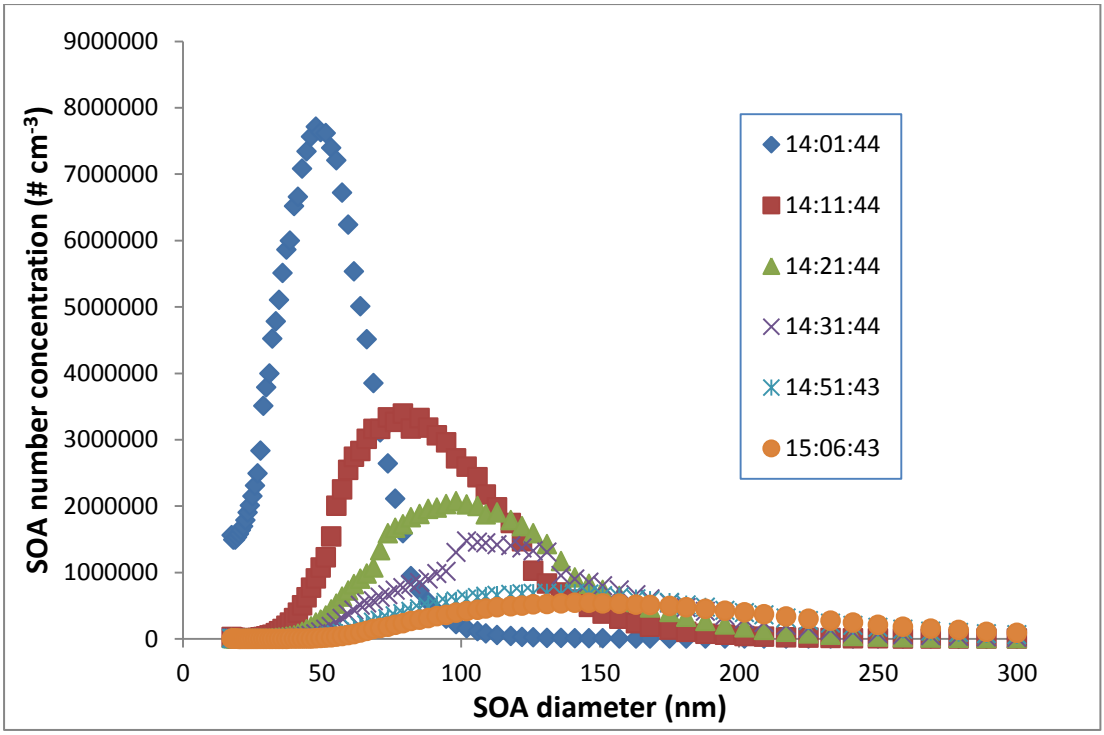


Figure 5.18 Number and size distribution of SOA generated at EUPHORE chamber on 13rd July 2009.

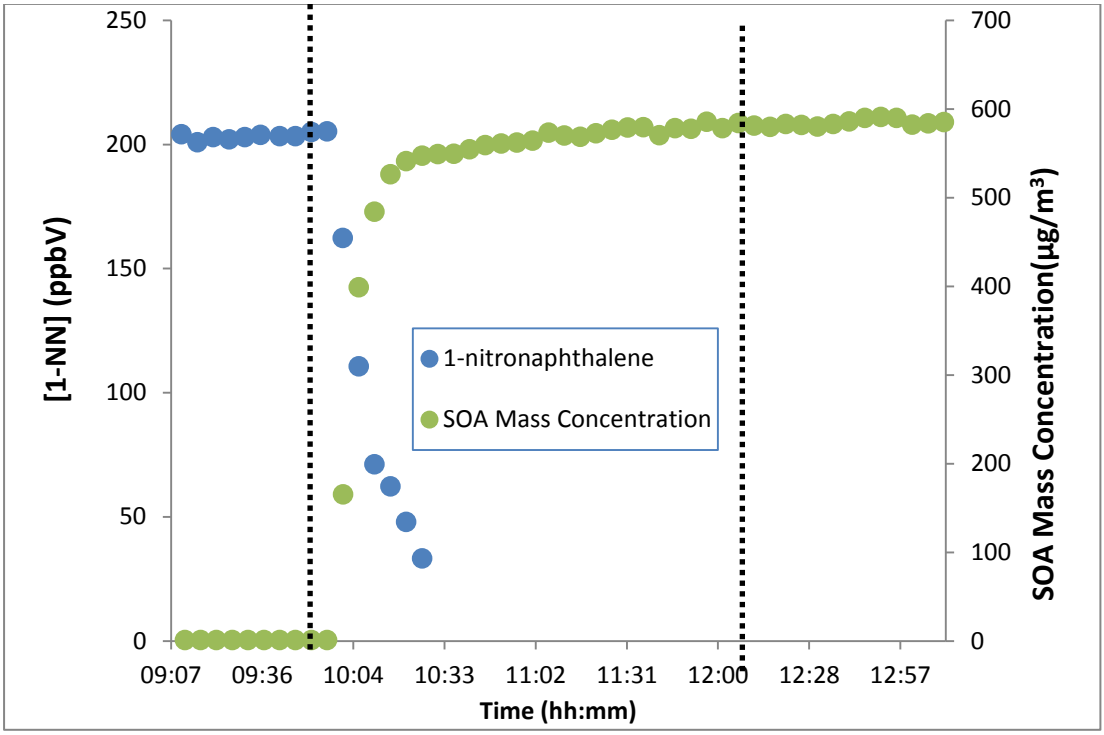


Figure 5.19 Concentration- time profile and SOA formation –time profile during the photolysis of 1-NN at EUPHORE on 14th July 2009, the vertical dash line indicating the time of chamber open (09:45) and chamber closed (12:06).

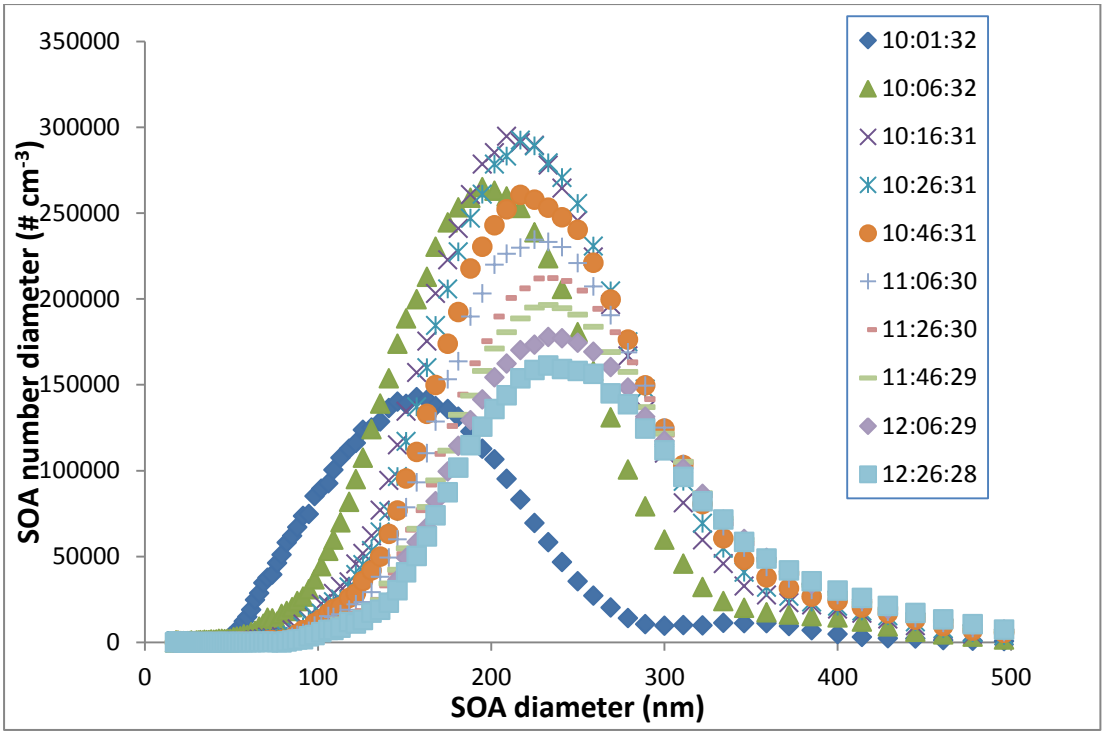


Figure 5.20 Number and size distribution of SOA generated at EUPHORE chamber on 14th July 2009.

The composition of SOA arising from photolysis of 1-NN without tracer or scavenger was analysed by GC-MS. Filter samples collected at the end of the experiment were treated in three different ways: extracted into a solvent and analysed by a direct injection method, derivatized by PFBHA in order to identify any carbonyls, derivatized by BSTFA to identify hydroxyl-containing products. Only 1,4-naphthoquinone was observed using the direct injection and PFBHA derivatization methods. The total ion chromatogram obtained from BSTFA derivatization of the filter extracts is shown in **Figure 5.21**. Two derivatized products were identified as 1-naphthol and 1,4-naphthalenediol based on their diagnostic ions listed in **Table 5.5**.

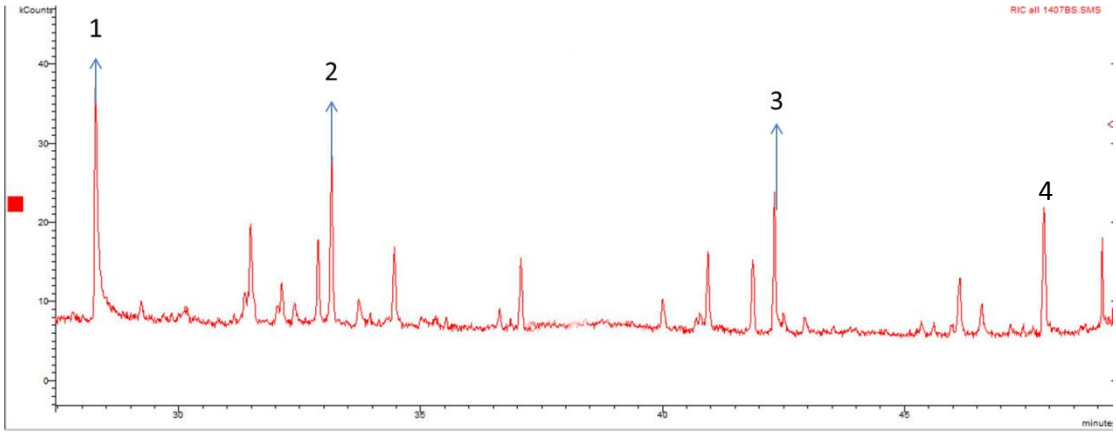
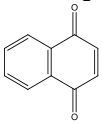
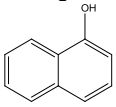
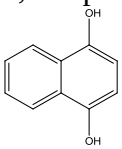
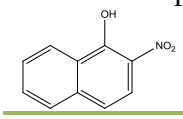


Figure 5.21 Total ion chromatogram of filter extracts obtained during the photolysis of 1-NN at EUPHORE (14th July 2009) and derivatized by BSTFA.

1) 1,4-naphthoquinone, 2) 1-naphthol,3) 1,4-naphthalenediol,41,4-naphthoquinone.

Table 5.5 Particle phase products identified by BSTFA derivatization GC-MS during the photolysis of 1-NN by natural sunlight in the EUPHORE chamber.

Compound	R.T. (min)	Peaks	Reference
1,4-naphthoquinone* 	28.32	76, 102, 130, 158(M)	a,b,
1-naphthol 	32.88	73, 101, 141, 185, 201, 216(M)	b
1,4-naphthalenediol 	42.30	73,201,304(M)	
2-nitro-1-naphthol 	46.61	73,147,229,261(M)	a

References: (a) Atkinson et al. (1989), (b) Phousongphouang et al. (2003).

** 1,4-naphthoquinone was identified but not derivatized by BSTFA.*

1,4-Naphthoquinone is an expected product from 1-NN photolysis likely formed in the gas-phase via the mechanism shown in **Figure 5.12**. This species has been detected in the particle phase in a number of previous studies (Bunce et al. 1997; Sasaki et al. 1997; Kautzman et al. 2010) and readily undergoes transfer to the particle

phase. The formation mechanisms for the other products are less certain and could involve further reactions of the naphthoxy radical in the gas-phase or particle-phase processes.

5.3.3.2 Indoor Chamber

Concentration-time profiles showing the decrease of 1-NN and increase in aerosol mass were generated for all experiments performed in the indoor chamber. The calculated aerosol yields are listed in **Table 5.3** and are in the same range as those measured in the EUPHORE experiments. The typical evolution of aerosol particle and size distribution during one of the photolysis experiments is shown in **Figure 5.22.** The pattern is very similar to that observed in the EUPHORE chamber, except that the mean particle diameters at the end of the experiments were slightly smaller.

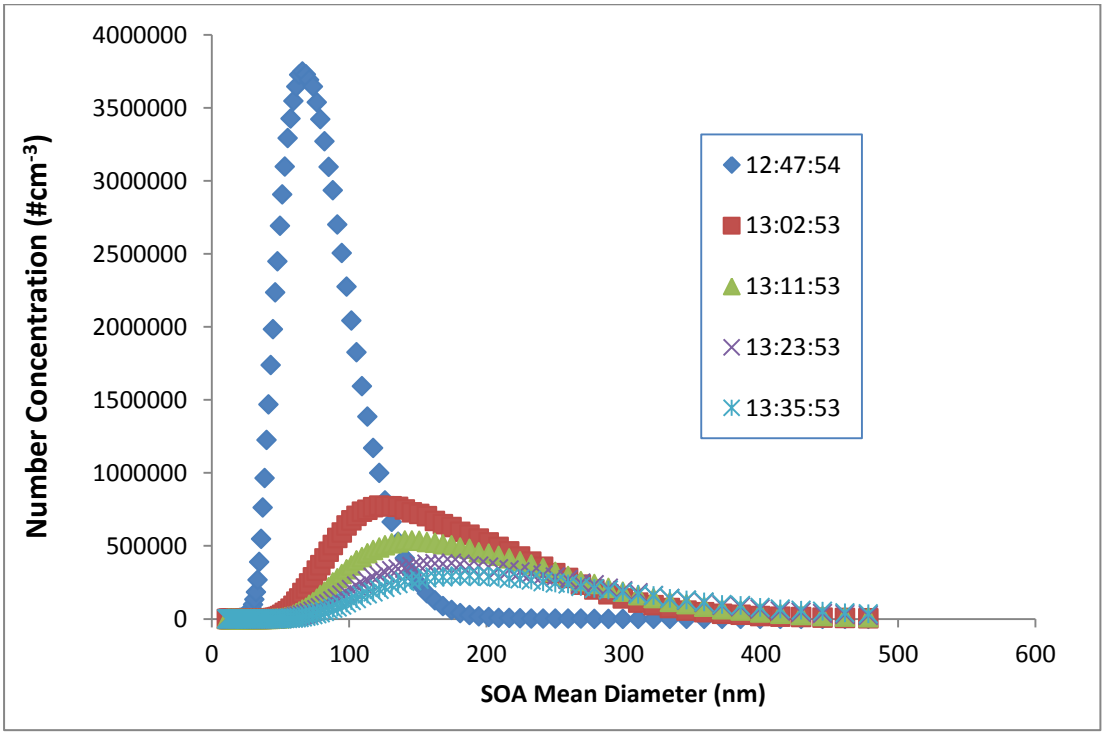


Figure 5.22 SOA number and size distribution from the photolysis of 1-NN in 28122012 at UCC chamber.

5.3.4 On-line Analysis of SOA using ATOFMS

A series of experiments was conducted to investigate the chemical composition of SOA formed in the photolysis of 1-NN in the 3.91 m^3 indoor simulation chamber. Experiments were performed using ca. 100 ppbV of 1-NN in the absence of seed aerosol, **Table 5.6**. The effect of changing the ionization laser power density, the

presence of an OH scavenger, and addition of NO and nitrobenzene were investigated. The absence of useful negative ions over 250 Da reduced the accuracy of the mass calibrations in this mass range, thus the high mass spectra over 250 Da were not very reproducible. The positive ion mass spectra were, however, much easier to calibrate in this range.

Table 5.6 Experimental conditions for ATOFMS studies of the composition of SOA produced from 1-NN photolysis in the indoor chamber.

Experiment	Reagents	Conc. (ppmV)	Irradiation time(min)
07112011	1-NN	0.1	90
11112011	1-NN	0.1	10
25112011	1-NN/n-butyl ether	0.1/10	10
07122011	1-NN/nitrobenzene	0.1/10	60
08122011	1-NN/NO	0.1/0.8	10

A typical contour plot of SOA formation monitored using the SMPS during one of the experiments is shown in **Figure 5.23**. The particles in the SOA grow very rapidly to mean diameters of around 150 nm in 3 minutes. Thus in this series of experiments, the irradiation time was limited to 10 minutes to avoid saturating the ATOFMS with high particle numbers, which results in particle coincidence in the sizing region and reduces the hit rate of the ATOFMS. The collection efficiency was around 10% when the standard ionization laser power density was used, while collection efficiency decreased at lower ionization laser energy, as expected. However, the hit rate remained satisfactory because the products formed exhibit relatively efficient absorption at 266 nm.

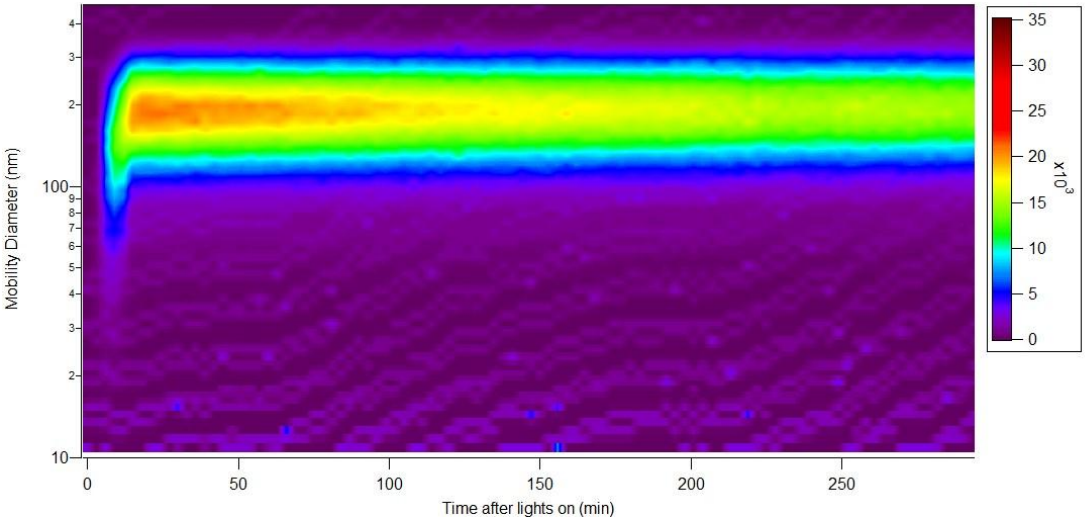


Figure 5.23 Typical contour plot of SOA number and size distribution in the photolysis of 1-NN.

5.3.4.1 Effect of Laser Power Density

The average dual ion mass spectra of the SOA formed in the photolysis of 1-NN using the standard laser power density (~ 1 mJ per pulse) are shown in **Figure 5.24**. In the positive mode, the peaks at *m/z* 27, 39, 51, 63 and 77 are due to aromatic fragment ions, while 89 ($C_7H_5^+$), 101 ($C_7H_4O^+$), 115 ($C_7H_4NO^+$) could be attributed to 1-NN, MW 173. The peak at *m/z* 143 ($C_{10}H_7O^+$) is attributed to 1-naphthol, which was also identified in the off-line analysis of the filter extracts collected during the photolysis of 1-NN at EUPHORE, **Section 5.3.3**. The high mass ions, such as *m/z* 187, 200, 212, 225, 237, 242, 264 and 282 are likely due to products arising from self-reactions of the naphthoxy radical, as explained below. The spectra in the negative ion mode contain strong peaks due to nitrate at *m/z* 46 (NO_2^-) and 62 (NO_3^-) and the aromatic fragment ion at *m/z* 25(C_2H^-). The *m/z* 143($C_{10}H_7O^-$) can be attributed to 1-naphthol, while the *m/z* 189 ($C_{10}H_7NO_3^-$) is assigned to 2-nitro-1-naphthol, previously identified during the photolysis of 1-NN by Atkinson et al. (Atkinson et al. 1989). The deduced formulae and tentative structures of the positive and negative and ions are summarised in **Table 5.7** and **Table 5.8** respectively.

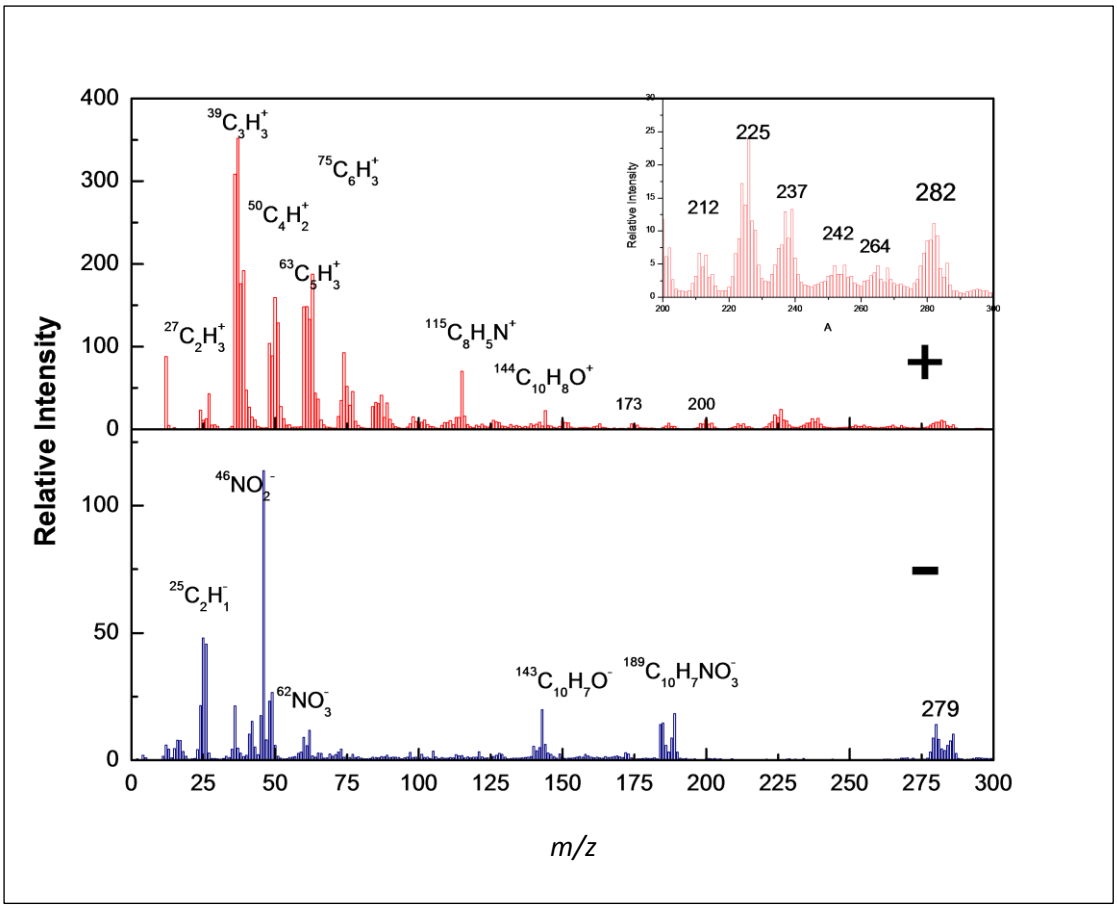


Figure 5.24 Average ATOFMS dual ion spectra obtained during the photolysis of 1-NN with normal laser power density.

Table 5.7 Positive Ions detected by ATOFMS during the photolysis of 1-NN.

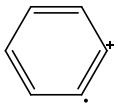
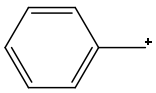
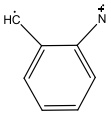
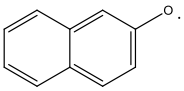
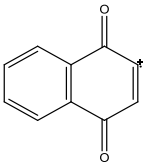
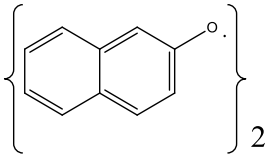
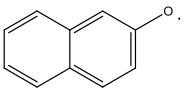
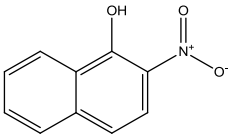
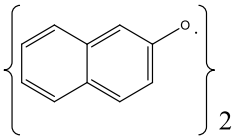
m/z	Formula	Proposed structure
27	$C_2H_3^+$	
39	$C_3H_3^+$	
51	$C_4H_3^+$	
63	$C_5H_3^+$	
75	$C_6H_3^+$	
90	$C_7H_6^+$,	
115	$C_8H_5N^+$	
143	$C_{10}H_7O^+$,	
156	$C_8H_5O_3^+$	
282-286	$C_{20}H_{14}O_2^+$	

Table 5.8 Negative Ions detected by ATOFMS during the photolysis of 1-NN.

m/z	**Formula**	**Proposed structure**
-25	C_2H^-	
-46	NO_2^-	
-62	NO_3^-	
-143	$C_{10}H_7O^-$,	
-(187-189)	$C_{10}H_7NO_3^-$	
-(282-286)	$C_{20}H_{14}O_2^-$	

The effect of reducing the laser power density was investigated in an attempt to acquire higher intensity molecular ion peaks in the ATOFMS (Fang et al. 2011). The positive ion spectra obtained at different relative laser power densities (100%, 60%, 20% and 15 %) is shown in **Figure 5.25**. The same ions were observed in all of the spectra. However, the relative intensities of the peaks change dramatically, with the clusters of high mass ion peaks centred around *m/z* 205, 212, 225, 237, 242, 264 and 281, becoming much more prominent at lower power density.

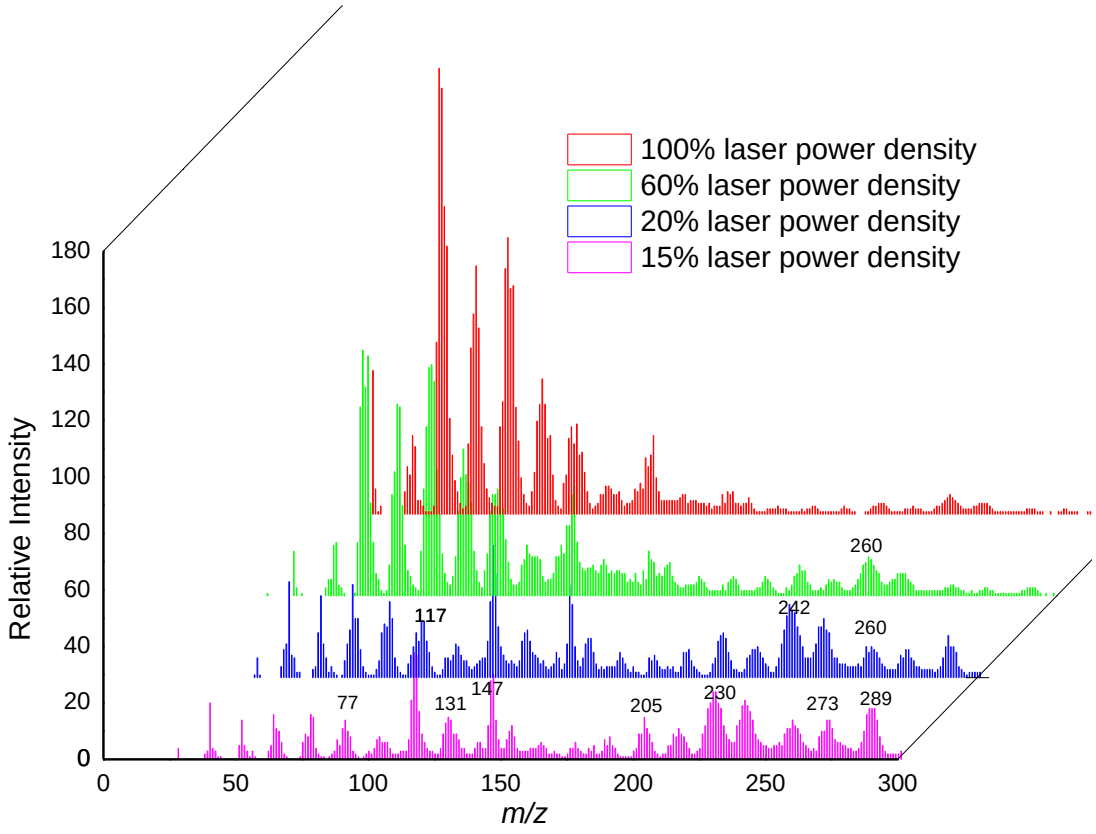


Figure 5.25 Positive ion mass spectra at 100%, 60%, 20% and 15% of the maximum ionization laser power density

Figure 5.26 shows dual ion mass spectra of the SOA from the photolysis of 1-NN at the lowest laser power density (15%). There are similarities with **Figure 5.24**, but also several differences. Firstly, the relative intensity of peak clusters centred around *m/z* 205, 230, 242, 260, 273 and 289 are much higher than they are in **Figure 5.24**. Secondly, new ion peaks were detected at *m/z* > 300. Thirdly, in the negative mode, the relative intensity of *m/z* 62 was much lower, while that of *m/z* 156, which is tentatively attributed to 1,4-naphthoquinone, was higher.

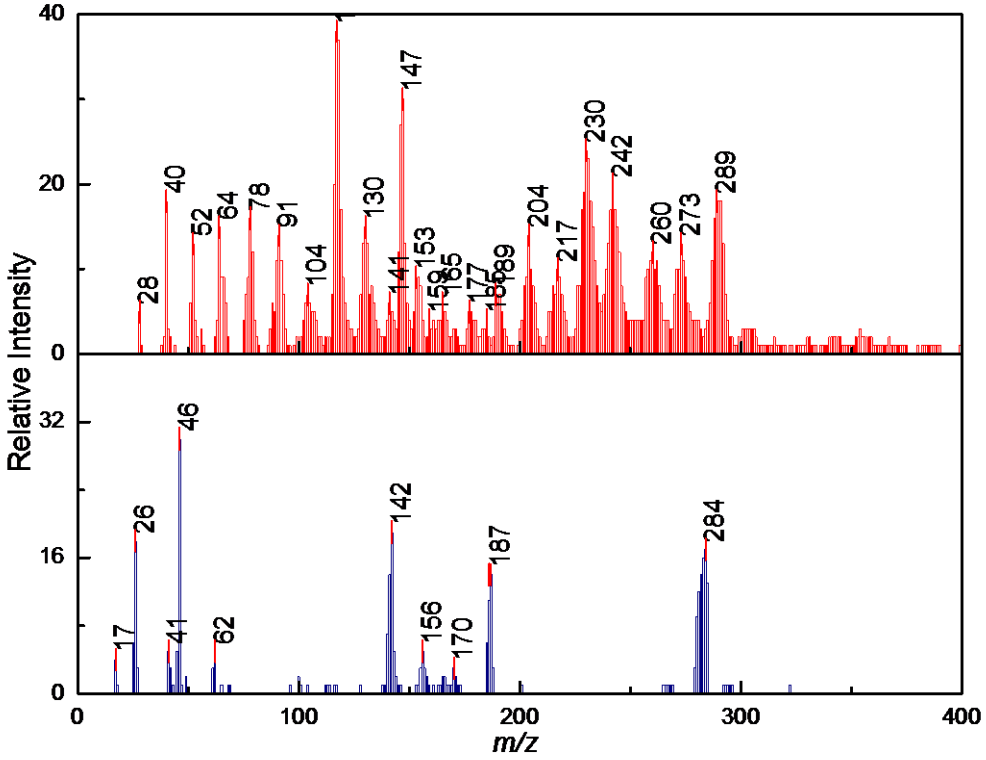


Figure 5.26 Average dual ion ATOFMS spectra of 1-NN SOA using a relative laser power density of 15%.

The particle-phase products detected in previous studies of the photooxidation of naphthalene have MW in the range 122-208 (Kautzman et al. 2010) and the presence of ions in the ATOFMS spectra with *m/z* considerably greater than 200 was therefore somewhat unexpected. However, a review of the literature indicates that the phenoxy radical ($C_6H_5O^{\cdot}$) is known to undergo dimerization in the gas-phase to generate a number of possible polycyclic species (Platz et al. 1998) with 4-phenoxyphenol detected as the major, if not sole product. It is therefore proposed that the naphthoxy radicals generated from the direct photolysis 1-NN undergo a similar process. The dimers have MW 286 and are expected to exist in two possible forms, shown in **Figure 5.27**, each of which has several positional isomers. These compounds could be responsible for the presence of the cluster of peaks centred around *m/z* 282-286 in the ATOFMS spectra and successive fragmentation of the molecular ions could give rise to the peak clusters observed at *m/z* 273, 260, 242, 230 etc. If the naphthoxy chemistry is completely analogous to the chemistry of phenoxy, formation of the compound containing the ether linkage is expected to be more favourable (Platz et al. 1998).

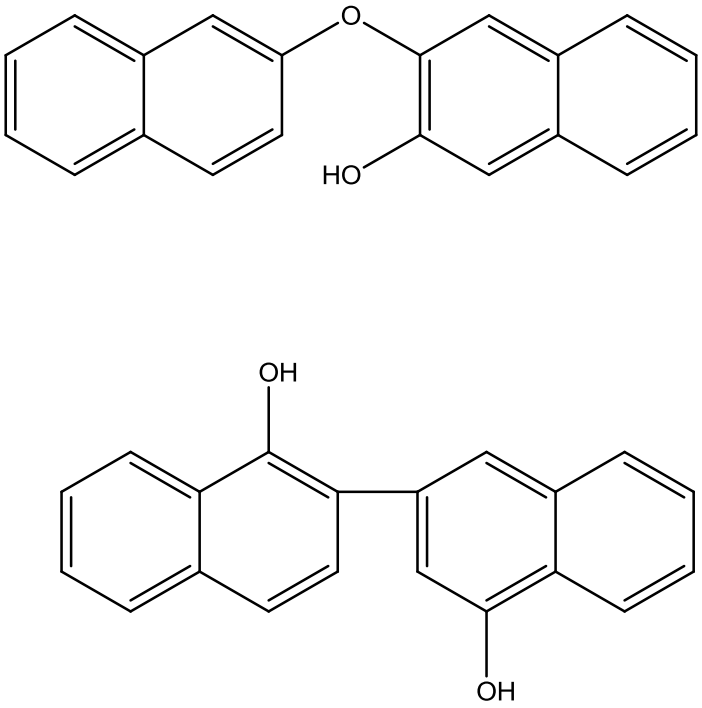


Figure 5.27 Chemical structures of compounds produced from dimerization of the naphthoxy radical.

5.3.4.2 Effect of OH Scavenger

The possible effect of OH radical reactions on the composition of the SOA was investigated by performing the photolysis of 1-NN in the presence of a large excess (10 ppmV) of n-butyl ether as OH scavenger. This compound is reactive towards OH and the resulting oxidation products are sufficiently volatile so that they do not contribute to SOA formation. The dual ion ATOFMS spectra for this experiment are shown in **Figure 5.28** and contain many of the same features as those shown in the previous spectra. This observation indicates that, although OH chemistry may play a part, the main components of the SOA are likely produced through the direct photolysis of 1-NN. Interestingly, the relative ion intensity of the peaks at *m/z* -186 and -143, attributed to 2-nitro-1-naphthol, is higher than in the experiment without scavenger. The formation of 2-nitro-1-naphthol is believed to proceed via reaction of naphthoxy with NO_2 and this observation indicates that the mixing ratio of NO_2 was higher in the presence of OH scavenger, presumably due to decreased efficiency in the removal of NO_2 via reaction with OH.

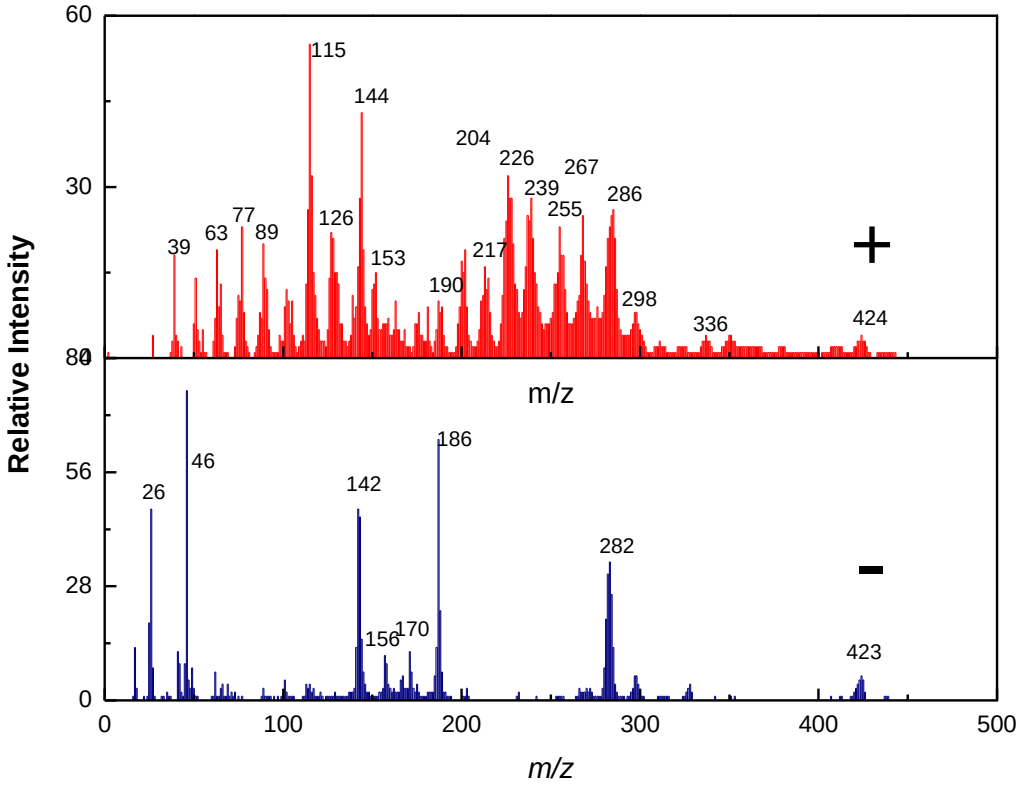


Figure 5.28 Average ATOFMS dual ion spectra obtained during the photolysis of 1-NN in the presence of excess *n*-butyl ether using a relative laser power density of 15%.

5.3.4.2 Effect of Nitrobenzene and NO on Naphthoxy Dimerization

Two additional experiments were conducted to further investigate the proposed role of naphthoxy radical self-reactions in the formation of dimers that contribute to SOA formation and growth. In the first experiment, the photolysis of 1-NN was performed in the presence of a large excess of nitrobenzene (10 ppmV), which is known to produce phenoxy radicals when irradiated with UV light (Osterheld et al. 1993; Kosmidis et al. 1994; Berho et al. 1998). The dual ion ATOFMS spectra for this experiment are shown in **Figure 5.29** and are significantly different to those obtained with only 1-NN in the chamber. Firstly, the high MW peaks at *m/z* 282-286 attributed to the dimer produced from the naphthoxy radical self-reaction are dramatically reduced in intensity. Secondly, the major peaks in the positive ion mode appear in a cluster centred on *m/z* 233, which may be attributed to a compound with MW formed from the reaction of phenoxy radicals with naphthoxy radicals, **Figure 5.30**. The large

peak observed at *m/z* 235 in the negative ion spectra may also be assigned to this compound. Finally, the relative ion intensity of the peaks at *m/z* -186 and -143, attributed to 2-nitro-1-naphthol, is higher, likely due to increased amounts of NO_2 in the reaction system.

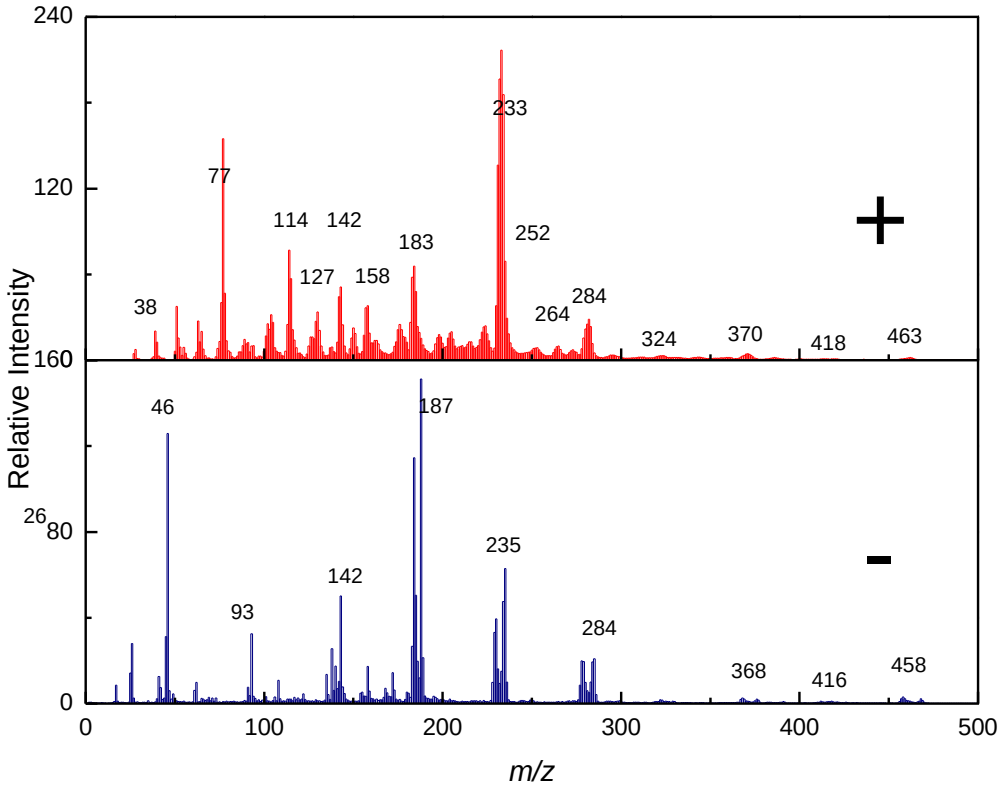


Figure 5.29 Average ATOFMS dual ion spectra obtained during the photolysis of 1-NN in the presence of excess nitrobenzene using a relative laser power density of 15%.

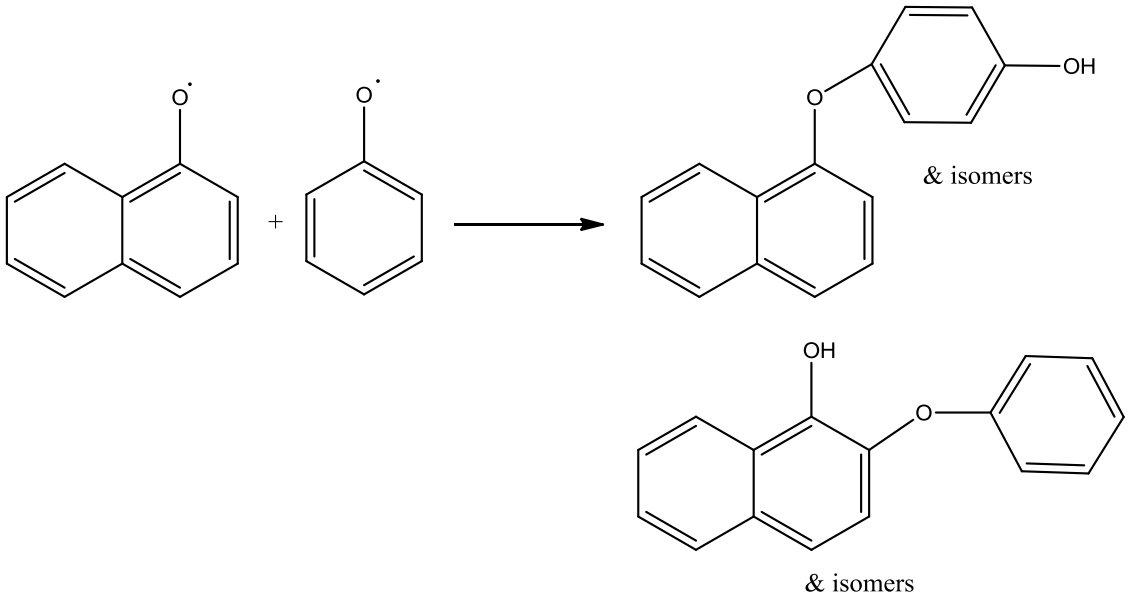


Figure 5.30 Proposed structure of the compound formed from the cross-reaction of phenoxy and naphthoxy radicals.

In the second experiment, the photolysis of 1-NN was performed in the presence of a large amount of NO (ca. 800 ppbV), which, by analogy with the phenoxy radical (Platz et al. 1998) is expected to react with the naphthoxy radical. The dual ion ATOFMS spectra for this experiment are shown in **Figure 5.31** and are different to those obtained with only 1-NN in the chamber. Firstly, the negative ion mass spectrum appears to be dominated by 2-nitro-1-naphthol, which is formed form the reaction of naphthoxy with NO_2. Secondly, the positive ion mass spectrum shows a similar pattern of peak clusters, but shifted to slightly higher *m/z* values, indicating that the composition is slightly different. Thus it appears that the naphthoxy radical self-reaction may be affected in the presence of excess NO but high molecular weight products are still formed. The results of this experiment suggest that the role of nitrogen oxides in the chemistry of naphthoxy radicals need further investigation.

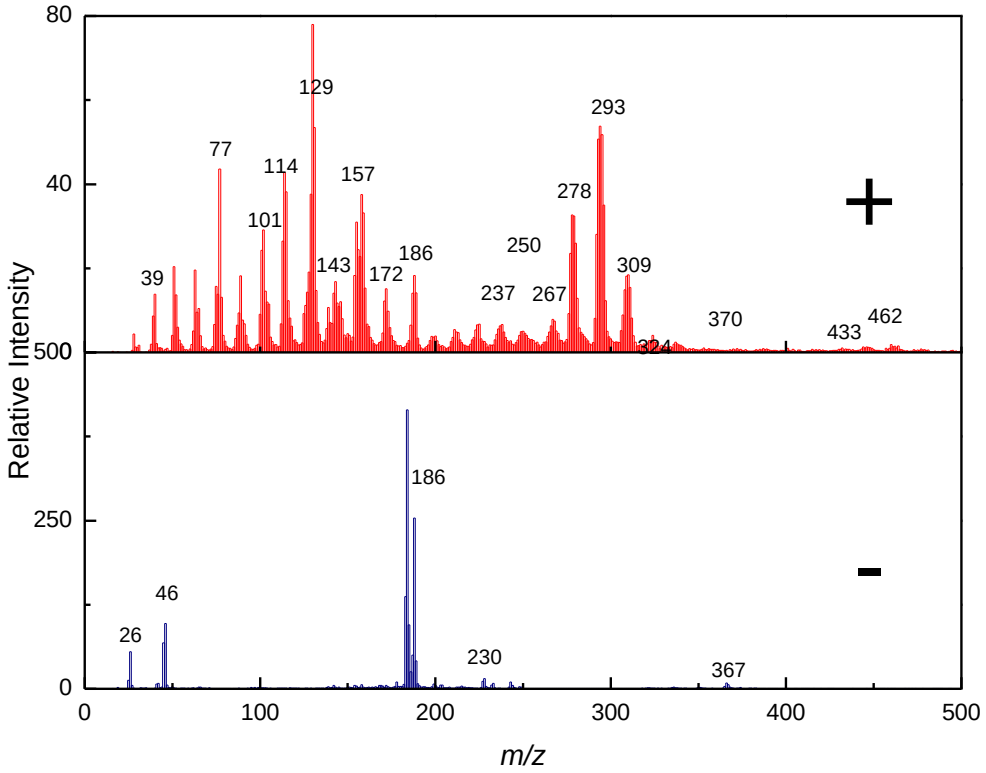


Figure 5.31Average ATOFMS dual ion spectra obtained during the photolysis of 1-NN in the presence of NO (800 ppbV) using a relative laser power density of 15%.

5.4 Conclusions

The photolysis of 1-nitronaphthalene was also investigated using natural light at the EUPHORE chamber in Valencia, Spain. The photolysis rate coefficient was measured directly and values in the range $(0.70 – 1.20) \times 10^{-3}$ s^{-1} were observed under different conditions. The corresponding lifetime due to photolysis is 14-24 min, confirming that photolysis is the major atmospheric loss process for 1-nitronaphthalene. The gas-phase photolysis products could not be identified. However, substantial amounts of NO were produced, consistent with the proposed mechanism which involves the direct formation of a naphthoxy radical and NO. SOA yields in the range 57-71% were measured in the presence and absence of OH radical tracer or scavenger. The major particle-phase products identified using off-line GC-MS analysis were 1,4-naphthoquinone, 1-naphthol and 1,4-naphthalenediol. On-line analysis of the SOA generated in an indoor chamber was performed using ATOFMS. A number of photolysis products were tentatively identified in the mass spectra and there was also evidence for the formation of one or more high MW products in the range 200-300. Further investigations revealed that these high MW products are oxygenated polycyclic compounds most likely produced from the dimerization of naphthoxy radicals.

5.5 References

Albinet, A., E. Leoz-Garziandia, H. Budzinski and E. Viłlenave (2007). "Polycyclic aromatic hydrocarbons (PAHs), nitrated PAHs and oxygenated PAHs in ambient air of the Marseilles area (South of France): Concentrations and sources." Science of the Total Environment **384**(1-3): 280-292.

Arey, J., R. Atkinson, B. Zielinska and P. A. McElroy (1989). "Diurnal concentrations of volatile polycyclic aromatic hydrocarbons and nitroarenes during a photochemical air pollution episode in Glendora, California." Environmental Science & Technology **23**(3): 321-327.

Arey, J., B. Zielinska, R. Atkinson and S. M. Aschmann (1989). "Nitroarene products from the gas‐phase reactions of volatile polycyclic aromatic hydrocarbons with the OH radical and N_2O_5." International Journal of Chemical Kinetics **21**(9): 775-799.

Arey, J., B. Zielinska, R. Atkinson and A. M. Winer (1987). "Polycyclic aromatic hydrocarbon and nitroarene concentrations in ambient air during a wintertime high-NO_x episode in the Los Angeles basin." Atmospheric Environment **21**(6): 1437-1444.

Atkinson, R. and J. Arey (2007). "Mechanisms of the gas-phase reactions of aromatic hydrocarbons and PAHs with OH and NO_3 radicals." Polycyclic Aromatic Compounds **27**(1): 15-40.

Atkinson, R., S. M. Aschmann, J. Arey, B. Zielinska and D. Schuetzle (1989). "Gas-Phase Atmospheric Chemistry of 1-Nitronaphthalene and 2-Nitronaphthalene and 1,4-Naphthoquinone." Atmospheric Environment **23**(12): 2679-2690.

Berho, F., F. Caralp, M.-T. Rayez, R. Lesclaux and E. Ratajczak (1998). "Kinetics and Thermochemistry of the Reversible Combination Reaction of the Phenoxy Radical with NO." The Journal of Physical Chemistry A **102**(1): 1-8.

Bunce, N. J., L. Liu, J. Zhu and D. A. Lane (1997). "Reaction of Naphthalene and Its Derivatives with Hydroxyl Radicals in the Gas Phase." Environmental Science & Technology **31**(8): 2252-2259.

Clifford, G. M., A. Hadj-A ïssa, R. M. Healy, A. Mellouki, A. Muñoz, K. Wirtz, M. Martín Reviejo, E. Borrás and J. C. Wenger (2011). "The Atmospheric Photolysis of *o*-Tolualdehyde." Environmental Science & Technology **45**(22): 9649-9657.

Crespo-Hernández, C. E., G. Burdzinski and R. Arce (2008). "Environmental Photochemistry of Nitro-PAHs: Direct Observation of Ultrafast Intersystem Crossing in 1-Nitropyrene." The Journal of Physical Chemistry A **112**(28): 6313-6319.

Dimashki, M., S. Harrad and R. M. Harrison (2000). "Measurements of nitro-PAH in the atmospheres of two cities." Atmospheric Environment **34**(15): 2459-2469.

Feilberg, A., R. M. Kamens, M. R. Strommen and T. Nielsen (1999a). "Modeling the formation, decay, and partitioning of semivolatile nitro-polycyclic aromatic hydrocarbons (nitronaphthalenes) in the atmosphere." Atmospheric Environment **33**(8): 1231-1243.

Feilberg, A., R. M. Kamens, M. R. Strommen and T. Nielsen (1999b). "Photochemistry and partitioning of semivolatile nitro-PAH in the atmosphere." Polycyclic Aromatic Compounds **14**: 151-160.

Galloway, D. B., J. A. Bartz, L. G. Huey and F. F. Crim (1993). "Pathways and kinetic energy disposal in the photodissociation of nitrobenzene." The Journal of Chemical Physics **98**(3): 2107-2114.

Hallquist, M., J. C. Wenger, U. Baltensperger, Y. Rudich, D. Simpson, M. Claeys, J. Dommen, N. M. Donahue, C. George, A. H. Goldstein, J. F. Hamilton, H. Herrmann, T. Hoffmann, Y. Iinuma, M. Jang, M. E. Jenkin, J. L. Jimenez, A. Kiendler-Scharr, W. Maenhaut, G. McFiggans, T. F. Mentel, A. Monod, A. S. H. Pravit, J. H. Seinfeld, J. D. Surratt, R. Szmigielski and J. Wildt (2009). "The formation, properties and impact of secondary organic aerosol: current and emerging issues." Atmospheric Chemistry and Physics **9**(14): 5155-5236.

Havey, C. D., A. J. Dane, C. Abbas-Hawks and K. J. Voorhees (2009). "Detection of nitro-polycyclic aromatic hydrocarbons in mainstream and sidestream tobacco smoke using electron monochromator-mass spectrometry." Environmental Chemistry Letters **7**(4): 331-336.

Kautzman, K. E., J. D. Surratt, M. N. Chan, A. W. H. Chan, S. P. Hersey, P. S. Chhabra, N. F. Dalleska, P. O. Wennberg, R. C. Flagan and J. H. Seinfeld (2010). "Chemical Composition of Gas- and Aerosol-Phase Products from the Photooxidation of Naphthalene." Journal of Physical Chemistry A **114**(2): 913-934.

Kosmidis, C., K. W. D. Ledingham, A. Clark, A. Marshall, R. Jennings, J. Sander and R. P. Singhal (1994). "On the dissociation pathways of nitrobenzene."

International Journal of Mass Spectrometry and Ion Processes **135**(2-3): 229-242.

Kramp, F. and S. E. Paulson (1998). "On the Uncertainties in the Rate Coefficients for OH Reactions with Hydrocarbons, and the Rate Coefficients of the 1,3,5-Trimethylbenzene and m-Xylene Reactions with OH Radicals in the Gas Phase." The Journal of Physical Chemistry A **102**(16): 2685-2690.

Landvik, N. E., M. Gorria, V. M. Arlt, N. Asare, A. Solhaug, D. Lagadic-Gossmann and J. A. Holme (2007). "Effects of nitrated-polycyclic aromatic hydrocarbons and diesel exhaust particle extracts on cell signalling related to apoptosis: Possible implications for their mutagenic and carcinogenic effects." Toxicology **231**(2–3): 159-174.

Lee, J. Y. and D. A. Lane (2009). "Unique products from the reaction of naphthalene with the hydroxyl radical." Atmospheric Environment **43**(32): 4886-4893.

Mihele, C. M., H. A. Wiebe and D. A. Lane (2002). "Particle Formation and Gas/Particle Partition Measurements of the Products of the Naphthalene-OH Radical Reaction in a Smog Chamber." Polycyclic Aromatic Compounds **22**(3-4): 729-736.

Nishino, N., R. Atkinson and J. Arey (2008). "Formation of Nitro Products from the Gas-Phase OH Radical-Initiated Reactions of Toluene, Naphthalene, and Biphenyl: Effect of NO_2 Concentration." Environmental Science & Technology **42**(24): 9203-9209.

Osterheld, T. H., T. Baer and J. I. Brauman (1993). "Infrared multiple-photon dissociation of the nitrobenzene radical cation. A paradigm for competitive reactions." Journal of the American Chemical Society **115**(14): 6284-6289.

Ozaki, N., N. Takemoto and T. Kindaichi (2010). "Nitro-PAHs and PAHs in Atmospheric Particulate Matters and Sea Sediments in Hiroshima Bay Area, Japan." Water, Air, & Soil Pollution **207**(1): 263-271.

Phousongphouang, P. T. and J. Arey (2003). "Rate constants for the photolysis of the nitronaphthalenes and methylnitronaphthalenes." Journal of Photochemistry and Photobiology a-Chemistry **157**(2-3): 301-309.

Platz, J., O. J. Nielsen, T. J. Wallington, J. C. Ball, M. D. Hurley, A. M. Straccia, W. F. Schneider and J. Sehested (1998). "Atmospheric Chemistry of the Phenoxy Radical, $C_6H_5O(\bullet)$: UV Spectrum and Kinetics of Its Reaction with NO, NO_2, and O_2." The Journal of Physical Chemistry A **102**(41): 7964-7974.

Reichardt, C., R. A. Vogt and E. Crespo-Hernandez (2009). "On the origin of ultrafast nonradiative transitions in nitro-polycyclic aromatic hydrocarbons: Excited-state dynamics in 1-nitronaphthalene." Journal of Chemical Physics **131**(22): -.

Reisen, F. and J. Arey (2004). "Atmospheric Reactions Influence Seasonal PAH and Nitro-PAH Concentrations in the Los Angeles Basin." Environmental Science & Technology **39**(1): 64-73.

Reisen, F., S. Wheeler and J. Arey (2003). "Methyl- and dimethyl-/ethyl-nitronaphthalenes measured in ambient air in Southern California." Atmospheric Environment **37**(26): 3653-3657.

Sasaki, J. C., J. Arey, D. A. Eastmond, K. K. Parks and A. J. Grosovsky (1997). "Genotoxicity induced in human lymphoblasts by atmospheric reaction products of naphthalene and phenanthrene." Mutation Research/Genetic Toxicology and Environmental Mutagenesis **393**: 23-35.

Tokiwa, H., R. Nakagawa, K. Morita and Y. Ohnishi (1981). "Mutagenicity of nitro derivatives induced by exposure of aromatic compounds to nitrogen dioxide." Mutation Research/Environmental Mutagenesis and Related Subjects **85**(4): 195-205.

Yu, C. W., D. H. Fine, K. S. Chiu and K. Biemann (1984). "Determination of nitrated polycyclic aromatic hydrocarbons in diesel particulates by gas chromatography with chemiluminescent detection." Analytical Chemistry **56**(7): 1158-1162.

Zugazagoitia, J. S., C. X. Almora-Diaz and J. Peon (2008). "Ultrafast Intersystem Crossing in 1-Nitronaphthalene. An Experimental and Computational Study." The Journal of Physical Chemistry A **112**(3): 358-365.

Chapter 6

Conclusions and Future Work

6.1 Conclusions

A detailed series of simulation chamber experiments has been performed on the atmospheric degradation pathways for naphthalene and two of its photooxidation products, phthaldialdehyde and 1-nitronaphthalene. The results will help to improve the current understanding of the environmental impact of this important PAH.

SOA formation yields from the photooxidation of naphthalene were determined in the absence of seed aerosol using nitrogen oxides (NO_x) and HONO as the OH radical precursor. The yields varied from 6-20% depending on hydrocarbon to NO_x ratio, precursor and relative humidity. Reactions with a higher hydrocarbon to NO_x ratio generated particles more quickly and produced higher yields of SOA. The SOA yield was also found to increase by up to a factor of 1.5 over the relative humidity range 0-50%. These results, along with those reported in similar studies (Chan et al. 2009; Shakya et al. 2010), indicate that naphthalene is a potentially large source of SOA in urban areas and should be included in atmospheric SOA models.

A combination of off-line and on-line analytical methods was employed to study the gas- and particle-phase photooxidation products of naphthalene. A wide range of carbonyls, nitro-compounds, phenols, carboxylic acids and quinones were identified using a denuder-filter sampling system combined with chemical derivatization and off-line analysis by GC-MS. On-line analysis of the chemical composition of naphthalene SOA was performed using ATOFMS for the first time. A number of oxidation products were tentatively identified in the mass spectra and there was also evidence for the formation of oligomers with MW in the range 200-500. The results of the off-line and on-line analyses indicate that larger amounts of carboxylic acids were present in naphthalene SOA formed at 50% relative humidity, suggesting that enhanced formation of carboxylic acids may contribute to the observed increase in SOA yields at higher relative humidity.

The photolysis of phthaldialdehyde was investigated using natural light at the EUPHORE chamber in Valencia, Spain. The photolysis rate coefficient was measured directly and values in the range $(1.01 - 1.89) \times 10^{-4}$ s^{-1} were observed under different conditions. The corresponding lifetime due to photolysis is 1-3 hours, confirming that photolysis is the major atmospheric loss process for phthaldialdehyde. The main

photolysis products identified in the gas-phase were phthalide and phthalic anhydride with average yields around 45% and 30% respectively. New mechanisms have been proposed to explain the formation of these products. SOA yields in the range 2-11% were measured and found to be highly dependent on the presence of an OH radical tracer or scavenger. The major particle-phase products identified using off-line GC-MS analysis were phthalic acid and dihydroxyphthalic acid. On-line analysis of the SOA generated in an indoor chamber was performed using ATOFMS. A number of photolysis products were tentatively identified in the mass spectra and the composition of the SOA was found to be slightly different when produced at higher relative humidity. There was also some evidence to suggest that species in the particle phase were slowly oxidized over a timescale of 4 hours.

The photolysis of 1-nitronaphthalene was also investigated using natural light at the EUPHORE chamber in Valencia, Spain. The photolysis rate coefficient was measured directly and values in the range $(0.70 – 1.20) \times 10^{-3}$ s^{-1} were observed under different conditions. The corresponding lifetime due to photolysis is 14-24 min, confirming that photolysis is the major atmospheric loss process for 1-nitronaphthalene. The gas-phase photolysis products could not be identified. However, substantial amounts of NO were produced, consistent with the proposed mechanism which involves the direct formation of a naphthoxy radical and NO. SOA yields in the range 57-71% were measured in the presence and absence of OH radical tracer or scavenger. The major particle-phase products identified using off-line GC-MS analysis were 1,4-naphthoquinone, 1-naphthol and 1,4-naphthalenediol. On-line analysis of the SOA generated in an indoor chamber was performed using ATOFMS. A number of photolysis products were tentatively identified in the mass spectra and there was also evidence for the formation of one or more high MW products in the range 200-300. Further investigations revealed that these high MW products are oxygenated polycyclic compounds most likely produced from the dimerization of naphthoxy radicals.

6.2 Suggestions for Future Work

The work presented in this thesis has extended our knowledge of the atmospheric degradation of naphthalene and two of its photooxidation products, phthaldialdehyde and 1-nitronaphthalene. There are however, a number of aspects that could be investigated further to provide a more complete understanding of the atmospheric chemistry of these compounds.

The formation yields and composition of SOA produced from the photooxidation of naphthalene has now been studied in some detail. However, further experiments should be performed to elucidate the mechanisms responsible for carboxylic acid formation in the particle phase and to clarify the role of relative humidity.

The photolysis rate coefficients for phthaldialdehyde and 1-nitronaphthalene are now well established. However, further experiments could be performed in order to improve our understanding of the mechanisms involved. Alternative techniques, such as proton transfer reaction – mass spectrometry (PTR-MS), could be employed for on-line monitoring of the gas-phase products.

One of the key findings of this work was that direct photolysis of phthaldialdehyde and 1-nitronaphthalene produces SOA. Similar experiments could be conducted on other photolabile photooxidation products of naphthalene, such as 2-formylcinnamaldehyde, 2-nitronaphthalene and 2-nitro-1-naphthol. In addition to chemical derivatization GC-MS, other off-line techniques could be used to identify the chemical components of the SOA. LC-MS, for example, does not cause heating of samples and is therefore useful in the identification of high MW polar species such as dimers and oligomers. The use of such methods would be particularly beneficial in the analysis of SOA produced from 1-nitronaphthalene photolysis and could help confirm the proposed pathway involving dimerization of naphthoxy radicals.

To date, the use of ATOFMS in simulation chamber studies has been very limited. However, the results of this work indicate that this technique has considerable potential for application to measurements of SOA composition. The high-time resolution afforded by the instrument means that it is particularly suited for monitoring the chemical evolution of SOA over time. Future applications of the ATOFMS could therefore involve monitoring the chemical changes to SOA while it is

subjected to oxidative ageing, e.g. via photolysis or reaction with atmospheric oxidants such as OH, NO_3 and O_3.

Finally, the results of this work and related studies could be compiled and used to generate the first detailed mechanism for the atmospheric degradation of naphthalene. The mechanism could be used in chemical models, such as the Master Chemical Mechanism (Bloss et al. 2005), that are used to predict the effect of VOC emissions on air quality.

6.3 References

Bloss, C., V. Wagner, M. E. Jenkin, R. Volkamer, W. J. Bloss, J. D. Lee, D. E. Heard, K. Wirtz, M. Martin-Reviejo, G. Rea, J. C. Wenger and M. J. Pilling (2005). "Development of a detailed chemical mechanism (MCMv3.1) for the atmospheric oxidation of aromatic hydrocarbons." Atmospheric Chemistry and Physics **5**(3): 641-664.

Chan, A. W. H., K. E. Kautzman, P. S. Chhabra, J. D. Surratt, M. N. Chan, J. D. Crounse, A. Karten, P. O. Wennberg, R. C. Flagan and J. H. Seinfeld (2009). "Secondary Organic Aerosol Formation from Photooxidation of Naphthalene and Alkylnaphthalenes: Implications for Oxidation of Intermediate Volatility Organic Compounds (IVOCs)." Atmospheric Chemistry and Physics **9**(9): 3049-3060.

Shakya, K. M. and R. J. Griffin (2010). "Secondary Organic Aerosol from Photooxidation of Polycyclic Aromatic Hydrocarbons." Environmental Science & Technology **44**(21): 8134-8139.